



UNIL | Université de Lausanne

Unicentre

CH-1015 Lausanne

<http://serval.unil.ch>

Year : 2011

ROLE OF PPARP IN IRRADIATION MEDIATED INTESTINAL DAMAGE

SAJIT THOTTATHIL OOMMEN

SAJIT THOTTATHIL OOMMEN, 2011, ROLE OF PPARP IN IRRADIATION MEDIATED
INTESTINAL DAMAGE

Originally published at : Thesis, University of Lausanne

Posted at the University of Lausanne Open Archive.

<http://serval.unil.ch>

Droits d'auteur

L'Université de Lausanne attire expressément l'attention des utilisateurs sur le fait que tous les documents publiés dans l'Archive SERVAL sont protégés par le droit d'auteur, conformément à la loi fédérale sur le droit d'auteur et les droits voisins (LDA). A ce titre, il est indispensable d'obtenir le consentement préalable de l'auteur et/ou de l'éditeur avant toute utilisation d'une oeuvre ou d'une partie d'une oeuvre ne relevant pas d'une utilisation à des fins personnelles au sens de la LDA (art. 19, al. 1 lettre a). A défaut, tout contrevenant s'expose aux sanctions prévues par cette loi. Nous déclinons toute responsabilité en la matière.

Copyright

The University of Lausanne expressly draws the attention of users to the fact that all documents published in the SERVAL Archive are protected by copyright in accordance with federal law on copyright and similar rights (LDA). Accordingly it is indispensable to obtain prior consent from the author and/or publisher before any use of a work or part of a work for purposes other than personal use within the meaning of LDA (art. 19, para. 1 letter a). Failure to do so will expose offenders to the sanctions laid down by this law. We accept no liability in this respect.



UNIL | Université de Lausanne

Faculté de biologie
et de médecine

Centre intégratif de génomique

**ROLE OF PPAR β IN IRRADIATION MEDIATED INTESTINAL
DAMAGE**

Thèse de doctorat ès sciences de la vie (PhD)

présentée à la

Faculté de biologie et de médecine
de l'Université de Lausanne

par

SAJIT THOTTATHIL OOMMEN

Master de l'Université de Mysore (L'Inde)...

Jury

Prof. Nicolas Fasel, Président
Prof. Béatrice Desvergne, Directrice de thèse
Prof. Freddy Radtke, Expert
Prof. Gisou Van Der Goot, Expert

Lausanne 2011

Imprimatur

Vu le rapport présenté par le jury d'examen, composé de

<i>Président</i>	Monsieur Prof. Nicolas Fasel
<i>Directeur de thèse</i>	Madame Prof. Béatrice Desvergne
<i>Experts</i>	Madame Prof. Gisou Van der Goot
	Monsieur Prof. Freddy Radtke

le Conseil de Faculté autorise l'impression de la thèse de

Monsieur Sajit Thottathil Oommen

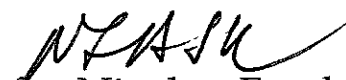
Master of Science of University of Mysore, India

intitulée

**ROLE OF PPAR beta
IN IRRADIATION MEDIATED INTESTINAL DAMAGE**

Lausanne, le 7 novembre 2011

pour Le Doyen
de la Faculté de Biologie et de Médecine



Prof. Nicolas Fasel

ACKNOWLEDGEMENTS

I would like to express my sincere gratitude to my supervisor, Prof. Beatrice Desvergne for giving me this opportunity to pursue my Ph.d in her laboratory at the Centre for Integrative Genomics (CIG). I especially thank her for her patience, understanding, guidance and all the constructive comments to improve my work.

I would also like to thank Prof. Freddy Radtke, Prof. Gisou Van Der Goot, and Prof. Pierre Michetti for being part of the thesis committee and for their detailed review, constructive criticism and excellent advice for the preparation of my thesis. I would especially like to thank Prof. Edward Farmer for being the President of the mid-thesis committee, for all his valuable suggestions and for taking the extra efforts to coordinate the thesis evaluation. My special thanks to Prof. Nicolas Fasel for being the President of the thesis committee in the absence of Prof. Edward Farmer and for the valuable discussions and his suggestions.

I am also thankful to my mentor - Prof. Bernard Thorens for his availability, his patient listening and his advises. My deep gratitude to Prof. Walter Wahli and Dr. Liliane Michalik for all their collaborations and their insightful comments during the PPAR group meetings.

My heartfelt thanks to Prof. Mathias Chamaillard for the collaboration on their project that resulted in a publication. My sincere thanks to Federic Varnat for his advice on primary cell culture technique and several aspects of the irradiation model. I would also like to take this opportunity to thank Laurent Dubuquoy for his collaboration and very expert and insightful comments for the in-vivo experiments.

I warmly thank Prof. Werner Held for his valuable advice and help with the Irradiation experiments. My sincere thanks to the members of the Transgenic Core Facility (TCF) and the Flow Cytometry Core facility (FCCF) at EPFL for their valuable help with the lentivirus production and FACS analysis respectively.

I am grateful to all the members of the CIG with whom I could work in an amiable environment. My sincere thanks to the members of the Genomic Technologies Facility for their help with Q-PCR and microarray experiments especially Manuel, Alexandra, Melanie and Hannes. I also wish to thank Sylvian Pradervand and Leonore Wigger for their help with the statistical analysis of the microarray data. I also extend my warm

thanks to Armelle Bauduret at the Genotyping facility and Catherine Roger at the Phenotyping facility for their invaluable support.

This work would not have been complete without the help of Josianne Bonnetti, Librarian of the University. Thank you for your help with making available many of the research articles that I needed. My sincere thanks are due to Christian Freymond, for her well-organised management of the lab that helped in very smooth flow of my work and also to Gilles Boss for all sorts of technical help at the CIG. I also wish to thank Nourra Egger and Marlyne Berger at the Central stores for their kind help and generosity. I would like to thank Corinne Hanggeli, Gergely and Edgar for their excellent informatics support at the CIG.

I am thankful to all the members at the animal facility particularly Patrick Gouait, Jose Huaman and Fabienne. Thanks for your help and support with maintaining the mice and all things I could learn from you. My sincere thanks to Carine for her valuable technical help and support all through out my thesis. I also wish to thank Elizabeth Joye, Genevieve, Maude, Fanny, Corinne Tallichet, Helene and Wanda who at one or the other time have offered their technical expertise and support.

I am greatly indebted to Marlene Petit for all her help with the administrative work without which my stay here would have been impossible. I really appreciate her special efforts and excellent secretarial skills in getting around things relating to my resident permit extension for my stay here in the last few months. I would also like to extend my thanks to Loyse Rebord for her help with administrative matters. I am grateful to many of the new and old colleagues and friends for the good ambience at the floor. I am especially grateful to Christoph, Laure, Cristina, Federica, Aurelien, Alex. M, Alex. K, Radina, Silvia, Nicolas. R, Pipat, Ilenia for their patient guidance and discussions. I also thank Jean-Marc, Jose, Virginie, Ilhelm, Matthew, He Fu, Imtiaz, Marta, Gwendoline for time spent in lab in meaningful discussions. I specially cherish the friendship of Chiara and Maria-giovanna for the time spent in our lab. My special thanks to Nathalie, particularly for her help with the translation of the abstract in French.

This work would be incomplete without the support of my friends in Lausanne – Shweta Tyagi, Shawon, Honey, Dhaval, Sandeep, Sujatha. Thanks to you for the homely feeling away from home. Thank you Shawon for all your help, support and your valuable suggestions. Words cannot convey the depth of my gratitude to you and I wouldn't have made it if not for your friendship and support.

This work would have been impossible without the prayers and support of my close friends Badri, Mary, Marc, Clara, Alice, Royson, Shaila, Lori, and Eva. Thank you for standing through the tough and testing times and for all your encouragement and invaluable support. Thank you Ibolya for the work in your lab in Hungary and to Betty for all your guidance that in a way laid the foundation for my work in Swiss.

This work would be incomplete without the prayers and invaluable support of my friends at Westlake church, Lausanne. My heartfelt thanks to the entire congregation, particularly to Tom, Martin, Alphonse for your guidance and spiritual insight. My heartfelt thanks to Clive and Daniel for walking along with me in the tough times. I extend my special thanks to the Zindlers, Karen Rizzo, Brandon, Meredith, Brian, Carolyn, Jonathan Olivier, Jonathan Schuler, Gustavo, Suleidy for your friendship and encouragement.

My special thanks to my friends in India – Sukumar anna, Sangeetha akka, Kiran uncle, Geetha Aunty, Soujanya, friends at Bethel fellowship and IISc BSF. Thanks for your invaluable support, friendship and prayers through out my entire work here. My heartfelt thanks to Prof. Cletus D’Souza for the constant encouragement, support, guidance and faith in me. I am so privileged to have you as my teacher.

I owe my loving thanks to my Family – my parents for their faith in me and their hopes for me. Special thanks to my brother Sanjay and Sister in law- Liji for taking care of responsibilities at home and letting me stay focussed on my studies, and to my niece – AnnaMaria you are such a darling and blessing to all of us.

There are many more people who have helped me in one or the other way through out this entire period of my thesis work and although I may not mention each of your names here, your help and support is warmly appreciated and my prayers for God’s blessings on your life.

And last but not the least, my sincere and heartfelt thanks to Almighty God. Thank you Lord for this gift of life and your plans for me in Switzerland and for the miracles you have done. Thank you that you are a loving, faithful and everlasting God who keeps his Promises.

TABLE OF CONTENTS

Abbreviations	4
Summary	6
Résumé	7
Chapter I. Introduction	9
1. The Intestine	9
1.1. General organization of the intestine.....	9
1.1.1. Composition of the intestinal epithelium	9
1.2. Signaling pathways in intestinal epithelial homeostasis	12
1.2.1. Wnt Signaling	12
1.2.2. Notch Signaling.....	16
1.2.2.1. The Notch pathway in lineage determination (Secretory vs Absorptive)	17
1.2.3. Hedgehog signaling.....	21
1.2.3.1. Hedgehog Secretion.....	21
1.2.3.2. The hedgehog-mediated transduction cascade	22
1.2.3.3. Identifying Hedgehog Target Cells	24
1.2.3.4. Hedgehog signaling and homeostasis of the adult gut	24
2. The nuclear receptor superfamily	26
2.1. Classification	26
2.2. The PPARs subfamily: a brief overview	27
2.2.1. PPAR β/δ	30
2.2.1.1. Structural properties	30
2.2.1.2. Ligand specificity	30
2.2.1.3. PPAR β : Functional properties.....	31
2.2.1.3.1. PPAR β in metabolism.....	31
2.2.1.3.2. PPAR β in cell fate.....	32
2.2.1.3.2.1. The anti-apoptotic activity of PPAR β	32
2.2.1.3.2.2. PPAR β in cell differentiation	34
2.2.1.3.2.2.1. In the placenta: Giant cell differentiation.....	34
2.2.1.3.2.2.2. In the skin: Keratinocyte differentiation	35
2.2.1.3.2.2.3. In the Central nervous system: neuronal and oligodendrocyte differentiation	35
2.2.1.3.2.2.4. In adipocyte differentiation	36
2.2.1.3.2.3. PPAR β in cell proliferation.	36
2.2.1.4. PPAR β in the intestine	37
2.2.1.4.1. Expression	37
2.2.1.4.2. PPAR β and paneth cell differentiation	37
2.2.1.4.3. A role for PPAR β in colorectal cancer	38
3. Irradiation: a medical concern and a tool for exploring cell and tissue repair	40
3.1. Signal transduction and cellular radiation responses.....	40
3.2. Irradiation and the intestine	43
3.2.1. Effects of radiation on the small intestinal cell types	44
3.2.1.1. The role of the intestinal adult epithelial stem cells	45
3.2.1.2. Radiation-induced apoptosis.....	45

3.2.1.3. The regenerative capacity of the epithelium after irradiation ...	47
3.2.1.4. Mechanisms of radioprotection.....	47
4. Aim of the work.....	49
Chapter II. Results.....	51
1. Consequences of PPAR β deletion at 8d post irradiation.....	51
1.1. Reduction of the number of mesenchymal cells in the lamina propria	51
1.2. Decrease of ECM components resulting in adhesion defect at 8d post-irradiation.....	55
2. In vivo analyses of the epithelia-mesenchyme crosstalk after irradiation	58
3. Exploring the molecular pathways controlled by PPAR β upon irradiation.....	60
3.1. Microarray analyses at 4 hours post-irradiation	60
3.2. Studies on cholesterol biosynthesis pathway using in vivo model.....	64
3.3. Validation of an in-vitro intestinal cell line model – HT-29	65
3.3.1. Estimation of basal levels of PPAR β and its activity in HT-29 cell model.....	65
3.3.2. Evaluation of PPAR β agonist and antagonist activities in HT-29 cell model.....	67
3.3.3. Generating lentivirus to mediate PPAR β silencing.....	70
3.3.4. Irradiation experiments: fine tuning the condition of cell irradiation	78
3.3.5. Studies on cholesterol biosynthesis pathway using HT-29 cell culture model.....	80
3.4. Global gene expression analysis using microarray to identify the effect of irradiation at 10Gy	82
3.4.1. Gene expression changes as an effect of 10Gy irradiation in HT-29 cells.....	85
3.4.2. GeneGo pathway analysis of the microarray data.....	87
3.4.3. Gene expression changes as an effect of treatment with agonist of PPAR β	89
3.4.4. Gene expression changes as an effect of treatment with antagonist of PPAR β	93
3.4.5. Validation of the genes of the microarray data by Q-PCR.....	96
3.4.6. Clonogenic survival assay in intestinal cell lines.....	97
3.4.7. Role of PPAR β in H ₂ O ₂ mediated damage in intestinal cell lines ...	100
Chapter III. Discussion and Perspectives	105
1. The late effects observed in gamma-irradiated PPAR β ^{-/-} mice	106
1.1. Alteration of the mesenchymal compartment.....	106
1.2. Alteration of the extra-cellular matrix of the mesenchymal compartment	107
1.3. The epithelial-mesenchymal cross-talk	108
1.4. The unexplored role of the endothelial microvasculature	108
2. New information gained from microarray data	109
2.1. Irradiation induces the cholesterol biosynthetic pathway.....	109
2.2. PPAR β -independent responses of HT29 to irradiation	110
2.3. PPAR β -dependent responses of HT29 to irradiation.....	111
3. How to reconcile in vivo and in vitro data?.....	111
Chapter IV. Materials and methods.....	113
1. Animal experiments	113

1.1. Generation of PPAR β ^{-/-} mice	113
1.2. Gamma-irradiation model	116
1.3. Histological analysis.....	116
1.4. Detection of apoptosis	117
1.5. Generation of PPAR β villin-Cre conditional KO mice	117
2. Experiments with cell cultures	119
2.1. Cell cultures.....	119
2.2. Transfections	119
2.3. Luciferase assays	120
2.4. Agonist/Antagonist treatments	120
3. Gamma irradiation experiments	120
4. Extraction of Total RNA	121
5. RT and Q-PCR.....	121
6. Microarray experiments.....	123
7. Extraction of proteins from cells	124
8. Western blot	124
9. PPAR β silencing using lentivirus.....	124
9.1. Lentivirus production	125
10. MTT assay	125
11. Caspase-3/7 assay	126
12. Clonogenic assay	127
12.1. Seeding after irradiation protocol	127
12.2. Seeding before irradiation protocol	127
12.3. Counting of colonies.....	128
13. H ₂ O ₂ assays.....	128
14. Statistical analysis.....	129
References.....	131
Annexes.....	153

ABBREVIATIONS

ADRP: Adipose Differentiation Related Protein
AF: Activation function
ANGPTL4: Angiopoietin-like 4
Apc: Adenomatous polyposis coli
BMP: Bone morphogenetic protein
BSA: Bovine serum albumin
CASP8: Caspase8
cDNA: Complementary DNA
cRNA: Complementary RNA
COL1A1: CollagenType I alpha1
COL2A1: CollagenType II alpha1
COL3A1: CollagenType III alpha1
CRC: Colorectal cancer
COX: Cyclooxygenase
DBD: DNA binding domain
DEPC: Diethylpyrocarbonate
DMEM: Dulbecco's Modified Eagle Medium
DMSO: Dimethyl sulfoxide
EEF1A1: Eukaryotic translation elongation factor 1 alpha 1
EGF: Epidermal growth factor
Elf3: E47-like factor 3
ES cells: Embryonic stem cells
FACS: Fluorescence activated cell sorting
FAP: Familial adenomatous polyposis
FCS: Fetal calf serum
FDFT1: Farnesyl-diphosphate farnesyl transferase 1
GAPDH: Glyceraldehyde 3-phosphate dehydrogenase
GFP: Green fluorescent protein
GUSB: Glucuronidase, beta
Gy: Gray (SI unit of absorbed radiation dose of ionizing radiation)
Hes1: Hairy/ Enhancer of Split 1
Hip: hedgehog interacting protein
HMGCR: 3-hydroxy-3-methylglutaryl-Coenzyme A reductase
HMGCS1: 3-hydroxy-3-methylglutaryl-Coenzyme A synthase1 (soluble)
IFN γ : Interferon γ
Ihh: Indian Hedgehog
ISC: Intestinal stem cell
LBD: Ligand binding domain
L-FABP: Liver fatty acid binding protein
LSS: Lanosterol synthase (2,3-oxidosqualene-lanosterol cyclase)
MMP: matrix metalloproteinase
MOI: Multiplicity of infection
MVD: Mevalonate (diphospho) decarboxylase
MTT: (3-(4,5-Dimethylthiazol-2-yl)-2,5-diphenyltetrazolium bromide
Ngn3: Neurogenin3
NF κ B: Nuclear factor- κ B

NSAIDS: Non-steroidal anti-inflammatory drugs
OD: Optical density
Klf4: kruppel-like factor 4
PATCH1: Patched-1 (hedgehog protein receptor)
PBS: Phosphate buffered saline
PDK1: Pyruvate dehydrogenase kinase, isoenzyme 1
PDK4: Pyruvate dehydrogenase kinase, isoenzyme 4
PFA: Paraformaldehyde
PPAR: Peroxisome proliferator-activated receptor
PPRE: PPAR response element
RNA: Ribonucleic acid
RNAi: RNA interference
RXR: Retinoid X receptor
siRNA: Small interfering RNA
Shh: Sonic hedgehog
Smo: Smoothened
TBP: TATA-binding protein
Tcf: T cell factor
TGF- β : Transforming growth factor- β
TNF α : Tumor necrosis factor α
TUNEL: Terminal deoxynucleotidyl transferase-mediated dUTP Nick –end labeling

SUMMARY

Peroxisome proliferator activated receptors (PPARs) belong to the nuclear receptor superfamily of transcription factors. Of the three known PPAR isotypes, PPAR β has been shown to regulate proliferation, apoptosis and differentiation in different tissues. Previous work from our lab have emphasized its role in cell survival and wound healing. In the small intestine, PPAR β is expressed in the intestinal crypts where it is known to regulate the differentiation of the Paneth cells by attenuating the expression of *Ihh*. Despite its remarkable potential of rapid self-renewal, small intestinal epithelium is sensitive to cytotoxic insults, especially to radiotherapy of cancers in the abdomino-pelvic region. Both acute and chronic exposure of the intestine to irradiation thus can lead to radiation-induced gastrointestinal syndrome. Due to the known protective role of PPAR β in inflammatory context, the aim of this thesis was to directly characterize the role of PPAR β in the molecular response to gamma-irradiation induced intestinal cell damage in a mouse model and in the human HT-29 colon carcinoma cell line. By comparing the effects of irradiation on HT-29 cells that were treated with or without PPAR β ligands, there was no evidence for a protective role of PPAR β . This contrasts with the situation *in-vivo*, since targeted deletion of PPAR β transiently increased the rate of apoptosis of intestinal stem cells 4hrs after irradiation. Furthermore, 8 days post irradiation, cell death was also increased in the mesenchyme, followed by impaired adhesion of the epithelia to the mesenchyme due to loss of collagen I and III of the extracellular matrix components. PPAR β thus appears to affect the crosstalk between the mesenchyme and the epithelium, consistent with the observed delay in tissue repair at 3.5 days post-irradiation in the PPAR β ^{-/-} mice. In cultured HT-29 cells lacking a mesenchymal component, the same crosstalk is unlikely to occur explaining perhaps the apparent discrepancy between our *in vivo* and *in vitro* results, if a protective role of PPAR β relies on the crosstalk between epithelia and mesenchyme. Overall, our findings are consistent with a possible involvement of PPAR β in attenuating intestinal tissue damage in conditions of radiotherapy for cancers. The exact molecular mechanism of PPAR β action still warrants further exploration to better understand its physiological role in this regard.

RÉSUMÉ

Les récepteurs activés proliférateurs de peroxisomes (PPARs) appartiennent à la grande famille des récepteurs nucléaires et ont été impliqués dans plusieurs processus physiologiques. Parmi les trois isotypes PPAR, PPAR β est bien connu pour son rôle dans les décisions déterminant le destin des cellules, notamment dans les processus de prolifération, de différenciation et d'apoptose. Ce rôle a particulièrement été souligné comme protecteur dans les contextes de survie cellulaire et de cicatrisation. Il est fortement exprimé dans l'intestin grêle. Notre groupe a déjà rapporté sa présence importante dans les cryptes duodénales, où se trouvent les cellules souches intestinales. Précédemment, nous avons aussi fait remarquer le rôle de PPAR β dans la différenciation des cellules de Paneth, par la régulation négative de la signalisation Ihh de l'épithélium intestinal. Malgré sa capacité de figurer parmi les tissus du corps qui se régénèrent le plus rapidement, l'épithélium intestinal est particulièrement sensible aux attaques cytotoxiques, surtout celles dues à la radiothérapie des cancers abdomino-pelviens. Cela peut donner lieu à des lésions gastro-intestinales en tant qu'effet indésirable d'une exposition aiguë et chronique à l'irradiation. En raison du rôle protecteur de PPAR β le but de cette étude était de comprendre les voies de signalisation moléculaires régulées par PPAR β qui sont impliquées dans les réponses des cellules intestinales aux dommages causés par l'irradiation.

Afin de déchiffrer les mécanismes moléculaires sous-jacents, un modèle in-vitro d'une lignée cellulaire - HT-29 a été utilisée. Il n'y a cependant pas de preuve d'un effet protecteur de PPAR β dans divers contextes d'endommagement cellulaire testés in-vitro. Ceci contraste avec les observations in-vivo qui indiquent que l'irradiation provoque une létalité supérieure dans les souris PPAR $\beta^{-/-}$ par rapport aux souris PPAR $\beta^{+/+}$, entre autre corrélée avec une apoptose augmentée des cellules souches intestinales à 4h après irradiation. En plus, le décès plus important de cellules mésenchymateuses a été observé dans les souris PPAR $\beta^{-/-}$, 8 jours après irradiation. Moins nombreuses, ces cellules se sont également détachées de la matrice extracellulaire reliant l'épithélium et le mésenchyme. Nous stipulons qu'in-vivo, PPAR β participe au dialogue entre le mésenchyme et l'épithélium, ce qui est concordant avec le délai observé lors de la réparation tissulaire. Ce

dialogue entre l'épithélium et le mésenchyme, n'existe pas de la même manière in-vitro. Il en résulte donc un défaut de réponse mésenchymale médiée par PPAR β , d'où le paradoxe entre les conditions in-vivo et in-vitro.

Ces observations indiquent l'implication possible de PPAR β dans les lésions actiniques, en tant que conséquence naturelle de la radiothérapie de patients avec un cancer. Les mécanismes précis de l'action de PPAR β nécessitent une exploration approfondie de son rôle physiologique dans ce contexte.

CHAPTER I:

INTRODUCTION

1. The Intestine

1.1 General organization of the intestine

The intestinal tract can be divided into the small intestine composed of the duodenum, jejunum and ileum and the large intestine composed of the colon and the rectum. The intestinal tract is a tubular structure composed of three different layers. The outer layer consists of layers of innervated smooth muscle cells that help in the process of peristalsis. The middle layer is composed of the stromal tissue and the inner layer is composed of epithelial cells, referred to as the mucosa that processes the nutrients and absorbs them.

The main function of the small intestine is to absorb the nutrients from the ingested food. To achieve this goal, the small intestinal mucosal surface area is enormously increased by numerous finger-like protrusions, termed villi. Deeply embedded structures into the submucosa are the crypts of Lieberkuhn. The functional unit of the small intestine is composed of the crypt-villus unit whereas the mucosa of the large intestine is composed of only crypts and surface epithelium, with no villi.

1.1.1 Composition of the intestinal epithelium

The intestinal crypts are the structures that contain the intestinal stem cells. The intestinal stem cells give rise to all the four different cell types namely enterocytes, goblet, enteroendocrine and the Paneth cells that form the crypt-villus unit (Fig.1, Crosnier et al., 2006). They divide to give rise to the transit-amplifying cells that then differentiate and migrate upward to form absorptive cells/ enterocytes, goblet cells and the enteroendocrine cells.

Enterocytes constitute more than 80% of all intestinal epithelial cells and cover almost the entire surface of the villi. Enterocytes secrete digestive enzymes and they mediate nutrient, ion and water uptake by expressing transporter proteins and by extending large numbers of microvilli that increase the total surface area.

Goblet cells are specialized secretory cells responsible for producing the mucus lining that fulfills an essential protective function, especially in the distal intestine where

these cells are most abundant. They secrete mucins and trefoil proteins that are necessary for proper movement and effective expulsion of gut contents. They also provide protection against stress caused by shearing and chemical damage.

Enteroendocrine cells secrete specific peptide hormones to coordinate important gut functions. These gut hormones include catecholamines, serotonin, substance P, and secretin (Hocker & Wiedenmann 1998). Based on their morphology and expression of these intestinal hormones, one can distinguish 15 different subtypes of enteroendocrine cells, which will not be described herein.

Paneth cells secrete antimicrobial proteins and enzymes like lysozymes, cryptidins and defensins (Porter et al. 2002). Along the crypt-villus axis, they are the only differentiated cells that migrate downward to occupy the crypt base next to the stem cells.

Table 1 (Adapted from Sancho et al., 2004) summarizes the markers used to identify the different intestinal epithelial cells.

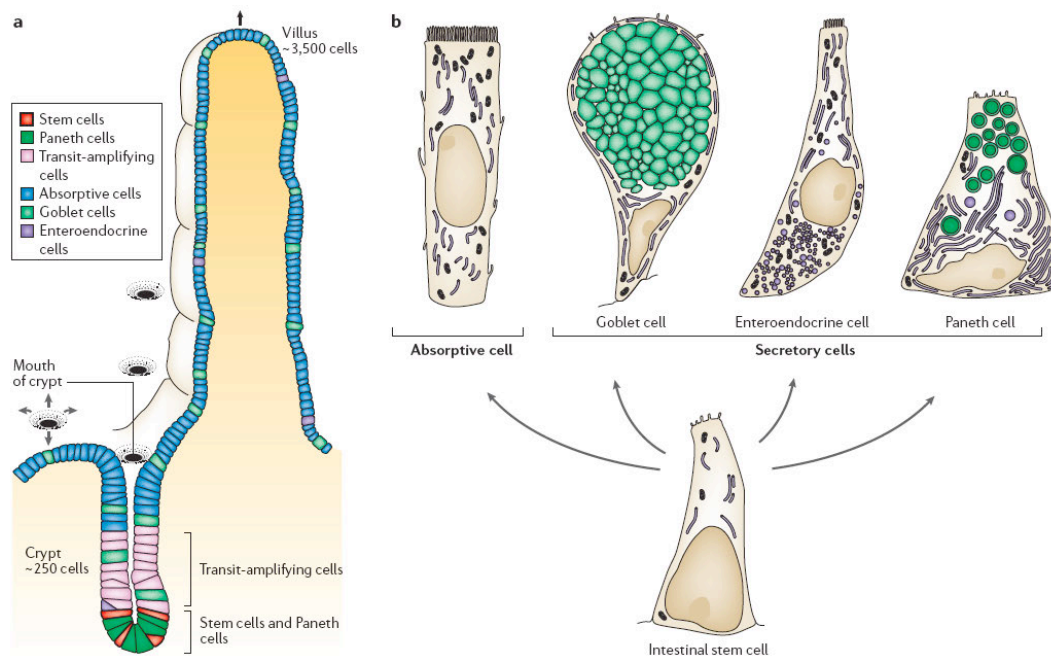


Fig. 1 | The distribution of epithelial cell types in the mammalian small intestine. a. A villus with one of the crypts that contribute to renewal of its epithelium. Arrows indicate the upwards flow of cells out of the crypts. Stem cells lie near the crypt base; it is uncertain whether they are mixed with, or just above, the Paneth cells. Above the stem cells are transit-amplifying cells (dividing progenitors, some of them already partially differentiated); and above these, in the neck of the crypt and on the villus, lie post-mitotic differentiated cells (absorptive cells, goblet cells and enteroendocrine cells; see panel **b**) (Adapted from Crosnier et al., 2006).

	Cell type
Proliferative	
Ki67	All proliferative cells
c-Myc	Proliferative—mainly bottom two thirds of crypts
NRP-B	All proliferative crypt cells
CD44	All proliferative crypt cells
SHH	Intervillus pockets in fetal small intestine
IHH	Intervillus pockets in fetal small intestine
Musashi-1	Stem cells + base columnar cells
EphB3	Stem cells + base columnar cells
EphB2	Decreasing gradient from bottom to top of crypt
Math-1	Goblet + enteroendocrine + Paneth precursors
Hes-1	Proliferative cells (specific precursors?)
Ngn-3	Enteroendocrine precursors
Differentiated	
P21waf1/Cip1	Cell cycle arrested cells
Ephrin-B1	Gradient from surface epithelium to crypt bottom
IHH	Top third and surface epithelium in adult colon
Carbonic anhydrase II	Top third and surface epithelium in colon
Phospho-smad 1/5/8	Differentiated cells in villus
Villin	Microvilli-increasing gradient from crypt to villus
Fabpi/FabpL	Enterocytes
Alkaline phosphatase	Enterocytes-brush border
Sucrose isomaltase	Enterocytes-brush border
Math-1	Mature goblet, enteroendocrine and Paneth cells
Muc2	Goblet cells
NeuroD/Beta	Enteroendocrine cells
Synaptophysin	Enteroendocrine cells
Secretin	Enteroendocrine cells
Serotonin	Enteroendocrine cells
Lysozyme	Paneth cells
Cryptdins	Paneth cells
EphB3	Paneth cells

Table 1: Markers of cell type or compartment in the intestinal epithelium (adapted from Sancho, E et al., 2004).

1.2 *Signaling pathways in intestinal epithelial homeostasis*

The intestinal epithelium is one of the most dynamic self-renewing systems of the body. The intestinal epithelium has the fastest turnover rate with the absorptive cells being replaced every 7 days. The pattern of renewal is quite uniquely organised by compartmentalization of the small intestinal crypt-villus unit, with proliferation ongoing at the bottom of the crypt and the differentiation at the top of the crypt. This pattern is followed by unidirectional migration of the cells starting from the crypt base to the tip of the villi, where they finally undergo apoptosis and are eliminated into the intestinal lumen. The intestinal stem cells are located at +4 position from the bottom of the crypts (Potten et al., 2003) and give rise to the transit-amplifying progenitor cells that migrate upwards towards the villi. They further divide and the differentiated cells move up the crypt neck and migrate to the villi, the only exception being the Paneth cells that migrate downward and remain there. The Paneth cells live longer than the other cells from the epithelium and are renewed only every 20 days.

As the entire small intestine is composed of numerous crypt-villus units with millions of cells, this entire mechanism of proliferation, differentiation and migration has to be tightly regulated to maintain a proper homeostasis. This is achieved by the compartmentalization of the small intestine and the numerous reciprocal signalling within the crypt-villus unit. The signaling pathways involved like Wnt, Indian hedgehog (Ihh), Bmp, Notch not only act independently but also in crosstalk with each other by expressing and regulating different components of the signaling pathway in different zones. Recent studies have elucidated the role of the interactions of these signals arising from the epithelium and the mesenchyme, as discussed below (reviewed in Crosnier et al., 2006).

1.2.1 *Wnt Signaling*

Wnt signaling has been recognized as indispensable in virtually every developmental process as all throughout the animal kingdom (Cadigan & Nusse 1997). The key player of the signaling pathway is β -catenin, a cytoplasmic protein. According to the classical model of Wnt signaling regulation, the tumor suppressor complex Apc controls the stability of β -catenin. In the absence of Wnt signal, the axin/GSK-3/Apc/Ck-1

destruction complex normally binds to β -catenin and phosphorylates it sequentially. Hyperphosphorylated β -catenin is then polyubiquitinated by an E3 ubiquitin ligase containing the F-box protein β -TrCP and destroyed by the proteasome, thereby preventing its nuclear translocation. This results in the repression of the Wnt responsive genes. In the presence of the activated Wnt signal, the secreted Wnt proteins bind to the cell surface receptor called frizzled (Frz), which usually interact with the transmembrane protein LRP (reviewed in Polakis 1999, Bienz & Clevers 2000, and Giles et al. 2003) and form a complex with the Disheveled (Dvl). Dvl is a cytoplasmic protein that functions upstream of β -catenin. In the presence of the Wnt signal, Dvl inhibits the Apc-containing destruction complex, resulting in hypophosphorylation of β -catenin that enables its translocation to the nucleus and further activation of the transcription of the target genes by its binding to the TCF/LEF complex.

Studies by Roberts et al. (2007) have led to the revision of the classical model of Wnt signaling. The authors show that Wnt binding to Frizzled triggers the recruitment and polymerization of Disheveled (DVL) to the membrane, itself recruiting the axin containing complex. This results in an inhibition of the Axin/GSK-3 β /CK-1/Apc complex formation, allowing the stabilization and accumulation of the cytoplasmic β -catenin. β -catenin then translocates to the nucleus where it interacts with the T cell factor/lymphoid-enhancing factor (TCF/LEF family). In the absence of β -catenin, the TCF/LEF factors repress transcription of their target genes, to which they bind. Upon binding to β -catenin, the TCF/LEF factors turn to activators and translate the Wnt signal into transcription of the target genes (Fig.2).

The expression pattern of all the Wnts, as well as that of other proteins belonging to this pathway, such as Frizzled, LRPs, and TCFs, are consistent for the presence of an active Wnt signaling in the epithelial cells of the crypt base (Gregorieff et al., 2005). Indeed, the role of Wnt signaling in the proliferation of the intestinal epithelial precursor cells has been reported by multiple *in-vivo* studies (Bienz & Clevers 2000, Booth et al. 2002, Kinzler & Vogelstein 1996), pointing Wnt as a master regulator of the intestinal epithelial proliferation and differentiation processes (Van de Wetering et al., 2002).

Various mice models have been used to inhibit the Wnt signaling in the small intestine (for example, mice lacking TCF4 transcription factor (Korinek et al., 1998); mice with a conditional deletion of β -catenin in the intestinal epithelium (Ireland et al., 2004;

Tea Fevr et al., 2007); adenoviral or transgenic expression of Dickkopf-1, a natural secreted Wnt antagonist (Kuhnert et al., 2004, Pinto et al., 2003)). In all these models, a considerable decrease of intestinal epithelial cell proliferation was observed. Further analyses demonstrated that indeed the maintenance of the crypt progenitor compartment in the intestine requires active Wnt signaling. On the contrary, transgenic expression of R-Spondin-1, a Wnt agonist, resulted in enormous hyperproliferation of the intestinal crypts due to activation of the Wnt pathway (Kim et al., 2005). Apart from regulating the proliferation of the transit-amplifying precursor cells, Wnt signaling is also involved in the terminal maturation of the Paneth cells via inducing Sox9 (Blache et al., 2004; Van Es et al., 2005).

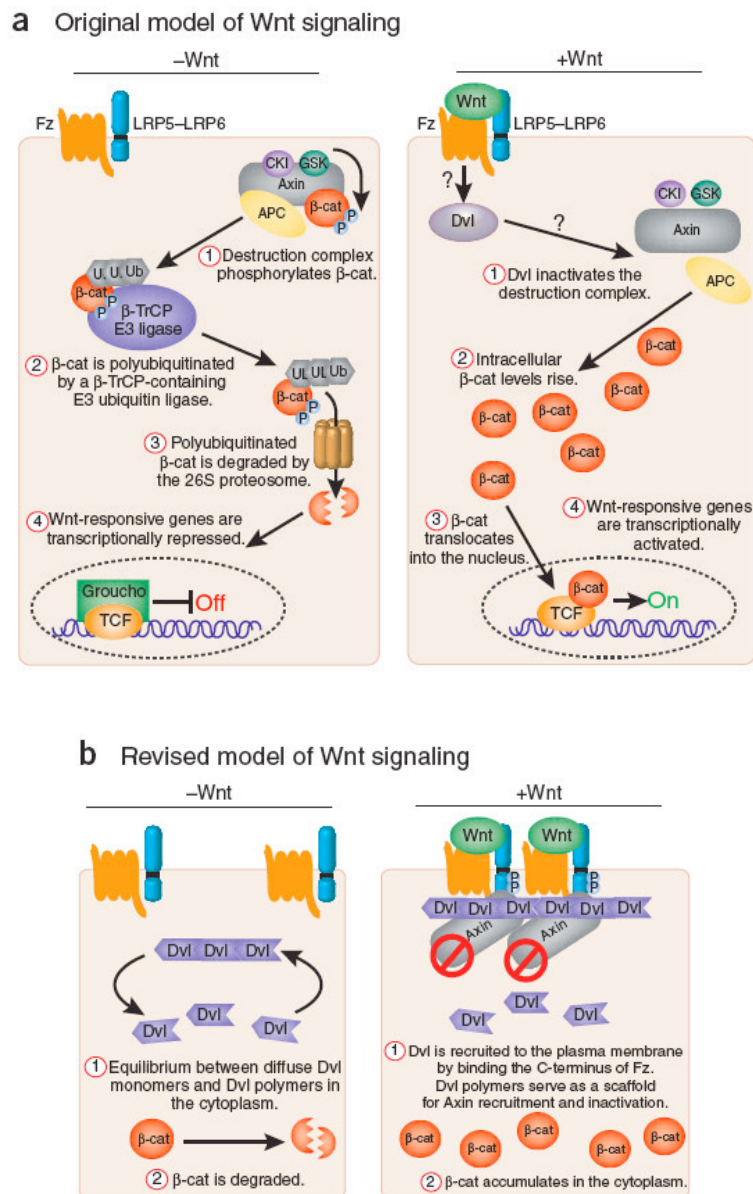


Fig. 2 | Models of Wnt signal transduction. (a) Classic model of Wnt signaling. See text for more details. **(b) Revised model of Wnt signaling.** In the absence of Wnt, Dvl remains cytoplasmic, in equilibrium between monomers and polymers. The destruction complex is active, and β -catenin is degraded. Wnt stimulation triggers Dvl recruitment to the plasma membrane by Frizzled (Fz) receptors, which function with LRP5–LRP6 coreceptors (reviewed in Clevers, 2006). Dvl binds the C-terminal tail of Fz using its PDZ domain (Wong et al., 2003). Dvl polymers at the membrane serve as a dynamic scaffold for Axin recruitment and inactivation (Cliffe et al., 2003). Wnt stimulation also leads to phosphorylation of LRP5–LRP6 by $\text{CKI}\gamma$ and GSK3 (reviewed in Clevers, 2006). Phosphorylated LRP5–LRP6 can interact with Axin, potentially providing another mechanism to recruit and inactivate Axin at the membrane (Tamai et al., 2004; Mao et al., 2001; Tolwinski et al., 2003). Several models have been proposed to explain Axin inactivation, including a conformational change upon Dvl and/or LRP5–LRP6 binding, and Axin degradation (reviewed in Clevers, 2006), (Adapted from Roberts et al., 2007).

1.2.2 Notch Signaling

Notch signaling has been implicated in cell fate decisions and morphogenesis in different species (Artavanis-Tsakonas et al. 1999). The Notch gene was first characterized in the fly *Drosophila melanogaster*, and encodes a 300-kD single-pass transmembrane receptor. Notch act as a receptor that is activated by transmembrane ligands known as DSL (Delta, Serrate, and Lag 2) proteins (Mumm & Kopan 2000). The interaction between Notch ligands and their receptor then occurs between two adjacent cells. This interaction enables proteolytic cleavage of the receptor to generate the Notch intracellular domain (NICD) that translocates into the nucleus. A key step in the cleavage process involves the activity of the gamma-secretase protease complex. In the absence of Notch signaling, the cofactor proteins collectively called CSL (CBF1, Su (H), Lag-1) act as transcriptional repressors. Their binding to NICD turns the complex into a transcriptional activator function that enables transcription of their target genes (e.g., HES, Hairy/Enhancer of Split genes)(Baron, 2003). This “core” Notch signaling pathway is depicted in Figure 3.

Notch signal regulates cell fate between adjacent cells in progenitor cell clusters. Signaling through Notch takes place when a cell gains levels of the ligand that is higher compared to their neighboring cells. This is mediated either through the intrinsic or extrinsic regulatory mechanisms, which are not well characterized, or through stochastic events that get instantly amplified through feedback regulatory mechanisms (Mumm & Kopan 2000). One of the best-characterized target genes of Notch is the hairy/enhancer of split (HES) transcriptional repressor, which belongs to the basic helix-loop-helix (bHLH) proteins. The HES protein is itself a transcription factor, which further regulates the downstream target genes (Artavanis-Tsakonas et al. 1999, Mumm & Kopan 2000, Baron, 2003).

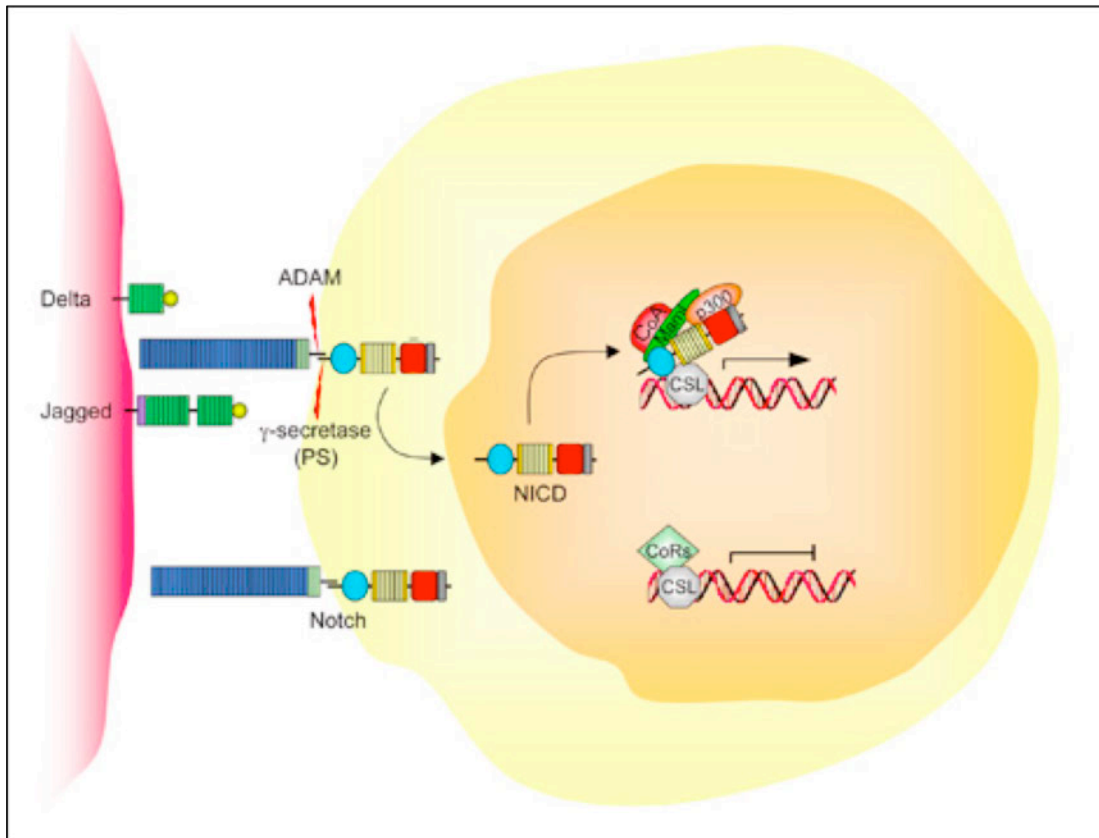


Fig. 3 | Core Notch signaling pathway. NOTCH1 signalling is initiated by the engagement of extracellular portions of NOTCH1 with its ligands, which are members of the Jagged/Delta family. This binding induces metalloprotease-dependent cleavage of the NOTCH1 heterodimerization domain (HD) with terminal cleavage that is dependent on gamma-secretase activity. This process releases Notch intracellular domain (NICD), which translocates to the nucleus to form a multimeric transcriptional factor complex with the transcription factor CSL and co-activators of the mastermind-like (MAML) family. These recruit additional co-activators, such as p300 and PCAF (CoA), to activate the transcription of target genes such as HES (Image adapted from www.google.com).

1.2.2.1 *The Notch pathway in lineage determination (Secretory vs Absorptive)*

As discussed previously, the transit amplifying cells differentiate to form the four different cell types, of which three are secretory (the goblet cells, the enteroendocrine cells, and the paneth cells) while the fourth one (the enterocytes) belong to the absorptive lineage. Figure 4 gives a schematic overview of the cell lineage specificity in the intestine. Similar to the role played by the Wnt signaling, the Notch pathway is vital to maintain the crypt compartment in its undifferentiated and proliferative state. Notch signaling deficiency in the intestinal epithelium either through conditional deletion of the CSL gene or through pharmacological gamma-secretase inhibitors results in the rapid and complete conversion of all epithelial cells into goblet cells (Milano et al., 2004; Wong et al., 2004).

Treatment of $Apc^{\text{min/+}}$ mice induced Math1 expression in adenomas and the conversion of proliferative adenoma cells into post-mitotic goblet cells (Van Es et al., 2005). Both the Notch1 and Notch2 receptors mediate Notch signals in the intestinal epithelium. These receptors work redundantly as evidenced by the complete conversion of the proliferative crypt cells into postmitotic goblet cells only upon conditional inactivation of both these receptors in the gut (Riccio et al., 2008). An opposite effect in the form of depletion of goblet cells and a reduction in enteroendocrine and Paneth cell differentiation are observed upon specific overexpression of the constitutively active Notch1 receptor (Fre et al., 2005; Stanger et al., 2005). Thus, in the intestinal epithelium, the Notch pathway regulates absorptive versus secretory cell fate decisions. There have been no reports of mutational alterations in Notch signaling in intestinal tumorigenesis so far.

A characteristic feature of Notch signaling is the regulation of the downstream effectors of Notch. As mentioned above, the first set of genes activated by Notch belongs to the Hairy/Enhancer of Split (Hes) class that encode transcriptional repressors. Hes repressors in turn repress transcription of a second set of genes, typically basic helix-loop-helix (bHLH) transcription factors that, when derepressed, induce differentiation along specific lineages. One of these is Math1 (Jensen et al., 2000). The epithelium of Math1 mutant mice is populated only by enterocytes indicating the fact that intestinal Math1 expression is required for the commitment towards the secretory lineage (Yang et al., 2001). The factors that are downstream of Math1 play specific roles in epithelial cell differentiation. For example, the zinc-finger transcriptional repressor Gfi1 is absent in Math1^{-/-} embryonic intestines, implying that it acts downstream of Math1. Gfi1^{-/-} mice lack paneth cells and display a clear reduction in the number of goblet cells. There is, however, an increase in the number of enteroendocrine cells (Shroyer et al., 2005). Other factors include kruppel-like factor 4 (Klf4), a zinc-finger transcription factor whose deletion results in the loss of goblet cells (Katz et al., 2002) and Neurogenin3 (Ngn3), a bHLH transcription factor that is downstream of the Notch-Hes1-Math1 signaling cascade. Ngn3^{-/-} mice do not develop any intestinal endocrine cells (Jenny et al., 2002).

Interestingly, Math1 expression is reduced in intestinal crypts in mouse models with impaired Wnt signaling, setting Math1 as the crossroad between the Wnt and Notch signaling. Indeed, as a functional consequence of the impaired Wnt signaling, the secretory lineages are depleted, and the villi are lined mainly with enterocytes (Ireland et al., 2004; Korinek et al., 1998; Pinto et al., 2003). Beside repressing Math1 activity and thereby repressing the secretory lineage, HES exert a positive activity on the

differentiation of the absorptive enterocytes, as suggested by the decrease in absorptive enterocytes in the *Hes1*^{-/-} animals (Jensen et al., 2000). These activities are mediated by HES acting on E47-like factor 3 (Elf3), a member of the Ets transcription family (Ng et al., 2002) and on the expression of transforming growth factor β type II receptor (Tgf- β RII) (Flentjar et al., 2007).

A summary of the proposed positioning of each component of the Notch and Wnt pathways acting on the epithelial cell lineage commitment is presented in the Figure 4 (Van der Flier and Clevers, 2009).

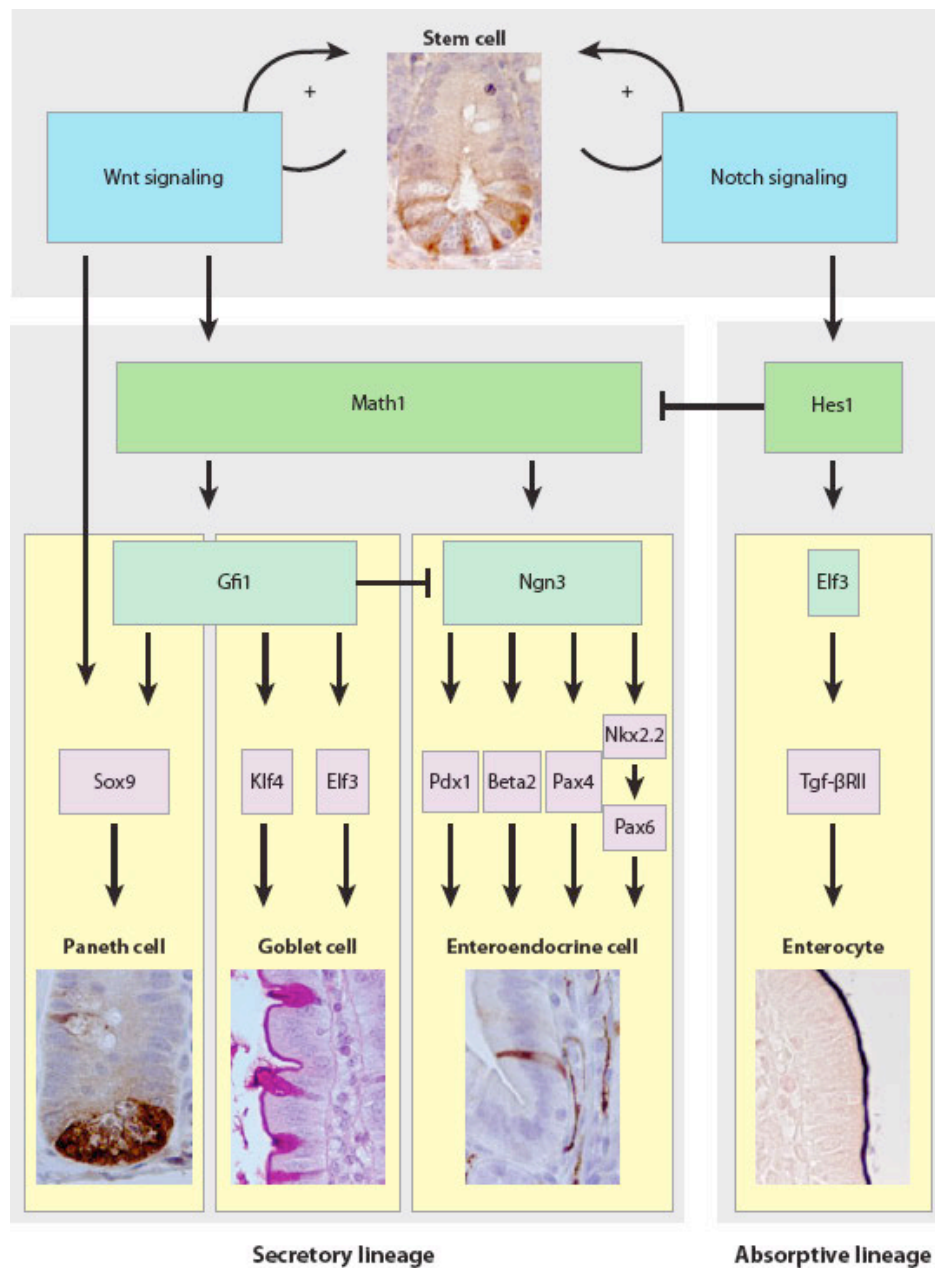


Fig. 4 | Schematic overview of the genetic hierarchy of epithelial cell lineage commitment in the intestine. Intestinal stem cells proliferate under control of both the Wnt and the Notch pathways and can differentiate into all four differentiated cell types present in the intestinal epithelium. Math1 is required for the commitment to the secretory lineage. Gfi1 and Sox9 are responsible for differentiation into Paneth cells. Gfi1, kruppel-like factor 4 (Klf4), and E47-like factor 3 (Elf3) are necessary for goblet cell development. Neurogenin3 (Ngn3) is required for endocrine cell fate specification. Downstream of Ngn3, a set of transcription factors is responsible for the specification of the various enteroendocrine hormone-expressing cell types. Hairy/ Enhancer of Split 1 (Hes1), through Elf3 and the transforming growth factor β type II receptor (Tgf- β RII), is responsible for differentiation into enterocytes of the absorptive lineage (Adapted from Van der Flier and Clevers, 2009).

1.2.3 *Hedgehog signaling*

➤ *Hedgehog Secretion*

The *Drosophila* Hedgehog mutant was first identified in 1980 (Nüsslein-Volhard and Wieschaus 1980), following which three separate groups identified the *Drosophila* hedgehog gene in 1992 (Lee et al., 1992; Mohler and Vani 1992; Tabata et al., 1992). Sonic hedgehog (Shh), desert hedgehog (Dhh), and Indian hedgehog (Ihh) are three murine homologs, which are highly conserved in mouse and humans (Marigo et al., 1995).

Hedgehog proteins undergo extensive post-translational modifications before they can function as a signaling molecule. Autocatalytic cleavage of a 45-kDa precursor protein results in a 19-kDa NH₂-terminal fragment that carries out the signaling function and a 26-kDa COOH-terminal fragment that acts as a cholesterol transferase apart from catalyzing the cleavage itself (Bumcrot et al., 1995; Lee et al., 1994; Porter et al., 1996; Porter et al., 1995). One characteristic feature of hedgehog proteins is that they are poorly soluble owing to dual lipid modification of the mature NH₂-terminal fragment that is linked covalently to a palmitate and a cholesterol group (Mann and Beachy, 2004). These modifications enable the hedgehog protein to fuse to the cell membrane and thus play a key role in directing the range of the hedgehog signaling in a tissue (Chen et al., 2004). In addition, both the above-mentioned modifications are necessary for the formation of multimers of NH₂-terminal hedgehog protein, required for the long range signaling (Chen et al., 2004; Zeng et al., 2001). Studies in *Drosophila* suggest that the lipid moieties of the hedgehog multimers associate with the outer phospholipid layer of lipoprotein particles and that this association is necessary for hedgehog signaling activity (Panakova et al., 2005).

The release of mature hedgehog protein from the hedgehog-producing cell requires Dispatched (Disp), a 12-pass transmembrane protein with a sterol-sensing domain. The significant role of Disp1 for hedgehog signaling activity was evident from Disp1^{-/-} mutant mice that showed phenotype similar to mice that lack hedgehog signaling receptor (Smo) (Caspary et al., 2002; Kawakami et al., 2002; Ma et al., 2002).

1.2.3.2 *The hedgehog-mediated transduction cascade*

Smoothed (Smo) is a seven-span transmembrane receptor that mediates the transmission of the Hedgehog signal. It binds to the cell membrane and intracellular vesicles (when overexpressed in cell lines) (Chen et al., 2002; Corbit et al., 2005; Incardona et al., 2002). Hedgehogs regulate the activity of Smo indirectly by binding to a second receptor Patched (PTCH1). In vertebrates, there exist two PTCH1 genes, PTCH1 (Goodrich, et al., 1996) and PTCH2 (Motoyama et al., 1998). PTCH is a 12-span transmembrane receptor with two large hydrophilic extracellular loops that mediate Hedgehog binding. Binding of Hedgehog to PTCH1 releases the inhibitory action of PTCH1 on Smo, which is now active (Fig. 5). Another component of this signaling cascade is Hedgehog-interacting protein (Hhip), which binds and somehow captures Hedgehog on receiving cells. It thus acts as a negative regulator of Hedgehog signaling (Chuang et al., 1999). Interestingly, PTCH1 and Hhip are transcriptional targets of Hedgehog signaling and function in a negative feedback loop thereby restricting the range of Hedgehog signaling in a tissue.

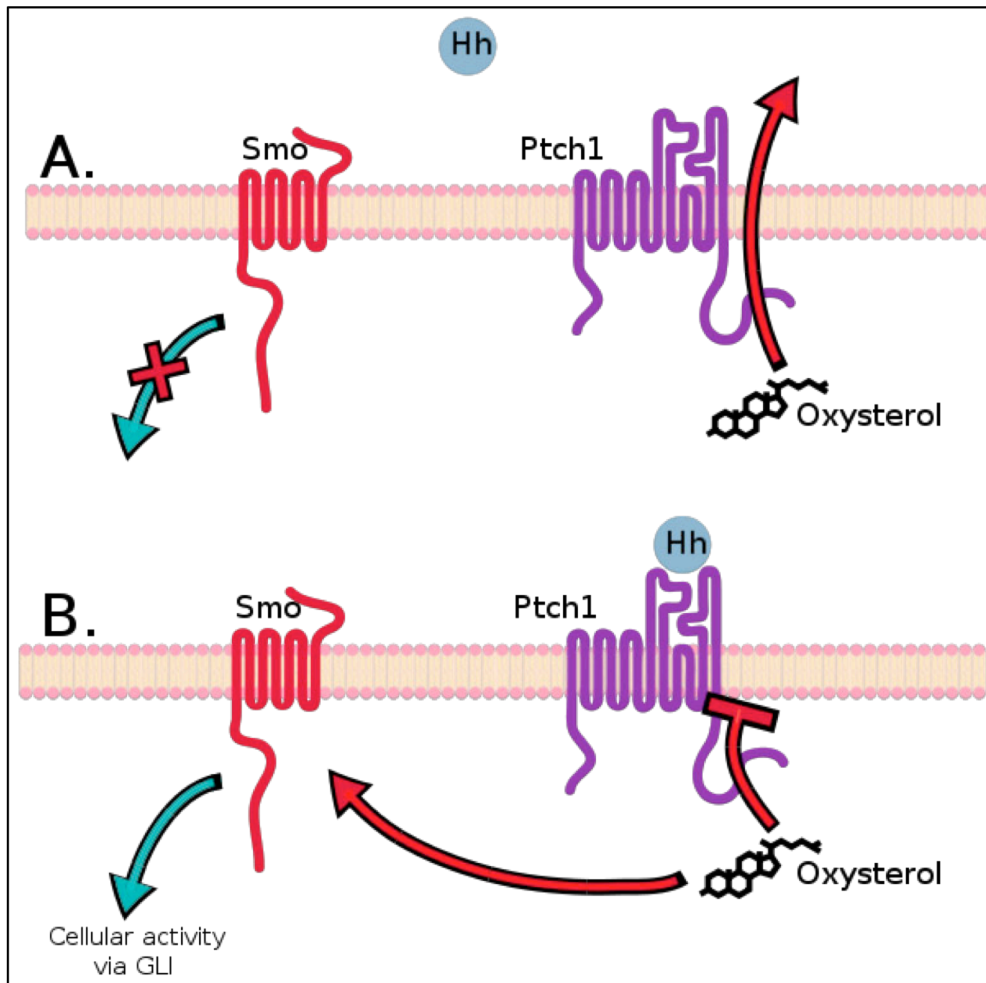


Fig. 5 | The current model of the mode of action of the Hedgehog receptor system.

Two key receptors involved in the Hedgehog pathway in normal adult cells are Smoothed (Smo), which initiates a signaling cascade, and Patched-1 (PTCH1), which inhibits this signaling mechanism potentially by preventing Smoothed from reaching the cell surface. **A:** In the absence of ligand, PTCH1 inhibits Smoothed (Smo), a downstream protein in the pathway. It has been suggested that Smo is regulated by a small molecule, the cellular localization of which is controlled by PTCH. PTCH1 has a sterol-sensing domain (SSD), which has been shown to be essential for suppression of Smo activity. **B:** Upon binding of Hedgehog to Patched-1 (PTCH1) receptor, it regulates Smo by removing oxysterols from Smo. PTCH acts like a sterol pump and removes oxysterols that have been created by 7-dehydrocholesterol reductase. Upon binding of an Hh protein or a mutation in the SSD of PTCH the pump is turned off allowing oxysterols to accumulate around Smo. This accumulation of sterols allows Smo to become active or stay on the membrane for a longer period of time. The binding of Shh relieves Smo inhibition, leading to activation of the Gli transcription factors (Image adapted from www.google.com).

Understanding of the vertebrate signal transduction operating downstream of Smo is far from complete, in part due to the relative lack of conservation of downstream targets of the Hedgehog signaling between *Drosophila* and vertebrates (Huangfu and Anderson, 2006; Osterlund and Kogerman, 2006). However, in both cases, the end-point target are transcription factors: Ci in *Drosophila*, and the glioblastoma (Gli) transcription factors in vertebrate –Gli1, Gli2, and Gli3– which mediate all aspects of Hedgehog signaling in

vertebrates (Hui et al., 1994). The major Glis to transduce the Hedgehog signal in the gut are Gli2 and Gli3.

1.2.3.3 Identifying Hedgehog Target Cells

It is essential to identify Hedgehog receiving cells to elucidate the role of Hedgehog signaling in any organ. Irrespective of the number of different target genes that have been identified, their regulation often differs in time or per organ. The expression pattern of two target genes – PTCH1 and Gli1 seems to be conserved particularly well throughout vertebrates. This expression pattern reflects the fact that Hedgehog signaling activity is seen in most if not all situations in vertebrates. However, a difference may exist for the sensitivity of the expression of PTCH1 and Gli1 for the range of the Hedgehog signal in the developing vertebrate gut. Both Shh and Ihh are expressed in the epithelium of the developing stomach and colon at E18.5. Expression of PTCH1 is high in a small zone very close to the Hedgehog expressing cells, whereas Gli1 is also expressed intensely in the smooth muscle layer at much greater distance (Ramalho-Santos et al., 2000).

1.2.3.4 Hedgehog signaling and homeostasis of the adult gut

There is very little information on the role of Hedgehog signaling in the adult small intestine. Low levels of Shh mRNA can be detected just above the Paneth cell position in the crypt. However when using gastric specimens as a positive control, expression levels are too low to be detected by immunohistochemistry (Van den Brink et al., 2002). Other reports confirmed, by quantitative PCR, this low expression of Shh in the small intestine and colon compared with the stomach (Suzuki et al., 2005). Batts et al., 2006 showed by in situ hybridization that Ihh is expressed at the crypt-villus junction with gradually diminishing expression towards the tip of the villus, and PTCH1 is expressed at low levels in the mesenchyme. Enterocytes on the upper half of the villus mainly express the Ihh protein (Jung et al., 1999). This partially overlapping expression pattern of mRNA and protein is typical for many enterocyte genes. An explanation for this is cells that have moved to the top of the villus often no longer transcribe mRNA from a given gene but still express the translated protein. The overall activity of the hedgehog pathway in intestinal homeostasis seems however modest as treatment of mice with cyclopamine, a potent inhibitor of Hh signaling, resulted in a modest 10% reduction of proliferation in the duodenum (Van den Brink et al., 2007).

While studying the role of PPAR β in the small intestinal homeostasis, our laboratory showed that Indian Hedgehog (Ihh) is important for Paneth cell differentiation. PPAR $\beta^{-/-}$ mice displayed approximately threefold induction of Ihh mRNA and protein. Treatment of wild-type mice with a PPAR β specific agonist strongly reduced Ihh mRNA levels, showing that PPAR β negatively regulates Ihh expression. Moreover, administration of the hedgehog pathway inhibitor cyclopamine increased the number of Paneth cells in the duodenum in both PPAR $\beta^{-/-}$ and wild-type mice, consistent with a role for Ihh in mediating inhibition of Paneth cell differentiation by PPAR β . In HT-29 colon cancer cells, upon treatment with recombinant Shh, expression of lysozyme, a Paneth cell marker was reduced, whereas treatment with cyclopamine increased lysozyme expression, thus recapitulating the effects of PPAR β *in-vitro*. These results agree with and corroborate the *in vivo* data and its interpretation that PPAR β inhibits Paneth cell differentiation at least in part by repressing Ihh expression. This is mediated by inhibiting the negative feed back loop operating between the mature paneth cells and the paneth cell precursors (Varnat et al., 2006). Figure 6 recapitulates the various signals at work in the small intestine and their cross talk.

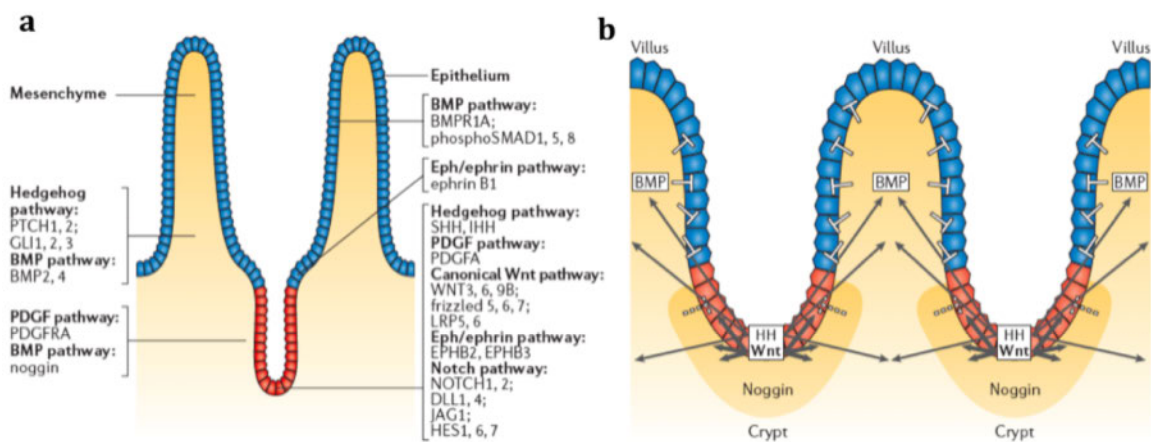


Fig. 6 | Signaling pathways in the small intestine. a | Components of the hedgehog (HH), platelet-derived growth factor (PDGF), bone morphogenetic protein (BMP), Wnt, Eph/ephrin and Notch pathways are expressed in different regions along the crypt–villus axis — some in the epithelium and some in the mesenchyme. **b** | A model of how the HH, BMP and Wnt signalling pathways combine to organize the pattern of villi and crypts or intervillus pockets. Epithelial cells in each crypt or intervillus pocket form a signalling centre, which functions as a source of long-range inhibition through the HH–BMP relay, and of short-range auto-activation through Wnt signalling. HH signalling activates the expression of BMP in the mesenchyme. BMP feeds back on the intestinal epithelium to repress Wnt signalling. The expression of the BMP inhibitor noggin in the neighbourhood of the crypts counteracts the effect of BMP so that Wnt activity is maintained in the crypt epithelium (Adapted from Crosnier et al., 2006).

2. The nuclear receptor superfamily

Nuclear receptors are transcription factors that are activated upon ligand binding. All nuclear receptors share some common features that include a DNA binding domain (DBD) and a ligand-binding domain (LBD). Upon ligand binding, the receptors are activated and these activated receptors then bind to specific response elements at the promoter of the target genes.

The nuclear receptors can bind DNA either as homodimers or heterodimers with RXR (retinoid X receptor) as the partner. A dual mode of action has been reported for these receptors: by default, they bind co-repressors that inhibit transcription of target genes, whereas in the presence of a ligand, they exchange co-repressor for co-activators to mediate transcriptional activation.

2.1. Classification

Nuclear receptors can be broadly classified into three categories:

1. Classical hormone receptors: these receptors recognise only few specific ligands and bind to them with a very high-affinity. Most of these are hormone binding receptors like thyroid hormone receptors (THR), glucocorticoid receptors, retinoic acid receptors (RAR), estrogen receptors (ERs), vitamin-D receptor (VDR), progesterone receptors (PR), mineralocorticoid and androgen receptors (AR).
2. Orphan receptors: these are the class of receptors which have a ligand binding domain but for which a specific ligand has not been identified so far. Some of the members of this group include SF-1, LRH-1, SHP, TLX, ROR- α , β , γ , GCNF, etc.
3. Adopted orphan receptors: these are receptors that have the ability to bind to a wide variety of molecules but with a relatively poor affinity. These receptors usually bind to molecules involved in metabolic pathways as substrates, intermediates or end products. Some examples are the pregnane X receptor (PXR), constitutive androstane receptor (CAR), farnesoid X receptor (FXR), liverX receptor (LXR) and peroxisome proliferator activated receptors (PPARs).

The latter group of receptors have gained importance due to their involvement as sensors in various metabolic pathways like fatty acid and cholesterol metabolism (reviewed in Desvergne et al., 2009). Many recent studies from various groups have elucidated their role in metabolism, cell proliferation and differentiation, cell survival and also tissue repair.

2.2 *The PPARs subfamily: a brief overview*

PPARs belong to the nuclear receptor family and can be classified into three isotypes: PPAR α , β/δ and γ . They were the first nuclear receptors identified as “sensors” rather than classic hormone receptors. They are nuclear, lipid-activable molecules that control a variety of genes in several pathways of lipid metabolism (Desvergne and Wahli, 1999). PPAR α (NR1C1) is highly expressed in tissue with high activity levels of lipid catabolism, e.g. liver, brown adipose tissue, skeletal and heart muscle. PPAR β (also called PPAR δ) is ubiquitously expressed. The PPAR γ gene gives rise to two isoforms, PPAR γ 1 and PPAR γ 2, the latter differing only by an additional stretch of 30 aminoacids in the N terminus. The expression of PPAR γ 2 remains restricted to adipose tissues whereas PPAR γ 1 is also detected in the colon, spleen, retina, hematopoietic cells and skeletal muscle.

All the three PPARs share a common modular structure containing the four major domains (Fig. 7) as follows:

- a. The A/B domain is the N-terminal region. This poorly structured N-terminal domain encompasses a weak ligand-independent transactivation domain in PPAR α and PPAR γ .
- b. The C-domain, which is the DNA binding domain, with its two zinc fingers is extremely well conserved and is the hallmark of the nuclear receptor family. It consists of 60-70 aminoacids and is responsible for the binding to the PPRE in the promoter region of the target genes.
- c. The D-domain or the hinge region connects the DBD to the LBD and is a poorly conserved region.
- d. The E/F domain is the ligand-binding domain and also helps in the dimerization. It carries the AF-2 site that is responsible for ligand dependent transcriptional activation. This ligand-binding cavity of PPAR is particularly large, a feature that likely explains the promiscuous behaviour of PPAR with respect to ligand binding.

In addition to the diverse substances grouped under their ability to provoke peroxisome proliferation, various fatty acids more particularly unsaturated fatty acids, and some eicosanoids mainly derived from arachidonic acid and linoleic acid, bind to the three PPARs with varying affinities. However, all the physiological ligands that could activate PPARs *in vivo* have most likely not been found yet.

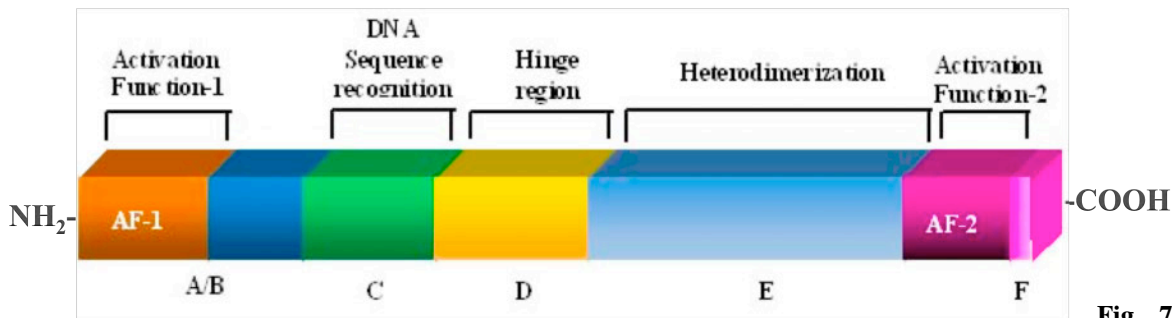


Fig. 7 |

Schematic representation of the structure of PPARs. PPAR proteins are organized in distinct domains that display specific function. The domain A/B contains the activating function 1 which is independent of the presence of ligand, the domain C is implicated in the DNA binding, the domain D is a hinge region and the domain E/F is implicated in the heterodimerization and ligand recognition, contains an activating function 2 which is dependent of the presence of ligand and is necessary for the heterodimerization with RXR.

PPARs bind to DNA as heterodimers with the retinoid X receptor (RXR), on PPAR response elements (PPRE) comprising direct repeats of two hexamers closely related to the sequence AGGTCA and separated by one nucleotide (DR-1 sequence). The classical model of PPAR-dependent transactivation proposes a two-step process (Fig. 8). In the absence of the ligand, the nuclear receptor dimer binds to a co-repressor protein, such as NCoR, that inhibits its transactivation properties. In the presence of the ligand, or due to an alternative pathway of activation such as phosphorylation, the co-repressor is released and PPAR recruits co-activators, most likely organized in large complexes (Surapureddi et al., 2002). The co-activators that can physically interact with PPARs include CBP, p300, and PGC-1.

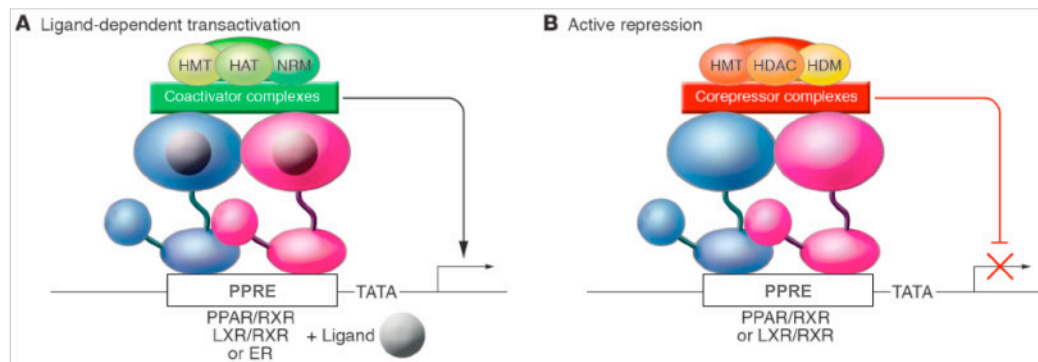


Fig. 8

Mechanisms of transcriptional activation and repression by heterodimeric nuclear receptors. (A) Ligand-dependent transactivation. The binding of natural or synthetic agonists causes the recruitment of coactivator complexes to the ligand-binding domain. In general, ligand-dependent transcription of nuclear receptor target genes is associated with the recruitment of numerous coactivator complexes that act in a combinatorial or sequential manner. These complexes are associated with a number of enzymatic activities, including histone acetyltransferase (HAT), histone methyltransferase (HMT), and nucleosome remodeling (NRM) activities. Structurally distinct ligands may alter the pattern of recruitment of these factors, resulting in altered patterns of gene activation. **(B) Active repression.** A subset of heterodimeric nuclear receptors, including PPAR/RXR and LXR/RXR heterodimers, are capable of binding to REs in the absence of ligand and recruiting corepressor complexes that actively repress transcription. A number of corepressor complexes are associated with histone deacetylase (HDAC) activities, as well as histone methyltransferase and nucleosome remodeling activities that are generally distinct from those associated with coactivator complexes. HDM, histone demethylase (Adapted from Glass, 2006).

Concerning the functional activities, PPAR α and PPAR γ perform opposing functions with respect to lipid metabolism. Most of PPAR α activity is linked to its ability to promote fatty acid oxidation, a vital process during fasting, and to govern many aspects of lipoprotein metabolism (Duval et al., 2007). In contrast, PPAR γ was first identified as a key regulator of adipogenesis, and necessary for intra-cellular lipid storage. Fibrates on the one hand and thiazolidinediones on the other hand are hypolipidemic and hypoglycemic drugs that act through their binding to PPAR α and PPAR γ respectively, making these two subtypes highly attractive as targets of drugs designed for metabolic disorders such as the type 2 diabetes. However, their therapeutic potentials go beyond the lipid and glucose metabolism as many research groups are now exploring their efficacious activity as anti-inflammatory regulators, particularly in the context of atherosclerosis and cardiovascular diseases (Zandbergen and Plutzky 2007; Széles et al., 2007). Due to the lack of appropriate tools and guided hypothesis for its functions, PPAR β was getting much less attention than the two other isotypes. However, identification of anti-obesity properties of PPAR β and conflicting reports so far on the role of PPAR β in the progression or attenuation of colon cancers has quite stimulated the field.

2.2.1 PPAR β/δ

2.2.1.1 Structural properties

Several structures have been determined for the ligand-binding domain of the human PPAR β (Reviewed in Zoete et al., 2007). The overall structure is common to other nuclear receptors, with a bundle of 13 helices and a small four-stranded β -sheet. PPARs accommodate an extra helix (H2') and are characterized by a very large Y-shaped cavity. A particularity of the PPAR β pocket is the narrowness of one of the Y arm, which thus cannot accommodate bulky polar heads (Xu et al., 2001). Interestingly, the structure of the PPAR β ligand-binding domain in the absence of ligand is not well defined and rather corresponds to equilibrium of different conformations, among which those favoring co-activator recruitment.

2.2.1.2 Ligand specificity

Natural ligands: Many unsaturated fatty acids can bind to PPAR β in a pattern closely resembling the binding to PPAR α (Desvergne and Wahli, 1999). The very large density lipoproteins (VLDL), through release of their triglycerides, are proposed to specifically deliver ligands to PPAR β in the macrophages (Chawla et al., 2003; Ziouzenkova and Plutzky, 2004). Arachidonic acid derivatives, and more particularly prostacyclin (PGI₂) formed upon cyclooxygenase 2 (COX-2) activation are strong candidates (Lim et al., 1999), and the stable synthetic analog carbaprostacyclin exhibits some binding properties (Forman et al., 1997). However, this activation seems to be tissue and/or context dependent. Other prostaglandins have also been diversely proposed as PPAR β ligands (Yu et al., 1995). Metabolites derivatives obtained through the 12/15-lipoxygenase activity, such as 9-HODE, 13-HODE, 12-HETE and 15-HETE, are low affinity PPAR γ activators (Nagy et al., 1998). They also activated PPAR β however with some intriguing results since 13-s HODE is reported to be an inhibitor of PPAR β in colon epithelial cells (Shureiqi et al., 2003), but an agonist in preadipocytes (Coleman et al., 2007). Finally, a recent report suggests that retinoic acid (RA) would be a ligand destined for either PPAR β

or RARs, depending on the relative expression of CRABP_{II} (delivering RA to RARs) and FABP5 (delivering RA to PPAR β) (Schug et al., 2007).

Synthetic ligands: Following the very first synthetic compound called L165041, which can give some PPAR γ activation at high doses, the most often used ligand in fundamental research is the glaxo compound GW501516. Presently, PPAR β specific antagonist–GSK0660 is also available commercially (Shearer et al., 2008).

2.2.1.3 PPAR β : Functional properties

2.2.1.3.1 PPAR β in metabolism

The most significant outcome of PPAR β activation concerns its anti-obesity effect. Indeed, PPAR β is implicated in energy consumption in peripheral tissue by controlling β -oxidation and energy uncoupling. The skeletal muscle is considered to be the prime site where PPAR β regulates genes mainly involved in β -oxidation and uncoupling such as FABP3, lipoprotein lipase, carnitine-*o*-palmitoyl transferase (CPT-1), or UCP-3, among others (Bedu et al., 2005). Consistently, *in-vivo* over-expression of PPAR β in skeletal muscle provokes a shift toward more oxidative fibres and promotes a general decrease of body fat content (Luquet et al., 2003). Quite similar results were obtained using a constitutively active PPAR β -VP16 fusion protein expressed under the control of the α -actin promoter, which increased the oxidative type I fibres in the muscle of PPAR β -VP16 transgenic mice. Importantly, these mice remained lean and insulin-sensitive on a high fat diet (Wang et al., 2004). A mirror image was obtained when specifically deleting PPAR β in skeletal muscles, with lower oxidative activity of the muscle fibres and an increased body fat mass leading to insulin resistance (Schuler et al., 2006). The fact that PPAR β expression increases upon exercise (Russell et al., 2005) suggests that PPAR β could be implicated in adaptive response of skeletal muscle to physical exercise (Reviewed in Grimaldi, 2007).

In parallel to acting on lipid metabolism, a role for PPAR β in regulating systemic lipid transport through lipoproteins adds to its potential therapeutic effects. In obese rhesus monkeys, an animal model for human obesity and associated metabolic disorders, as well

as in diabetic db/db mice, a selective PPAR β agonist caused a beneficial increase in serum HDL cholesterol and a decrease in small-dense LDL (Leibowitz et al., 2000; Oliver et al., 2001). Conversely, PPAR β deficient mice exhibit LDL hypertriglyceremia, due to increased hepatic production of VLDL and decreased LPL-mediated catabolism (Akiyama et al., 2004). One important mechanism for these effects is an increase in reverse cholesterol transport via increased expression of ABCA1 (Oliver et al., 2001), as well as a reduced cholesterol absorption in mutant intestine that is associated with a decrease in Niemann-Pick C1 like 1 (NPC1L1) protein (Van der Veen et al., 2005).

In the context of atherosclerosis, the role of PPAR β in macrophages remains difficult to explore as the three PPAR isotypes are coexpressed and have significant overlapping activities, particularly with respect to anti-inflammation properties. In macrophages, a direct interaction of PPAR β with BCL6 or p65 negatively regulates NF- κ B driven promoters. However, this mechanism is likely tissue- or context-dependent (Trifilieff et al., 2003; Kharroubi et al., 2006). Other studies of PPAR β in macrophages have focused on its capacity to act as a VLDL sensor, to which it responds by increasing carnitine synthesis and lipase activation.

2.2.1.3.2 PPAR β in cell fate

2.2.1.3.2.1 *The anti-apoptotic activity of PPAR β*

Apoptotic cell death can take place by two major mechanisms: either through the activation of the death receptor pathways by the binding of TNF-or Fas-Ligand (Fas-L), or through activation of the mitochondrial pathway through the Bcl-2 family of proteins. Cell death through both of these major apoptotic mechanisms can be prevented by the activation of the Akt1 pathway. Phosphorylation of Akt1 at threonine 308 (T308) by the 3-phosphoinositide-dependent kinase-1 (PDK1) and of serine 473 (S473) by the integrin-linked kinase (ILK) (Nicholson and Anderson, 2002) or other kinases is necessary for the maximal Akt 1 activity.

In skin wound healing, PPAR β protects keratinocytes from anoikis and growth factor deprivation-induced apoptosis through the activation of Akt1 pathway (Di-poï et al, 2002). In this context, the Akt1 phosphorylates Bad, the proapoptotic member of the Bcl-2

family, thus preventing cytochrome c release which can trigger the activation of the initiator caspase-9. PPAR β exerts regulation of Akt1 phosphorylation through transcriptional upregulation of ILK and PDK1, and repression of PTEN (phosphatase and tensin homolog deleted on chromosome 10). Keratinocytes derived from PPAR $\beta^{+/+}$ or PPAR $\beta^{-/-}$ showed no difference in the expression of Akt1. However, the expression of ILK and PDK1 was reduced in the PPAR $\beta^{-/-}$ cells as compared to their wt counterparts whereas the expression of PTEN was 2-fold higher in PPAR $\beta^{-/-}$ cells. Consistent with this decreased PDK1/ILK protein levels in PPAR $\beta^{-/-}$ cells, is the reduced phosphorylation of Akt1 at T308 and S473 in PPAR $\beta^{-/-}$ cells. Further, treatment of PPAR $\beta^{+/+}$ keratinocytes with the PPAR β ligand L-165041 resulted in an increase of both PDK1 and ILK and a decrease in PTEN expression, indicating that it is a direct PPAR β target that is further strengthened by the fact that it was unaffected by protein synthesis inhibitor cycloheximide (CH). However, in the case of PTEN regulation it turned out to be an indirect regulation by PPAR β . These results clearly show that in keratinocytes, PPAR β controls cell fate decision by directly controlling apoptosis through the Akt1 pathway (Fig. 9).

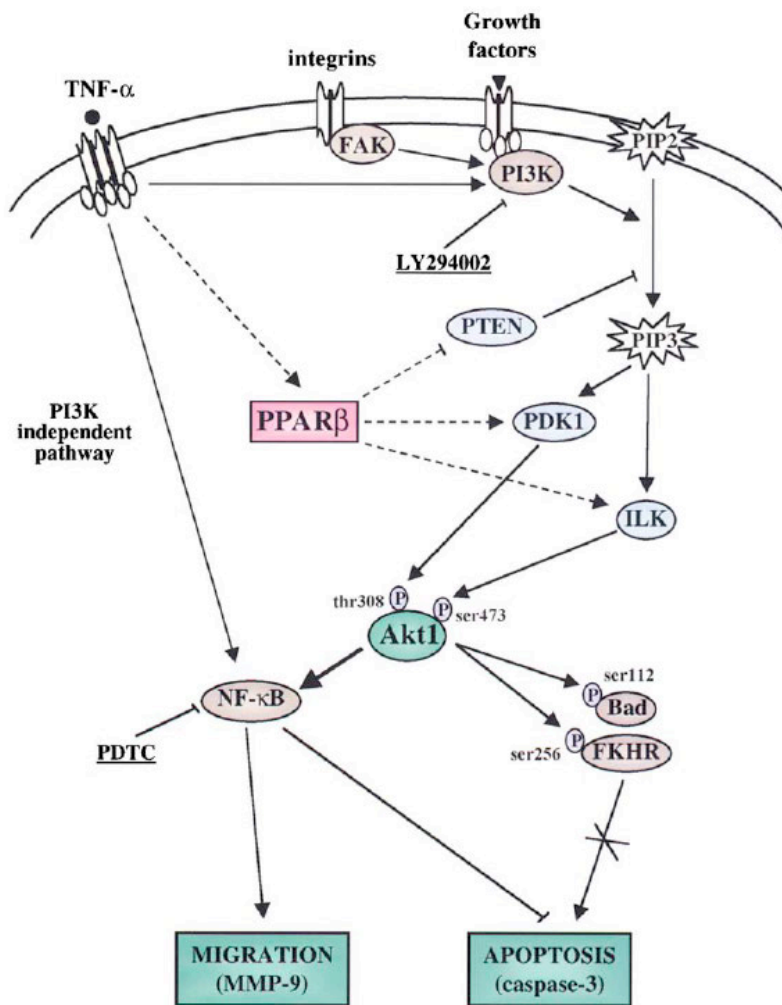


Fig. 9 | Model for the anti-apoptotic role of PPAR β in keratinocytes. Following stimulation by TNF- α , PPAR β directly upregulates ILK and PDK1 and downregulates PTEN, leading to the activation of Akt1 in a PI3K-dependent manner. In response to this activation, the activity of several of its targets, including Bad, FKHR, and NF- κ B, is modified, leading to the inhibition of apoptosis and changes in cell adhesion/migration. Dotted lines represent a modification at the transcriptional level, and continuous lines represent a modification of the protein activity. Inhibitors of PI3K (LY294002) and NF- κ B (PDTC) are indicated (Adapted from Di-Poi et al., 2002).

2.2.1.3.2.2 PPAR β in cell differentiation

2.2.1.3.2.2.1 In the placenta: Giant cell differentiation

Early evidence for the role of PPAR β in development came from the observation that null mutation of PPAR β showed embryonic lethality at E9.5 to E10.5, with the trophoblast giant cell layer being the most affected. Interestingly, treatment of a rat trophoblast cell line (RCHO cells) with PPAR β ligand markedly accelerated giant cell

differentiation via increased expression of PDK1 and ILK, subsequent phosphorylation of Akt, and Id2 inhibition of expression. The links between PPAR β activity in giant cells and its role on Akt activity is further strengthened by the remarkable pattern of phospho-Akt expression *in-vivo* at E 9.5, specifically in the nucleus of the giant cells. In addition to this main pathway, PPAR β also induced giant cell differentiation via increased expression of I-mfa, an inhibitor of Mash-2 activity. Thus, PPAR β is a major regulator of secondary giant cell differentiation, which plays a major role in the establishment of the placental structure and has important endocrine function (Nadra et al., 2006).

2.2.1.3.2.2.2 *In the skin: Keratinocyte differentiation*

Inflammatory signals from skin wounding results in generation of TNF- α and IFN- γ . These inflammatory signals activate the stress-associated signaling pathway and also further stimulate PPAR β expression via an AP-1 site in its promoter. These signals also promote the synthesis of a PPAR β ligand that is so far unidentified. The resulting increase in PPAR β transcriptional activity strongly accelerates the differentiation of keratinocytes that increases their resistance to apoptotic signals. (Tan et al., 2001). Also PPAR β promotes hair follicle morphogenesis by regulating the balance between the proliferation and apoptosis required for this process by the anti-apoptotic action mediated via the Akt/PKB pathway (Di-poi et al., 2005).

2.2.1.3.2.2.3 *In the Central nervous system: neuronal and oligodendrocyte differentiation*

A role for PPAR β in neuronal differentiation is suggested due to the high level of expression of PPAR β in the CNS (Woods et al., 2003; Moreno et al., 2004; Cullingford et al., 1998) and in neurons in culture (Di Loreto et al., 2006; Cimini et al., 2005). In the primary glial culture as well as in enriched oligodendrocyte culture, PPAR β agonist strongly accelerates the differentiation of the oligodendrocytes, increasing both the number of oligodendrocytes and the size of the membrane sheets they produce (Saluja et al., 2001).

2.2.1.3.2.2.4 *In adipocyte differentiation*

The implication of PPAR β in adipocyte differentiation is more complex. PPAR β is highly expressed in the preadipocytes where it mediates long-chain fatty acid effects on the expression of adipose-related genes. The reduced fat mass observed in some PPAR β null mice is consistent with a role in adipogenesis (Barak et al., 2002; Peters et al., 2000). In contrast, the adipose tissue specific deletion of PPAR β at a later stage did not affect adiposity of the mice (Barak et al., 2002). Taking into account some contradictory observations in cell in culture (Brun R et al., 1996; Holst et al., 2003; Matsusue et al., 2004), as well as *in-vivo* (Akiyama et al., 2004; Wang et al., 2003), the role of PPAR β in adipogenesis seems strongly intertwined with its general metabolic activity rather than specifically acting on the differentiation program.

2.2.1.3.2.3 *PPAR β in cell proliferation*

The influence of PPAR β on proliferation is complex. As mentioned above, PPAR β promotes terminal differentiation and inhibits proliferation of keratinocytes, at least in part through down-regulation of cyclin A (Tan et al, 2001) or through increased ubiquitination of PKCa (Kim et al, 2005). Assays performed in a variety of cell lines did not demonstrate any pro-proliferation activity of a PPAR β agonist (Hollingshead et al., 2007). In contrast, PPAR β can promote proliferation of hepatic stellate cells (Hellemans et al., 2003) and vascular smooth muscle cells (Zhang et al., 2002). Thus a direct anti- or pro- proliferative activity of PPAR β agonist has yet to be further studied. Attention must be paid to the fact that a higher degree of cell survival rather than a direct proliferation activity may account for an increased cell population. Thus, the anti-apoptotic role of PPAR β might be essential to be taken into consideration in some experimental settings aimed at evaluating cell proliferation.

2.2.1.4 *PPAR β in the intestine*

2.2.1.4.1 *Expression*

PPAR β is ubiquitously expressed in the body. It has been reported that of the three PPAR isotypes, PPAR β is the major isotype expressed in the gastrointestinal tract (**Fig.10**; Escher et al., 2001). Also it has been shown that PPAR β is highly expressed at the bottom of the crypt and the expression reduces towards the tip of the villi (Varnat et al., 2006).

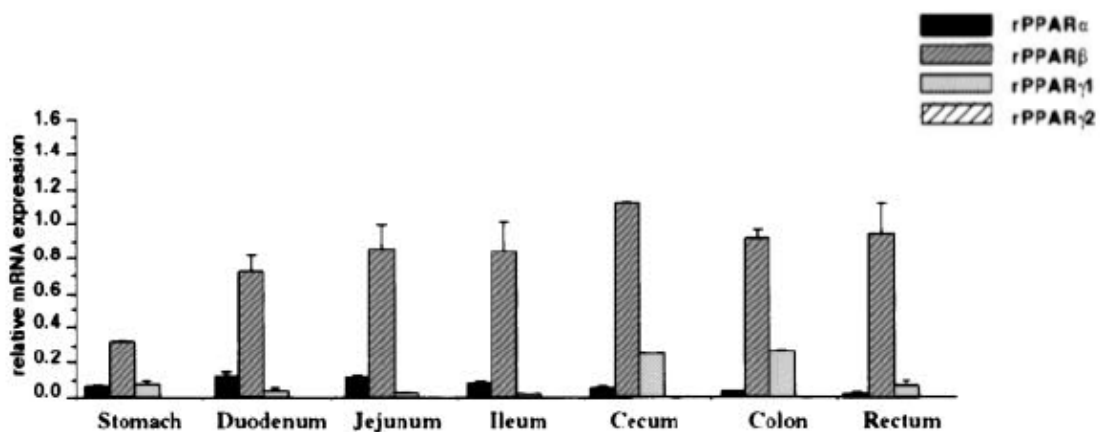


Fig. 10 | Comparative analysis of PPAR α , PPAR β , and PPAR γ expression in the gastrointestinal tract. Histograms show quantifications (in relative values) of PPAR mRNA levels \pm SD, normalized to L27 mRNA expression, derived from RNase protection assays, [n=3](Adapted from Escher et al., 2001).

2.2.1.4.2 *PPAR β and paneth cell differentiation*

In the gut, PPAR β is involved in the differentiation of the Paneth cells, but does not significantly affect the three other cell types. Mature Paneth cells signal to their precursors through the *Ihh* to negatively regulate their differentiation. PPAR β acts by inhibiting the negative feed back loop operating between the mature Paneth cells and the paneth cell precursors (Varnat et al., 2006). The intensity of the *Ihh* signal received by the precursor cells determines the number of mature Paneth cells in the crypt. High levels of *Ihh* lead to the suppression of the maturation of the PATCH-1-positive cells, limiting them in their precursor state. On the contrary, weak *Ihh* signal inhibits the positive feedback loop on PATCH-1 expression stimulating the terminal differentiation of precursor cells to fully mature Paneth cells. Although the total number of mature Paneth cells is reduced in

the PPAR β -null mice, the levels of Ihh are particularly high, thus falsely signaling the precursor cells to delay differentiation (Fig. 11).

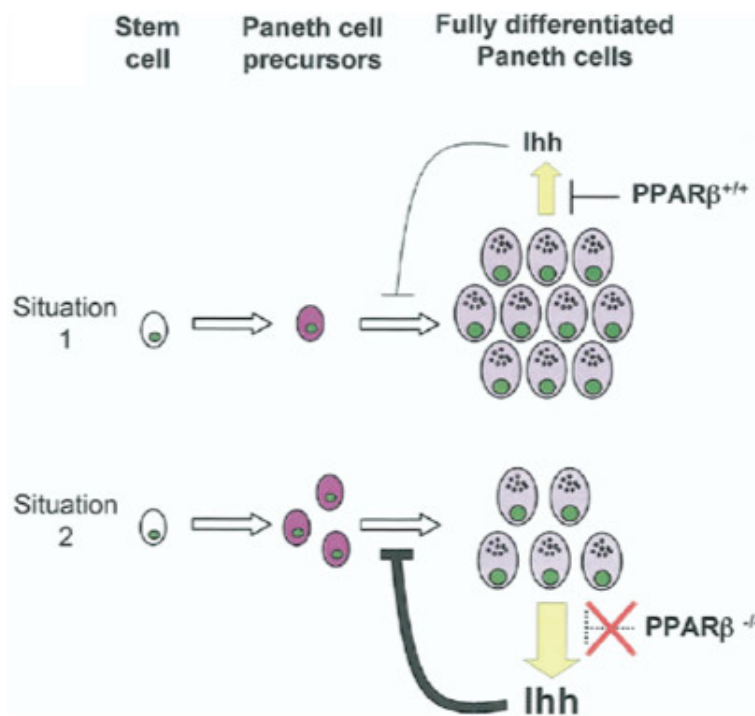


Fig. 11 | Model for PPAR β action on the level of Ihh, resulting in the alteration of Paneth cell homeostasis. PPAR β controls the number of Paneth cells by regulating the differentiation of their precursors; for details see text (Adapted from Varnat et al., 2006).

2.2.1.4.3 A role for PPAR β in colorectal cancer

PPAR β is a target of Wnt signaling and is also involved in the progression of colorectal cancer (He et al., 1999). There are conflicting reports so far on the role of PPAR β in the progression or attenuation of colon cancers. Inactivation of Apc gene or treatment with azoxymethane has been shown to increase the levels of PPAR β in colorectal tumors (He et al., 1999; Gupta et al., 2000). This increased levels of PPAR β in colorectal tumors compared to the normal mucosa is consistent with the hypothesis that Apc suppresses activity of β -catenin /TCF-4 transcription of target genes including PPAR β , cyclin D1 (He et al., 1999). A decrease in tumor formation was observed when the PPAR β -null HCT cells were xenografted in nude mice (Park et al., 2001). In addition, it has been shown that treatment of Apc^{min/+} mice with PPAR β -specific ligand (GW501516) leads to the increase in the number and size of the small intestinal adenomas

(Gupta et al., 2004). In summary, these studies suggest that loss of Apc leads to the increase in expression of PPAR β through β -catenin /TCF-4 transcriptional pathway, thus promoting tumorigenesis. On the other hand, several studies show conflicting results. Comparative studies on the normal colonic mucosa and adenomas from Apc^{min/+} mice as well as in humans between normal and cancer tissue show decrease in the expression of PPAR β (Chen et al., 2004). This is consistent with the observations in mice with targeted deletion of Apc in intestine, that show decrease in PPAR β mRNA and protein levels and increase in c-myc levels along with accumulation of β -catenin (Reed et al., 2004). Since then, a certain numbers of papers have continued to feed the controversy but do not give clues on the reasons for such discrepancies.

However, a particular attention has recently been brought on the angiogenesis that accompanies tumor formation. In addition to the role of Akt signaling in regulating angiogenesis (Shiojima and Walsh, 2002), PPAR β upregulates VEGF expression (Wang et al., 2006; Piqueras et al., 2007). It is now further proposed that PPAR β plays an essential role for the formation of functional tumor microvessels (Müller-Brüsselbach et al., 2007).

3. Irradiation: a medical concern and a tool for exploring cell and tissue repair

After surgery, radiotherapy is one of the most used therapeutic actions for cancers, especially for those that are localized and have not metastasized yet. Ionizing radiations have variable success rates depending on the type of solid tumor involved. For e.g., lymphomas and seminomas are quite responsive to low doses of irradiation where as some like melanoma and glioblastoma are very radioresistant and show higher resistance even after high doses (Jung and Dritschilo, 1996). Failures in patients treated with ionizing radiation have been correlated to various features attributed to distant metastases as well as to the primary site. Indeed, precise localisation, size, and inadequate vascular supply (hypoxia) of the tumor can all play a role in the non-responsiveness to ionizing radiation. However, the most important factors that contribute to radiation resistance are cellular and genetic factors such as differential tissue-specific gene expression (e.g., p53, ataxia telangiectasia mutated (ATM) status (Peters et al., 1982; Deacon et al., 1984). These observations emphasize the need to well understand the molecular responses to radiation and their modulation, as discussed below.

3.1 Signal transduction and cellular radiation responses

Numerous radiobiological studies have proven the activation of existing cellular response pathways of the mammalian cells in response to ionizing radiation over a wide dose ranges. These pathways can either activate the cytoprotective or the cytotoxic responses thereby mediating the cell survival or the cell death, respectively. The mitogen-activated protein kinase (MAPK) and the phosphatidyl inositol-3 phosphate kinase (PI3 kinase) mediate the cytoprotective responses. They activate the cellular biosynthetic machinery and may also act by stimulating the cellular proliferation if the cell is able to repair the radiation-induced damage. The most direct cytotoxic response involves Jun N-terminal kinase (JNK no known as MAPK8) and results in cellular death due to apoptosis and/or some other form of cell death (reviewed in Schmidt-Ullrich et al., 2000).

The production of radiation-induced radicals forms the primary ionizing events and is the immediate response of cells to irradiation. The primary radical generated $\bullet\text{OH}$ is

short lived with diffusion range about 4nm before reacting (Roots and Okada, 1972). Cellular Reactive Oxygen Species (ROS) and Reactive Nitrogen Species (RNS) play a role in the cytoplasmic amplification mechanisms that are responsive to relatively low radiation doses. Figure 12 summarizes the potential sources and sensors of these ROS/RNS. O_2^- and H_2O_2 form the secondary ROS molecules and H_2O_2 can react with cellular metal ions to produce additional $\bullet OH$.

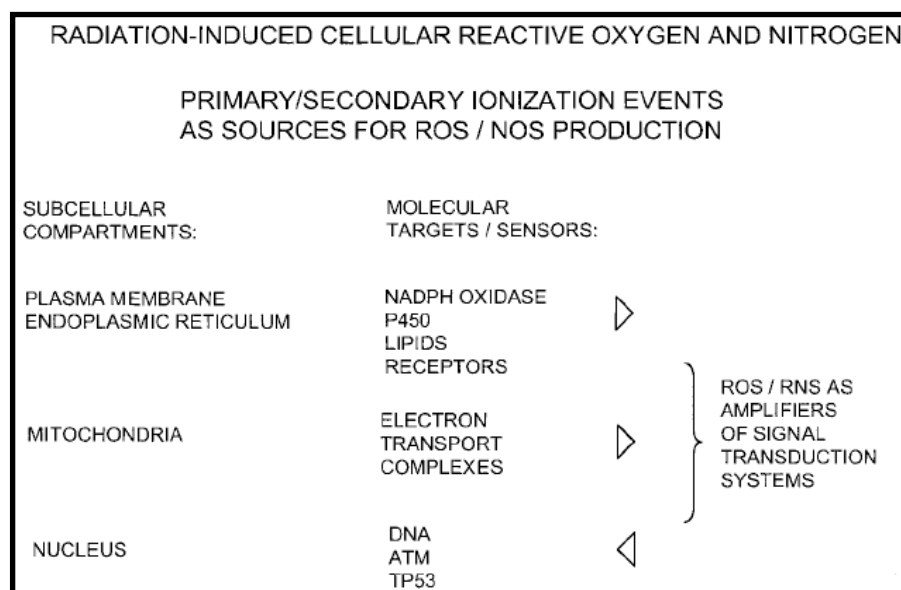


Fig. 12 | Radiation-induced cellular reactive oxygen/ nitrogen species (ROS/ NOS), sources and targets. Targets and sensors of radiation-induced ROS/RNS are localized in subcellular compartments including membranes, mitochondria and the nucleus. In each of these compartments, sensors and amplifiers of primary and secondary radicals are in proximity. While the cellular amplification systems enhance signal transduction responses, the effector molecules of these pathways feed into nuclear DNA damage recognition and repair functions (Adapted from Schmidt-Ullrich et al., 2000).

Some of these ROS/RNS remain sufficiently stable to diffuse significant distances within cells, e.g H_2O_2 , nitric oxide and peroxynitrite, and contribute to the subsequent cellular damages. First, they are membrane permeant and can also change the membrane structure via lipid peroxidation (Berroud et al., 1996; Ritov et al., 1996). Second, they can interact with protein. A particularly interesting example is the interconversion of reduced and oxidized Cys, which change a protein conformation and therefore its activity, as it has been shown for Tyr phosphatase 1B, whose inhibition could lead to enhanced phosphorylation and activation of target proteins, such as EGFR (Bae et al., 1997; Lee et al., 1998).

Finally, exposure to ionizing radiation induces the formation of DNA double-strand breaks, which can provoke a P53-mediated response. The tumor suppressor TP53

and the protein mutated in ataxia telangiectasia cells, ATM, were identified to function as sensors of DNA damage (Morgan and Kastan, 1997; Giaccia and Kastan, 1998). They regulate cell cycle checkpoints, apoptosis and DNA repair (Reviewed in Schmidt-Ullrich, et al., 2000). They are known to activate signaling systems, to initiate damage repair or responses of cell death or apoptosis. In general, the cells deficient in TP53 or carrying a TP53 mutation are more radioresistant than cells expressing wild-type TP53 (Lee and Bernstein, 1993). However, the effect of mutant TP53 on radiosensitivity depends on the specific mutant and the cell type involved. In cells expressing wild-type TP53, irradiation results in cell cycle arrest mainly at the G1-phase checkpoint via transcriptional activation of CDKN1A, a potent inhibitor of CDKs, (Fig. 13; Canman et al., 1994; Kuerbitz et al., 1992). This cell cycle regulation is thus significantly linked to the vital cellular processes of biosynthesis, such as DNA repair, transcriptional regulation, the initiation of cell proliferation, or cell death and apoptosis. The complex interplay between such response systems reflects the extent of surveillance mechanism cells possess to maintain the integrity of the nuclear material against genotoxic stress.

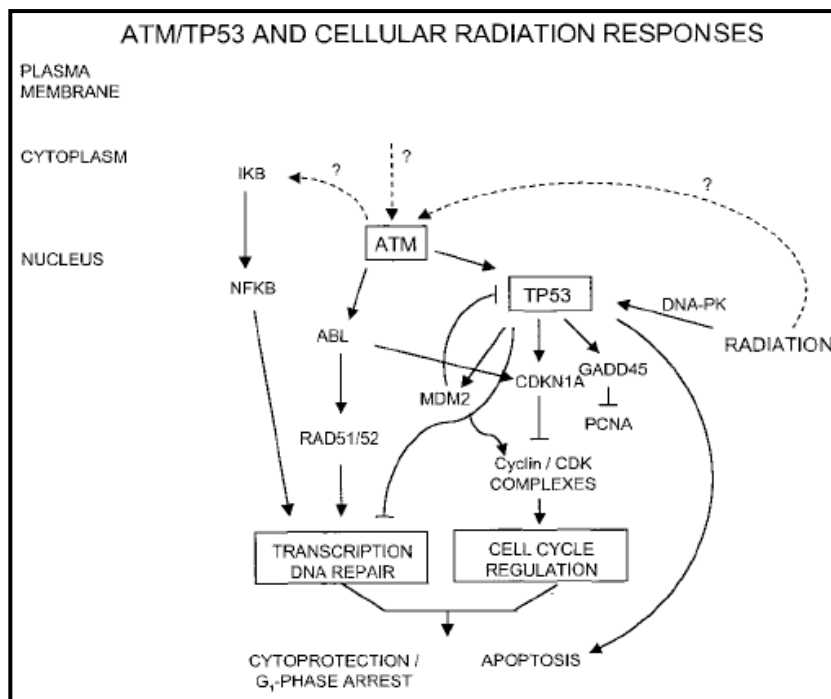


Fig. 13 | ATM/ TP53 and cellular radiation responses. The nuclear sensor proteins of DNA damage, TP53 and ATM, play a central role in modulating cellular responses that may directly or indirectly affect apoptosis or DNA repair and survival. Radiation may activate TP53 directly through DNA-PK or indirectly through ATM. In addition, ATM may directly affect repair through ABL and RAD51/52. Alternatively, ATM may regulate transcription through the cytoplasmic IKB and NFKB. The modulation of cell cycle progression at the G1/S-phase checkpoint by TP53 is mediated by a complex network of positive and negative regulators including MDM2, CDKN1A, GADD45 and PCNA. Arrows and blocks represent stimulatory and inhibitory signals, respectively (Adapted from Schmidt-Ullrich et al., 2000).

3.2 *Irradiation and the intestine*

Treatment for abdominal and pelvic cancers by radiotherapy is one of the main source for patients to get exposed to irradiation and may induce adverse effects on the intestine, first described by Walsh, 1897. Walsh concluded that radiation caused a direct inflammation of the gastrointestinal mucous membranes. In studies on domestic animals, X-ray irradiation induced injuries of the small intestine were dose-dependent as reported by Krause and Ziegler (1906-1907). Proliferation of the intestinal bacteria was believed to be the cause of the observed harmful effects. Contrary to this, delayed changes caused by X-irradiation was observed by Regaud et al., 1912 in dog small intestine. A mode of acute radiation death, the so-called GI-syndrome was described in 1956 by Quastler, which had a well-defined time course using dose ranging from 10 to 100 Gy of X-ray irradiation. The high sensitivity of the GI tract to X-irradiation makes it a target for complications in accidentally exposed persons and during the course of treatments for cancers by radiotherapy. Indeed, as abdomino-pelvic cancers increase with the aging of the population and lead to increased utilization of radiotherapy, the requirement of a better and thorough knowledge of the effects of radiation on the cells and organism as a whole has to be emphasized.

On clinical levels, radiation-induced intestinal damages are well documented and can be caused by various types of irradiation (X-ray, neutron, gamma). Ionizing radiation effects on the GI tract can be categorized into two main groups: early effects that occur at relatively low doses equivalent to 1 Gy and the GI syndrome that occur at high doses of radiation doses (more than 10Gy). The effects of ionizing radiation on the gut can be followed in a time dependent manner and can be categorized as initial phase (1-3 days after exposure) followed by the acute, subacute and the late phases of the illness (Berthrong and Fajardo 1981; Anno et al., 1989; Rubio and Jalnas, 1996).

The acute phase is the early response of the radiation-induced stress and is characterized by the damage to the intestinal epithelium (depletion of epithelium or complete denuding of epithelial layer). This loss of integrity of the intestinal epithelium is the usual major effect on the intestine followed by the symptoms of nausea, vomiting, diarrhoea, loss of electrolytes and fluids, haemorrhage, anorexia, bacterial infection and endotoxemia. Alteration in the balance of electrolytes and fluids may be responsible directly for the effect on changes in cellular transport processes (Young, 1987). Ionizing

radiation mediated loss of intestinal epithelia leads to bacterial infection and endotoxemia and the bacterial products released thereafter can result in altered cellular communications.

Subacute and late responses of the ionizing radiation-induced GI damage result in radiation enteritis or radiation-induced enteropathy. Abdominal pain, gut perforation, haemorrhage, gut obstruction, diarrhea, malabsorption and dysmotility are the most frequent clinical consequences. The late effects of ionizing radiation are seen after almost 2 months after treatment and can be seen to last until a year later. Severe collagen accumulation results from aggregation of scattered thin fibrils in the submucosa from the second month after exposure to irradiation. In addition, the other compartments like the connective tissue and vascular tissue respond slowly to these radiation effects and contribute to the appearance of fibrosis (Langberg et al., 1996).

However, the cause of fibrosis remains poorly understood. The possible mechanisms may include direct effects of radiation on collagen or other constituents of the extracellular matrix, modified production or degradation of extracellular materials, direct or indirect effects of radiation to the vascular and/or parenchymal cell constituents, consequences of non-specific inflammatory or autoimmune processes, as reviewed by (Hauer-Jensen, 1990) and (Followill et al., 1993; Somosy et al., 2002).

3.2.1. Effects of radiation on the small intestinal cell types

Experimentally, radiation can be a very useful tool to induce damage to the tissues (Potten, 2004), thus allowing studying how the cells and tissues recognize the occurrence of damages and thus their repair response. Thus, radiation is an ideal cytotoxic agent for such studies. Using mouse models of total body irradiation, it was shown that in the first three to six hours after a moderate irradiation, the low levels of spontaneous p53-dependent apoptosis in the intestinal crypt dramatically increase. This cell death associated to a cell cycle arrest lead to shrinkage of the villi and loss of protective barrier observed 18 to 24 hours post-irradiation. Release from mitotic arrest occurs at about 36 hours and is associated with a rapid increase in the proliferative activity. At doses < 15Gy, surviving progenitor cells lead to crypt recovery identified at 3.5 days post-irradiation as typical hyperplastic regenerative crypts that exceed the size of control crypts by more than 2 folds. Large regenerating crypts split or bud to generate new crypts, until the intestinal mucosa regains a normal architecture at about 2 weeks after irradiation (Potten, 2004).

3.2.1.1 *The role of the intestinal adult epithelial stem cells*

Tissue homeostasis and regeneration upon injury are the key processes presumed to be under the control of adult tissue stem cells. Several studies in mice showed that Lgr5 (Barker et al., 2007), CD133/Prominin 1 (Zhu et al., 2009) and Bmi-1 (Sangiorgi and Capecchi, 2008) expressing cells at or near crypt base are intestinal stem cells (ISCs). The cells that exhibit the properties of ISCs are seen to be located in two different positions: the columnar cells at the crypt base called Crypt Base Columnar cells (CBCs) and some +4 position cells just above the Paneth cells. Work from several groups has identified that apoptosis in these cells is mainly responsible for the acute intestinal damage and rapid onset of gastrointestinal (GI) syndrome and death using a whole body radiation model (Potten, 2004; Ch'ang et al., 2005; Qiu et al., 2008).

3.2.1.2 *Radiation-induced apoptosis*

Many early reports show that damages to stem cells are an early response to irradiation (Potten et al., 1983, 1994). These damages to stem cells provoke apoptosis and mitotic inhibition (G2 block) (Potten et al., 1983; Carr et al., 1996). Mitotic inhibition is observed as early as 30min post irradiation, and lasts for the next 8-20 h (Potten et al., 1983). Soon after irradiation, there is initiation of apoptotic processes, and apoptotic cells appear after 2-3 h post irradiation that are visible by morphological analysis of the fine ultra structural features (Ijiri and Potten, 1984; Potten, 1992; Merritt et al., 1995; Arai et al., 1996).

Radiation induced apoptosis is one of the key events responsible for the acute intestinal damage and rapid onset of gastrointestinal syndrome (Potten 2004). Studies on mice have shown that as early as within 3- 6 h after gamma-irradiation, numerous apoptotic cells are observed in the region towards the bottom of the small intestinal crypts where the putative stem cells reside. The highest levels of apoptosis are seen following radiation doses >1Gy. Similarly in the proliferative zone of the murine colonic crypts, apoptosis can be observed within a few hours of gamma-irradiation. Nevertheless, the colonic epithelium is more resistant when compared to the small intestinal epithelium in

the context of radiation induced apoptosis as evidenced by maximal apoptosis occurring only above doses of 8Gy (Potten and Grant, 1998).

Using transgenic mice studies, two broad types of apoptosis has been characterized in the mouse intestine. In the normal, unstressed intestine, spontaneous apoptosis occurs constantly at low levels and the stress-induced apoptosis occurs as a result of genotoxic insult like exposure to gamma rays or DNA damaging drugs. Spontaneous apoptosis occurs at the base of the crypts at or near the position of the epithelial stem cells. Studies using p-53 and Bcl2 knockout mice have shown that in both the small and the large intestine, spontaneous apoptosis is independent of p53 and Bax, but Bcl2 only regulates spontaneous apoptosis in the colon. On the contrary, studies using p-53 knockout mice have shown that both p53 and Bcl2 are important regulators of stress-induced apoptosis. Bax only plays a minor role in the regulation of stress-induced apoptosis (Watson and Pritchard, 2000).

Studies on radiation induced apoptosis by Potten et al., 2004 indicate that there were about six apoptosis-susceptible cells per crypt located at around cell positions 4–5. These cells lacked repair capacity and instead initiated a TP53-dependent cell suicide to delete the damaged cell. This occurred fairly rapidly within a period of 3–6 h. This apoptotic response may be part of the mechanism operating in the stem cells of the small intestine to protect their genome. Interestingly, the response of the large intestine is strikingly different owing to two factors. First, apoptosis in the large intestine occurs randomly throughout the crypt and is not limited specifically to the stem cell position, which is at the base of the crypt. Second, the apoptosis-susceptible cells are more resistant to radiation since higher doses are required to induce similar total yields. Lastly, the stem cells of the large intestine express the protein associated with the cell survival gene Bcl2 that prevents them from undergoing apoptosis. In contrast, the small intestinal stem cells do not express this gene as determined by immunohistochemistry and confirmed by studies of the yield of apoptotic cells in the small and large intestines of Bcl2 knockout mice (Merritt et al., 1995).

The Bcl-2 family of proteins is evolutionarily conserved regulators of apoptosis and the BH3-only subgroup of proteins appears to initiate and promote apoptosis in a cell type and stimulus specific manner (Yu and Zhang, 2004; Labi et al., 2006). Several groups have shown that the p53 upregulated modulator of apoptosis (PUMA) is a BH3-only protein and is a transcriptional target of p53 that has an essential role in p-53 dependent and independent apoptosis through the mitochondrial pathway (Han et al., 2001; Nakano

and Vousden, 2001; Yu et al., 2001). Recent studies by Qiu et al., 2008 indicate that PUMA deficiency protects the ISCs (both CBCs and +4 position cells) and progenitors from radiation induced apoptosis and improve crypt regeneration.

3.2.1.3 The regenerative capacity of the epithelium after irradiation

The regenerative capacity of the crypts upon radiation-induced damage is initiated by the survival of one or more clonogenic cells by a process referred to as clonal regeneration. The clonal regeneration process was studied in detail by Rod Withers in the late 1960s and published as the crypt microcolony assay (Withers and Elkind, 1969; 1970). The assay involves counting the number of regenerating crypt-like foci between 3–4 days after different doses of radiation to generate crypt radiation survival curves. This is achieved by routine staining of paraffin-embedded tissue sections on day 3-4.

Several studies indicate that the estimates of the number of clonogenic cells in a crypt depends somewhat on the intensity of the dose that one uses to investigate them. Small doses tend to give lower estimates, whereas high doses, or more severe stress, tend to give higher estimates. These conclusions are well accepted and have been seen to be consistent with the data obtained by other cell kinetic, lineage-tracking and mathematical modeling exercises.

According to Potten et al., 2004, at low doses of radiation damage, the crypt contains a relatively small number (about six per crypt) of clonogenic regenerators of the crypt, where as at higher doses the number is greater (up to about 30–40 potential clonal regenerators that can be recruited into action). This suggests that the crypt may be composed of a small number of lineage ancestor stem cells (four to six per crypt) that function as the day-to-day actual stem cells and a larger population of cells (from six to 30–40) that have not lost the potential to function as stem cells if the tissue is severely damaged, i.e. potential stem cells (Cai et al., 1997). However, there is still quite a lot of debate about what could determine the overall gastrointestinal damage.

3.2.1.4 Mechanisms of Radioprotection

It has been shown by Booth and Potten, 2001 that growth factors protect against radiation or chemotherapy induced mucosal injury. For example, the various growth

factors like the insulin-like growth factor 1 (IGF-1), keratinocyte growth factor and fibroblast growth factor-2 (or basic fibroblast growth factor-2 (bFGF-2)) have been shown to protect the +4 position cells and increase animal survival after whole body radiation (Booth and Potten, 2001; Paris et al., 2001; Wilkins et al., 2002). But what is not well understood are the targets and the mechanism of intestinal protection provided by these growth factors. Recently, Qui et al., 2010 have shown that the suppression of PUMA has a critical role in IGF-1 and bFGF- mediated radioprotection in the gastrointestinal system through a PI3K/AKT/p53- dependent mechanism. More recently, it has been shown by Jones et al., 2011 that Flagellin pretreatment protected mice from radiation-induced intestinal mucosal injury and apoptosis via a toll-like receptor 5 (TLR5)- dependent mechanism.

It is noteworthy that apart from growth factors, prostaglandin E2 (PGE2), a prostaglandin produced by the intestinal epithelial cells in response to gamma-irradiation (Murmu et al., 2004) has a remarkable radioprotective effect on ISC (Tessner et al., 2004). It has been shown that PGE2 can activate PI3K/ Akt signaling through PPAR β activation in colon cancer cell line model (Gupta et al., 2004; Wang et al., 2004). It then could be speculated that PGE2 exert its radioprotective effect through the activation of PPAR β .

While many studies concerned the intestinal epithelium responses to ionizing radiation, many different cell types besides the epithelial cell layer of the GI tract are also affected. Some studies have shown that stromal pericryptal fibroblasts are highly sensitive to irradiation (Potten et al., 1983). Finally, there is strong evidence for the vital role of fibroblasts in radiation-induced late inflammation and altered composition of the extracellular matrix (Barcellos-Hoff, 1998; Hauer-Jensen et al., 1998).

AIM OF THE WORK

AIM OF THE WORK

Of the known three PPAR isotypes, PPAR β remains the least known. Works in our laboratory has revealed the importance of this particular isotype in apoptosis, cell survival and proliferation. Furthermore, previous work from our group has shown that PPAR β plays a role in the differentiation of Paneth cells of the intestine by inhibiting the Ihh pathway. Considering the previous works from our laboratory on the role of PPAR β in cell survival and tissue repair (Di-Poi et al., 2002; and Letavernier et al., 2005), it was important to disturb the intestinal epithelial cell homeostasis and assess whether PPAR β might affect the healing process. Reports in the literature substantiate that gamma-irradiation is a very powerful tool that can be used to induce intestinal epithelial cell death, and follow the regenerative process of the gut (Potten, 2004). Thus PPAR $\beta^{+/+}$ and PPAR $\beta^{-/-}$ mice were exposed to 10Gy irradiation and the animals were sacrificed at 4h and at 3.5 days post-irradiation. At 4h post-irradiation, PPAR $\beta^{-/-}$ mice showed significantly higher apoptosis of the epithelial cells when compared to the control animals, more particularly at the level of the proposed location of the stem cell niche within the duodenal crypts (position +4 or +5 from the crypt bottom). Indeed, a BrdU staining protocol that allows the identification of stem cells in forms of “label retaining cells” further suggested that stem cells that were particularly damaged as an effect of irradiation. This correlated then with a significant reduction of epithelial cell proliferation at 3.5 days post-irradiation in the PPAR $\beta^{-/-}$ animals accompanied with a strong reduction of crypt survival.

The aim of my thesis work was thus to elucidate the molecular signalling mechanism mediated by PPAR β in the intestine upon gamma irradiation and more broadly to explore the possible role of PPAR β in intestinal epithelium repair.

More specifically, our goals and corresponding strategies were to answer the following questions:

- a. *Is the poor recovery state of the PPAR $\beta^{-/-}$ small intestine at 3.5d post irradiation a permanent damage or does it only reflect a delay in the healing process?*

With that respect, we will explore the phenotype at 8 day post-irradiation, by classical histological and immunohistological analyses, focusing on the two different compartments: epithelial and the intra-villus mesenchyme.

b. Which cell population is primarily affected by PPAR β deletion?

The intestinal homeostasis is maintained as a result of interplay of signals arising from two main compartments - the epithelial and the mesenchymal compartments. Using PPAR β conditional KO mice (PPAR β L2/L2) crossed with mice carrying the villin-Cre-ER^{T2} transgene, we planned to obtain mice where deletion of PPAR β in the intestinal epithelial cells can be provoked by Tamoxifen injection. The comparison of the phenotype provoked by the gamma-irradiation in PPAR β L2/L2 Cre⁺ treated vs PPAR β L2/L2 Cre⁻ treated with tamoxifen will tell us how much of the phenotype is due to the epithelial compartment vs the mesenchymal response.

c. Which PPAR β -dependent pathways are solicited in the irradiated intestine?

Starting from the previous demonstration that PPAR β is downstream of Wnt, as one of its target gene, and upstream of Ihh as one negative regulator of Ihh expression (Varnat et al., 2006), we wanted to pursue our quest for the molecular mechanisms utilized by the epithelial cells wounded by gamma-irradiation and the role played by PPAR β in the cell survival and repair process. For that purpose, primary enterocytes in culture represent an ideal tool. For ease of manipulation, we also considered to use the HT-29 cells, which are intestinal colon adenocarcinoma cells of human origin.

CHAPTER II:

RESULTS

1. Consequences of PPAR β deletion at 8d post irradiation

The apparent poor proliferation responses observed in the small intestine of PPAR $\beta^{-/-}$ at 3.5d post irradiation prompted us to explore further the repair mechanism of the PPAR $\beta^{-/-}$ mice at 8d post irradiation. For that purpose, we irradiated five 12- week old male mice with two rounds of 5Gy each. Mice were sacrificed at 8 days post-irradiation and we made histological analysis of the duodenal tissue sections of these mice.

1.1 Reduction of the number of mesenchymal cells in the lamina propria

Analyses by haematoxylin-eosin (HE) of the duodenum from PPAR $\beta^{+/+}$ and the PPAR $\beta^{-/-}$ mice at 8 d post-irradiation revealed that at that late time, the epithelial layer seems equally restored in both genotypes, the height of the villi are also of similar size (Fig. 14). Intriguingly, the mesenchymal compartment in the PPAR $\beta^{-/-}$ mice appeared less dense compared to that of the PPAR $\beta^{+/+}$ mice. This result in a thinning of each villi, as can be seen in Figure 14. This loosening of the lamina propria might be better seen on longitudinal section of the villi, shown in inserts within figure 14b. To document this subtle phenotype, we quantified the number of epithelial and mesenchymal cells within each crypt-villi unit from both the genotypes. The calculation was made as follows: the HE stained sections from both the PPAR $\beta^{+/+}$ and the PPAR $\beta^{-/-}$ mice were used to take images of full length crypt- villi unit. These images were then processed using the Image J software and we counted the number of epithelial and the mesenchymal cells within 200 crypt-villi unit from each animal totalling 1000 villi from five different animals for each genotype (five different fields of each section, and two different sections from four different slides from each animal).

To overcome the difficulties bound to the fact that small intestinal sections cannot be easily positioned such as the sections run by the central crypt-villus axis, we also calculated the ratio of epithelial cells to the mesenchymal cells in the transversal section of each villus unit. As shown in the Fig. 15, this ratio was significantly higher in the PPAR $\beta^{-/-}$

$\beta^{-/-}$ mice when compared to the $\text{PPAR}\beta^{+/+}$ mice, confirming the relative low density of mesenchymal cells in the lamina propria.

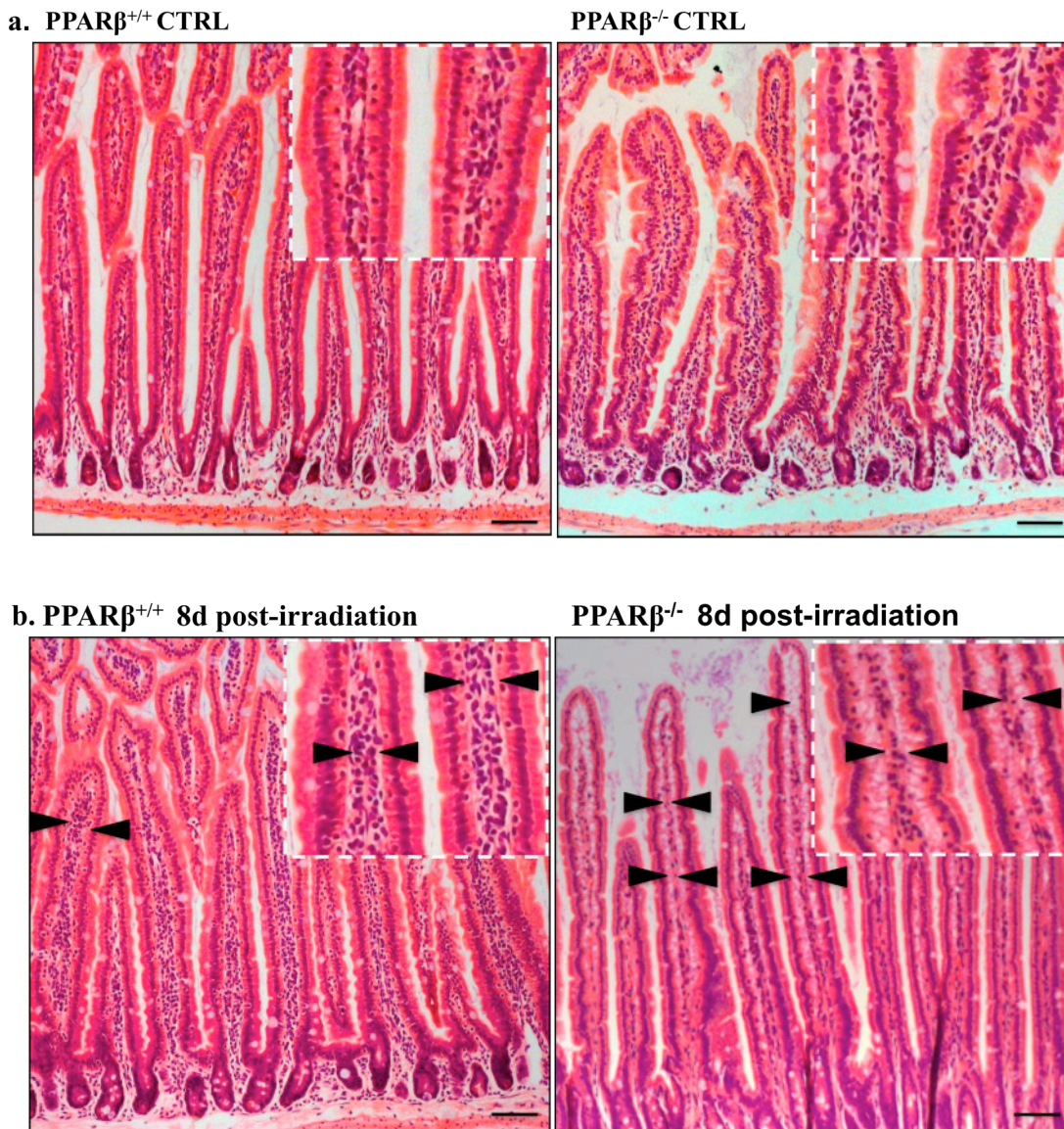


Fig. 14a and b | Haematoxylin-eosin staining of **a. $\text{PPAR}\beta^{+/+}$ and $\text{PPAR}\beta^{-/-}$ control samples. b. $\text{PPAR}\beta^{+/+}$ and $\text{PPAR}\beta^{-/-}$ at 8 days post-irradiation.** Panel **a**: $\text{PPAR}\beta^{+/+}$ and $\text{PPAR}\beta^{-/-}$ (n=5 for each genotype) samples do not show any difference in length of the villi and arrangement of cells in the intra-villus mesenchyme but in **Panel b**: After 8 days post-irradiation, $\text{PPAR}\beta^{-/-}$ show thin and long villus with fewer cells and loosely organised mesenchyme in the intra-villus region. Black arrows point to regions where there are mesenchymal cells. (Scale bar = 100 μm).

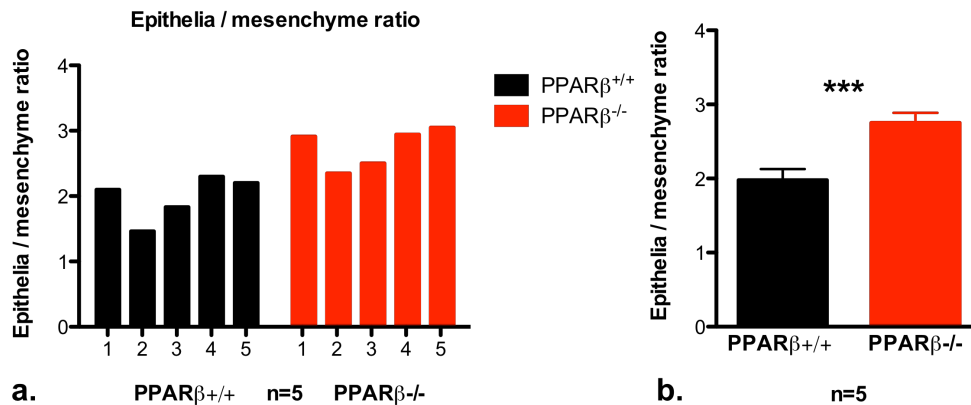


Fig. 15 | Epithelia/ mesenchyme ratio as calculated by counting the epithelial and mesenchymal cells within 1000 crypt-villi unit using the Image J software. A total of 5 PPAR $\beta^{+/+}$ and PPAR $\beta^{-/-}$ mice were analysed at 8 days post-irradiation and the epithelia/ mesenchyme ratio is presented for (a) each individual of both genotypes and (b) the average for 5 mice of both genotypes. Images of HE stained sections from both the PPAR $\beta^{+/+}$ and the PPAR $\beta^{-/-}$ mice were processed using the Image J software. Data represented was obtained by taking a count of the number of epithelial and the mesenchymal cells within 200 crypt-villi unit of each animal totalling 1000 villi for five different animals of each genotype. Statistical analysis was performed by paired t-test. *** Statistically significant at $p < 0.001$ when PPAR $\beta^{+/+}$ is compared with the PPAR $\beta^{-/-}$.

These differences observed at 8 days post irradiation might reflect differences in the rate of proliferation and/or apoptosis of these two cell types in the previous stages of recovery. Hence, we performed an immunostaining on paraffin sections of the duodenal samples at 3.5 d post irradiation from PPAR $\beta^{+/+}$ and PPAR $\beta^{-/-}$ mice, using an antibody against Ki-67, a marker for proliferation. As seen in Fig. 16, there are rather few cells labelled in the mesenchymal compartment when compared to highly proliferative crypts. The number of Ki-67 positive cells is even lower in the mesenchyme of PPAR $\beta^{-/-}$ mice when compared to PPAR $\beta^{+/+}$ mice, confirming that the mesenchyme cells of the PPAR $\beta^{-/-}$ mice underwent lower proliferation.

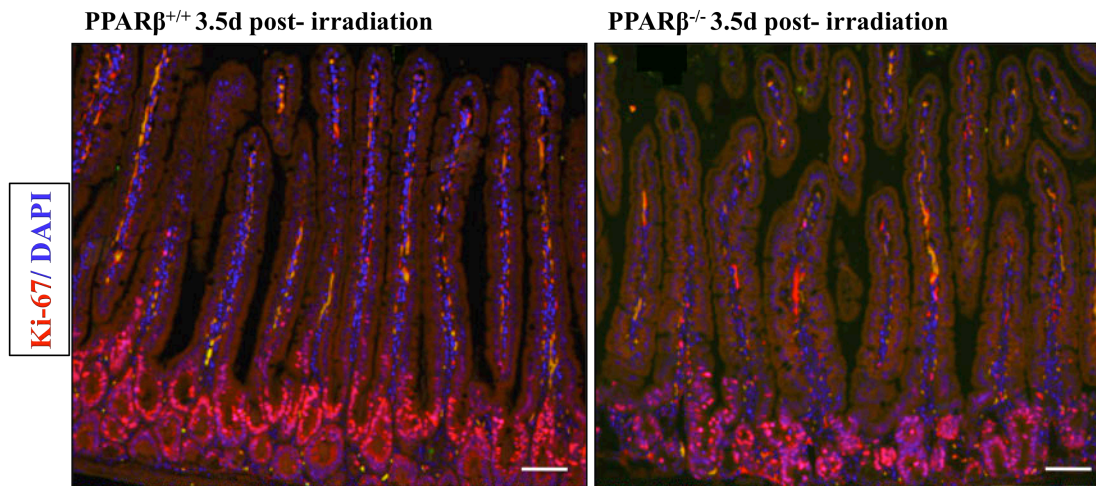


Fig. 16 | Evaluation of proliferation in the PPAR $\beta^{+/+}$ and PPAR $\beta^{-/-}$ samples at 3.5 days post irradiation. Immunostaining of the proliferation marker Ki-67 on paraffin sections from PPAR $\beta^{+/+}$ and PPAR $\beta^{-/-}$ samples at 3.5 days post-irradiation (n=3 for each genotype). PPAR $\beta^{-/-}$ show less number of mesenchymal cells as evident by the DAPI staining in the intravillus mesenchyme and also less number of proliferative cells in this region as evident by co-staining of Ki-67 (red) and Dapi(blue) in comparison to PPAR $\beta^{+/+}$. (Scale bar = 100 μ m).

In parallel, we performed a TUNEL assay on paraffin sections of the duodenal samples from PPAR $\beta^{+/+}$ and PPAR $\beta^{-/-}$ mice, to evaluate the number of apoptotic cells at 3.5 d post irradiation in the epithelial and the mesenchymal compartments (Fig. 17). As expected, TUNEL staining is mainly found along the epithelial sheet, with reinforcement at the top of the villi. Interestingly, PPAR $\beta^{-/-}$ mice showed a higher number of TUNEL positive cells in the mesenchyme compared to the epithelia confirming that the mesenchymal cells underwent higher apoptosis. Intriguingly, there were fewer apoptotic events in the epithelial sheet of PPAR $\beta^{-/-}$ intestine.

Altogether these results suggest that the low mesenchymal cell density in PPAR $\beta^{-/-}$ mice after irradiation is in part caused by a decreased proliferation and increased apoptosis rate in the mesenchymal compartment. This also emphasizes a differential response to gamma irradiation of the cell types constituting these two compartments.

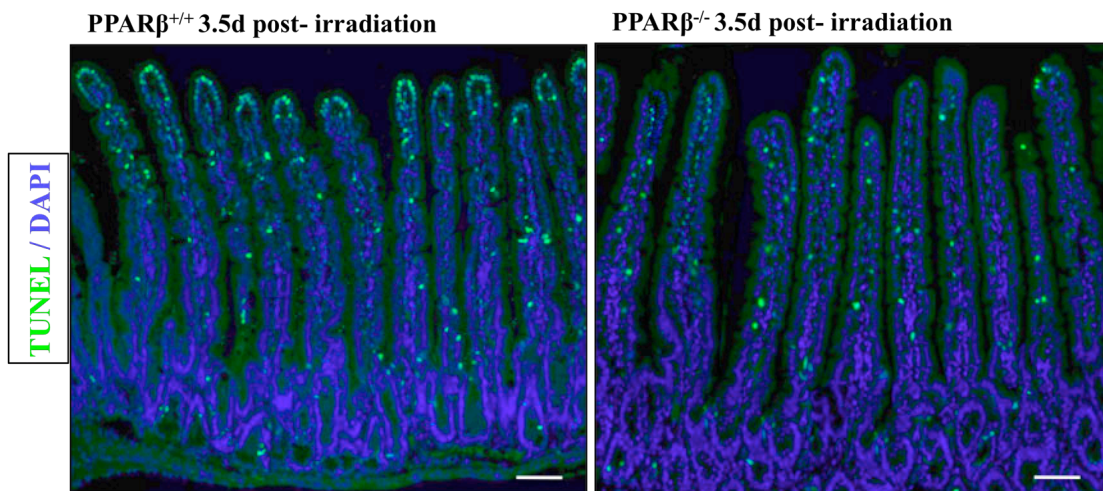


Fig. 17 | Evaluation of apoptosis in the $PPAR\beta^{+/+}$ and $PPAR\beta^{-/-}$ samples at 3.5 days post irradiation. Immunostaining using TUNEL assay on the paraffin sections from $PPAR\beta^{+/+}$ and $PPAR\beta^{-/-}$ samples at 3.5 days post-irradiation (n=3 for each genotype). $PPAR\beta^{-/-}$ show positive staining for TUNEL mainly in the intra-villus mesenchyme, indicating death of mesenchymal cells in this region where as $PPAR\beta^{+/+}$ stain positive for TUNEL mainly in the villi tip where apoptosis of epithelial cells takes place normally as a result of homeostasis. (Scale bar = 100 μ m).

1.2 *Decrease of ECM components resulting in adhesion defect at 8d post-irradiation*

The looseness of the structure of the lamina propria at day 8 post-irradiation in $PPAR\beta^{-/-}$ mice is also exemplified by a particular phenotype shown in Figure 18. On HE staining, the mesenchymal cells in the $PPAR\beta^{-/-}$ mice appeared to be contracted from the epithelial basement membrane and concentrated towards the centre of the lamina propria leaving an empty space between the epithelia and the mesenchyme.

While quite unlikely, we first check whether this empty space might be due to an inappropriate secretion of mucus towards the baso-lateral side of the gut epithelial cells, hence pushing the mesenchymal cells towards the centre of the lamina propria. To evaluate this, we performed alcian blue staining of the duodenal sections from both the $PPAR\beta^{+/+}$ and $PPAR\beta^{-/-}$ mice at 8d post irradiation to detect the mucopolysaccharides and glucosaminoglycans of the mucus secreted by Goblet cells. However, we did not observe any mucus staining in this empty space (Fig. 19).

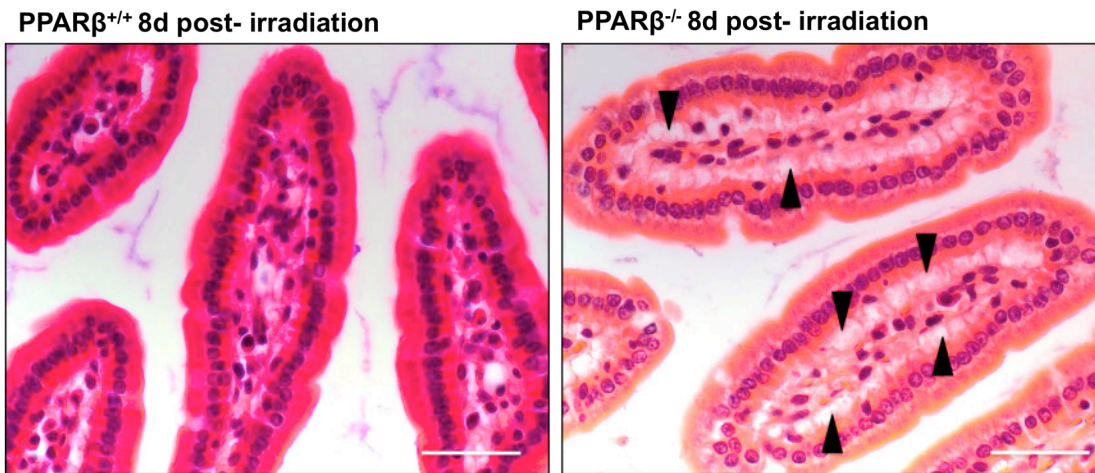


Fig. 18 | Haematoxylin-eosin staining of PPAR $\beta^{+/+}$ and PPAR $\beta^{-/-}$ at 8 days post-irradiation. At 8 days post-irradiation (n=5 for each genotype) PPAR $\beta^{-/-}$ show detachment of the epithelial layer from the basal mesenchymal layer as seen by gaps between the two layers. Black arrows show regions in the PPAR $\beta^{-/-}$ where detachment is clearly seen. (Scale bar = 20 μ m).

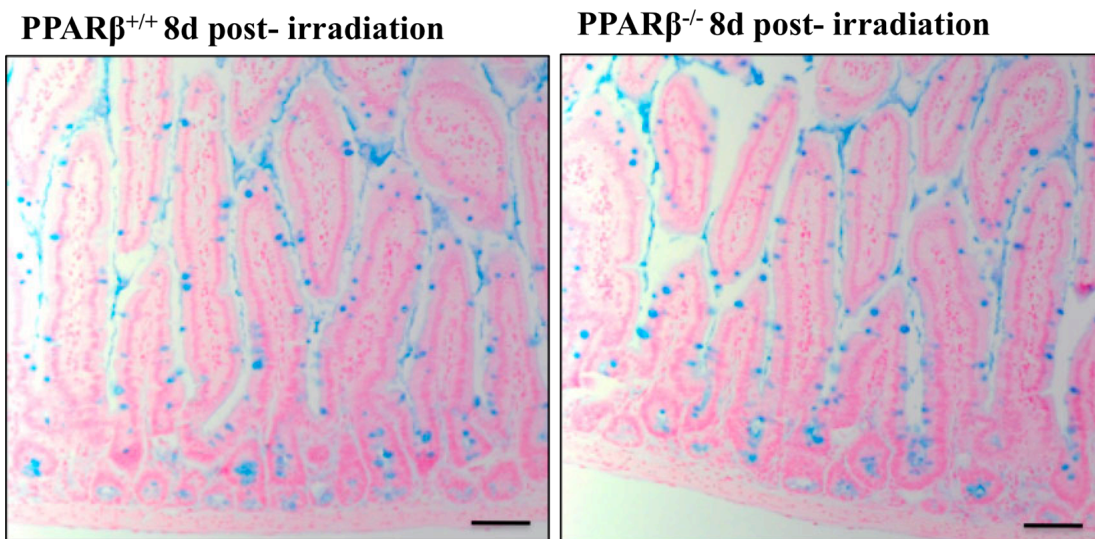


Fig. 19 | Alcian blue staining of the PPAR $\beta^{+/+}$ and PPAR $\beta^{-/-}$ samples at 8d post irradiation. Immunohistochemistry on paraffin sections from PPAR $\beta^{+/+}$ and PPAR $\beta^{-/-}$ samples at 8 days post-irradiation (n=3 for each genotype). Alcian blue stains the mucopolysaccharides in the mucus. The PPAR $\beta^{-/-}$ does not show any staining for alcian blue (blue in colour) in the intra-villus mesenchyme as compared to the PPAR $\beta^{+/+}$ (Scale bar= 50 μ m).

We thus explored whether the deposition of the extra-cellular matrix and the contact with the basal membrane of the epithelium was affected. To evaluate the collagen fibres of the extra cellular matrix, we performed Sirius red staining of the sections of the duodenal samples from both the PPAR $\beta^{+/+}$ and PPAR $\beta^{-/-}$ mice at 8d post irradiation. We observed that PPAR $\beta^{-/-}$ showed a less intense staining for the collagen fibres I and III

when compared to the $\text{PPAR}\beta^{+/+}$ that had a very intense staining (Fig. 20). This indicates a relative loss of collagen fibres in the lamina propria of $\text{PPAR}\beta^{-/-}$ mice after irradiation. It is thus possible that the empty space observed between the epithelial basement membrane and the collagen fibres attached to the mesenchymal layer in these mice is an outcome of the loss of the collagen fibres resulting in a gap between the two layers. Hence, these observations hint to the possible defect in components of the extracellular matrix in the $\text{PPAR}\beta^{-/-}$ mice due to irradiation. Alternately, the decreased amount of extra-cellular matrix in the lamina propria might mainly reflect the low cellular density present in this compartment.

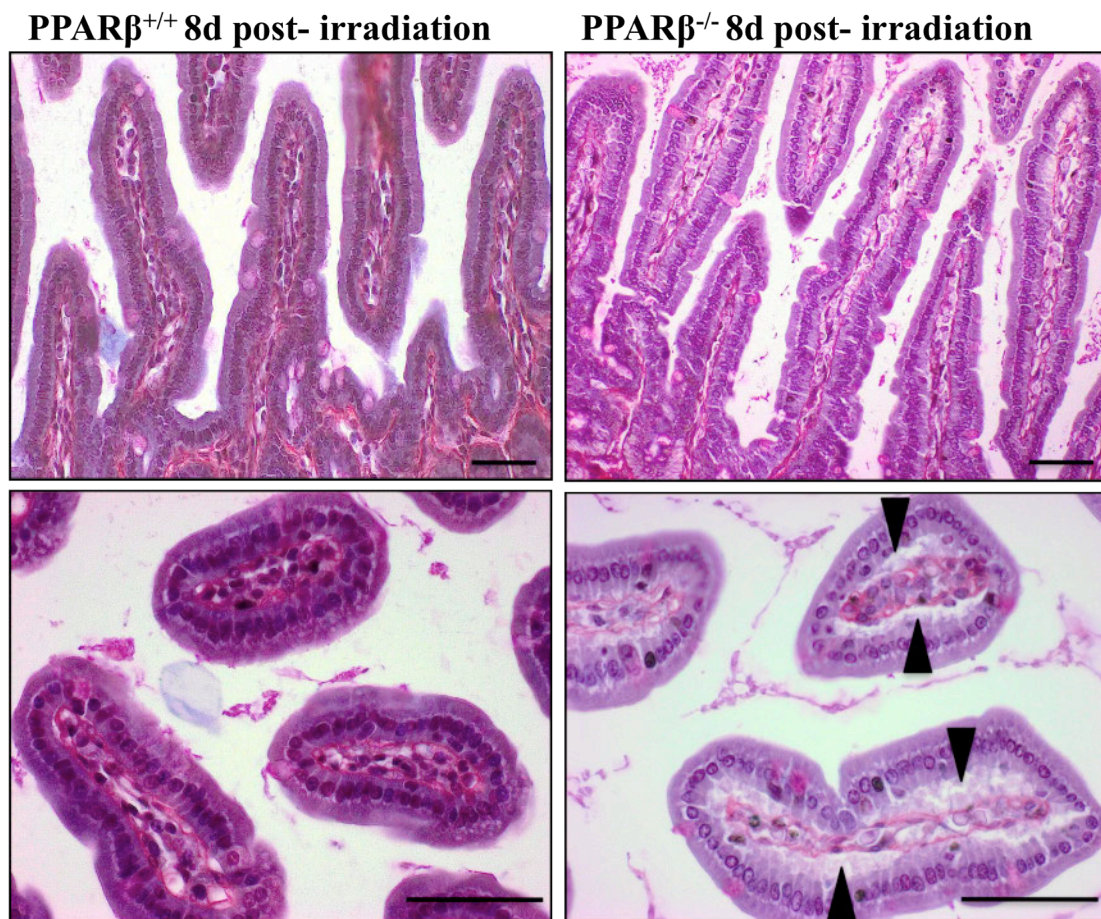


Fig. 20 | Sirius red staining of the $\text{PPAR}\beta^{+/+}$ and $\text{PPAR}\beta^{-/-}$ samples at 8 days post-irradiation [$\text{PPAR}\beta^{+/+}$ (left lane) and $\text{PPAR}\beta^{-/-}$ (right lane)]. Sirius red stains collagen I and III fibres red in colour. At 8 days post-irradiation $\text{PPAR}\beta^{-/-}$ show detachment of the epithelial layer from the basal mesenchymal layer as seen by detachment of collagen fibres stained in red between the two layers as compared to the $\text{PPAR}\beta^{+/+}$. Black arrows show regions in $\text{PPAR}\beta^{-/-}$ where detachment of collagen is clearly seen. (n=3 for each genotype);(Scale bar for top lane: 100 μm and for bottom lane: 50 μm).

2. In vivo analyses of the epithelia-mesenchyme crosstalk after irradiation.

Intestinal homeostasis is maintained through a coordination of signals arising from two different compartments (see introduction). To analyse the respective role of PPAR β in the epithelial sheet versus the mesenchymal compartment, we used the villin-Cre-Lox system, to knockdown PPAR β in the epithelial cells of the intestine.

El Marjou, et al. (2004) have reported generation of two complementary systems for Cre-mediated recombination of target genes in the mouse digestive epithelium. Accordingly, we crossed the PPAR β L2/L2 floxed mice with the villin Cre-ER^{T2} to obtain the PPAR β L2/L2 villin Cre⁺ and the PPAR β L2/L2 villin Cre⁻. The PPAR β L2/L2 Villin Cre⁺ mice bear a tamoxifen-dependent Cre recombinase expressed under the control of the villin promoter. Upon tamoxifen treatment, the Cre expressing cells undergo a somatic recombination of the PPAR β L2/L2 alleles. This recombination was detectable throughout the digestive epithelium and persisted for 60 days.

For our experimental purpose, we had three groups of 12 weeks old mice: PPAR β L2/L2 (n=4), which served as wild type controls, PPAR β L2/L2 Villin Cre⁺ (n=5) and the PPAR β L2/L2 villin Cre⁻ (n=4). Each of the three groups was treated with tamoxifen and vehicle. Tamoxifen was administered intraperitoneally at a dose of 1mg/ml/kg per day for 5 consecutive days. For the vehicle treated group, equal volume of sunflower oil was administered. The tamoxifen-mediated deletion was allowed for one week and after one week the animals were irradiated and then sacrificed at 3.5 and 8 days post irradiation.

We performed a histological analysis to evaluate the phenotype at 8 days post irradiation. Histological analysis by haematoxylin-eosin staining showed that the Villin Cre⁺ mice (n=5) have the similar kind of defect like that of the PPAR β ^{-/-} mice with reduction in the number of mesenchymal cells and also detachment of mesenchyme from the basement membrane and separation from the epithelia (Fig. 21).

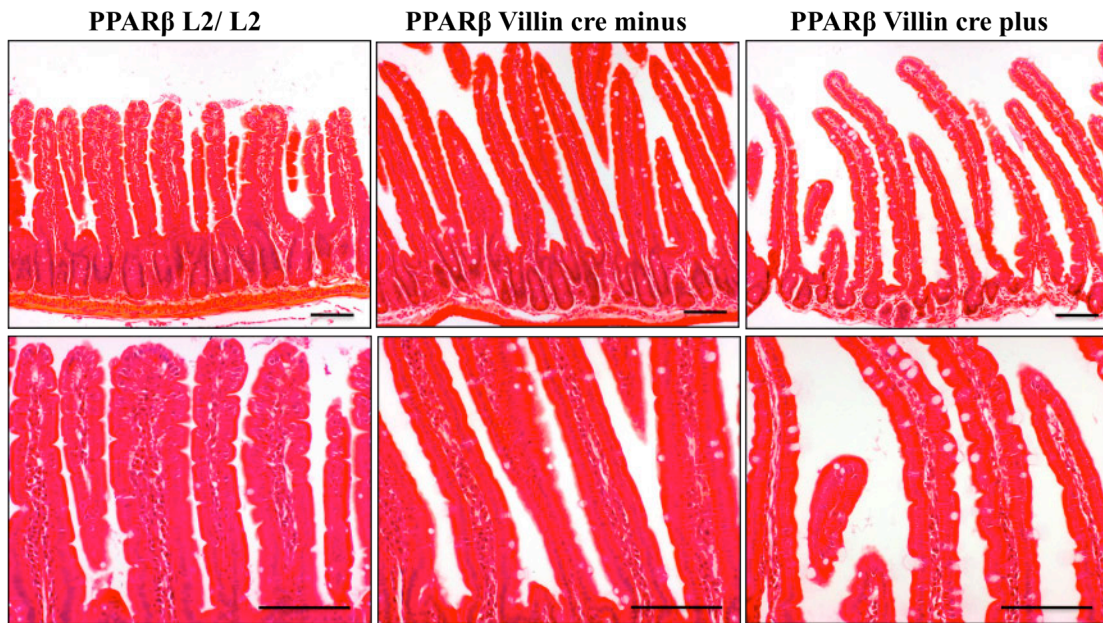


Fig. 21 | Haematoxylin-eosin staining of PPAR β L2/L2, PPAR β Villin cre⁻ and PPAR β villin cre⁺ conditional KO at 8 days post irradiation. Tissue specific knockdown of PPAR β was brought about by the Cre-Lox system as explained in the text. The figure shows normal architecture of the villus in the PPAR β L2/L2 mice and the PPAR β villin cre⁻ which served as controls where as the PPAR β villin cre⁺ KO shows thinner villi with reduced number of mesenchymal cells. (Scale bar for top lane: 100 μ m and bottom lane: 50 μ m; n=5).

On the other hand, the PPAR β L2/L2 control group (n=3) does not show any defect. Thus, these set of experiments suggest a possible role of PPAR β in initiating the signal from the epithelia to the mesenchyme in response to damage upon irradiation. Thus, this model of the epithelial specific PPAR β conditional KO may be a good model to confirm the signaling crosstalk between the epithelia and the mesenchyme during the recovery from irradiation mediated damage. However, high variability in the results prevented us to pursue along this experimental line.

3. Exploring the molecular pathways controlled by PPAR β upon irradiation

3.1 Microarray analyses at 4 hours post-irradiation

In the course of his thesis work, Frederic Varnat had prepared a microarray analysis, performed on scraped intestinal mucosa before and at 4 hours post-irradiation, comparing PPAR $\beta^{+/+}$ and PPAR $\beta^{-/-}$ mice.

To help in identifying the first molecular event along the irradiation, we first analysed the results obtained from this study. A global view of the results is shown in Figure 22. A total of 2527 genes were observed to be differentially modulated between the PPAR $\beta^{-/-}$ and the PPAR $\beta^{+/+}$ mice in non-irradiated condition (i.e, at 0h) whereas 1994 genes were found to be altered between the PPAR $\beta^{-/-}$ and the PPAR $\beta^{+/+}$ at 4h post-irradiation. Of these, 587 genes were found to be modulated at both time-points.

We also observed that as an effect of irradiation, 2561 genes were modulated in the PPAR $\beta^{+/+}$ when compared to non-irradiated condition. The same comparison give 1783 modulated genes in PPAR $\beta^{-/-}$, i.e. around 800 genes less than in PPAR $\beta^{+/+}$. Finally, 2907 genes were found that were commonly modulated between the strains (PPAR $\beta^{+/+}$ 4h vs PPAR $\beta^{+/+}$ 0h and PPAR $\beta^{-/-}$ 4h vs PPAR $\beta^{-/-}$ 0h).

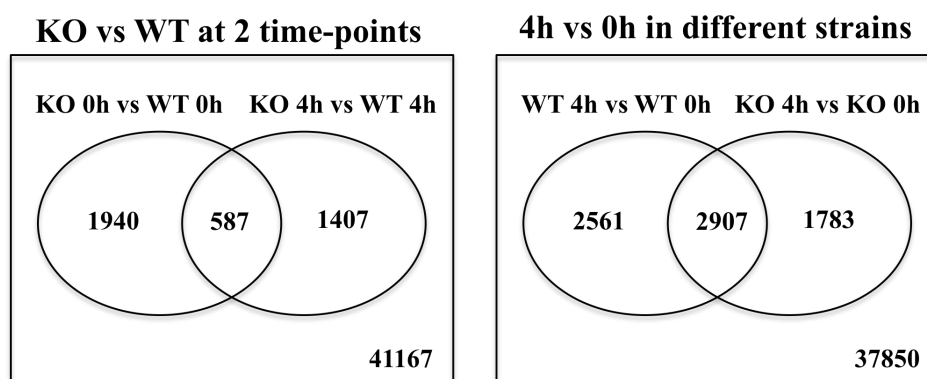


Fig. 22 | Venn diagrams showing results from microarray done on scraped intestinal mucosa from PPAR $\beta^{+/+}$ (WT) and PPAR $\beta^{-/-}$ (KO) mice at 0h and 4h post-irradiation showing number of genes that were modulated in each group. A comparison between PPAR $\beta^{+/+}$ (WT) and PPAR $\beta^{-/-}$ (KO) at the two different timepoints and between non-irradiated (0h) and irradiated at 4h in the two different genotypes is represented.

We then used a powerful analytical method called Gene Set Enrichment Analysis (GSEA) for interpreting gene expression data. The purpose of Gene Set Enrichment Analysis (GSEA) is to determine whether the members of a gene set S distributes randomly throughout the whole reference gene list L or is just primarily found at the top or bottom. The GSEA has the relative robustness to noise and outliers in the data, which is a big advantage.

The analysis shows that the cholesterol biosynthesis pathway was remarkably affected upon irradiation (Fig. 23 and 24). As seen in these figures, the genes of the cholesterol biosynthesis pathway (Fig. 25) were significantly (Geneset Rank-6) upregulated in the group $\text{PPAR}\beta^{+/+}$ 4h when compared to $\text{PPAR}\beta^{+/+}$ 0h. This same pathway was found to be significantly (Geneset rank-2) down-regulated in the $\text{PPAR}\beta^{-/-}$ 4h when compared to $\text{PPAR}\beta^{+/+}$ 4h. Thus, this clearly indicates that irradiation affects transcription of the genes involved in the cholesterol biosynthesis pathway. The analysis is summarised in Fig. 26.

Before vs after 4h irradiation in WT mice - \uparrow by irradiation

Gene set rank: 6

Statistics

Normalized Enrichment Score (NES)	-2.19
Nominal p-value	0.00
FDR q-value	0.002



Fig. 23 | Heat map from Gene Set Enrichment Analysis (GSEA) showing cholesterol biosynthesis pathway geneset that is upregulated in $\text{PPAR}\beta^{+/+}$ mice as a result of irradiation.

PPAR β WT vs KO after 4h irradiation - ↓ in KO

Gene set rank: 2

Statistics

Normalized Enrichment Score (NES)	2.40
Nominal p-value	0.0
FDR q-value	0.0

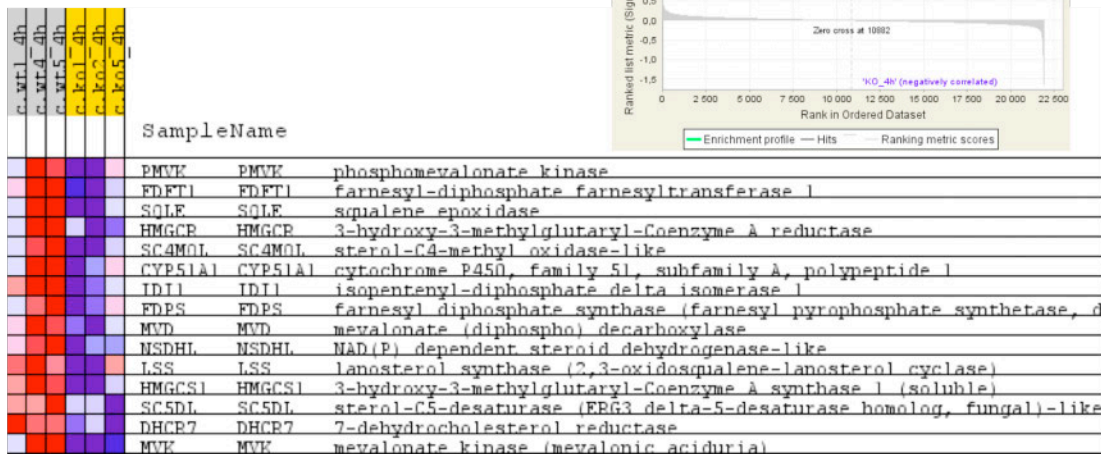


Fig. 24 | Heat map from Gene Set Enrichment Analysis (GSEA) showing cholesterol biosynthesis pathway geneset that is downregulated in PPAR β ^{-/-} mice when compared to PPAR β ^{+/+} mice at 4hr post- irradiation.

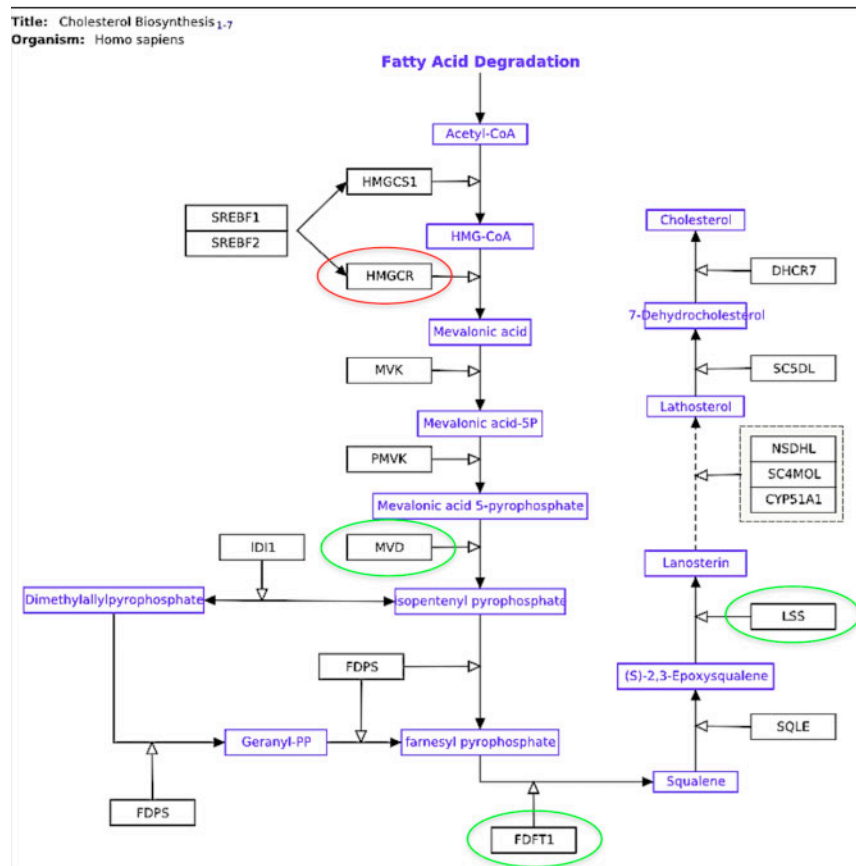


Fig. 25 | Overview of the various enzymes involved in cholesterol biosynthesis pathway (adapted from GENMAPP2.0). The boxes in blue indicate the various products formed in the pathway brought about by the specific enzymes of the pathway (highlighted in black). All the genes encoding for all these enzymes of the pathway were found to be modulated in the microarray data. The rate-limiting enzyme of the pathway-HMG-CoA reductase (HMGCR) is highlighted in red and the genes coding for the enzymes highlighted in green were selected based on their p-value significance for further validation of the microarray results.

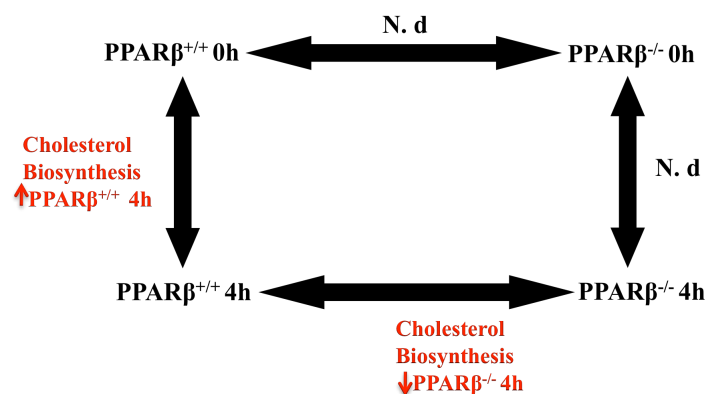


Fig. 26 | Summary of the results of the microarray data showing the modulation of cholesterol biosynthetic pathway genes when comparison is made between the genotypes $PPAR\beta^{+/+}$ and $PPAR\beta^{-/-}$ at the two different the timepoints- 0h (non-irradiated) and 4h post irradiation [N. d= no difference].

3.2 Studies on cholesterol biosynthesis pathway using in vivo model

To validate the observations from the microarray experiment, we performed qPCR analysis of the selected set of genes, namely- Farnesyl-diphosphate farnesyl transferase 1 (FDFT1), Mevalonate (diphospho) decarboxylase (MVD), Lanosterol synthase (LSS), 3-hydroxy-3methylglutaryl-Coenzyme A reductase (HMGCR), and 3-hydroxy-3-methylglutaryl-Coenzyme A synthase1 (HMGCS1), involved in the cholesterol biosynthesis pathway that was found to be significantly modulated in $PPAR\beta^{+/+}$ and $PPAR\beta^{-/-}$ mice in response to irradiation. These control analyses were performed on a new preparation of samples. A remarkable up-regulation was observed in all the above-mentioned genes in the $PPAR\beta^{+/+}$ upon irradiation (Fig. 27). Interestingly, the response was attenuated in $PPAR\beta^{-/-}$ mice but not absent.

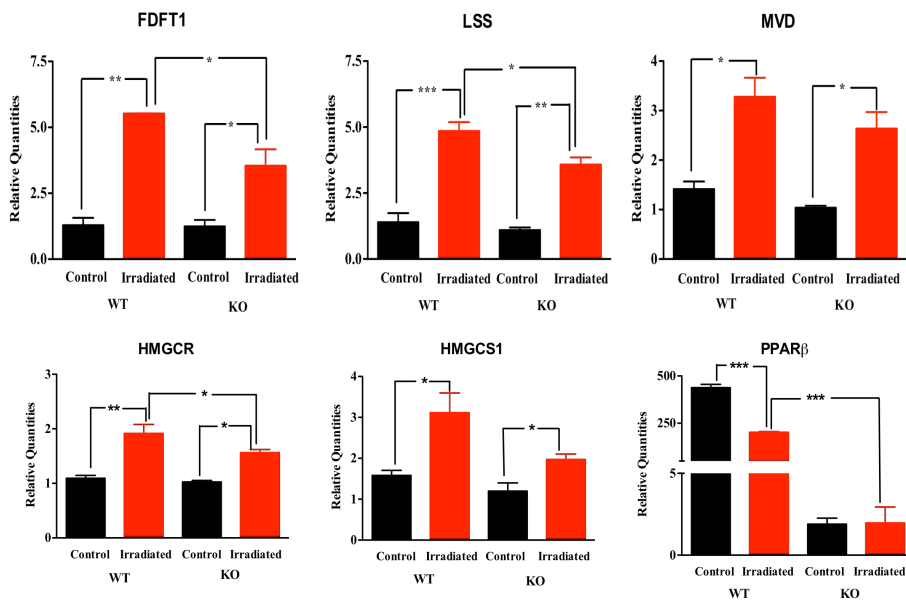


Fig. 27 | Gene expression analysis by QPCR on scraped mucosa samples from the intestine of $PPAR\beta^{+/+}$ (WT) and $PPAR\beta^{-/-}$ (KO) control (non-irradiated) and 4h post-irradiated samples. Gene expression analysis was performed by SYBR green assay on the following genes of the cholesterol biosynthesis pathway that were found to be significantly modulated by 10Gy irradiation in $PPAR\beta^{+/+}$ (WT) and $PPAR\beta^{-/-}$ (KO) mice: Farnesyl-diphosphate farnesyl transferase 1 (FDFT1), Mevalonate (diphospho) decarboxylase (MVD), Lanosterol synthase (LSS), 3-hydroxy-3methylglutaryl-Coenzyme A reductase (HMGCR), and 3-hydroxy-3-methylglutaryl-Coenzyme A synthase1 (HMGCS1), Peroxisome proliferator-activated receptor β ($PPAR\beta$). All samples were normalized using two housekeeping genes namely Glyceraldehyde-3-phosphate dehydrogenase (GAPDH) and Tata-box binding protein (TBP). Data expressed are mean \pm SEM. Statistical analysis was performed by one-way ANOVA followed by Newman-Keuls multiple comparison test. (* Statistically significant at $p < 0.05$, ** $p < 0.01$, and *** $p < 0.001$ in comparison to control).

Finally, it is also of interest to note that the levels of PPAR β expression was significantly reduced upon irradiation in the PPAR $\beta^{+/+}$ mice when compared to the PPAR $\beta^{+/+}$ non-irradiated mice. These results emphasize the importance of the cholesterol metabolism pathway in the early response to irradiation. It also suggests that PPAR β might be an important contributor to this response, albeit we have not been able to observe the dramatic differences obtained in the microarray analyses.

3.3 *Validation of an in-vitro intestinal cell line model: HT-29*

The difficulties in obtaining a solid and reproducible molecular phenotype led us to consider a simplified model system to validate our *in-vivo* data. With that in mind, we decided to use an intestinal colon adenocarcinoma cell line – HT-29.

3.3.1 *Estimation of basal levels of PPAR β and its activity in HT-29 cell model*

Estimations with qPCR were performed to identify the basal levels of expression of PPAR β in HT-29 cells. The Ct values averaging to ~24 indicates that PPAR β has a high expression level in HT-29 cell line. The levels of PPAR β activity were then estimated with Luciferase assay. The HT-29 cells were transfected with PPRE 3XTk luc (peroxisome proliferator response element with luciferase construct driven by thymidine kinase promoter). 6h after transfection, the cells were treated with PPAR β specific agonist (500nM GW501516) and/or antagonist (900nM GSK0660). 24h after the administration of the ligands, luciferase reporter assays were performed (Fig. 28).

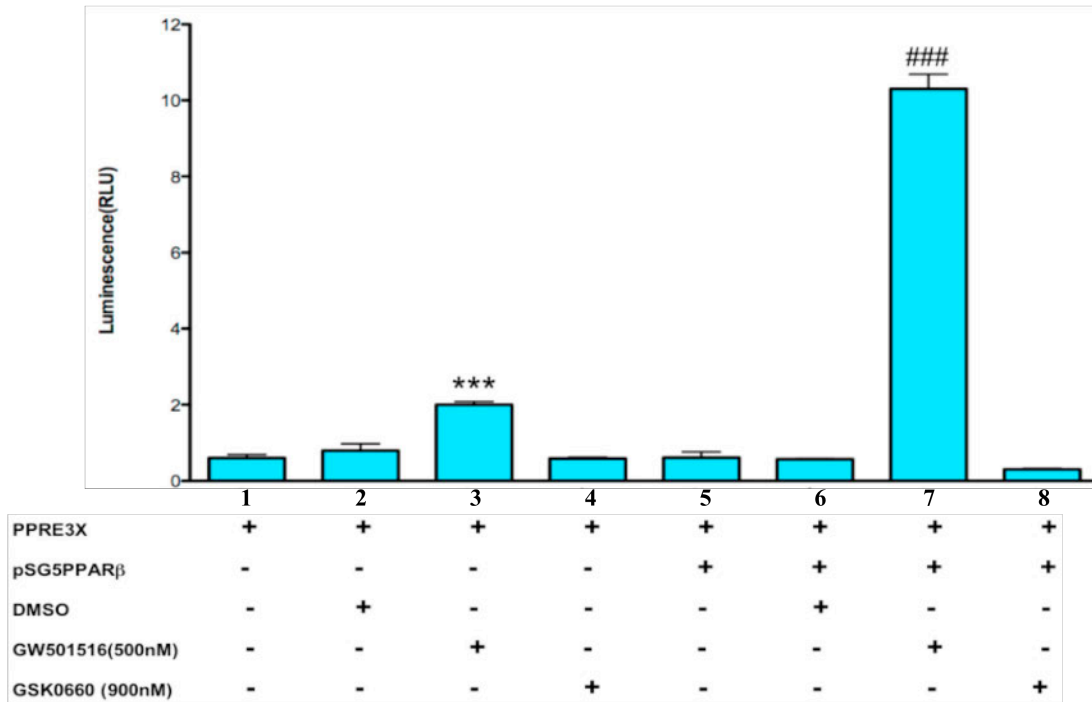


Fig. 28 | Luciferase assay showing PPAR β activity levels in HT-29 cells. Cells were transfected with luciferase construct carrying 3X PPRE and treated with different doses of the agonist GW501516 and the antagonist GSK0660. 24h after initiating the treatment, cells were lysed and luminescence was measured. Data expressed as a mean \pm SEM. Statistical analysis was performed by one-way ANOVA followed by Newman-Keuls multiple comparison test. *** Statistically significant at $p < 0.001$ and when lane 3 compared with lane 2 observed and ### statistically significant at $p < 0.001$ when lane 7 compared with lane 6.

Basal activity of PPAR β was moderate as evident from the control group (lane1), and its over-expression in absence of exogenous ligand did not significantly up-regulate its activity (lane5). In response to the agonist, PPAR β activity was significantly induced in cells, both at basal levels of PPAR β (lane3) as well with over-expression of PPAR β using the plasmid pSG5 PPAR β (lane7). The antagonist GSK0660 was not able to down-regulate the activity levels of PPAR β significantly, in both basal and over-expressed states of PPAR β in these cells. This observation indicates that GW501516 at a dose of 500nM can activate PPAR β in HT29 cells. This ligand and dose was thus used for further tests.

3.3.2. Evaluation of PPAR β agonist and antagonist activities in HT-29 cell model

In order to confirm the efficiency of the treatment with PPAR β specific ligands, their effects on endogenous PPAR β target genes were estimated (Fig. 29). After treating HT-29 cells with two different doses (100nM and 500nM) of PPAR β specific agonist (GW501516), we tested by qRT-PCR six known target genes of PPAR β namely Adipose Differentiation Related Protein (ADRP), Angiopoietin-like 4 (ANGPTL4), Indian hedgehog (Ihh), Transforming growth factor β (TGF β), Pyruvate dehydrogenase kinase, isozyme 1 (PDK1), and Pyruvate dehydrogenase kinase, isozyme 4 (PDK4).

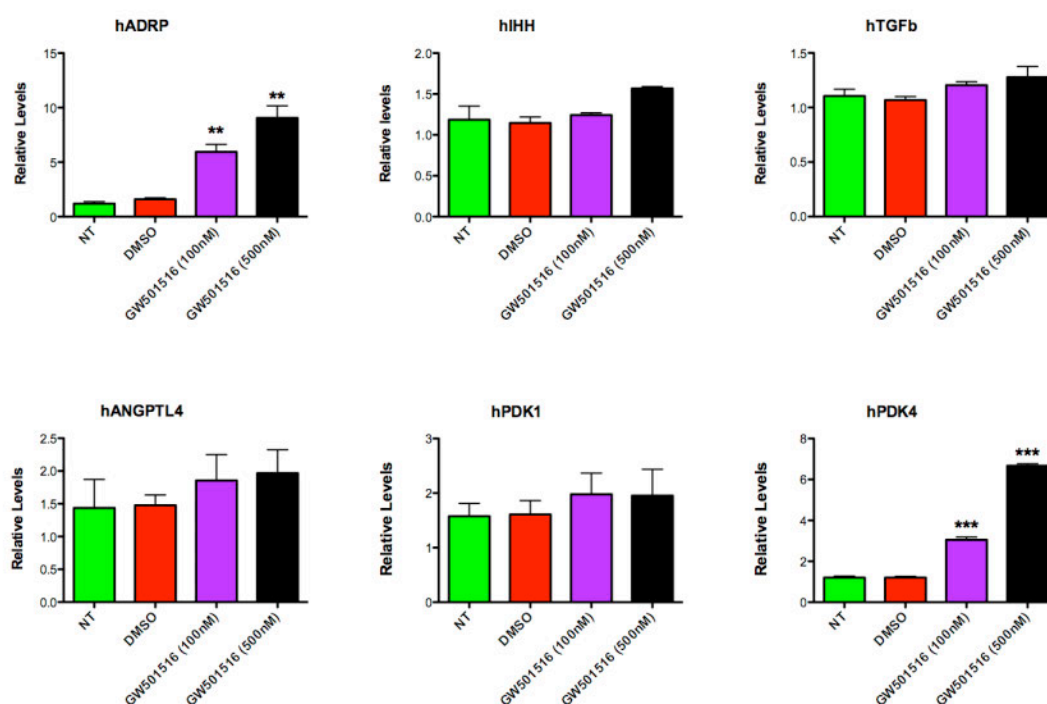


Fig. 29 | Effects of PPAR β specific agonist (GW501516) on gene expression in HT-29 cells. Gene expression analysis was performed by SYBR green assay on the following genes - Adipose Differentiation Related Protein (ADRP), Angiopoietin-like 4 (ANGPTL4), Indian hedgehog (Ihh), Transforming growth factor β (TGF β), Pyruvate dehydrogenase kinase, isozyme 1 (PDK1), and Pyruvate dehydrogenase kinase, isozyme 4 (PDK4). All samples were normalized using two housekeeping genes namely human eukaryotic translation elongation factor 1 alpha 1 (hEEF1A1) and human glucuronidase, beta (hGusB). Data expressed are mean \pm SEM. Statistical analysis was performed by one-way ANOVA followed by Newman-Keuls multiple comparison tests. (**Statistically significant at $p < 0.01$ and *** at $p < 0.001$ in comparison to DMSO treatment). NT= no treatment).

Only PDK4 and ADRP were significantly up regulated in a dose-dependent manner when the cells were challenged with both 100nM and 500nM of GW501516. As the levels of up-regulation of PDK4 were more significant than that of ADRP, we thus considered PDK4 as our choice to validate PPAR β activity in HT-29 cells.

Alongside using already available PPAR β antagonist in the lab (GSK0660), we decided to test a newly identified molecule VP80 (provided by Rolf Müller) that is considered to be a more specific antagonist of PPAR β . We used luciferase assay system to evaluate its efficacy in our cell system and compared it with the existing potent antagonist GSK0660. In order to compare the antagonizing effects of the two antagonists, we performed an experiment using both VP80 and GSK0660 at a dose range of 1-10 μ M and tested its efficacy against GW501516-induced PPAR β activity at a constant dose of 100 nM, so that we can observe the maximum antagonizing effect of these antagonists at a lower effective dose of the agonist (Fig. 30).

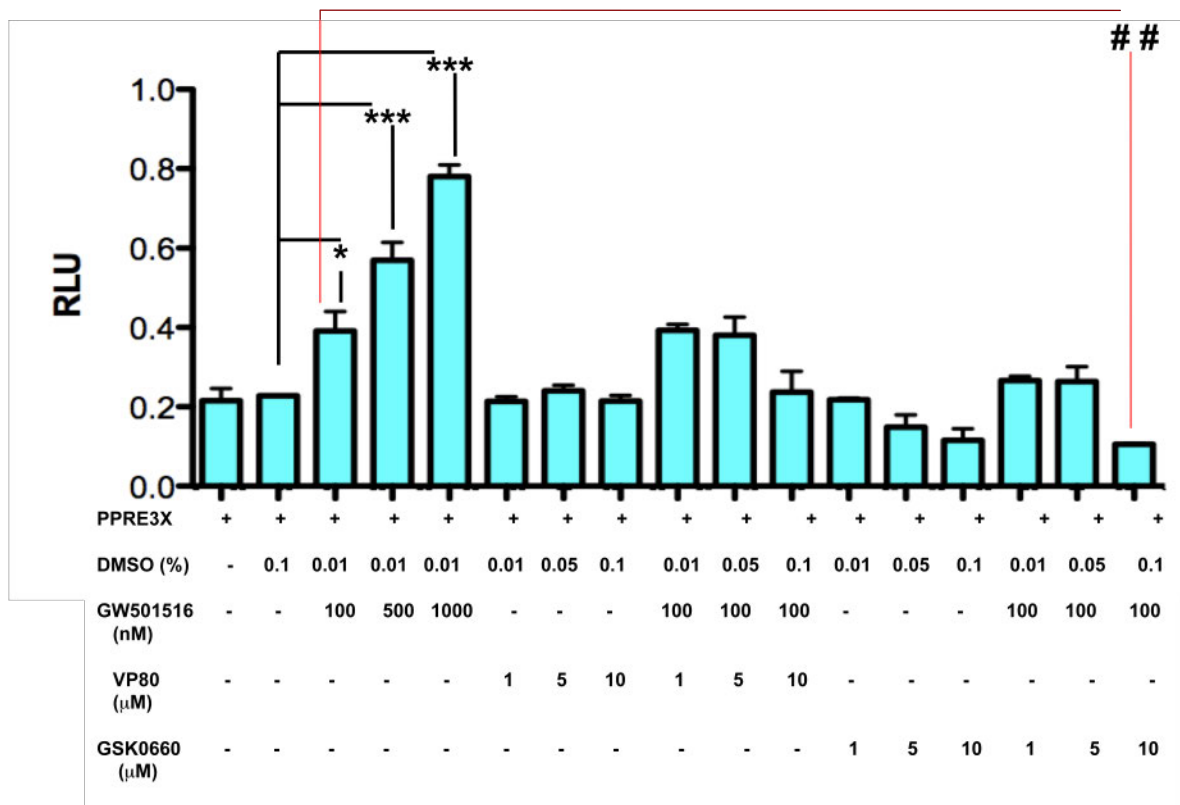


Fig. 30 | Comparison of PPAR β antagonists - GSK0660 and VP80 activity in HT-29 cells. Cells were transfected with luciferase construct carrying 3X PPRE and treated with 100-1000nM of GW501516 without or with the addition of various concentrations of GSK0660 and VP80. GSK0660 and VP80 can compete with GW501516 and decrease the efficacy of the agonist GW501516. 24h after initiating the treatment, cells were lysed and luminescence was measured. Data expressed are mean \pm SEM. Statistical analysis was performed by one-way ANOVA followed by Newman-Keuls multiple comparison tests. (*= $p < 0.05$, ##= $p < 0.01$; *** statistically significant at $p < 0.001$).

GW501516 was able to induce significant PPAR β activity dose dependently (100, 500 and 1000 nM) at basal conditions as observed in the Fig.30. Neither VP80 nor GSK0660 were able to inhibit the basal levels of PPAR β activity. GSK0660 at a dose of 10 μ M could significantly down-regulate GW501516-induced PPAR β activation by 73 %. Furthermore, GSK0660 had no significant cytotoxic effects in comparison to VP80, which showed significant cytotoxic effect at doses of both 5 and 10 μ M, as evident by the MTT assay (Fig. 31). Significant cytotoxic effects were also observed at higher concentrations of GW501516 at 500 and 1000 nM but not at a concentration of 100 nM.

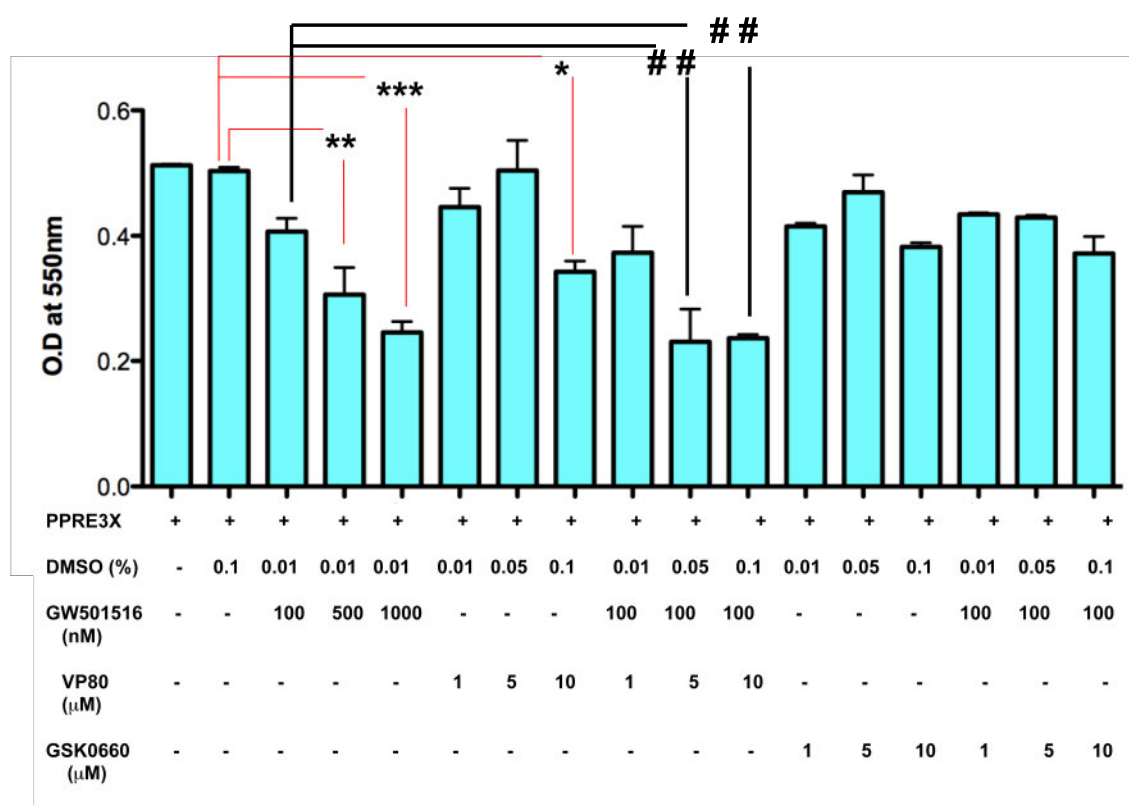


Fig. 31 | MTT assay to assess cytotoxicity due to the PPAR β antagonists GSK0660 and VP80 at different doses in HT-29 cells. Cells were transfected with luciferase construct carrying 3X PPRE and treated with 100-1000nM of GW501516 without or with the addition of various concentrations of GSK0660 and VP80. An MTT assay was performed on cells 24h after initiating the treatment. MTT assay is a colorimetric assay for measuring the activity of enzymes that reduce MTT to formazan dye, giving a purple color in living cells as against dead cells. Thus, MTT assay gives a measure of the cytotoxicity due to the treatment with the ligands. The absorbance at O.D 550nm is inversely proportional to the cytotoxicity. The higher the absorbance the lesser the cytotoxicity and vice-versa. Data expressed are mean \pm SEM. Statistical analysis was performed by one-way ANOVA followed by Newman-Keuls multiple comparison test (*Statistically significant at $p < 0.05$; ** = $p < 0.01$; *** at $p < 0.001$ and ## at $p < 0.01$).

These observations suggest that GSK0660 had higher inhibitory effect with lesser cytotoxicity. It was chosen as the best candidate to antagonize PPAR β mediated effects and was used at a concentration of 10 μ M for further studies.

3.3.3. *Generating lentivirus to mediate PPAR β silencing*

In the framework of identifying the irradiation effects mediated by PPAR β in the *in-vitro* conditions, we decided to use the lentivirus-based approach to knock down PPAR β in HT-29 cells. Although we had in the lab a lentivirus based vector construct carrying silencing sequence for PPAR β (pLVTHsi PPAR β) that recognize human and mouse PPAR β [Nadra et al., 2006], we had to spend considerable time standardizing the various steps in the production of the lentivirus. For this, we collaborated with the Transgenesis Core Facility (TCF) at EPFL to learn to produce and titrate the lentivirus efficiently. The pLVTH vector carries a marker gene (GFP) downstream of an internal EF1- α promoter allowing an easy detection (or selection by FACS) of infected cells. The vectors can be readily generated at quite high titers (more than a million particles per ml) by cotransfection into 293T cells together with the relevant packaging vectors, pCMV- Δ R8.74 and pMD2G-VSVG, encoding for the envelop and the packaging genes respectively.

We first amplified the vector pLVTHsi PPAR β (for PPAR β knockdown), the control vector- pLVTHsi PPAR β ctrl along with pCMV- Δ R8.74 and pMD2G-VSVG. These vectors were used further to produce the lentivirus by transfecting cell lines having good transfection efficiency - 293T cells. In order to verify the efficiency of the pLVTHsi PPAR β lentivirus produced, the pSuper-siRNA vectors were initially transfected in 293T cells, along with vectors expressing our target gene (PPAR β) fused to green fluorescent protein (GFP). The biological titer of the lentivirus produced was then estimated by FACS analysis. Further, this lentivirus was tested in different concentrations in the HT-29 cell system in order to identify the appropriate Multiplicity of infection (MOI) of virus required to obtain the maximal silencing of our target gene. The knockdown efficiency was also tested at different time-points post infection to ascertain the desired silencing of our gene of interest.

Thus in collaboration with the Transgenesis Core Facility (TCF) at EPFL, we generated the first batch of the lentivirus pLVTHsi PPAR β (S) containing the sequence to silence PPAR β and its control pLVTHsi PPAR β ctrl (SC) with a titer of 1.85×10^6 TU/ μ l and 2.6×10^6 TU/ μ l respectively (Fig. 32).

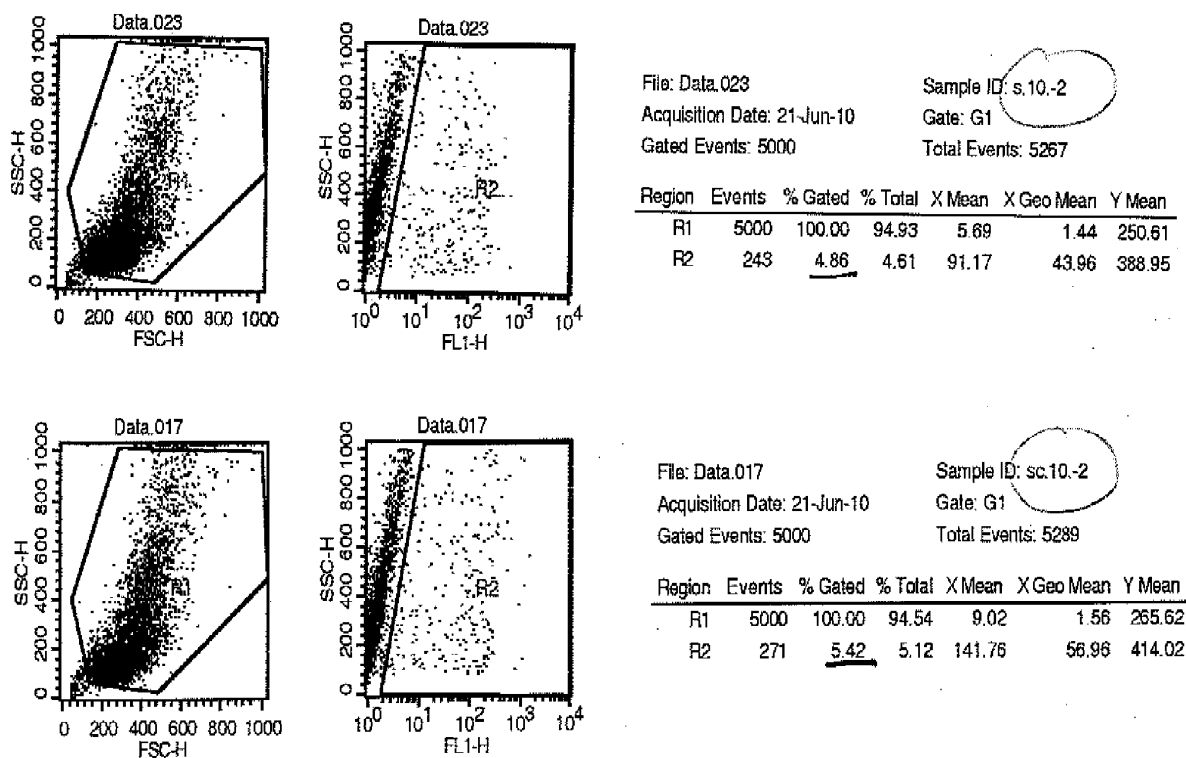


Fig. 32 | Flow cytometric analysis of Green fluorescent protein (GFP) in 293T cells.

293T cells were infected with various dilutions (10^1 , 10^{-1} to 10^{-4}) of either lentivirus construct carrying si PPAR β (S) or si PPAR β ctrl (SC) with a GFP tag. 72h post-infection cells were fixed and analysed by Flow cytometry. Non-infected cells were used for gating. The cells were separated into two populations- the GFP positive and GFP negative cells. The percentage of GFP positive cells in each dilution was used to calculate the titer of the virus. Note that only dilutions yielding 1% to 20% GFP positives were used for titer calculations.

We first determined the appropriate MOI of both S and SC in HT-29 cells by infecting the cells with different MOI (MOI 1, MOI 25, MOI 50, MOI 75 and MOI 100). The efficiency of infection was observed both by fluorescence microscopy (Fig. 33) and FACS for the reporter gene-green fluorescent protein (GFP), which is tagged with our gene of interest PPAR β (Fig. 34 a, b). The results are as summarized in Table-2.

MOI	si PPAR β (S)	si PPAR β Ctrl (SC)
MOI 25	88 %	85.6%
MOI 50	90.2%	89.9%
MOI 75	93.6%	92.1%
MOI 100	94.7%	93.4%

Table- 2 | Multiplicity of infection (MOI) analysis by FACS. HT-29 cells were infected with various concentrations of either lentivirus construct carrying si PPAR β (S) or si PPAR β ctrl (SC) with a GFP tag. 48h post-infection cells were fixed and analysed by Flow cytometry. Non-infected cells were used for gating. The cells were separated into two populations- the GFP positive and GFP negative cells. The percentage of GFP positive cells in each concentration was used to calculate the percentage infection.

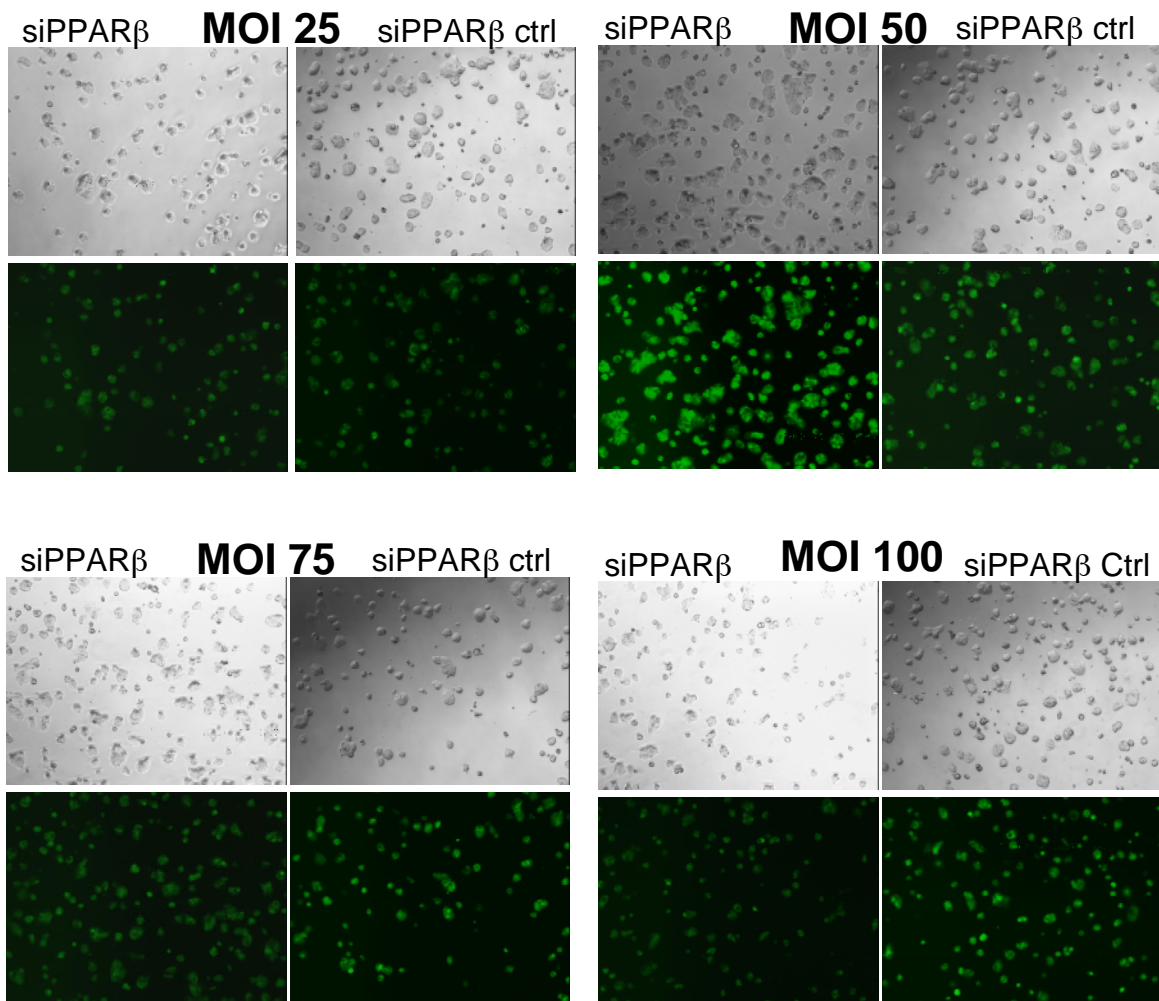


Fig. 33 | Fluorescence microscopy pictures of HT-29 cells infected with lentivirus for either lentivirus construct carrying si PPAR β (S) or si PPAR β ctrl (SC) with a GFP tag. Concentrations ranging from MOI 25 to MOI 100 of each type of virus were used to infect the cells and 48h post-infection cells were analysed by fluorescence microscopy. Non-infected cells were used as negative control. Scale bar: 100 μ m.

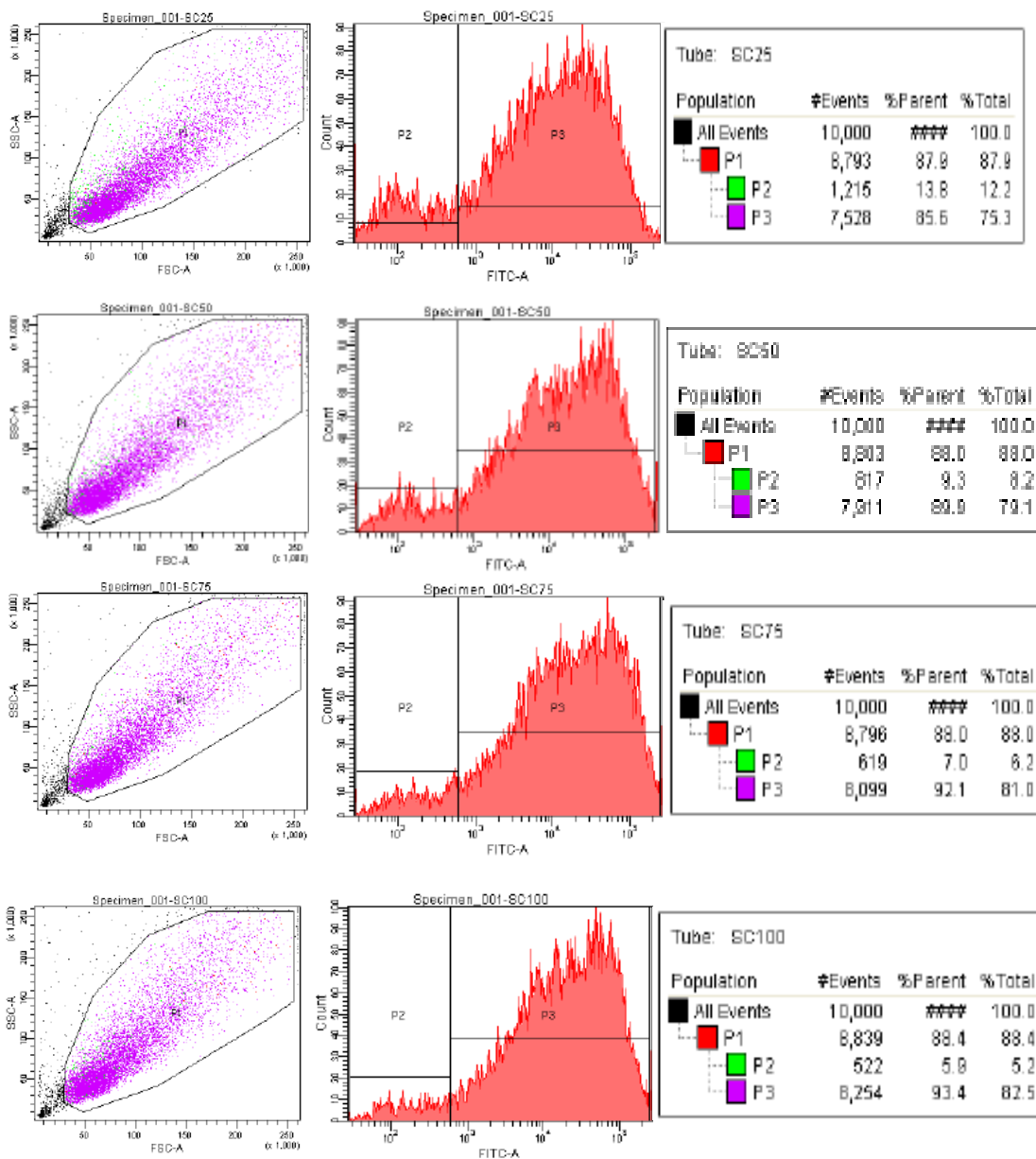


Fig. 34 a | Multiplicity of infection (MOI) analysis by FACS. HT-29 cells were infected with various concentrations of lentivirus construct carrying si PPAR β ctrl (SC) with a GFP tag [SC25, SC50, SC75, SC100]. 48h post-infection cells were fixed and analysed by Flow cytometry. Non-infected cells were used for gating. The cells were separated into two populations- the GFP positive and GFP negative cells. The percentage of GFP positive cells in each concentration was used to calculate the percentage infection.

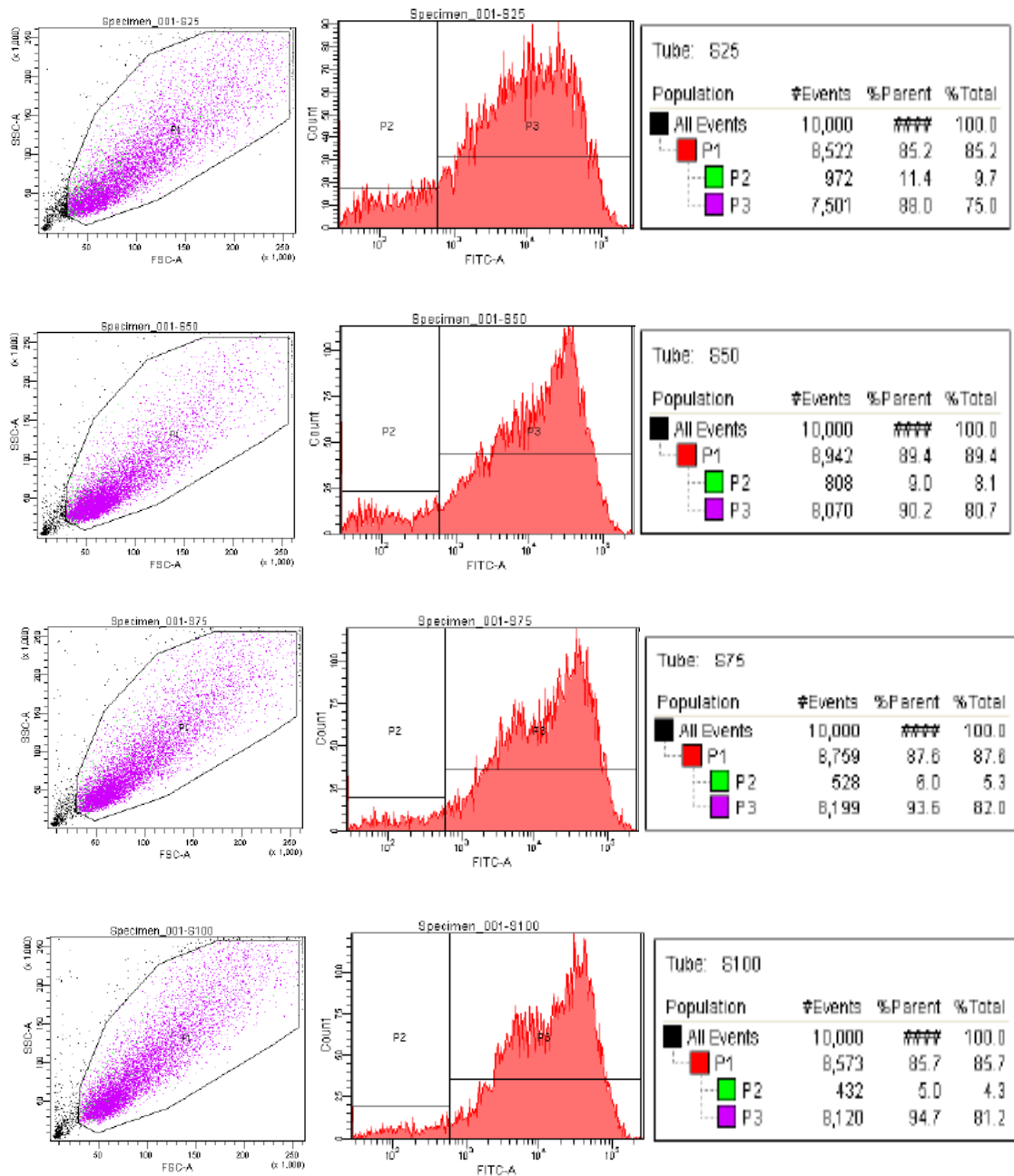


Fig. 34 b | Multiplicity of infection (MOI) analysis by FACS. HT-29 cells were infected with various concentrations of lentivirus construct carrying SiPPAR β (S) with a GFP tag [S25, S50, S75, S100]. 48h post-infection cells were fixed and analysed by Flow cytometry. Non-infected cells were used for gating. The cells were separated into two populations- the GFP positive and GFP negative cells. The percentage of GFP positive cells in each concentration was used to calculate the percentage infection.

From the observations it was evident that both MOI 50 and 75 can effectively infect about 90% of the cells. Further, in order to confirm whether this MOI can efficiently inhibit PPAR β and its activity, we evaluated the relative levels of expression of PPAR β and PDK4 by qPCR analysis in response to MOI 50 (Fig. 35 a, b) and MOI 75 (Fig. 36 a, b) at 24, 36 and 48 hrs after infection.

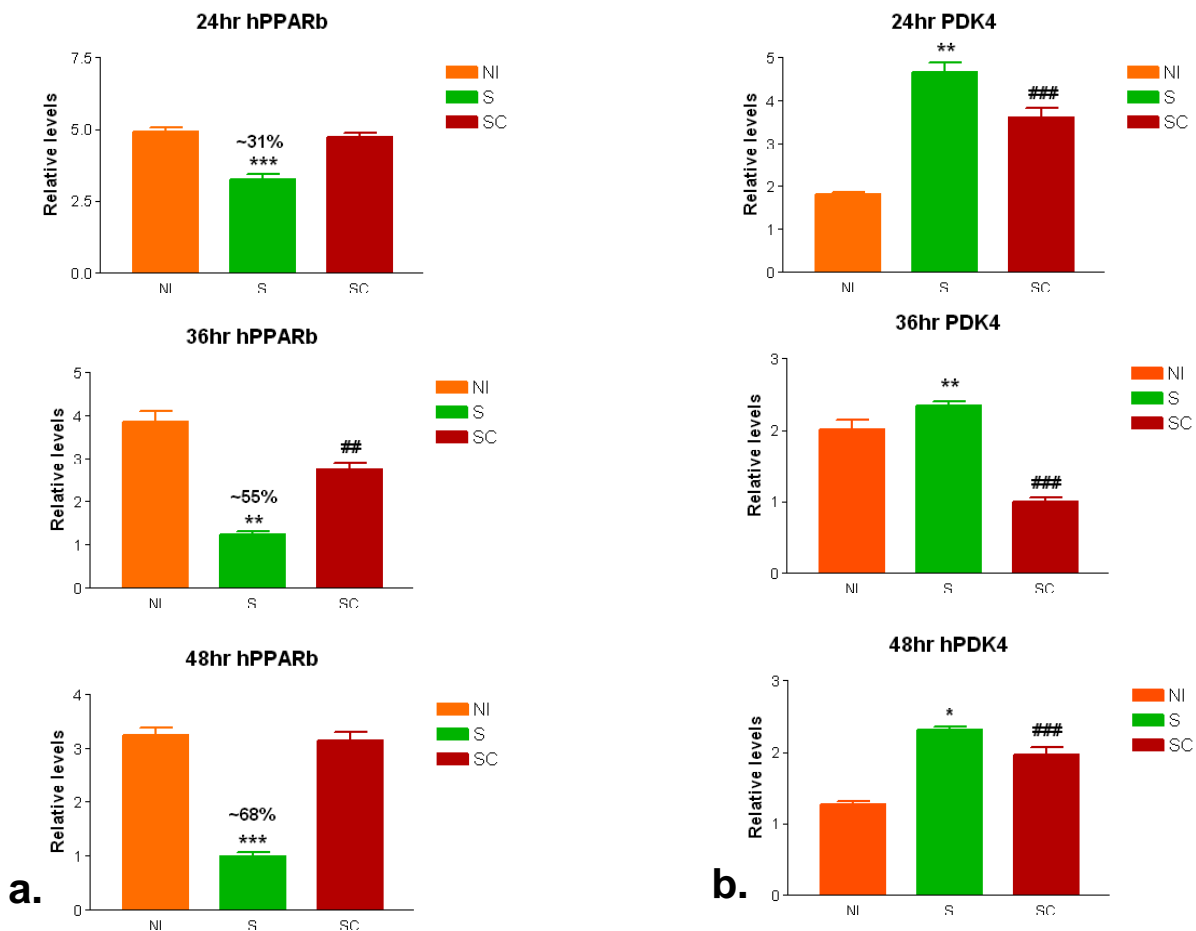


Fig. 35 a, b | Relative expression of (a) PPAR β and (b) PDK4 after infection with S (si PPAR β) and SC (si PPAR β ctrl) at MOI 50 and at three different timepoints - 24, 36, 48h post infection. HT-29 cells were infected with S (si PPAR β) and SC (si PPAR β ctrl) at MOI 50 and at 24, 36, and 48h post-infection, RNA was extracted from cells. Gene expression analysis was performed by SYBR green assay on PPAR β and PDK4. All samples were normalized using two housekeeping genes namely human eukaryotic translation elongation factor 1 alpha 1 (hEEF1A1) and human glucuronidase, beta (hGusB). Note that infection with S was compared with SC and infection with SC compared to non-infected (NI) to determine percentage significance. Data expressed are mean \pm SEM. Statistical analysis was performed by one-way ANOVA followed by Newman-Keuls multiple comparison test. (*Statistically significant at $p < 0.05$, ** $p < 0.01$ and *** $p < 0.001$ when compared to SC; # Statistically significant at $p < 0.01$ and ### at $p < 0.001$ when compared to NI.

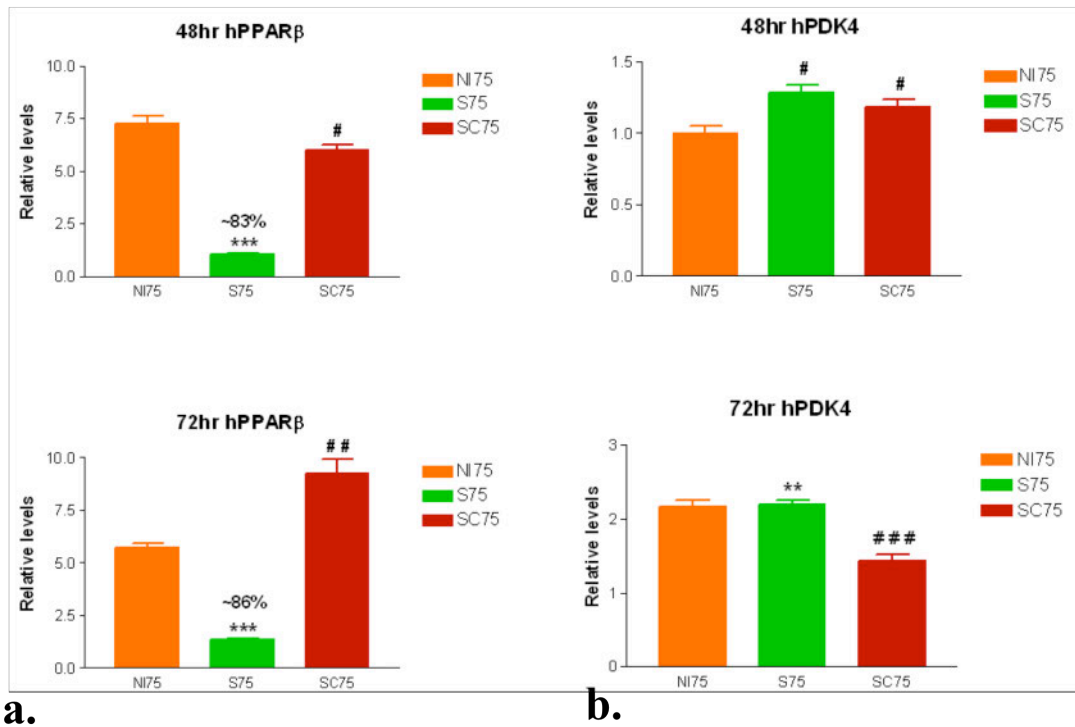
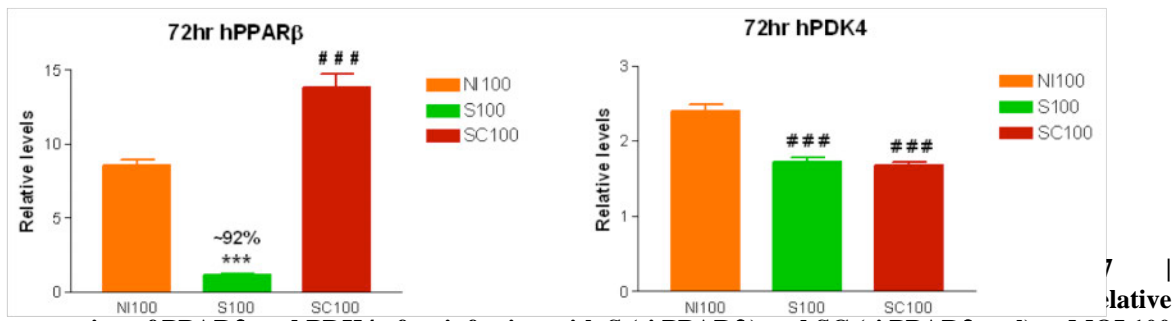


Fig. 36 a, b | Relative expression of (a) PPAR β and (b) PDK4 after infection with S (si PPAR β) and SC (si PPAR β ctrl) at MOI 75 and at 48 and 72h post infection. HT-29 cells were infected with S (si PPAR β) and SC (si PPAR β ctrl) at MOI 75 and at 48h and 72h post-infection, RNA was extracted from cells. Gene expression analysis was performed by SYBR green assay on PPAR β and PDK4. All samples were normalized using two housekeeping genes namely human eukaryotic translation elongation factor 1 alpha 1 (hEEF1A1) and human glucuronidase, beta (hGusB). Note that infection with S was compared with SC and infection with SC compared to non-infected (NI) to determine percentage significance. Data expressed are mean \pm SEM. Statistical analysis was performed by one-way ANOVA followed by Newman-Keuls multiple comparison test. (**Statistically significant at $p < 0.01$ and *** at $p < 0.001$ when compared to SC; # Statistically significant at $p < 0.05$, ## at $p < 0.01$ and ### at $p < 0.001$ when compared to NI).

We also tested the effect of MOI 100 at 72 hrs post infection (Fig. 37) in order to check whether further better inhibition could be attained in comparison to MOI 75. But there was not much difference in the levels of inhibition of PPAR β by MOI 100 in comparison to MOI 75 at 72 h post-infection.



expression of PPAR β and PDK4 after infection with S (si PPAR β) and SC (si PPAR β ctrl) at MOI 100 and at - 72h post infection. HT-29 cells were infected with S (si PPAR β) and SC (si PPAR β ctrl) at MOI 100 and at 72h post-infection, RNA was extracted from cells. Gene expression analysis was performed by SYBR green assay on PPAR β and PDK4. All samples were normalized using two housekeeping genes namely human eukaryotic translation elongation factor 1 alpha 1 (hEEF1A1) and human glucuronidase, beta (hGusB). Note that infection with S was compared with SC and infection with SC compared to non-infected (NI) to determine percentage significance. Data expressed are mean \pm SEM. Statistical analysis was performed by one-way ANOVA followed by Newman-Keuls multiple comparison test. (***)Statistically significant at $p < 0.001$ when compared to SC; ### Statistically significant at $p < 0.001$ when compared to NI).

Of all the different MOI and different time-points post-infection, MOI 75 at 48 hrs post-infection was the most effective condition to silence PPAR β by 83% and was thus considered for further microarray studies. Paradoxically, PDK4 that we used a target gene of PPAR β and for which we expected a down-regulation parallel to that of PPAR β remained stably expressed, if not induced, upon lentivirus infection. This effect is likely due to the fact that PDK4 is an important enzyme in metabolism and is regulated by many other factors than PPAR β . The condition of lentivirus infection might therefore perturb the pathway to which PDK4 belongs, overriding a possible response generated by the lack of PPAR β .

3.3.4. Irradiation experiments: fine-tuning the condition of cell irradiation

To observe irradiation-mediated cell damage in HT-29, we performed a study to evaluate the effect of different doses of irradiation (ranging from 0-30 Gy) at different timepoints post-irradiation. In order to confirm cell damage, we assessed apoptosis using Caspase- 3/7 as a marker for early apoptosis using the Caspase-Glo® 3/7 Assay kit (Promega).

The Caspase-Glo® 3/7 Assay kit provides a homogeneous luminescent assay that measures caspase-3/7 activities (see materials and methods). We used this Caspase assay at different time-points, i.e. 4h, 6h, and 24h post irradiation. As there were no signs of apoptosis at 4h post irradiation (data not shown), we decided to keep 6h and 24h time-point post irradiation.

We observed that at 6h post-irradiation (Fig. 38), there was significant increase in the Caspase-3/7 activity at doses starting from 10Gy till 30Gy, whereas at 6Gy it remained unaltered. As Caspase-3/7 is a marker of early apoptosis, this indicates that a dose of 10Gy could damage the cells sufficiently enough to initiate apoptosis as early as 6h post-irradiation.

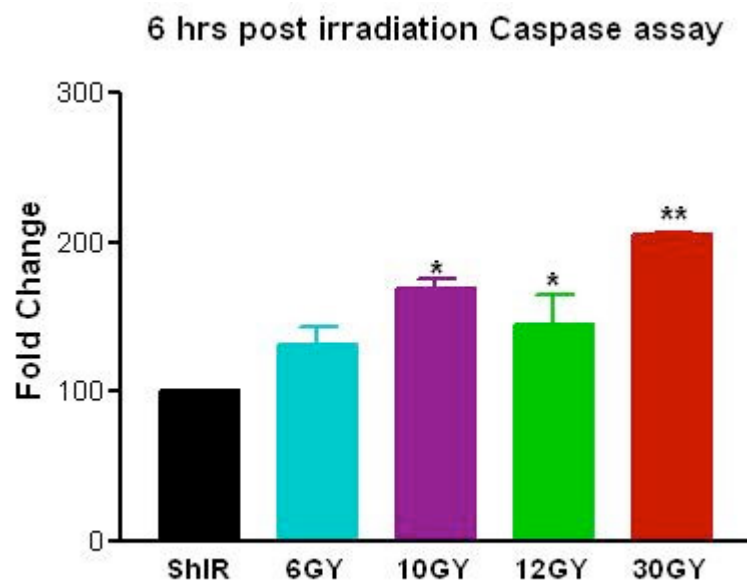


Fig. 38 | Caspase-3/7 assay at 6h post-irradiation with different doses of irradiation. HT-29 cells were irradiated with different doses of irradiation ranging from 0-30Gy and sham-irradiated (ShIR) cells served as control. At 6h post-irradiation, all sets of cells were lysed and analysed using the Caspase- 3/7 assay kit. Luminescence emitted due to caspase-3/7 cleavage of the luminogenic substrate was measured for each dose at 6h post irradiation. Luminescence measured was proportional to the caspase activity present and the signal from no cell control was subtracted from the signal from the treated and untreated controls. The fold change values were calculated with Sham irradiated cells (ShIR) as control group for statistical calculations. Data expressed are mean \pm SEM. Statistical analysis was performed by one-way ANOVA followed by Newman-Keuls multiple comparison tests. (*Statistically significant at $p < 0.05$ and ** $p < 0.01$ when compared to sham ShIR).

We also observed the effects of irradiation till 24h post-irradiation (Fig. 39). We could see significant apoptosis in cells irradiated with 10Gy and 30Gy, but the basal levels

of Caspase-3/7 activation in the control group was too low suggesting that a repair process might be already in progress to rescue the cells from the damage.

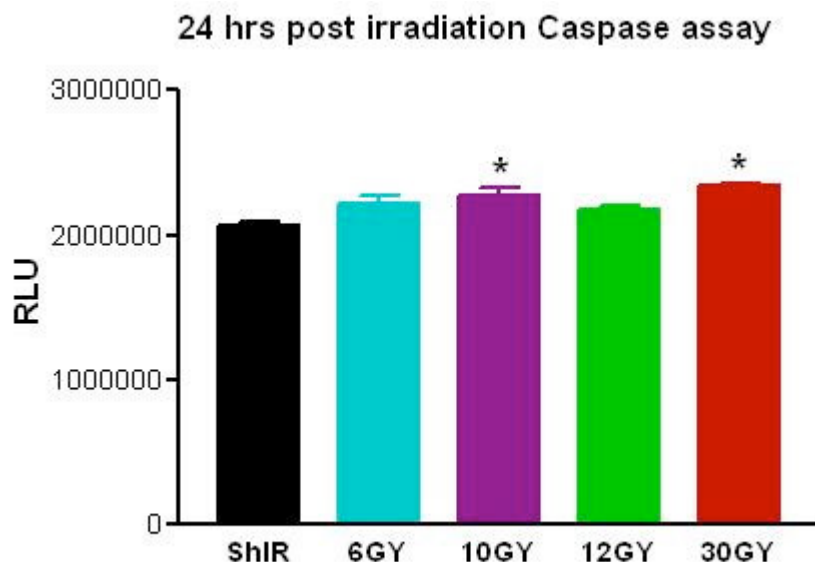


Fig. 39 | Caspase-3/7 assay at 24h post-irradiation with different doses of irradiation. HT-29 cells were irradiated with different doses of irradiation ranging from 0-30Gy and sham-irradiated (ShIR) cells served as control. At 6h post-irradiation, all sets of cells were lysed and analysed using the Caspase- 3/7 assay kit. Luminescence emitted due to caspase-3/7 cleavage of the luminogenic substrate was measured for each dose at 24h post irradiation. Luminescence measured was proportional to the caspase activity present and the signal from no cell control was subtracted from the signal from the treated and untreated controls. The fold change values were calculated with Sham irradiated cells (Sh.I) as control group for statistical calculations. Data expressed are mean \pm SEM. Statistical analysis was performed by one-way ANOVA followed by Newman-Keuls multiple comparison test. (*Statistically significant at $p < 0.05$ when compared to sham ShIR).

3.3.5. Studies on cholesterol biosynthesis pathway using HT-29 cell culture model

In order to reconfirm our *in-vivo* observations and to decipher the molecular mechanism by which PPAR β contributes to the cell response to irradiation, and along the setup based on the results discussed above, we irradiated HT-29 cells at a dose of 10Gy. qPCR analyses of a set of genes of interest were then performed in samples retrieved at different time points, 4h, 24h, 48h and 72h. Sham-irradiated HT-29 cells served as control. The genes to be tested were selected based on their p-value from the microarray data of Federic Varnat.

We observed an upregulation at 24h post-irradiation of PDK1, a target gene of PPAR β , indicating that PPAR β is activated in this condition (Fig. 40). While FDFT1, LSS and MVD were found to be upregulated significantly in the scraped mucosa samples from PPAR $\beta^{+/+}$ mouse intestine at 4hr post-irradiation, this response was delayed in HT-29 at 24hr post irradiation, with increased expression of FDFT1 and LSS of the cholesterol biosynthetic pathway whereas MVD remained unaltered. At this time point also, the expression levels of PPAR β remain unaltered but the levels of caspase-8 (the effector caspase for apoptosis) were significantly upregulated.

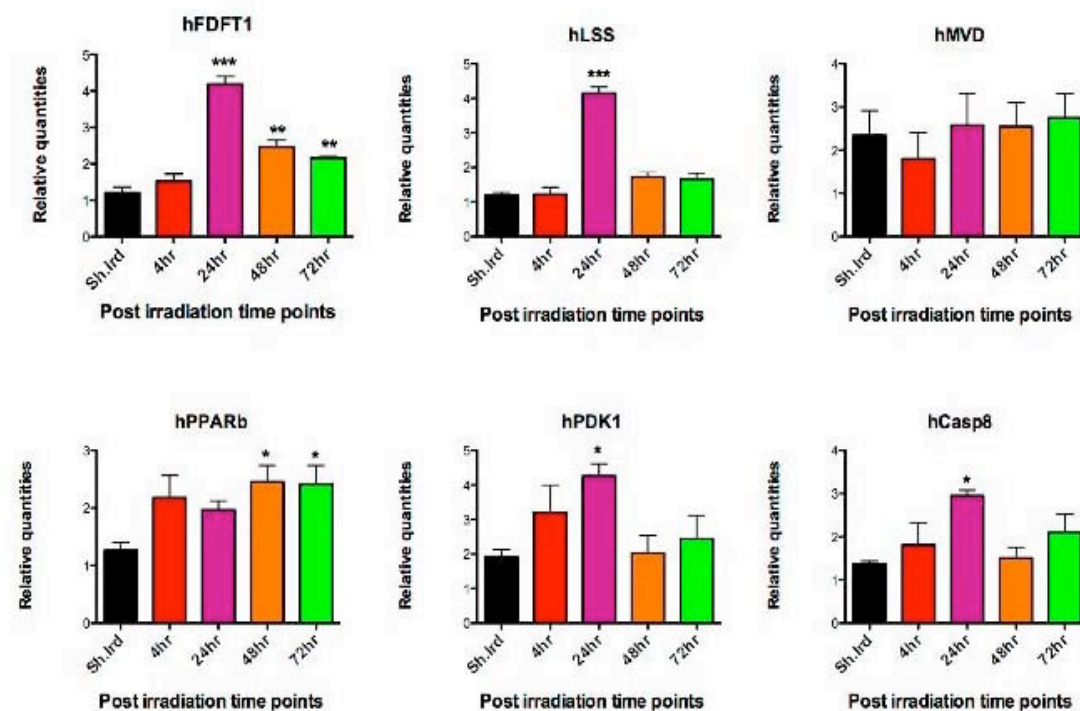


Fig. 40 | Effect of 10Gy irradiation on gene expression in HT-29 cells at different time-points (4, 24, 48 and 72h) post- irradiation. HT-29 cells were irradiated with a dose of 10Gy and sham-irradiated (ShIR) cells served as control. At 4, 24, 48, and 72h post-irradiation, RNA was extracted from cells. Gene expression analysis was performed by SYBR green assay on the following genes - Farnesyl-diphosphate farnesyl transferase 1 (FDFT1), Lanosterol synthase (LSS), Mevalonate (diphospho) decarboxylase (MVD), Peroxisome proliferator-activated receptor β (PPAR β), Pyruvate dehydrogenase kinase isozyme 1 (PDK1), Caspase8 (Casp8- effector capsase). All samples were normalized using two housekeeping genes namely human eukaryotic translation elongation factor 1 alpha 1 (hEEF1A1) and human glucuronidase, beta (hGusB). Data expressed are mean \pm SEM. Statistical analysis was performed by one-way ANOVA followed by Newman-Keuls multiple comparison tests. (*Statistically significant at $p < 0.05$, **at $p < 0.01$ and *** at $p < 0.001$ in comparison to sham-irradiated (ShIR) cells).

3.4 Global gene expression analysis using microarray to identify the effect of irradiation at 10Gy.

Microarray studies have been the method of choice in the recent years to evaluate the large-scale gene expression changes in tissues or cells in response to physical or chemical stimuli (DeRisi 1997; Axelson et al., 2007). A global gene expression analysis using microarray was thus performed to identify the effect of irradiation at 10Gy in an *in-vitro* intestinal cell line model of HT-29. The experimental design was as follows.

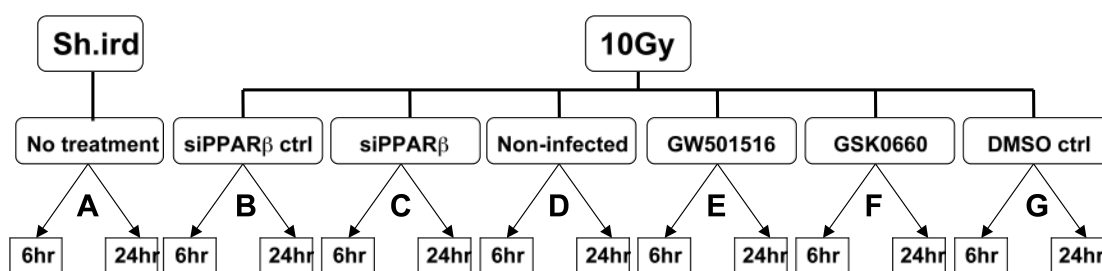


Fig. 41: Experimental design for microarray. Seven groups (A-G) were planned to evaluate the effect of 10Gy irradiation on HT-29 cells at two different timepoints post-irradiation (6h and 24h) and also to explore the role of PPAR β by either silencing it using lentivirus or with PPAR β specific agonist (500nM GW501516) and antagonist (10 μ M GSK0660) treatment. Sham-irradiated group-A (Sh.ird) without any other treatment would serve as control for all six groups (B-G) of 10Gy-irradiation (10Gy) with various other treatments. Infection with si PPAR β ctrl (B) would serve as control for si PPAR β infection(C). Non-infected group (D) would serve as control for infection with si PPAR β ctrl and si PPAR β (B, C). DMSO ctrl (G) would serve as control for both group-E: agonist (GW501516) and group-F: antagonist (GSK0660) treatment.

According to the above-mentioned set-up, we performed the RNA extraction for each sample, followed by some qPCRs to assess the quality of the experiment and evaluate PPAR β silencing. Unfortunately, the results showed that PPAR β silencing was extremely mild, with an expression levels remaining at around 70% of the control infected cells. This led us to perform a series of tests to identify the cause of this problem. We finally could demonstrate that the quality of the virus preparation was responsible of this failure. Therefore, the following microarrays analyses were only performed on the set of conditions with no viral infection.

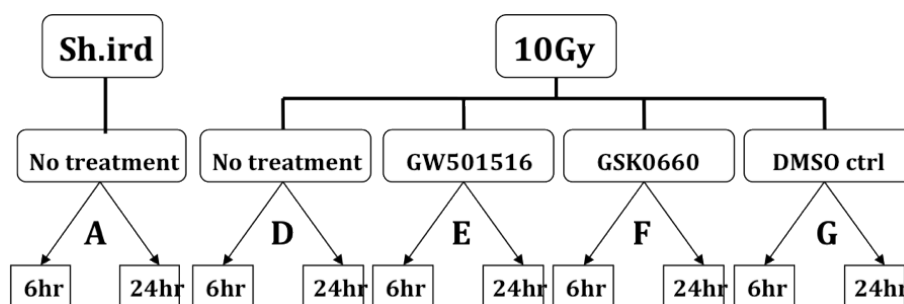


Fig. 42: Final modified experimental design used for the microarray analyses. Originally seven groups (Fig. 41, A-G) were planned to evaluate the effect of 10Gy irradiation on HT-29 cells at two different timepoints post-irradiation (6h and 24h). Of these two groups that were designed to explore the role of PPAR β by silencing it using lentivirus were eliminated due to mild silencing effects. Instead, we evaluated the role of PPAR β with PPAR β specific agonist (500nM GW501516) and antagonist (10 μ M GSK0660) treatment. Sham-irradiated group-A (Sh.ird) without any other treatment would serve as control for all four groups (D-G) of 10Gy-irradiation (10Gy) with various other treatments. DMSO ctrl (G) would serve as control for both group-E: agonist (GW501516) and group-F: antagonist (GSK0660) treatment.

Using the microarray data, we first analyzed the expression profiles of HT-29 cells treated with 10Gy irradiation at 6h and 24h post irradiation, in comparison with that of control sham-irradiated cells, at the same time points post irradiation. It was observed that most genes that were differentially expressed show low fold-change. Hence, in the data shown below, we have not made any fold-change cut-offs, but have only kept those for which the p-value was significant.

Clustering analysis of the microarray results was performed using ‘R’ for quality control (Fig. 43). The cluster analysis for all the 33,297 probesets on the chip groups the biological replicates together as expected. The timepoint effect, i.e. gene expression changes during the course of time from 6h to 24h were found to be the highest as observed by longer distance in the cluster map. The effect of irradiation i.e. gene expression modulated between the irradiated and the sham-irradiated group is seen to be prominent at 24h post-irradiation as compared to the 6h post-irradiation, as observed by longer distance in the cluster map. This same pattern was observed for both the timepoint effect and irradiation effect when the cluster analysis was done for a small subset of 1000 most differentially expressed genes. As an effect of the irradiation upon treatment with the ligands, we see very few changes during the course of time from 6h to 24h but the effect is higher at 6h upon treatment with ligands in comparison to untreated group.

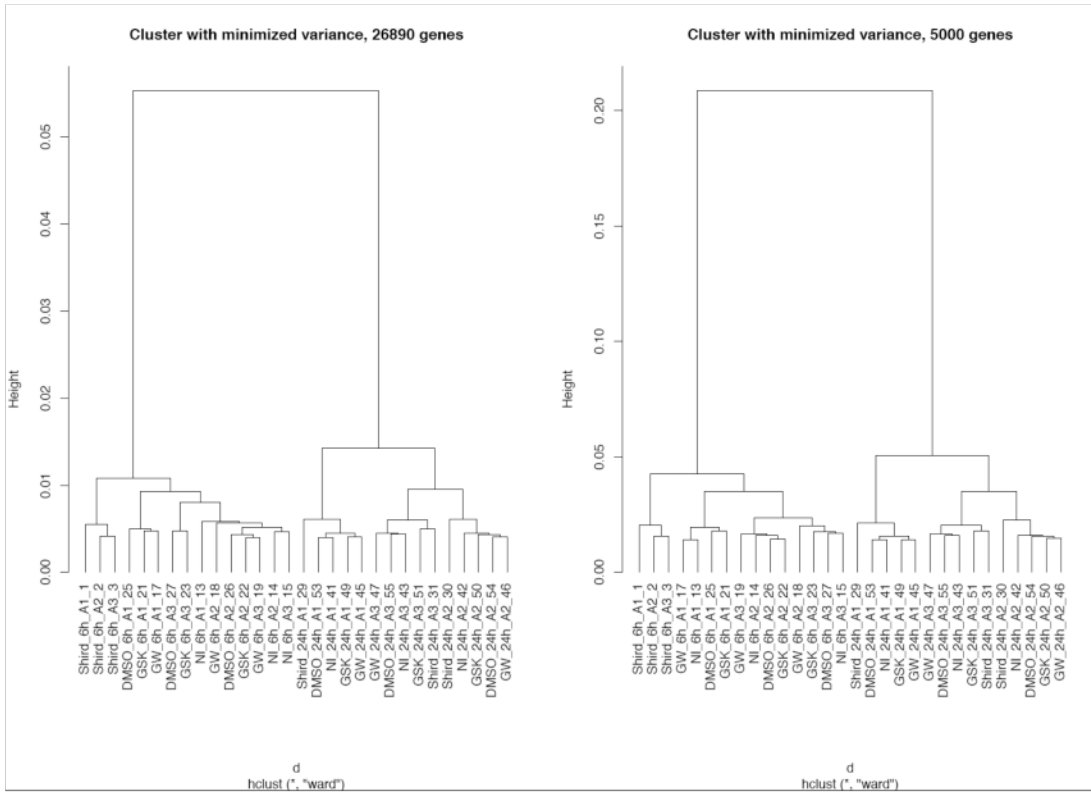


Fig. 43 | Cluster analysis of the gene expression datasets from microarray experiments showing clustering of the most differentially regulated genes with the different number of probesets (26890, 5000) on the chip. Gene expression analysis was carried out on cRNA samples obtained from the various groups outlined in figure- 42 using Affymetrix Human Gene 1.0 ST arrays (Affymetrix, SC, USA). Gene expression was analysed using the software Expression Console and the data was submitted to one-way ANOVA with $p < 0.05$ considered significant. Clustering analysis of the data was performed using ‘R’ for quality control. Legends: Shird_6h and Shird_24h (Sham-irradiated at 6 and 24h post sham-irradiation; group- A), NI_6h and NI_24h (No treatment except 10Gy at 6 and 24h post- irradiation), GW_6h and GW_24h (PPAR β agonist GW501516 treatment at 6 and 24h post 10Gy irradiation), GSK_6h and GSK_24h (PPAR β antagonist GSK0660 treatment at 6 and 24h post 10Gy irradiation), DMSO_6h and DMSO_24h (DMSO vehicle control for agonist and antagonist treatment at 6 and 24h post 10Gy irradiation), A1, A2, A3 were the three biological replicates for each group of sample.

2.4.4 Gene expression changes as an effect of 10Gy Irradiation in HT-29 cells

From the analysis of the microarray data, as an effect of irradiation, we observed a total of 418 genes modulated at 6h and 1168 genes at 24h with a p-value cut-off of 0.05 (Fig. 44). Of these, 144 genes were common to both time points.

In our experiments, 10 Gy irradiation induced increase in expression levels of NFκB2, decrease of Cyclin B1 prominently and several other genes were regulated moderately at 6h post-irradiation (Table 3). We observed increase in the expression of the cyclin dependent kinase inhibitor CDKN2B/ p15, that forms a complex with CDK4/CDK6 and inhibits the activation of the CDK kinases. This protein thus functions as a cell growth regulator that controls cell cycle G1 progression. It is believed to play a role in TGF-β induced growth inhibition. We did not observe the modulation of the most commonly upregulated p53 target gene – CDKN1A (p21/WAF1/Cip1), that acts as an inhibitor of the CDK2/CDK4 complex and thus regulates the cell cycle G1 progression in a p53 dependent manner. Also, we did not observe the modulation of any other p53 dependent DNA damage response target genes like MDM2, Gadd45. Thus, this indicates a p53-independent activation of the process of cellular repair.

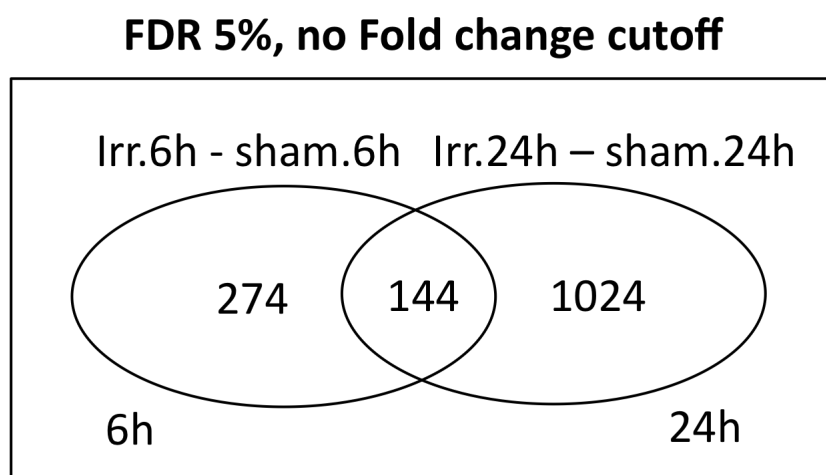


Fig. 44 | Venn diagram showing the most differentially regulated genes obtained in the microarray experiments between 10Gy irradiated and sham-irradiated groups at two different timepoints post irradiation. This comparison gives us information on expression of genes as an effect of irradiation. [Irr.6h= 10Gy irradiated at 6h, sham.6h= sham-irradiated at 6h, Irr.24h= 10Gy irradiated at 24h, sham.24h= sham-irradiated at 24h].

ID	FoldChange	adj.p.val	Gene.Symbol
7930074	2.51	1.62E-06	NFKB2
8125512	2.26	8.38E-05	TAP1
8178867	2.26	8.38E-05	TAP1
8180061	2.26	8.38E-05	TAP1
8124650	2.95	8.38E-05	UBD
8178295	2.82	9.27E-05	UBD
7992828	2.36	0.000145999	IL32
8101126	2.68	0.000182832	CXCL10
8161610	2.09	0.000246076	C9orf71
8029580	2.36	0.000246076	RELB
7958895	1.61	0.000320707	OAS3
7900699	-1.74	0.000444479	CDC20
8046861	1.55	0.000444479	ITGAV
7957850	-2.05	0.000444479	GAS2L3
8056361	-1.62	0.000467284	---
8082100	1.62	0.000589789	PARP14
8112139	1.40	0.000700155	IL6ST
7926239	1.53	0.000748975	OPTN
8041170	-2.06	0.000883865	---
8178977	1.41	0.000883865	TAPBP
8004167	-1.75	0.000883865	FAM64A
8006531	1.60	0.000943684	SLFN5
8115147	1.42	0.00096581	CD74
8122265	1.80	0.001056807	TNFAIP3
8084524	-1.52	0.001056807	EPHB3
8086125	1.58	0.001056807	TRANK1
8180166	1.40	0.001056807	TAPBP
8173444	1.69	0.001301434	IL2RG
8150889	1.52	0.001301434	SDR16C5
8112260	-1.45	0.001343433	DEPDC1B
8105828	-1.69	0.00138559	CCNB1
8143327	1.42	0.001402071	PARP12
7983969	-1.46	0.001413742	CCNB2
8021653	1.41	0.001466214	SERPINB8
8125713	1.40	0.001471355	TAPBP
7977046	2.63	0.001482346	TNFAIP2
8040712	-1.55	0.00148968	CENPA
8095680	1.94	0.001497825	IL8
8077786	1.41	0.001509738	IRAK2
8108301	-2.28	0.001509738	KIF20A
8160452	1.39	0.001509738	CDKN2B
8152719	-1.64	0.00164887	ANXA13
8140967	1.47	0.001935472	SAMD9
8066247	-1.36	0.001980552	LOC388796
7952601	1.53	0.001983989	ETS1
8096635	1.34	0.002025303	NFKB1
8010260	-1.30	0.002200225	BIRC5
8038725	1.42	0.002200225	KLK10
7909146	-1.80	0.002200225	FAM72D

Table - 3 | The list of top 50 genes regulated as an effect of 10Gy irradiation in HT-29 cells at 6h post-irradiation.

Interestingly, the irradiation effects at 24h post irradiation were mainly targeted at the histone proteins (Table 4). This correlates with previous reports by Meador et al.

(2011) where they confirm that both high- and low-Linear energy transfer (LET) radiation exposure negatively regulate histone gene expression in human lymphoblastoid and colon cancer cell lines independent of p53 status.

ID	FoldChange	adj.p.val	Gene.Symbol
8117580	-1.67	0.0038	HIST1H2AI
8124510	-1.68	0.0038	HIST1H2BL
8085350	-1.37	0.0038	C3orf31
8096335	2.04	0.0038	HERC6
8140967	1.96	0.0038	SAMD9
7929052	3.08	0.0038	IFIT3
8124430	-1.68	0.0038	HIST1H1D
8124524	-2.00	0.0038	HIST1H2AK
8050537	1.72	0.0038	MATN3
8117589	-1.49	0.0040	HIST1H3H
8096301	-1.72	0.0040	SPP1
8103601	2.11	0.0040	DDX60L
7929047	3.55	0.0041	IFIT2
8124397	-1.52	0.0044	HIST1H1C
7961413	1.57	0.0044	C12orf36
7927710	1.52	0.0044	CDK1
8103563	2.91	0.0045	DDX60
8001133	1.46	0.0045	SHCBP1
8048926	1.88	0.0046	SP140L
8161892	-1.60	0.0046	GNA14

Table- 4 | The list of top 20 genes regulated as an effect of 10Gy irradiation in HT-29 cells at 24h post-irradiation. Genes highlighted indicate key genes coding for various histone proteins and cell cycle regulatory proteins (For details, see text).

3.4.2. GeneGo pathway analysis of the microarray data

Analysis of the microarray data was also done using the GeneGO Metacore pathway analysis software to determine the cellular pathways affected upon Irradiation. MetaCore™ is an integrated knowledge database and software suite for pathway analysis of experimental data and gene lists generated by various studies like microarray, sequence based gene expression studies, etc. It is based on a proprietary manually curated database of human protein-protein, protein-DNA and protein compound interactions, metabolic and signaling pathways for human, mouse and rat, supported by proprietary ontologies and controlled vocabulary (<http://www.genego.com/metacore.php>).

The GeneGO analysis of the top-10 modulated canonical pathways throughout the entire dataset indicates that the most modulated probe sets belong to cell cycle (metaphase

checkpoint, role of APC in cell cycle regulation), apoptosis and survival (anti-apoptotic TNFs/NF- κ B/Bcl-2 pathway, APRIL and BAFF signaling), immune response (IL-2 activation and signaling pathway, signaling pathway mediated by IL-6 and IL-1) (Fig. 45). Thus, it gives us a clear picture that the irradiation effects are mainly targeting important cellular processes such as cell cycle checkpoint regulation, immune response and apoptosis and survival pathways.



Fig. 45 | GeneGo analysis of the top 10 modulated canonical pathways throughout the entire dataset across two different timepoints - 6h and 24h post irradiation. The first 10 Canonical pathways generating significant score are displayed as a bar chart along the Y-axis. The X-axis represents the score; the taller the bar, the better the score for the indicated pathway.

3.4.3. Gene expression changes as an effect of treatment with agonist of PPAR β

To identify the role of PPAR β in irradiation-mediated effects, we pre-treated the cells with PPAR β agonist (GW) and antagonist (GSK) at the previously determined dose at which they showed optimal activity in this cell type. As an effect of the agonist (GW) treatment, we observed a total of 3 genes modulated at 6h and 13 genes at 24h with a p-value cut-off of 0.05 (Fig. 46A).

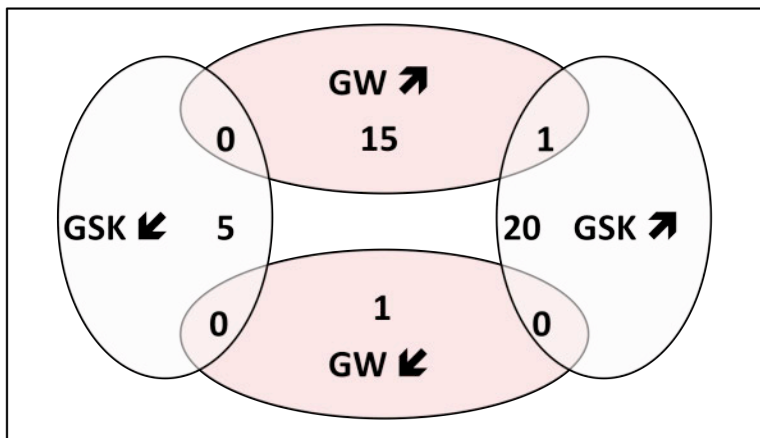
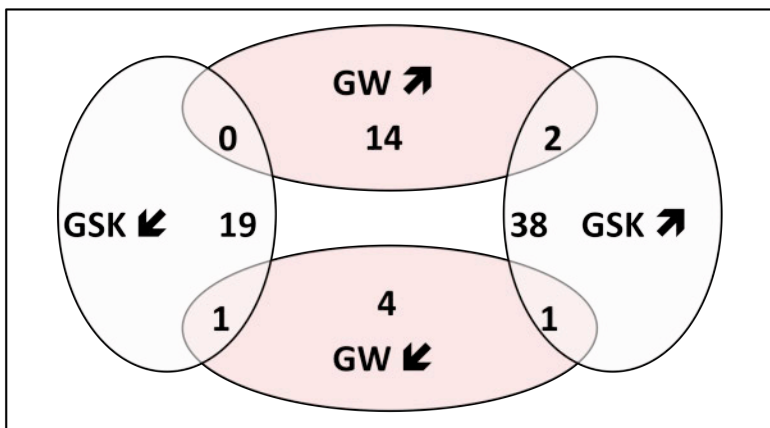
A : FDR 5%, no fold change cut off**B : FDR 10%, no fold change cut off**

Fig. 46 | Venn diagram showing the most differentially regulated genes between 10Gy-irradiated pretreated with PPAR β ligands - agonist (GW), antagonist (GSK), and 10Gy-irradiated DMSO treated control group. A: With a false discovery rate (FDR) of 5% and B: with a FDR of 10%. This comparison gives us information on expression pattern of genes upon ligand treatment and irradiation.

The genes that were modulated at 6h are PDK4, SLC25A20, and ACADVL. PDK4 showed three fold increase at 6h post-irradiation. This upregulation of PDK4 (pyruvate dehydrogenase kinase, isoenzyme 4) - a known PPAR β target gene indicates that the ligand treatment in this cell type and experiment is functional. SLC25A20 - solute carrier family 25 (carnitine/acylcarnitine translocase), member 20 is a mitochondrial-membrane carrier protein that mediates the transport of acylcarnitines into mitochondrial matrix for their oxidation by the mitochondrial fatty acid-oxidation pathway. ACADVL (acyl-CoA dehydrogenase, very long chain) is transported to the inner mitochondrial membrane

where it catalyzes the first step of the mitochondrial fatty acid beta-oxidation pathway. It is specific to long-chain and very-long-chain fatty acids.

At 24h, we observed an increase in the expression of known PPAR β target genes such as PDK4 and ANGPTL4, PLIN2/ADRP and HMGCS2 (Table-5). PDK4 and ANGPTL4 increased to five and three fold respectively at 24h post-irradiation. The expression of ADRP/PLIN2 and HMGCS2 were increased 2.5 and 2 fold respectively at 24h post-irradiation. The top modulated genes at both 6h and 24h post irradiation belonged to various metabolic pathways like lipid metabolism, mitochondrial long chain fatty acid beta-oxidation, mitochondrial unsaturated fatty acid beta-oxidation, ketone bodies biosynthesis and metabolism (Fig. 47).

ID	FoldChange	adj.P.Val	Gene.Symbol
8141094	5.07	2.16E-08	PDK4
7949971	1.88	4.61E-06	CPT1A
8160297	2.73	0.000194207	PLIN2
8025402	2.70	0.000194207	ANGPTL4
8087224	1.88	0.000194207	SLC25A20
7939298	1.29	0.008564907	CAT
7919055	1.86	0.009225528	HMGCS2
8004271	1.40	0.009225528	ACADVL
8103951	1.28	0.013944265	ACSL1
8160284	1.32	0.035157544	HAUS6
7940341	1.25	0.035157544	MS4A10
8023261	1.29	0.039168928	ACAA2
8092021	1.47	0.039168928	LRRC31
7960730	1.21	0.050480634	LPCAT3

Table-5 | The list of top 15 genes regulated as an effect of agonist pre-treatment followed by 10Gy irradiation in HT-29 cells at 24h post-irradiation. The genes have been selected based on the cut-off of p-value at $p < 0.05$.

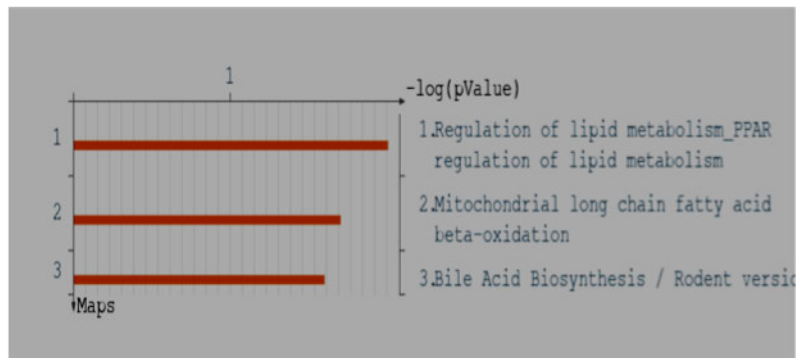
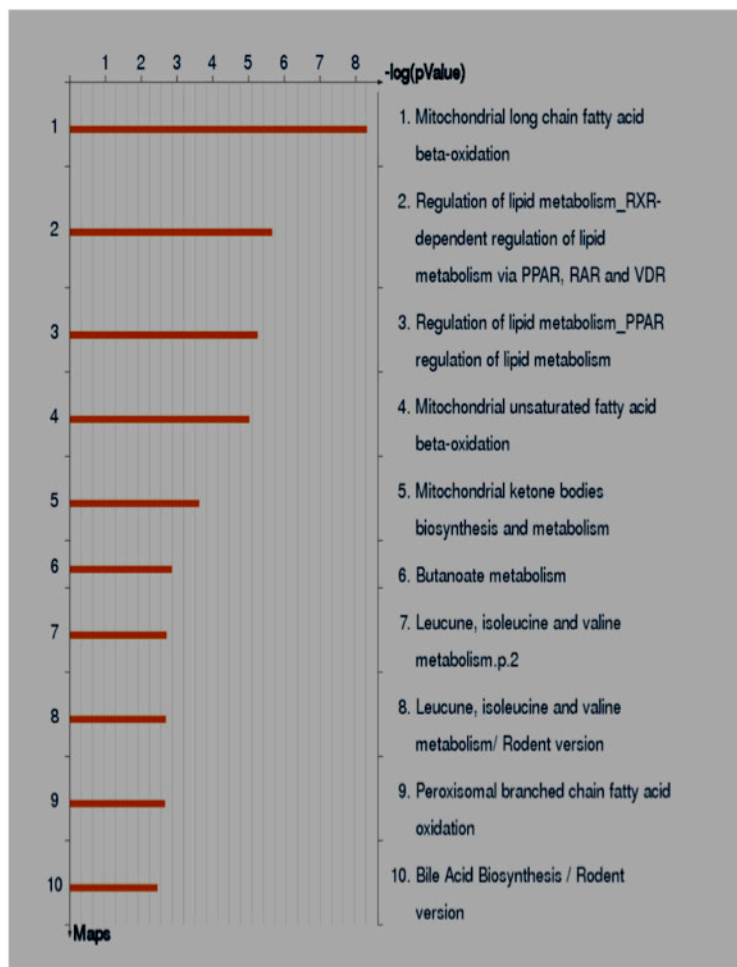
GW vs DMSO at 6h**GW vs DMSO at 24h**

Fig. 47 | GeneGo analysis of the top 10 modulated canonical pathways upon agonist (GW) treatment throughout the entire dataset across two different timepoints - 6h and 24h post irradiation. The first 10 Canonical pathways generating significant score are displayed as a bar chart along the Y-axis. The X-axis represents the score; the taller the bar, the better the score for the indicated pathway.

3.4.4. *Gene expression changes as an effect of treatment with antagonist of PPAR β*

As an effect of the antagonist (GSK) treatment, with a p-value cutoff of 0.05, only 2 genes were modulated at 6h. At 24h, 23 genes were modulated (Fig. 48A), among which the 2 genes [(LRRRC31-Leucine rich repeat containing 31) and (AKR1B10-Aldo-keto reductase family 1, member B10)] found in the 6h time-point. The LRRRC31-Leucine rich repeat containing 31 belongs to the family of proteins containing the LRR motif. LRR is a 20-29 residue sequence motif present in many proteins that participate in protein-protein interactions and have different functions and cellular locations. LRRs correspond to structural units consisting of a beta strand (LxxLxLxxN/CxL conserved pattern) and an alpha helix. AKR1B10 (aldo-keto reductase family 1, member B10 (aldose reductase)) is a member of the aldo/keto reductase superfamily and can efficiently reduce aliphatic and aromatic aldehydes. There is data from literature that suggest that AKR1B10 affects cell survival through modulating lipid synthesis, mitochondrial function, and oxidative status, as well as carbonyl levels, thereby being an important cell survival protein.

At 24h post irradiation, we found the androstenedione and testosterone metabolism, estradiol metabolism and cortisone biosynthesis and metabolism, tyrosine metabolism pathways being modulated (Fig. 48). With a very strict *p*-value cut-off of 0.05, we found only 23 genes modulated (Table-6) and thus we tested with a higher *p*-value cut-off of 0.1 (Fig. 48B) and still we found very few genes modulated upon antagonist treatments. The GeneGo pathway analysis of the microarray data gave us a clear picture that the antagonist treatments mainly targeted the important metabolic pathways at 6h and at 24h post irradiation.

ID	FoldChange	adj.P.Val	Gene.Symbol
8136336	1.55	0.002	AKR1B10
8096116	1.45	0.004	AGPAT9
8124707	1.42	0.007	TRIM31
7925929	1.33	0.008	AKR1C3
8115397	-1.34	0.008	C5orf4
8179617	1.41	0.008	TRIM31
8005475	1.28	0.008	TRIM16L
8178330	1.41	0.010	TRIM31
7958174	1.23	0.015	TXNRD1
8172204	1.33	0.015	MAOB
7931832	1.58	0.015	AKR1C2
8171435	1.34	0.015	PIR
7955297	-1.32	0.017	AQP5
8127158	1.37	0.017	GCLC
8049349	1.39	0.017	UGT1A1
7987565	-1.35	0.019	PPP1R14D
8098246	1.48	0.023	ANXA10
8013384	1.45	0.023	ALDH3A1
8021584	1.31	0.026	SERPINB5
7929388	1.41	0.030	PLCE1
8140984	-1.53	0.030	HEPACAM2
8101675	1.37	0.034	ABCG2
8138466	-1.24	0.040	MACC1

Table - 6 | The list of top genes regulated as an effect of antagonist pre-treatment followed by 10Gy irradiation in HT-29 cells at 24h post-irradiation. The genes have been selected based on the cut-off of p-value at $p < 0.05$.

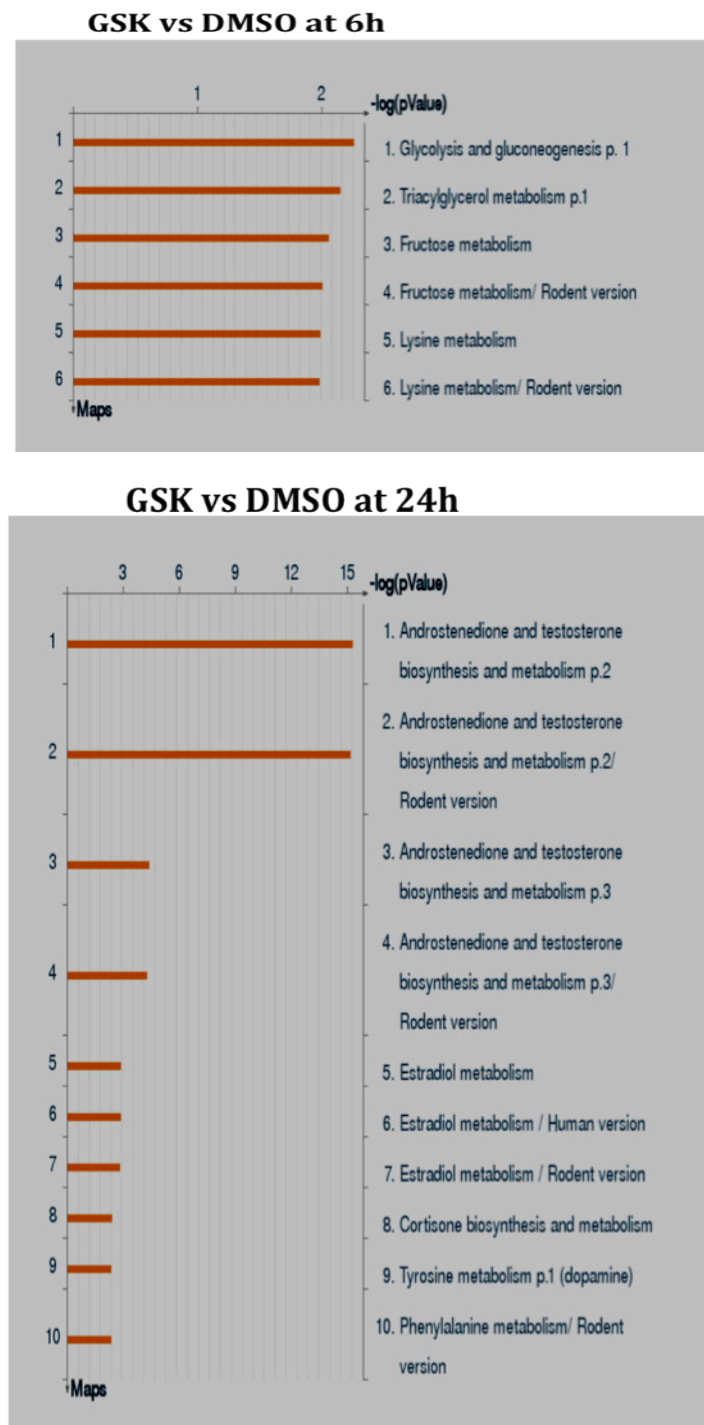


Fig. 48 | GeneGo analysis of the top 10 modulated canonical pathways upon antagonist (GSK) treatment throughout the entire dataset across two different timepoints - 6h and 24h post irradiation. The first 10 Canonical pathways generating significant score are displayed as a bar chart along the Y-axis. The X-axis represents the score; the taller the bar, the better the score for the indicated pathway.

3.4.5. Validation of the genes of the microarray data by Q-PCR

We performed Q-PCR on RNA samples from HT-29 cells irradiated at 10Gy with control non-irradiated cells and we observed increase in the expression of the inflammatory marker NF κ B2 at 6h post irradiation and decrease at 24h post irradiation (Fig. 49). On the other hand, we observed decrease in the expression of the CCNB1 at 6h post irradiation and increase at 24h post irradiation. This data correlates with the data obtained by microarray experiments.

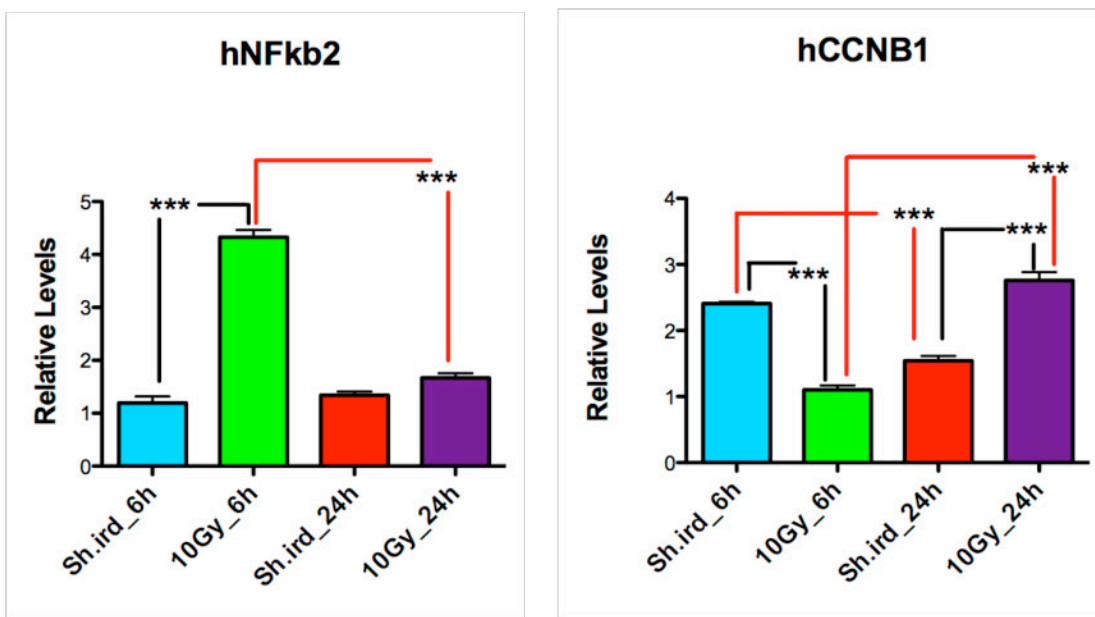


Fig. 49 | Relative expression levels of NF κ B2 and CCNB1 as analysed by Q-PCR at two different timepoints - 6h and 24h post 10Gy irradiation compared with sham-irradiated controls. HT-29 cells were irradiated with a dose of 10Gy and sham-irradiated (Sh.ird) cells served as control. At 6 and 24h post-irradiation, RNA was extracted from cells. Gene expression analysis was performed by SYBR green assay on the following genes - nuclear factor of kappa light polypeptide gene enhancer in B-cells 2 (NF κ B2) and cyclin B1 (CCNB1). All samples were normalized using two housekeeping genes namely human eukaryotic translation elongation factor 1 alpha 1 (hEEF1A1) and human glucuronidase, beta (hGusB). Data expressed are mean \pm SEM. Statistical analysis was performed by one-way ANOVA followed by Newman-Keuls multiple comparison tests. (***) Statistically significant at $p < 0.001$ in comparison to sham-irradiated (Sh.ird) cells).

3.5 *Clonogenic survival assay in intestinal cell lines*

The little effect of PPAR β ligands in modifying the cellular responses to irradiation was quite unexpected and in contradiction with the severe damages seen in PPAR $\beta^{-/-}$ mice at 3.5 days post-irradiation. We thus looked for more sensitive means to assess the possible activity of PPAR β ligand in shaping cell radiosensitivity. In the field of radiobiology, clonogenic assays are considered gold standards to determine the cytotoxic effect of radiotherapy using ionizing radiations and chemotherapy using several chemical agents and also the latest intervention of dual treatments of chemo-radiotherapy. Thus determining the clone forming ability of these cells upon irradiation and subsequently attempting to modulate this clonogenic capacity and thus a modulation of their intrinsic radiosensitivities using pretreatments with drugs (ligands for PPAR β in this case) would be a promising technique for searching new therapeutic interventions involving chemo-radiotherapy.

The intrinsic radiosensitivity of the two colorectal cell lines, HT-29 and HCT-116 was determined by the colony-forming assay. The two cell lines mentioned above have differences in their p53 status and hence considered to have different radioresistance. HT-29 with null p53 has previously been shown to be more radioresistant than HCT-116 with a functional p53 (Williams et al., 2008).

We tested the survival capacity of these two intestinal cell lines on exposure to different doses of gamma-irradiation ranging from 0-10Gy. In order to determine proper plating efficiency two different protocols were initially tested. In the first, cells were first irradiated and then seeded for the colony-forming assay. The second protocol involved irradiation of the cells after they were seeded and continued for survival assay (Williams et al., 2008). The cells responded better in terms of plating efficiency when they were irradiated after being seeded (data not shown). Hence, this protocol was used for further set of experiments (Pomp et al., 1996; Franken et al., 2006).

On exposure to different doses of gamma-irradiation ranging from 0-10 Gy, it was evident that HCT 116 was a sensitive cell line showing a survival fraction of only 50% at a dose level of 2Gy, whereas HT-29 showed 70% survival at the same dose (Fig. 50). At 4Gy, HCT116 showed very low survivability (15%) in comparison to HT29 that had close to 40% survival fraction at this dose. More importantly HT29 cells could survive maximally till 6Gy though with a very low survival fraction (14%) whereas, HCT-116

cells were unable to survive at all at this high dose indicating their sensitivity towards irradiation. These results are in accordance with previous findings reporting enhanced radiosensitivity in HCT in comparison to HT-29 (Williams et al., 2008).

We then tested if pretreatment with PPAR β agonist or antagonist could promote survival of HT-29 and HCT cell types upon challenge with irradiation and thus a modulation of their intrinsic radiosensitivities.

To test this hypothesis, we pretreated the two cell types with the previously validated doses of the agonist and the antagonist and then exposed them to different doses of gamma-irradiation ranging from 0-10 Gy.

It was clearly evident that the ligand treatments (both agonist and the antagonist) did not bring much expected differences in the radiosensitivity of HCT 116, a sensitive cell line that showed a survival fraction of only 58% at a dose level of 2Gy (Fig. 51), which is very similar to the DMSO control group. On the other hand HT-29 showed a 74% survival at a dose level of 2Gy that is quite comparable to the DMSO control group.

This similar pattern was observed in the two cell types at the several different doses tested suggesting clearly that the ligands for PPAR β had little effects in modulating the radiosensitivity of the two cell types. In addition, no conclusion can be drawn from their p53 status as they likely diverge in many different aspects apart from their p53 status.

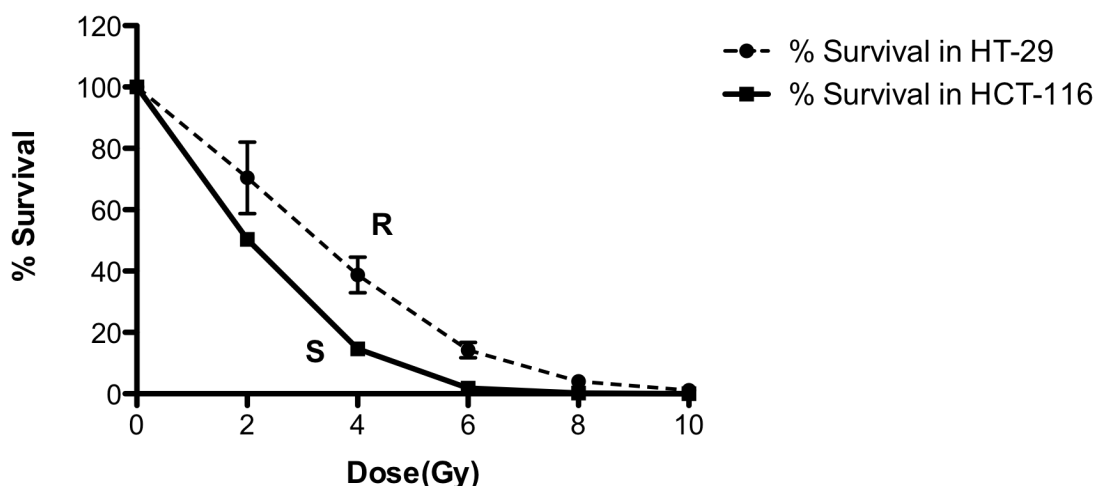


Fig. 50 | Survival curves for HT-29 (dashed line) and HCT-116 (continuous line) cells irradiated with graded doses (0- 10Gy) of gamma rays. The letters R (resistant), S (Sensitive) refers to the radiosensitivity group to which these cell lines belong as defined by Williams et al. (2007). HT-29 and HCT-116 single cell suspensions were seeded at very low densities and cells were irradiated with graded doses (0-10Gy) after overnight incubation. After irradiation, HCT-116 cells were cultured for 8 days and HT-29 for 12 days to form colonies. At the end of this period, cells were fixed and stained and the colonies formed were counted. Colonies with less than 50 cells were not counted. Colonies counted were used to arrive at percentage survival using formula described. (See Materials and Methods). Data expressed are mean \pm SEM. Means at each point represent 6 replicates from two independent experiments and the error bars represent the standard error of the mean when they are larger than the symbol.

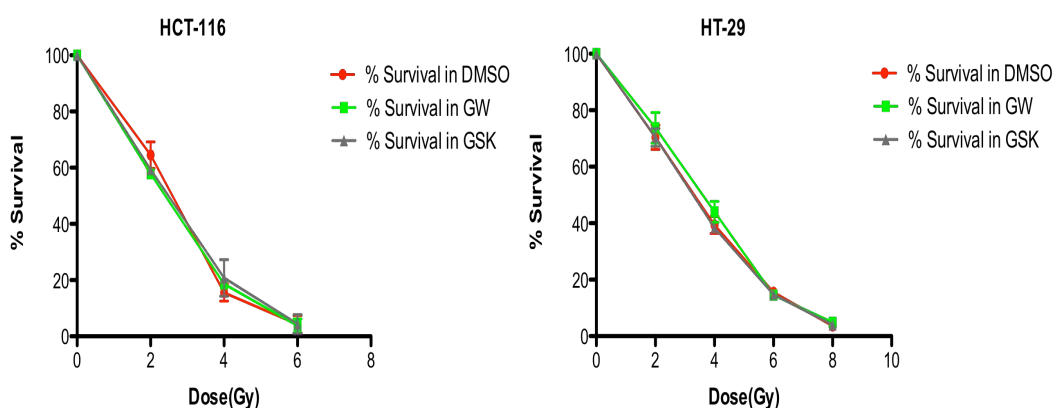


Fig. 51 | Comparison of changes in percentage survival as an effect of pretreatment with ligands for PPAR β in HCT-116 and HT-29 cells after irradiation with graded doses of gamma rays. HT-29 and HCT-116 single cell suspensions were seeded at very low densities in media with agonist (GW) and antagonist (GSK) for PPAR β , with DMSO treated and untreated cells serving as control. Cells were irradiated with graded doses (0-10Gy) after overnight incubation. After irradiation, HCT-116 cells were cultured for 8 days and HT-29 for 12 days with or without GW, GSK, and DMSO to form colonies. At the end of this period, cells were fixed and stained and the colonies formed were counted. Colonies with less than 50 cells were not counted. Colonies counted were used to arrive at percentage survival using formula described. (See Materials and Methods). Data expressed are mean \pm SEM. The slopes represent the treatments with irradiation and either the PPAR β agonist (GW), antagonist (GSK) or the vehicle control (DMSO). Each data point represents the mean of two independent experiments and the error bars represent the standard error of the mean when they are larger than the symbol.

3.6 *Role of PPAR β in H₂O₂ mediated damage in intestinal cell lines*

The lack of activity of PPAR β in radiosensitization was unexpected for two main reasons. First, the observations in vivo clearly showed that PPAR β null mice are more severely affected by irradiation than their WT counterpart. Second, our group had previously demonstrated in two different models the important role of PPAR β in cell survival. In a first instance, PPAR β promotes keratinocyte survival in the context of inflammation (Di-Poi, et al., 2002). Even more dramatic is the protection conferred by PPAR β to kidney epithelial cells in the context of acute ischemic renal failure. This was demonstrated in vivo, by performing acute renal ischemia in PPAR β null mice and PPAR $\beta^{+/+}$ mice, pretreated or not with a PPAR β agonist (Letavernier et al., 2005). Along this study, in vitro tests demonstrated again the pro-survival activity of PPAR β agonist on kidney epithelial cells exposed to high doses of H₂O₂.

Previously, it has been reported that irradiation results in an oxidative stress by the generation of reactive oxygen metabolites, which have been implicated in causing epithelial cell injury. Watson et al., 1994 have generated a model of oxidant injury using the intestinal epithelial cells HT-29 and treating them with graded concentrations of H₂O₂. Therefore we tested the role of PPAR β in this model of oxidant injury induced by the production of reactive oxygen metabolites by administration of H₂O₂ to in the two intestinal cell lines, HT-29 and HCT-116.

Graded concentrations of hydrogen peroxide (0.1mM-5mM) were administered to both these cell lines and the extent of damage was characterized by MTT test. The MTT test is a validated assay for cytotoxicity. The MTT (3-(4,5-Dimethylthiazol-2-yl)-2,5-diphenyltetrazolium bromide, a yellow tetrazole) measures the mitochondrial dehydrogenase activity as it is reduced to purple formazan in living cells. The amount of purple formazan produced by cells treated with an agent (in this case H₂O₂) is compared with the amount of formazan produced by untreated control cells, thus giving an index of the effectiveness of the agent in causing death, or changing metabolism of cells, that can be deduced through the production of a dose-response curve. In our experiments, we measured the O.D of the purple formazon product formed and normalized it with the untreated cells and correlated it to the cell survivability upon treatment with H₂O₂.

In HT-29 cells, we observed that H_2O_2 dose dependently decreased the survivability of the cells, with 5mM H_2O_2 showing approximately 50% survivability (Fig. 52a). However, on pre-treatment with PPAR β agonist (GW), we did not observe any significant change in the survivability percentage of the cells (Fig. 52b).

Interestingly, HCT cells had a survivability of only around 25% at the highest dose, much less than that observed in HT-29 at the same concentration of H_2O_2 (Fig. 53a). We also observed a significant increase, ~ 50% in the percentage of survivability of these HCT cells on pre-treatment with PPAR β agonist (GW), when compared to the H_2O_2 treated cells (Fig. 53b).

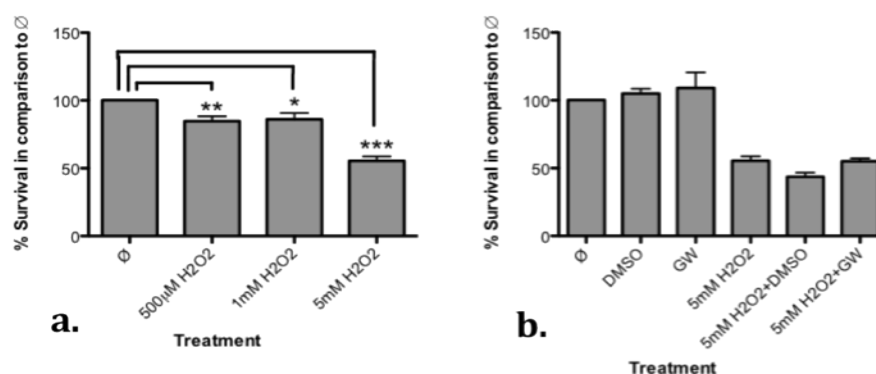


Fig. 52 | Assay of cell survivability with MTT test after treatment of HT-29 cells with H_2O_2 .

HT-29 cells untreated or pretreated with PPAR β agonist (GW501516) for 24h were treated with graded doses of H_2O_2 (100µM- 5mM) for 1h after which an MTT assay was performed. The absorbance at O.D 550nm is inversely proportional to the cytotoxicity. The absorbance values obtained for untreated cells (ϕ) were used as control and all data were normalised to control to obtain percentage survival. **52a:** Cell survivability upon different doses of H_2O_2 in comparison to untreated cells. **52b:** Cell survivability upon treatment with PPAR β agonist (GW) or the vehicle control DMSO. Data presented represent data from three independent experiments. Data expressed are mean \pm SEM. Statistical analysis was performed by one-way ANOVA followed by Dunnett's multiple comparison tests. (* Statistically significant at $p < 0.05$, ** $p < 0.01$ and *** $p < 0.001$ when compared to untreated cells).

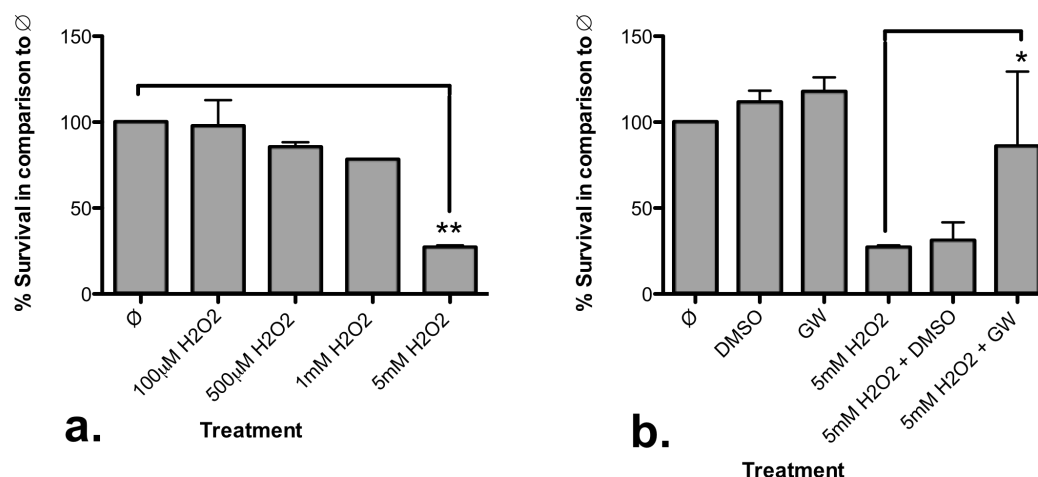


Fig. 53 | Assay of cell survivability with MTT test after treatment of HCT cells with H₂O₂. HCT-116 cells untreated or pretreated with PPAR β agonist (GW501516) for 24h were treated with graded doses of H₂O₂ (100 μ M- 5mM) for 1h after which an MTT assay was performed. The absorbance at O.D 550nm is inversely proportional to the cytotoxicity. The absorbance values obtained for untreated cells (\emptyset) were used as control and all data were normalised to control to obtain percentage survival. **53a:** Cell survivability upon different doses of H₂O₂ in comparison to no treatment (\emptyset). **53b:** Cell survivability upon treatment with PPAR β agonist (GW) or the vehicle control DMSO. Data expressed are mean \pm SEM. Statistical analysis was performed by one-way ANOVA followed by Dunnett's multiple comparison tests. (* Statistically significant at $p < 0.05$, and ** $p < 0.01$ when compared to untreated cells).

In the protective function of PPAR β in the skin wound healing model (Di Poi et al., 2003), PPAR β acts in response to inflammatory signals by activation of Akt1 pathway that increases the survival of keratinocytes. Also, it has been shown that PPAR β plays a protective role in a renal ischemia/reperfusion model by activating the Akt pathway (Letavernier et al., 2005).

In order to test if HT-29 cells are resistant to oxidative stress induced by H₂O₂ and hence to radiotherapy as well, we checked the levels of activation of PI3kinase/Akt signaling pathway. We tested for p-Akt levels and found that upon 5mM H₂O₂ treatment, Akt was phosphorylated at Ser473 and this phosphorylation was reduced upon GW pre-treatment (Fig. 54 a, b).

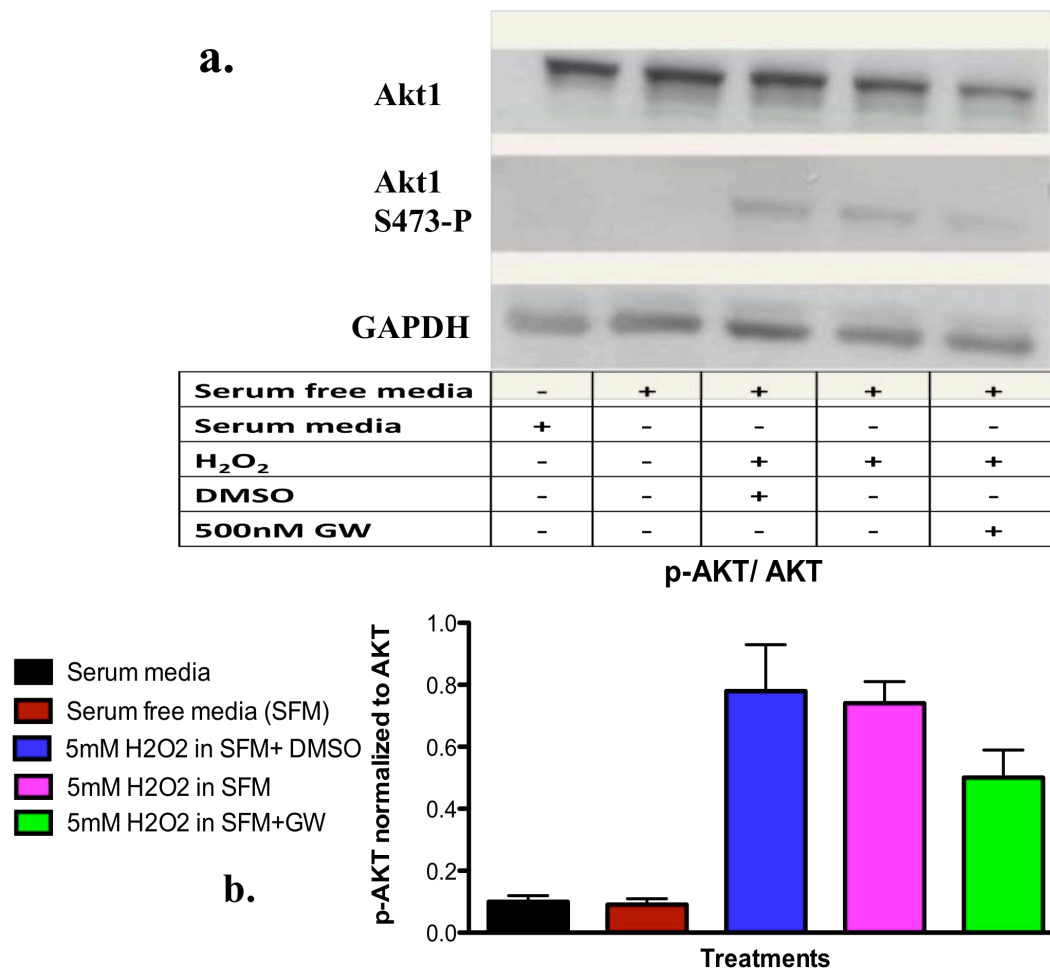


Fig. 54 | Akt1 phosphorylation and the role of PPAR β in H₂O₂ mediated stress response. HT-29 cells untreated or pretreated with PPAR β agonist (GW501516) for 24h were then treated with 5mM H₂O₂ for 1h after which total cellular proteins were isolated from these cells. PPAR β agonist (GW) or DMSO as vehicle for GW treatment was diluted in serum free media (SFM) and hence there were two sets of control cells. One set consisting of cells treated without 10% serum in media that served as control for treatment with GW and cells treated with serum media as control for SFM. **(a)** Equal concentration (20 μ g) of cellular proteins from various groups was analysed for Akt1 and phospho-Akt1 expression by western blot. **(b)** Bands obtained by Western blot for Phospho- Akt1 normalized to Akt-1 [Quantity One 1-D software analysis (Bio-Rad)]. Data represent the mean \pm SEM of two independent experiments.

Thus in our hands, we do not see phosphorylation of Akt1 in untreated HT-29 cells but we see phosphorylation of Akt1 upon H₂O₂ treatment.

CHAPTER III:

DISCUSSION AND PERSPECTIVES

DISCUSSION

Radiotherapy for cancers can affect organs in the vicinity of the tissue affected. Small intestine has the highest turnover rate in terms of cell proliferation and differentiation and thus is one of the key radiosensitive organs of the abdomen. Studies have highlighted the importance of PPAR β as therapeutic target for gastrointestinal complications (He et al., 1999). However, the role of PPAR β in intestinal damage after radiation exposure has not been deciphered so far. In the present study, we tried to elucidate the mechanism through which PPAR β might influence events post irradiation. Both, in vitro and in vivo approaches were utilized to confirm the potential effects of PPAR β activation in intestinal cells in response to irradiation. When PPAR $\beta^{-/-}$ mice were exposed to whole-body irradiation, we observed that irradiation aggravated mesenchymal cell death in duodenum of PPAR $\beta^{-/-}$ compared to the PPAR $\beta^{+/+}$ mice and also defect in the adhesion between epithelia and mesenchyme indicating the involvement of PPAR β in irradiation-mediated intestinal damage. Microarray analysis of PPAR $\beta^{+/+}$ and PPAR $\beta^{-/-}$ mice showed downregulation of the entire set of genes involved in the cholesterol biosynthesis pathway after irradiation in PPAR $\beta^{-/-}$ mice when compared to the PPAR $\beta^{+/+}$.

To confirm these observations, we established an in vitro model system in HT-29 cell lines to evaluate the effect of PPAR β specific ligand post irradiation. Upon irradiation, we observed changes in the expression levels of genes involved in the cell cycle regulation through microarray analysis, but with ligand treatment we failed to observe any differences between the agonist treated and the vehicle treated cells post irradiation. On treatment with PPAR β agonist, we observed upregulation of its target genes and genes involved in lipid metabolism and fatty acid oxidation for which the role of PPAR β has already been established.

We also tested if PPAR β activation can alter the radiosensitivity of the intestinal cells in both radioresistant and radiosensitive cell lines, but did not observe any significant difference with PPAR β activation indicating that it is not involved in the radiosensitization mechanism.

1. The late effects observed in gamma-irradiated PPAR β ^{-/-} mice

1.1 Alteration of the mesenchymal compartment

Previous observations from our lab has revealed a delay in the regenerative proliferation in the small intestine and the colon of the PPAR β ^{-/-} mice on exposure to irradiation when compared to the wild type counterpart at 3.5d post-irradiation. This was attributed, at least in part, to a significant increase in the apoptotic bodies observed in the crypts of the PPAR β ^{-/-} mice in comparison to the PPAR β ^{+/+} at 4h post-irradiation. This increased apoptosis was observed in the cell position 4 (position of intestinal stem cells) from the bottom of the crypts that indicate that the delay in the regenerative proliferation observed at 3.5 d post-irradiation might be partly due to an increased apoptosis in the stem cell compartment (i.e, immediate effects).

At 8d post-irradiation, the observed phenotype was a reduction in the mesenchymal cells in PPAR β ^{-/-} mice. This could arise from a differential rate of cell death or cell renewal in the two compartments of epithelia and the mesenchyme that occurred at an early time point after irradiation, i.e., 3.5d. Observations from our *in-vivo* studies indicate increased apoptosis of not only the epithelial cells but also the mesenchymal cells occupying the intra-villus region of the small intestines of PPAR β ^{-/-} mice at 3.5 and 8 days post-irradiation respectively. The mesenchymal cells in PPAR β ^{-/-} mice are more sensitive to irradiation than the epithelia as evident from Tunel assay and thus responds stronger to the damaging effects of irradiation than the epithelia.

1.2 *Alteration of the extra-cellular matrix of the mesenchymal compartment*

We also observed detachment of the mesenchymal layer from the epithelial layer in the $\text{PPAR}\beta^{-/-}$ mice, indicative of weak ECM. Literature supports the role of *Ihh* and *Foxf* genes as critical regulators of epithelial-mesenchymal interactions and extracellular matrix production respectively (Ormestad et al., 2005; Van Dop et al., 2010). Deletion of the intestinal epithelial *Ihh* has been shown to result in the loss of the muscularis mucosae, deterioration of the ECM, and reductions in numbers of the crypt myofibroblasts hence leading to the disruption of the intestinal mesenchymal architecture (Kosinski et al., 2010).

Further, *Foxf2* mutants result in striking deficiency of fibrillar (type I) as well as sheet-forming (type IV) collagens throughout the intestine (Ormestad et al., 2005). They also reported that in these mutants the basal laminae surrounding smooth muscle cells as well as the basement membrane underneath the epithelium were indistinct and frequently replaced by gaps of extracellular space and mesodermal cells of the colon had poorly developed endoplasmic reticulum (Kosinski et al., 2010).

Earlier from our group a role of $\text{PPAR}\beta$ in the proper organization of the secretory pathway of the paneth cells has been shown as the $\text{PPAR}\beta^{-/-}$ mice had less compact endoplasmic reticulum in the intestinal cells, suggesting a role in the differentiation of the paneth cells (Varnat et al, 2006). In that study it was identified that *Ihh* is negatively controlled by $\text{PPAR}\beta$ in the small intestine as its expression was significantly higher in the $\text{PPAR}\beta^{-/-}$ than the $\text{PPAR}\beta^{+/+}$ mice with a corresponding increase in the expression of BMP-4, a well established target of the hedgehog signaling. But these observations were made without any irradiation challenge to the mice and hence, it will be difficult to speculate the role of any of these genes, if any, in our present context. Thus the mechanism behind the phenotype observed in $\text{PPAR}\beta^{-/-}$ mice showing damage in the mesenchymal ECM on irradiation exposure needs further elucidation.

1.3 *The epithelial-mesenchymal cross-talk*

One of the key question raised for the delayed effects seen in the mesenchymal compartment in irradiated PPAR β ^{-/-} mice is whether this was a cell autonomous effect or was it due to a defective crosstalk between epithelia – mesenchyme. In other words, what is the source of the signals that cause these delayed effects?

Analysis of the results from the PPAR β villin-cre conditional KO mice at 8 days post-irradiation show that the villin Cre⁺ mice, i.e. with a deletion of PPAR β alleles restricted to the epithelial cells, have the similar kind of defect like that of the PPAR β ^{-/-} mice with detachment of the mesenchyme from the basement membrane and separation from epithelia and reduction in the number of mesenchymal cells. The PPAR β L2/L2 control group does not show any defect. Albeit the Villin Cre⁻ group also shows some damages, it was not seen in all animals and thus is not fully penetrant unlike the Villin Cre⁺. Thus we can speculate that PPAR β in the epithelia is essential for the process of healing in the absence of which is there is a defect. It is therefore interesting to understand the mechanisms by which PPAR β in the epithelia mediates survival signal for the recovery of both the epithelia and the mesenchyme.

1.4 *The unexplored role of the endothelial microvasculature*

The intra-villus region is made up of mesenchymal cells as well as endothelial microvasculature. According to a previous report (Paris et al., 2001) endothelial vascular damage precedes the epithelial damage and it is the earliest event even prior to the crypt damage at 4-6h post irradiation. This signifies endothelial dysfunctions to be one of the important factors contributing to epithelial lethality. Moreover, microvascular function regulates expression of radiation-induced crypt stem cell clonogenic alteration (Maj, et al., 2003). The mechanism for this involves the inhibition of radiation-induced crypt shrinkage but not the enhancement of crypt regeneration. These studies provide evidence that microvascular endothelial apoptosis is ordered upstream of the mitotic dysfunction of the clonogenic compartment that occurs during the early phase of radiation-induced damage to the intestines. As the microvascular endothelium and the mesenchymal cells are placed spatially in the same intravillus mesenchymal compartment, thus we could speculate that

the mesenchymal damage like the microvascular endothelium damage could be responsible for the radiation induced crypt stem cell clonogen damage in the PPAR β ^{-/-} mice as evidenced by the observed defects at 4h post-irradiation in comparison to the PPAR β ^{+/+}.

2. New information gained from microarray data

2.1 Irradiation induces the cholesterol biosynthetic pathway

Microarray experiment comparing the PPAR β ^{+/+} and PPAR β ^{-/-} in response to 4 hrs post irradiation showed modulation of large number of genes of which the most significant being those involved in the cholesterol biosynthesis pathway which were also validated through qPCR. These observations were further tested in *in-vitro* conditions using adenocarcinoma cell line, HT-29, on exposure to irradiation. In HT-29, at 24hr post irradiation we observed significant upregulation of two of the genes involved in cholesterol biosynthesis, FDFT1 and LSS, that were also upregulated in PPAR β ^{+/+} mouse intestine at 4h post-irradiation. A previous report on elucidating the mechanism involved in the regulation of cholesterol synthesis in human intestinal cells (Caco-2), has shown that levels of HMG-CoA reductase mRNA were increased under conditions of cholesterol efflux (Field et al., 1991). Furthermore, it has also been shown that ionizing radiation induces cholesterologenesis in different cells of mammalian organism as an early reaction to the harmful effect necessary for restoration of biomembranes (Kolomiitseva, 1986).

We also observed similar induction of genes including the one encoding for the rate-limiting enzyme, HMGCR, in the PPAR β ^{+/+} mice on irradiation. Also, up- regulation of several genes encoding the key enzymes in the cholesterol biosynthesis pathway in the HT29 cell line in response to irradiation was observed, thus allowing us to speculate for a possible increment in the cellular cholesterol efflux in response to irradiation. This is presumably because of the increase in the requirement of cholesterol for synthesis of new membranes in response to the injury to radiosensitive cells in order to make them recover and compensate for their functions.

Since we observed a decrease in the levels of gene expression of these enzymes involved in cholesterol biosynthesis pathway in PPAR β ^{-/-} mice post-irradiation in

comparison to the PPAR $\beta^{+/+}$, this might attenuate cellular cholesterol increase indicating to the involvement of PPAR β in irradiation mediated intestinal damage.

2.2 *PPAR β -independent responses of HT29 to irradiation*

Our global analyses of the microarrays obtained from HT29 cells, pretreated or not with agonist and antagonist of PPAR β , revealed little interference if any of PPAR β activity in the radiation-induced responses.

Following exposure to 10Gy irradiation, as an effect of irradiation, we observed a total of 418 genes modulated at 6h and 1168 genes at 24h. This is in accordance with previous reports (Rødningen et al., 2005; Tachiiri et al., 2006) where they observe a higher number of genes modulated at a later timepoint post exposure than an early timepoint.

Genotoxic stress can activate or suppress a variety of genes and pathways. In our experiments, 10 Gy irradiation induced increase in the expression levels of NF κ B2, CDKN2B and several other genes at 6h post-irradiation (Table 3). We observed that the upregulation of the cyclin dependent kinase inhibitors (CDKN2B) lead to the downregulation of cyclin dependent kinases (Cyclin B1 and B2) thereby regulating the cell cycle in the G2/M phase. This data correlates with the previously reported studies that cells respond to irradiation by modulation of the cell cycle regulators (Schmidt-Ullrich et al., 2000; Pawlik et al., 2004). We also observed increase in the expression of NF κ B2 – a known marker of inflammation at 6h post irradiation and decrease at 24h post irradiation. This fits well with previously reported observation in human KG-I myeloid leukemia cells, that as an effect of 20Gy, there was a detectable increase in NF κ B expression at 3 and 6h post irradiation. This effect was transient and levels of NF- κ B transcripts returned to that in control cells by 15h. These findings indicated that ionizing radiation regulates NF- κ B expression at the mRNA level (Brach et al., 1991).

At the same time at 24h post irradiation, we see decrease in various histone proteins (Table 4) that suggests that the cell cycle is in the G2 phase as reported by Heintz 1991; Osley 1991. Thus, these above results clearly indicate that the cell cycle has been

stalled at the G2/M phase as a protective response mechanism of the cells against irradiation mediated damage (Pawlik et al., 2004).

2.3 PPAR β dependent responses of HT-29 to irradiation

In our experiments, the effect of irradiation upon the treatment with the agonist for PPAR β clearly show an increase in the expression of some known PPAR β target genes, e.g. PDK4 and ANGPTL4, in a time dependent manner. However, these genes modulated in response to the agonist treatment upon irradiation belong to the various lipid metabolic processes that are one of the main well-known functions of PPAR β in the cells (Bedu et al., 2005; Desvergne et al., 2009). This clearly indicates that the agonist treatment is functional in this set of experiments. However, we did not see modulation of any other genes relevant to cell cycle regulation, apoptosis and survival. This was unexpected but consistent with the caspase assays and clonogenic assays which revealed that PPAR β activity did not modify the radiation-induced response of HT29 and HCT116 cells.

Intriguingly, pre-treatment with an antagonist for PPAR β provoked an increase in few genes that are not found down-regulated in the presence of an agonist as could have been expected. The AKR1B10 was regulated at both 6hr and 24 hrs. It is a aldose reductase and data from literature suggest that AKR1B10 affects cell survival through modulating lipid synthesis, mitochondrial function, and oxidative status, as well as carbonyl levels, thereby being an important cell survival protein in colorectal cancers (Tammali et al., 2007; Wang et al., 2009). However, in the absence of any other genes of AKR1B10 mediated survival pathway being modulated it is hard to confirm the above mechanism in this cell model. Thus, from the present set of experiments, it is hard to decipher the function of PPAR β on irradiation-mediated damage.

3. How to reconcile in vivo and in vitro data?

It has been shown by Bonnaud et al., 2010 that despite an enhancement of crypt survival and an inhibition of crypt epithelial cell mitotic catastrophe by S1P (Sphingosine-1

phosphate), direct protection of irradiated epithelial cells by S1P seems to be excluded in *in-vitro* studies using IEC-6 cells, as well as in transformed intestinal T84, colonic tumor Caco2, and HCT116 epithelial cell lines. Thus, S1P enhances crypt radioprotection but not *in-vitro* epithelial cell radioresistance. It is very similar to what we see in our *in-vivo* data where PPAR β is seen to bring about a crypt radioprotection in the PPAR $\beta^{+/+}$ mice but we do not see any enhancement of radioresistance in *in-vitro* studies using HCT-116 cells.

Edwards et al., 2002 have shown that phospho-AKT staining was untraceable in small intestine sections from untreated mice and AKTi (inhibitor) treatment did not modulate death of 15 Gy-irradiated mice. From their studies, they considered this as a first proof of the specificity of the AKT inhibition strategy in tumor but not in normal tissue endothelium. This correlates with our data where we do not see phosphorylation of AKT1 in untreated HT-29 cells but we see phosphohorylation of AKT1 upon H₂O₂ treatment.

As a summary, experiments in *in-vitro* cell lines did not show any response to pre-treatment of PPAR β agonist in modulating the expression levels of radiation induced genes or radiosensitivity or H₂O₂ induced oxidative stress. Thus there is no clear evidence for a protective effect of PPAR β in various contexts of cell damages tested *in-vitro*. Of quite significance is the fact that the crosstalk between the epithelia and the mesenchyme is necessary for the proper development of the crypt-villus unit (reviewed in Crosnier et al., 2006). Thus, this could probably explain why we do not see any defects in *in-vitro* model where we have only the intestinal crypt phenotype and lack the crosstalk with the mesenchyme.

We propose that *in-vivo* PPAR β affects the crosstalk between the mesenchyme and the epithelium consistent with the observed delay in tissue repair in the PPAR $\beta^{-/-}$ mice. These observations indicate the possible involvement of PPAR β in radiation-induced injury. The exact molecular mechanism of PPAR β action still demands further exploration to better understand its physiological role in this regard. Particularly, a better understanding of the mechanism by which PPAR β controls epithelial and mesenchymal crosstalk in normal and tumor tissue responses to radiation need further development such as elaborating an *in-vitro* model of a co-culture of epithelia and mesenchyme to better mimic *in-vivo* conditions.

CHAPTER IV:

MATERIALS AND METHODS

1. Animal experiments

All animals had free access to a standard laboratory chow diet with a 12hour light and dark cycle. PPAR $\beta^{-/-}$ and their control PPAR $\beta^{+/+}$ were bred on a mixed genetic background (Sv129 and C57BL/6) and were used at 12 weeks of age unless otherwise mentioned. All animal procedures were performed with authorization from the cantonal veterinary service of the Canton of Vaud.

1.1 Generation of PPAR $\beta^{-/-}$ mice

(i) Construction of a replacement vector for PPAR β . Nine overlapping mouse PPAR β genomic clones were isolated from an Sv129 mouse embryonic stem (ES) cell genomic library (gift from F. Conquet), and their restriction maps were established (Fig. 55). A targeting vector was designed to delete the two exons encoding the DNA binding domain (i.e., exons 4 and 5), according to the organization of the Xenopus PPAR β/δ gene. The targeting vector (derived from TK-NEO-UMS, a vector comprised of the thymidine kinase gene, neomycin resistance sequence, and upstream mouse sequence; a gift from Charles Weissman) contained 1.7 kb of homologous sequence at the 5' end, 7 kb of homologous sequence at the 3' end, and a phosphoglycerate kinase-neomycin (PGK-neo) cassette (Fig. 55A).

(ii) ES cell transfection. D3 ES cells were cultured as previously described (Guillemot et al., 1993), and electroporation was performed as previously reported (Van der Hoeven et al., 1996). Twenty- four hours after electroporation, positive selection by G418 at 350 $\mu\text{g/ml}$ (geneticin) was performed for 9 days. Resistant clones were then transferred onto 48-well plates (Costar) and subsequently grown to confluence on duplicate 24- well plates for either genomic analysis or storage of master plates at -80°C .

(iii) Genotyping. Genomic DNA was prepared from ES cells, yolk sacs of embryos, or tail samples following the classical procedures. A first round of genotyping was performed by two independent PCRs. Primers b19 (5'-ATCCA GAGTGTTTCGTATGAC-3') and UMS1 (5'-TCTTATGCTCCTGAAGTCCAC-3') amplified a 2.2- kb fragment from the recombinant allele, whereas the primers b3 (5'-AGCCTCAACATGGAATGTCG-3') and b4 (5'-GATCGCAC TTCTCATACTCG-3')

amplified a 1.6-kb product from the wild-type (wt) allele. Five percent of the neomycin-resistant ES cell clones were positive for homologous recombination. All mutant clones and/or embryos or mice were subsequently confirmed by Southern analyses using a digoxigenin-labeled probe (CDP-Star protocol; Boehringer Mannheim), located 160 bp upstream of the 5' homology region. Digested genomic DNA samples were blotted on a Zetaprobe GT membrane and processed following the manufacturer's protocol (Bio-Rad). Probes, restriction digestion, and hybridized fragments from wt and recombinant alleles are indicated in Fig. 55.

(iv) Generation of chimeric mice and germ line transmission. Positive D3 clones were microinjected into the blastocoel of 3.5-day-old embryos at the blastocyst stage and isolated from C57BL/6 females (10 to 15 ES cells per blastocyst). Between five and seven injected blastocysts were reimplanted into each uterine horn of pseudopregnant foster mothers. Male chimeric animals were mated for germ line transmission with Sv129 mice. One chimeric male transmitted the mutation from which the colony of mice has been obtained.

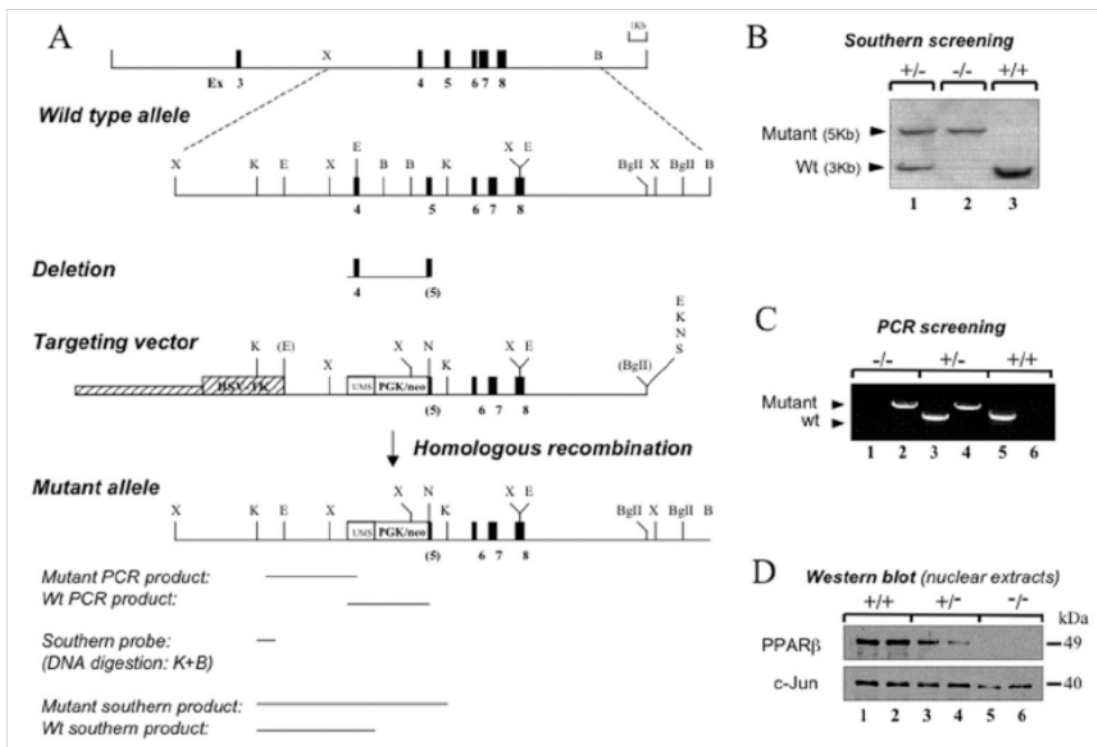


Fig. 55 | Targeted disruption of the PPAR β gene in mouse. The PPAR β gene was disrupted in ES cells by homologous recombination with a replacement-type vector, using an approach based on positive-negative selection (A). In this vector, PPAR β genomic sequences containing the exons encoding the DNA-binding domain of the receptor (exon 4 and part of exon 5) were replaced with a PGK-neo cassette. Homologous recombination at the PPAR β locus in ES cells led to the deletion of both exon 4 and part of exon 5 encoding the two zinc fingers of the DNA-binding domain. ES cells carrying the mutant allele were confirmed by Southern blot analysis (B). Two independent positive ES cell clones were injected into blastocysts to generate chimeras, and heterozygous mice were obtained from a germ line transmitter chimera. Panel A shows the structure of the wt PPAR β allele, targeting vector, and recombinant PPAR β allele. The exons as well as locations of restriction sites and probes for PCR and southern blot are indicated. B, BamHI; E, EcoRI; K, KpnI; N, NotI; X, XhoI. Panel B shows a Southern blot analysis of genomic DNA digested with BamHI and KpnI from E9.5 embryos produced by a PPAR β heterozygous intercross. (C) PCR analysis of yolk sac DNA derived from E9.5 embryos. (D) Western blot analysis performed on nuclear extracts with a specific PPAR β antibody. The nuclear protein c-Jun was used as an internal control. In order to obtain a sufficient amount of material, the control at the protein level was performed on pups obtained from homozygous matings.

(From Nadra et al., 2006).

1.2 *Gamma-irradiation model*

In the gamma-irradiation protocol, the PPAR $\beta^{+/+}$ and PPAR $\beta^{-/-}$ mice were exposed to whole body irradiation at a dose of 10Gy (two doses of 5Gy) and the animals were sacrificed at different time-points: 4hr, 3.5d and 8d post irradiation (Fig. 56). After death by cervical dislocation, the abdomen was opened and the duodenum, jejunum, ileum and colon were dissected out and flushed with cold phosphate buffered saline (PBS). Tissue samples were frozen in liquid nitrogen for subsequent RNA and protein analysis or processed for histological analyses after fixing in 4% paraformaldehyde (PFA)-PBS for 2hours at 4°C.

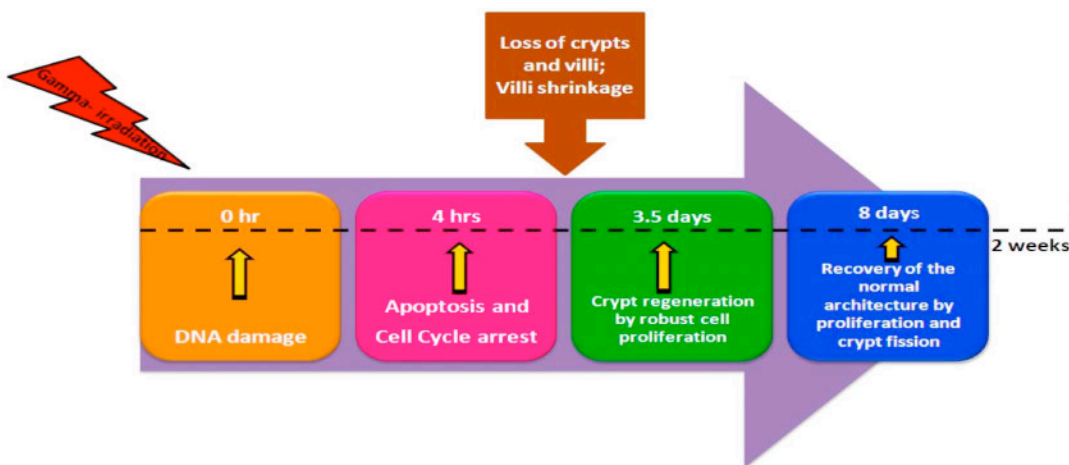


Fig. 56 | Schematic representation of gamma-irradiation model (adapted from Somosy et al.2002; Potten 2004).

1.3 *Histological analysis*

Intestines were fixed in 4% paraformaldehyde- in phosphate buffer saline (PFA-PBS), dehydrated and embedded in paraffin according to standard procedures. Sections of 4 μ m were processed for staining or immunohistological analysis. For immunohistochemistry, paraffin sections were hydrated and boiled for 15 minutes in 0.01M sodium citrate, pH=6. Sections were subsequently washed in PBS. Sections were

incubated in 1% bovine serum albumin (BSA) before incubation with the primary antibody. For immunofluorescence, sections were further incubated with a fluorescein isothiocyanate (FITC)- coupled secondary antibody. Sections were then counterstained with DAPI to stain the nuclei. Primary anti-Ki-67 was purchased from Abcam (ab 15580).

1.4 *Detection of apoptosis*

Apoptosis detection was performed using TUNEL assay. This assay was performed on paraffin sections as described by the manufacturers instructions (In situ cell death detection kit, Fluorescein, Roche).

1.5 *Generation of PPAR β villin- Cre conditional KO mice*

The Cre protein is a site-specific DNA recombinase that recognizes a 34-bp loxP sequence and, in the presence of two directly repeating loxP sites, excises the intervening DNA sequence (Abremski and Hoess, 1984). The use of the Cre/ lox system involves both mice expressing Cre enzyme (villin- Cre- ERT²) and mice with loxP sites (PPAR β L2/L2) inserted at a selected transgenic locus of interest. The mating of the two strains generates progeny in which Cre is expressed and excises the sequences between the loxP sites.

To specifically inactivate PPAR β in intestinal epithelia *in-vivo*, we combined this powerful site-specific recombination system with the tissue specificity of the murine villin promoter. A 9-kb regulatory region of the villin gene has been shown to target stable and homogeneous expression of transgenes in small and large intestine along the crypt- villus axis, in differentiated enterocytes, as well as in the immature, undifferentiated cells of the crypt (Janssen et al., 2002; Pinto et al., 1999; Robine et al., 1997). The approach used here allowed recombination of target genes in the intestinal epithelia, at any time during postnatal life. We have generated transgenes containing a tamoxifen-dependent recombinase (vil-Cre-ERT²), shown schematically in Figure 57. The vil-Cre-ERT² construct is based on a fusion of the Cre recombinase with a mutated ligand-binding

domain of the human estrogen receptor, resulting in a tamoxifen- dependent Cre recombinase (Feil et al., 1996; Metzger and Chambon, 2001, Metzger et al., 2003).

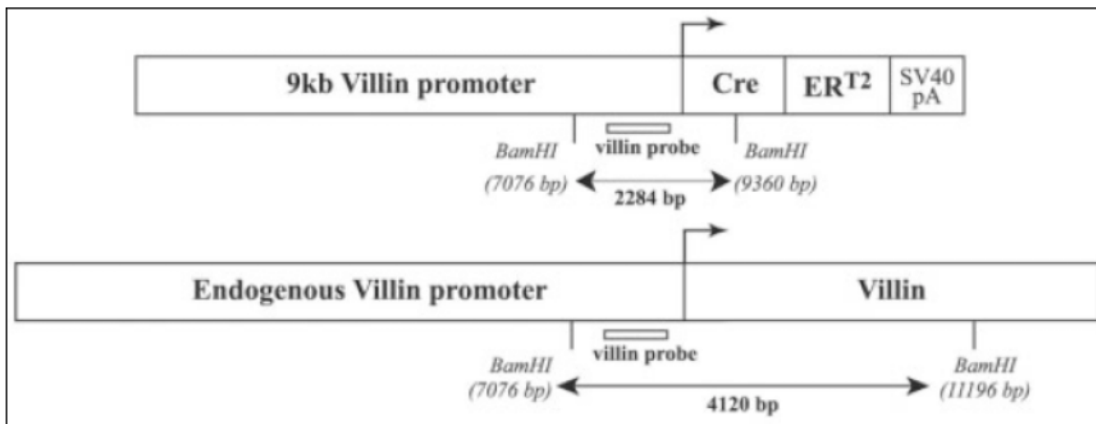


Fig. 57: | Generation of villin-Cre-ER^{T2} transgene. A 9-kb region of the villin promoter drives the expression of the tamoxifen-dependent Cre-ER^{T2}. *BamHI* sites and the expected sizes of the resulting DNA fragments are indicated. The villin probe obtained by PCR is indicated (Adapted from El Marjou et al., 2004).

To generate PPAR β villin- Cre conditional KO, we crossed the PPAR β L2/L2 with the villin- Cre- ER^{T2}. The Cre-mediated deletion is obtained by induction through tamoxifen. For experimental purpose, we had three groups: PPAR β L2/L2, which served as wild type controls, PPAR β L2/L2 villin- Cre⁺ and the PPAR β L2/L2 villin- Cre⁻. Each of the three groups was treated with tamoxifen and vehicle. Chemical treatments were administered to 12 weeks old mice. Tamoxifen (Sigma) solubilized in sunflower oil was administered intraperitoneally at a dose of 1mg/ml/kg per day for 5 consecutive days. For the vehicle treated group, equal volume of sunflower oil was administered. The tamoxifen-mediated deletion was allowed for one week and after one week the animals were irradiated and then sacrificed at 3.5 days post irradiation. RNA, protein and tissue samples for histology were collected as described in later sections.

2. Experiments with Cell cultures

2.1 Cell cultures (HT-29 and HCT-116)

The HT-29 cells are human colon adenocarcinoma cells that were originally isolated from carcinoma of the human colon and hence have retained some characteristics, including expression of hormone receptors (Jan Mester et al., 1989). There is a G-> A mutation in codon 273 of the p53 gene resulting in an Arg-> His substitution. The p53 antigen is thus overproduced in these cell lines. The line is also positive for expression of c-myc, K-ras, H-ras, N-ras, Myb, Sis and fos oncogenes. They have the ability to grow as monolayers and under special culture conditions, they can differentiate to form mucus secreting and/or absorptive cells. When cultured in high glucose media and 10%FCS, the cells remain undifferentiated and grow as multilayers but when glucose is absent or replaced they undergo differentiation after confluence.

For our experiments, HT-29 cells were cultured in DMEM + Glutamax I (Gibco) containing 4.5mg/L glucose supplemented with 10% fetal bovine serum (FBS). HCT-116 cells are also human colon adenocarcinoma cells and were cultured in DMEM + Glutamax I (Gibco) containing 4.5mg/L glucose supplemented with 10% FBS.

2.2 Transfections

HT-29 cells were cultured in DMEM + Glutamax I (Gibco) containing 4.5mg/L glucose supplemented with 10% FBS. The cells were seeded at a density of 0.5million/ml per well of a 12 well plate and allowed to grow to 30% confluency before transfection. Transfections were carried out using Lipofectamine LTX (Invitrogen) in low serum media using OptiMEM 1X (GIBCO) and allowed to incubate at 37°C for 4h. At this point, the cells were incubated with serum media for a period of 4 hours followed by serum free media for those requiring agonist or antagonist treatment. Appropriate doses of specific agonist/antagonist of PPAR β were given in DMEM + Glutamax I without serum and incubated at 37°C for 24hrs. The cells were then washed once with PBS and processed further for luciferase assay.

2.3 *Luciferase assays*

After cells were transfected with the luciferase constructs, cells were either untreated or treated with agonist and/ or antagonist for 24h. The cells were washed with PBS before lysis using 1X passive lysis buffer (Dual luciferase assay Kit, promega) and samples were further processed according to the manufacturer's instructions and analysed using a luminometer (Promega corporation).

2.4 *Agonist/ Antagonist treatments*

PPAR β specific agonist GW501516 was used at a concentration ranging from 100-1000nM in DMSO. Two types of antagonist were used – GSK0660 (shearer et al., 2008) and a new candidate VP80. Both were used at concentrations ranging from 1-10 μ M in DMSO. For transfection experiments, agonist or antagonist treatment were given in serum free media but for microarray experiment, it was given in normal serum media to avoid variations arising from serum free treatment.

3. *Gamma-irradiation experiments*

For our *in-vivo* studies, we used a Caesium-137 (Cs-137) gamma-irradiator under the guidance of Prof. Werner Held at the Ludwig Institute of Cancer Research (LICR), Lausanne. The PPAR $\beta^{+/+}$ and PPAR $\beta^{-/-}$ mice were exposed to whole body irradiation at a dose of 10Gy (two doses of 5Gy) at room temperature and the animals were sacrificed at different time-points: 4hr, 3.5d and 8d post irradiation.

For our *in-vitro* studies, we used an irradiator (RS2000, Rad Source Technologies Inc.) that is specially designed for cell and small animal studies with the irradiation source being non-isotope, an alternative to traditional radioactive isotope based irradiators but with the capacity to produce a dose, equivalent to gamma-irradiators. Dose-dependent studies using different doses, ranging from 0-30 Gy (in accordance to informations from literature) were performed to identify the effective dose. Furthermore, different timepoints

post-irradiation were also assessed with the effective dose, at which the cell death could be observed indicating the levels of injury mediated by irradiation.

For irradiation of HT-29 cells, we cultured them on six or twelve well plates to confluence and had two groups: one that was irradiated with a dose of 10Gy and the other was a sham-irradiated control group. The sham-irradiated group received all treatments similar to the irradiated group in terms of culture media and transport from the incubators to irradiators but with the exception of not receiving gamma-irradiation. We isolated the RNA samples at different timepoints post irradiation- 4hr, 24hr, 48hr and 72hr and checked for the alterations in the gene expression levels of various genes by Q-PCR at these time-points and compared them to the sham irradiated control group.

4. Extraction of Total RNA

Total RNA from tissues was extracted using TRIzol LS reagent (Invitrogen). Tissues were homogenized at medium speed with a polytron apparatus for 30 sec on ice in TRIzol reagent (800ul/100mg of tissue). After 10 minutes of incubation on ice, the samples were centrifuged at 4°C and 13,000 rpm. The supernatants were then subjected to choloform extraction and incubated 5 minutes on ice and centrifuged at 13,000 rpm for 20 minutes at 4°C. Total RNA was precipitated using isopropanol during 20 minutes at 4°C followed by a centrifugation at 13,000 rpm at 4°C. The pellets were washed twice in cold 70% ethanol-DEPC treated and resuspended in DEPC treated water. OD measurements were done using a Nanodrop (Nanodrop®) and the integrity of RNA was assessed by capillary electrophoresis (Bio-analyzer, Agilent Biotechnology). For extraction of total RNA from cells in culture, we used the RNeasy plus mini kit from Qiagen and followed the manufacturers instructions.

5. RT and Q-PCR

One microgram of the total RNA was reverse transcribed with random hexamer primers (Promega) using SuperscriptTM II reverse transcriptase (Invitrogen). Real-time PCR was performed with SYBR® Green PCR matermix (Applied Biosystems) using ABI PRISM® 7900 PCR machine (Applied Biosystems). Primers were designed to generate a PCR amplification product of 100- 200 bp. Expression was related to the control

housekeeping genes: mouse glyceraldehyde-3-phosphate dehydrogenase (GAPDH) and Tata-box binding protein (TBP) for mouse tissue samples and human eukaryotic translation elongation factor α 1 (EEF1A1) and Glucuronidase β (GusB) for HT-29 samples. The expression of the housekeeping genes- EEF1A1 and GusB did not change under the experimental conditions studied. The primers for NF κ B2, CCNB1, PDK4, ANGPTL4, PLIN2/ADRP were obtained from Qiagen's QuantiTech® primer assay. The other primer sequences are as follows:

Human primer sequences

EEF1A1_Hs:

Hs_EEF1A1-1039F: CTGAACCATCCAGGCCAAAT

Hs_EEF1A1-1097R: GCCGTGTGGCAATCCAAT

GusB_Hs:

Hs_GusB-544F: CCACCAGGGACCATCCAAT

Hs_GusB-622R: AGTCAAAATATGTGTTCTGGACAAAGTAA

FDFT1_Hs:

H_FDFT1_F: CCCTTGAGTTTAGAAATCTGGCT

H_FDFT1_R: CCACTCCTGTTCAGAGGTCAC

LSS_Hs:

H_LSS_F: CTGCCAGCCGGATACAGAG

H_LSS_R: TCCCAAACACGGTGGACTTAT

MVD_Hs:

H_MVD_F: GCTGACAGGCAGTACCGTG

H_MVD_R: GCATTGAGGTAAGAGATGGGC

PPAR β _Hs:

H_PPAR β _F: GCATGAAGCTGGAGTACGAGAAG

H_PPAR β _R: GCATCCGACCAAAACGGATA

PDK1_Hs:

H_PDK1_F: TGTAACCAGAGAGCGGGATGT

H_PDK1_R: TTTTGGCATAACTAAGGCCGAA

CASP8_Hs:

H_CASP8_F: GGCTTTGACCACGACCTTTGA

H_CASP8_R: AGTGAAGTACTGAGATGTCAGCTCAT

Mouse primer sequences

Ms_Fdft1:

Ms_F_Fdft1: TCC CAC TGC TGT GTA ACT TCC

Ms_R_Fdft1: TGT CTA CAA ATT CTG CCA TCC C

Ms_Lss:

Ms_F_Lss: TCG TGG GGG ACC CTA TAA AAC

Ms_R_Lss: CGT CCT CCG CTT GAT AAT AAG TC

Ms_Mvd :

Ms_F_Mvd: ACC AGC TAA AAA CGA CCA CAA

Ms_R_Mvd: CTG AGG GGT AGA GTG TCC C

Ms_HMGCR:

Ms_HMGCR_F: TCGTCATTCATTTCTCGACAAA

Ms_HMGCR_R: GATTGCCATTCCACGAGCTAT

Ms_HMGCS1:

Ms_HMGCS1_F: AACTGGTGCAGAAATCTCTAGC

Ms_HMGCS1_R: GGTTGAATAGCTCAGAACTAGCC

Ms_PPAR β :Ms_PPAR β _F: CGGCAGCCTCAACATGGMs_PPAR β _R: AGATCCGATCGCACTTCTCATAAC*6. Microarray experiments*

A global gene expression analysis using microarray was performed to identify the effect of irradiation at 10Gy in an in-vitro intestinal cell line model of HT-29. The experimental design is as described in Fig. 42. For all the five groups of samples, total RNA was extracted from quadruplicate experiments using RNeasy Plus mini Kit (Qiagen, USA) according to manufacturer's instructions. cDNA was synthesized from 1 μ g total RNA using the WT expression kit Ambion (Applied biosystems). After fragmentation, 10 μ g cRNA was hybridized with the Human Gene 1.0 ST arrays (Affymetrix,SC,USA).

Gene chips were then scanned in an Affymetrix Scanner, and gene expression was analyzed using the Software Expression Console. The data was submitted to one-way ANOVA (a value of $p < 0.05$ was considered significant). Clustering analysis of the microarray results was performed using 'R' for quality control. Analysis of the microarray data was done using the GeneGO Metacore pathway analysis software to determine the cellular pathways affected upon Irradiation.

7. *Extraction of proteins from cells*

Cells were first washed gently with ice-cold PBS (1X). Cells were then lysed by scraping and pipetting in ice-cold RIPA lysis buffer (50 mM Tris pH=7.4, 150 mM NaCl, 0.5% sodium deoxycholate, 1% NP-40, 0.1% SDS) supplemented with proteases and phosphatases inhibitors (1mM Na_3VO_4 , 1mM PMSF, 10 $\mu\text{g/ml}$ Aprotinin, 10 $\mu\text{g/ml}$ Leupeptin) just before use. Cell lysis was continued by agitation on the spin wheel at 4°C for 40 minutes. The samples were then centrifuged for 15min, 14,000rpm at 4°C. The supernatants were collected and stored at -80°C for further protein analysis.

8. *Western blot*

Proteins extracted from cells using RIPA lysis buffer were denatured for 5 min at 95°C. Equal amounts of protein extracts were then resolved by 10% SDS-PAGE gel. Electrotransfer of proteins onto nitrocellulose membrane was done in 10 min using the iBlot™ device (Invitrogen). Membranes were then blocked for 1h at room temperature (RT) with 5% of milk powder in Tris buffered saline (TBS) with 0.1% Tween-20 and incubated at 4°C overnight with the primary antibodies diluted (1:1000 for all antibodies) in primary antibody dilution buffer (1X TBS, 0.1% Tween-20 with 5% Bovine serum albumin (BSA)). The membranes were then washed in 1X TBST (TBS with 0.1% Tween-20) thrice and incubated for 1 h at RT with anti- IgG, HRP-conjugated secondary antibody in 1X TBST with 5% milk powder and detected by chemiluminescence (GE Healthcare). Blots were then analysed using the Quantity-1® software from BIORAD. Primary anti-Akt and anti-Phospho-Akt (Ser473) (from Cell signaling) and Anti-GAPDH antibodies were purchased from Sigma.

9. *PPAR β silencing using lentivirus*

A lentivirus based vector construct carrying silencing sequence for PPAR β (pLVTHSi PPAR β) [Nadra et al., 2006], was available in the lab. We first amplified the vector pLVTHSi PPAR β , the control vector- pLVTHSi PPAR β ctrl along with pCMV- Δ R8.74 and pMD2G-VSVG that encode for the viral envelope and the packaging genes respectively. These vectors were used further to transfect 293-T cells to produce the

lentivirus. The biological titer of the lentivirus produced was then estimated by FACS analysis. Further, this lentivirus was tested in different concentrations in the HT-29 cell system in order to identify the appropriate Multiplicity of infection (MOI) of virus required to obtain the maximal silencing of our target gene. The knockdown efficiency was also tested at different time-points post infection to ascertain the desired silencing of our gene of interest.

9.1 *Lentivirus production*

All recombinant lentiviruses were produced by transient transfection of 293T cells according to standard protocols. Briefly, subconfluent 293T cells were cotransfected with 112.5 μg of the control vector pLV-THsiPPAR β ctrl or the PPAR β -targeted vector pLV-THsiPPAR β , 73 μg of pCMV- Δ R8.4, and 39.55 μg of pMD2G-VSVG (where CMV is cytomegalovirus and VSVG is vesicular stomatitis virus protein G) by calcium phosphate precipitation. The medium was changed after 16 h, and recombinant lentiviruses in the supernatant were harvested two or three times every 8-12h. The Supernatant were stored at 4°C until used for ultracentrifugation. The pooled supernatant was filtered using a 0.22- μm filter unit. Ultracentrifuge 120 min at 50,000 \times g, 16°C. Resuspend the pellet (not always visible) with PBS1X. Clear the final concentrate by a brief centrifugation (around 5 seconds) at maximum speed on a bench top centrifuge. Aliquot the supernatant and store at 80°C.

10. *MTT assay*

MTT (3-(4,5-Dimethylthiazol-2-yl)-2,5-diphenyltetrazolium bromide, a yellow tetrazole), is a dye that is reduced to purple formazan in living cells. MTT assay is a colorimetric assay for measuring the activity of enzymes that reduce MTT to formazan dye, giving a purple color. A main application allows assessing the viability (cell counting) and the proliferation of cells (cell culture assays). It can also be used to determine cytotoxicity of potential drugs, since those agents would stimulate or inhibit cell viability and growth. MTT assay is based on the inverse relation between the absorbance and the cytotoxicity. The higher the absorbance the lesser the cytotoxicity and vice-versa.

We used the MTT assay to assess cytotoxicity in response to PPAR β agonist and antagonist treatment at different doses in HT-29 and HCT-116 cells.

MTT (Sigma) stock solution was prepared at a concentration of 5mg/ml. After the treatment with the agonist or antagonist for appropriate time, the medium was removed and the diluted MTT working solution (0.5mg/ml) was added. The cells were incubated at 37°C for 3 hrs and were observed by phase contrast microscopy for color development at regular intervals. At that point, the MTT working solution was eliminated and the solubilization solution (90% isopropanol + 10% DMSO) was added and incubated at 37°C for 20 min. After this, 100ul of the colored solution was transferred to a 96well plate and the absorbance was read at 550nm.

11. *Caspase- 3/7 assay*

The Caspase-3/7 assay Kit (Promega) provides a proluminescent caspase-3/7 DEVD-aminoluciferin substrate and a thermostable luciferase in a reagent optimized for caspase-3/7 activity, luciferase activity and cell lysis. To assay Caspase activity, an equal volume of Caspase-Glo® 3/7 reagent is added to the sample in the assay well and after mixing well, results in cell lysis. This is followed by caspase cleavage of the substrate that liberates free aminoluciferin, which is consumed by the luciferase, generating a "glow-type" luminescent signal. And this light generated is measured with a luminometer (Promega corp.). The signal is proportional to caspase-3/7 activity.

HT-29 cells were seeded in 96 well plates and cultured overnight at 37°C, 5% CO₂. They were irradiated with different doses ranging from 0-30Gy and samples were prepared according to the manufacturer's instructions in Caspase-Glo 3/7 assay kit (Promega). Luminescence emitted due to caspase-3/7 cleavage of the luminogenic substrate was measured for each dose at 6h and 24h post irradiation. Luminescence measured was proportional to the caspase activity present and the signal from no cell control was subtracted from the signal from the treated and untreated controls. The fold change values were calculated with Sham irradiated cells (Sh.I) as control group for statistical calculations.

12. *Clonogenic assay*

Clonogenic assays are considered gold standards to determine the cytotoxic effect of radiotherapy using ionizing radiations and chemotherapy using several chemical agents and also the latest intervention of dual treatments of chemo-radiotherapy. The intrinsic radiosensitivity of the two colorectal cell lines, HT-29 and HCT-116 was determined by this colony-forming assay. We tested two different protocols as outlined below and found that the seeding before irradiation protocol gave better results and thus used it for all our experiments.

12.1 *Seeding after irradiation protocol:*

Seed several T-25cm² flasks with appropriate number of cells and incubate them at 37°C in the incubator so as to have cells in the logarithmic growth phase after 2 days in culture. Irradiate these cells at the appropriate doses. Remove media from these flasks and wash them with PBS. Trypsinize each flask with 1 ml of 0.05% Trypsin-EDTA. Observe under microscope and make a single cell suspension in warm culture media (DMEM-10 + 10% FCS). Serially dilute and seed appropriate dilutions onto six well plates. Mix well for uniform distribution of cells and incubate at 37°C, 5% CO₂. For HCT-116 cells, we allowed them to grow for 8days post-irradiation and for HT-29 cells we allowed them to grow for 12 days post-irradiation.

12.2 *Seeding before irradiation protocol:*

Label all the six-well plates (TPP) appropriately and add 2ml of media (DMEM-10 + 10% FCS) with or without the ligands for PPAR β and let it warm at 37°C in the incubator. Trypsinize a T-25cm² flask with 1ml of Trypsin and make a single cell suspension. Serially dilute in media with or without PPAR β ligands and seed appropriate dilutions on respective plates so as to have 100, 200, 400, 800 cells per well. Incubate overnight at 37°C, 5% CO₂ and four hours before irradiation add fresh media. Irradiate at the desired doses and culture at 37°C, 5% CO₂ for the desired time post-irradiation to allow colony formation. For HCT-116 cells, we allowed them to grow for 8days post-irradiation and for HT-29 cells we allowed them to grow for 12 days post-irradiation.

12.3 Counting of colonies

We followed the standard procedure to count the colonies using the stereobinocular microscope. The number of colonies in each set of treatment for the different grades of irradiation doses was counted, with untreated and non-irradiated group serving as control. The plating efficiency (PE) is the ratio of the number of colonies to the number of cells seeded and was calculated as follows:

$$PE = \frac{\text{Number of colonies counted}}{\text{Number of cells plated}} \times 100$$

The number of colonies that arise after treatment of cells, expressed in terms of PE, is called the surviving fraction (SF):

$$SF = \frac{\text{no. of colonies formed after treatment}}{\text{no. of cells seeded} \times PE}$$

We determined the PE of control cells, that is, the fraction of colonies from cells not exposed to irradiation and ligand treatments. The surviving fraction of cells after any treatment was always calculated taking into account the PE of control cells (For details, see Franken et al., 2006).

13. H_2O_2 assays

We tested the role of PPAR β in a model of oxidant injury induced by the production of reactive oxygen metabolites by administration of H_2O_2 to intestinal cell lines, HT-29 and HCT-116.

HT-29 cells were seeded at a density of 0.01×10^6 cells per well of a 96 well plate in media containing DMEM-10 with 10% FBS. HCT-116 cells were seeded at a density of 0.05×10^6 cells per well of a 24 well plate in media containing DMEM-10 with 10% FBS. Both the cell types were incubated for 24h at 37°C, 5% CO_2 in an incubator. Further they were pre-treated with the PPAR β ligands for 24h in serum free media. The liganded media was then replaced with different concentrations of H_2O_2 (500 μ M – 5mM) prepared in serum free media and allowed to incubate at 37°C, 5% CO_2 for 1 hour. The media was

then removed and an MTT assay was performed as mentioned previously. The O.D reading at 550 nm was directly linked to the used to calculate the surviving fraction with cells without H₂O₂ serving as controls.

14. Statistical analysis

Data are expressed as mean \pm S.E.M. All analysis was performed with Graphpad Prism version 5.0 software using one-way analysis of variance (ANOVA) followed by Newman–Keul’s multiple comparison tests, and paired two-tailed t-test where applicable. $p < 0.05$ was considered to be statistically significant.

REFERENCES

- Akiyama TE, Lambert G, Nicol CJ, Matsusue K, Peters JM, Brewer HB Jr, Gonzalez FJ. Peroxisome proliferator-activated receptor beta/delta regulates very low density lipoprotein production and catabolism in mice on a Western diet. *J Biol Chem* 2004; 279: 20874-20881.
- Anno GH, Baum SJ, Withers HR, Young RW. Symptomatology of acute radiation effects in humans after exposure to doses of 0.5-30Gy. *Health Phys* 1989; 56:821-838.
- Arai T, Kida Y, Harmon BV, Gobé GC. Expression and localization of clusterin mRNA in the small and large intestine of the irradiated rat: its relationship with apoptosis. *Int J Radiat Biol* 1996; 69: 547-553.
- Aung CS, Faddy HM, Lister EJ, Monteith GR, Roberts-Thomson SJ. Isoform specific changes in PPAR α and β in colon and breast cancer with differentiation. *Biochem Biophys Res Commun* 2006; 340: 656-660.
- Axelsen JB, Bock-Axelsen J, Lotem J, Sachs L, Domany E. Genes overexpressed in different human solid cancers exhibit different tissue-specific expression profiles. *Proc Natl Acad Sci USA* 2007; 104: 13122-13127.
- Babbar N, Ignatenko NA, Casero RA Jr, Gerner EW. Cyclooxygenase-independent induction of apoptosis by sulindac sulfone is mediated by polyamines in colon cancer. *J Biol Chem* 2003; 278: 47762-47775.
- Bae YS, Kang SW, Seo MS, Baines IC, Tekle E, Chock PB, Rhee SG. Epidermal growth factor (EGF)-induced generation of hydrogen peroxide. Role in EGF receptor-mediated tyrosine phosphorylation. *J Biol Chem* 1997; 272: 217-221.
- Barak Y, Liao D, He W, Ong ES, Nelson MC, Olefsky JM, Boland R, Evans RM. Effects of peroxisome proliferator-activated receptor delta on placentation, adiposity, and colorectal cancer. *Proc Natl Acad Sci USA* 2002; 99: 303-308.
- Barcellos-Hoff MH. How do tissues respond to damage at the cellular level? The role of cytokines in irradiated tissues. *Radiat Res* 1998; 150: S109-S120.
- Barker N, Clevers H. Tracking down the stem cells of the intestine: strategies to identify adult stem cells. *Gastroenterology* 2007; 133: 1755-1760.
- Bastide P, Darido C, Pannequin J, Kist R, Robine S, Marty-Double C, Bibeau F, Scherer G, Joubert D, Hollande F, Blache P, Jay P. Sox9 regulates cell proliferation and is required for Paneth cell differentiation in the intestinal epithelium. *J Cell Biol* 2007; 178: 635-648.
- Beckman JS, Koppenol WH. Nitric oxide, superoxide and peroxynitrite: the good, the bad, and the ugly. *Am J Physiol* 1996; 271: C1424-C1437.
- Bedu E, Wahli W, Desvergne B. Peroxisome proliferator-activated receptor beta/delta as a therapeutic target for metabolic diseases. *Expert Opin Ther Targets* 2005;9:861-873.
- Berroud A, Le Roy A, Voisin P. Membrane oxidative damage induced by ionizing radiation detected by fluorescence polarization. *Radiat Environ Biophys* 1996; 35: 289-295.

Berthrong M, Fajardo LF. Radiation injury in surgical pathology. Part II. Alimentary tract. *Am J Surg Pathol* 1981; 5: 153-178.

Bonnaud S, Niaudet C, Legoux F, Corre I, Delpon G, Saulquin X, Fuks Z, Gaugler M-H, Kolesnick R, Paris F. Sphingosine-1-phosphate activates the AKT pathway to protect small intestines from radiation-induced endothelial apoptosis. *Cancer Res* 2010; 70: 9905–9915.

Brach MA, Hass R, Sherman ML, Gunji H, Weichselbaum R, Kufe D. Ionizing radiation induces expression and binding activity of the nuclear factor kappa B. *J Clin Invest* 1991; 88: 691-695.

Blache P, van de Wetering M, Duluc I, Domon C, Berta P, Freund JN, Clevers H, Jay P. SOX9 is an intestine crypt transcription factor, is regulated by the Wnt pathway, and represses the CDX2 and MUC2 genes. *J Cell Biol* 2004; 166: 37-47.

Booth D, Potten CS. Protection against mucosal injury by growth factors and cytokines. *J Natl Cancer Inst Monogr* 2001; 29: 16-20.

Briscoe J, Chen Y, Jessell TM, Struhl G. A hedgehog-insensitive form of patched provides evidence for direct long-range morphogen activity of sonic hedgehog in the neural tube. *Mol Cell* 2001; 7: 1279-1291.

Brun RP, Tontonoz P, Forman BM, Ellis R, Chen J, Evans RM, Spiegelman BM. Differential activation of adipogenesis by multiple PPAR isoforms. *Genes Dev* 1996; 10: 974-984.

Brunelli L, Cieslik KA, Alcorn JL, Vatta M, Baldini A. Peroxisome proliferator-activated receptor-delta upregulates 14-3-3 epsilon in human endothelial cells via CCAAT/enhancer binding protein-beta. *Circ Res* 2007; 100: e59-e71.

Bumcrot DA, Takada R, McMahon AP. Proteolytic processing yields two secreted forms of sonic hedgehog. *Mol Cell Biol* 1995; 15: 2294–2303.

Burdick AD, Kim DJ, Peraza MA, Gonzalez FJ, Peters JM. The role of peroxisome proliferator-activated receptor-beta/delta in epithelial cell growth and differentiation. *Cell Signal* 2006; 18: 9-20.

Bussink J, van der Kogel AJ, Kaanders JHAM. Activation of the PI3-K/AKT pathway and implications for radioresistance mechanisms in head and neck cancer. *Lancet Oncol* 2008; 9: 288–296.

Cadigan KM, Nusse R. Wnt signaling: a common theme in animal development. *Genes Dev* 1997; 11: 3286–3305.

Cai WB, Roberts SA, Potten CS. The number of clonogenic cells in crypts in three regions of murine large intestine. *Int J Radiat Biol* 1997; 71: 573-579.

Canman CE, Wolff AC, Chen CY, Fornace AJ Jr, Kastan MB. The p53-dependent G1 cell cycle checkpoint pathway and ataxia-telangiectasia. *Cancer Res* 1994; 54: 5054–5058.

- Carr KE, Bullock C, Ryan SS, McAlinden MG, Boyle FC. Radioprotectant effects of atropine on small intestinal villous shape. *J Submicrosc Cytol Pathol* 1991; 23: 569-577.
- Carr KE, Hume SP, Nelson AC, O'Shea O, Hazzard RA, McCullough JS. Morphological profiles of neutron and X-irradiated small intestine. *J Radiat Res* 1996; 37: 38-48.
- Caspary T, Garcia-Garcia MJ, Huangfu D, Eggenschwiler JT, Wyler MR, Rakeman AS, Alcorn HL, Anderson KV. Mouse Dispatched homolog1 is required for long-range, but not juxtacrine, Hh signaling. *Curr Biol* 2002; 12: 1628-1632.
- Ch'ang HJ, Maj JG, Paris F, Xing HR, Zhang J, Truman JP, Cardon-Cardo C, Haimovitz-Friedman A, Kolesnick R, Fuks Z. ATM regulates target switching to escalating doses of radiation in the intestines. *Nat Med* 2005; 11: 484-490.
- Chawla A, Lee CH, Barak Y, He W, Rosenfeld J, Liao D, Han J, Kang H, Evans RM. PPARdelta is a very low-density lipoprotein sensor in macrophages. *Proc Natl Acad Sci USA* 2003; 100: 1268-1273.
- Chen JK, Taipale J, Cooper MK, Beachy PA. Inhibition of Hedgehog signaling by direct binding of cyclopamine to Smoothened. *Genes Dev* 2002; 16: 2743-2748.
- Chen LC, Hao CY, Chiu YS, Wong P, Melnick JS, Brotman M, Moretto J, Mendes F, Smith AP, Bennington JL, Moore D, Lee NM. Alteration of gene expression in normal-appearing colon mucosa of APC (min) mice and human cancer patients. *Cancer Res* 2004; 64: 3694-3700.
- Chen MH, Li YJ, Kawakami T, Xu SM, Chuang PT. Palmitoylation is required for the production of a soluble multimeric Hedgehog protein complex and long-range signaling in vertebrates. *Genes Dev* 2004; 18: 641-659.
- Chuang PT, McMahon AP. Vertebrate Hedgehog signalling modulated by induction of a Hedgehog-binding protein. *Nature* 1999; 397: 617-621.
- Cimini A, Benedetti E, Cristiano L, Sebastiani P, D'Amico MA, D'Angelo B, Di Loreto S. Expression of peroxisome proliferator-activated receptors (PPARs) and retinoic acid receptors (RXRs) in rat cortical neurons. *Neuroscience* 2005; 130: 325-337.
- Clarke AR, Gledhill S, Hooper ML, Bird CC, Wyllie A H. p53 dependence of early apoptotic and proliferative responses within the mouse intestinal epithelium following gamma-irradiation. *Oncogene* 1994; 9: 1767-1773.
- Clevers H. Wnt/beta-catenin signaling in development and disease. *Cell* 2006; 127: 469-480.
- Cliffe A, Hamada F, Bienz M. A role of Dishevelled in relocating Axin to the plasma membrane during wingless signaling. *Curr Biol* 2003; 27:13:960-966.
- Coleman JD, Prabhu KS, Thompson JT, Reddy PS, Peters JM, Peterson BR, Reddy CC, Vanden Heuvel JP. The oxidative stress mediator 4-hydroxynonenal is an intracellular agonist of the nuclear receptor peroxisome proliferator-activated receptor-beta/delta (PPARbeta/delta). *Free Radic Biol Med* 2007;42:1155-1164.

Corbit KC, Aanstad P, Singla V, Norman AR, Stainier DY, Reiter JF. Vertebrate Smoothed functions at the primary cilium. *Nature* 2005;437:1018–1021.

Cordes N, Blaese MA, Meineke V, Van BD. Ionizing radiation induces up-regulation of functional beta1-integrin in human lung tumour cell lines in vitro. *Int J Radiat Biol* 2002;78:347-357.

Crosnier C, Stamatakis D, Lewis J. Organizing cell renewal in the intestine: stem cells, signals and combinatorial control. *Nat Rev Genet* 2006;7:349-359.

Cullingford TE, Bhakoo K, Peuchen S, Dolphin CT, Patel R, Clark JB. Distribution of mRNAs encoding the peroxisome proliferator-activated receptor alpha, beta, and gamma and the retinoid X receptor alpha, beta, and gamma in rat central nervous system. *J Neurochem* 1998;70:1366-1375.

D'Errico I, Moschetta A. Nuclear receptors, intestinal architecture and colon cancer: an intriguing link. *Cell Mol Life Sci* 2008;65:1523-1543.

Deacon J, Peckham MJ, Steel GG. The radioresponsiveness of human tumours and the initial slope of the cell survival curve. *Radiother Oncol* 1984;2:317–323.

DeRisi JL. Exploring the Metabolic and Genetic Control of Gene Expression on a Genomic Scale. *Science* 1997;278:680–686.

Desvergne B, Feige JN, Casals-Casas C. PPAR-mediated activity of phthalates: A link to the obesity epidemic? *Mol Cell Endocrinol* 2009;304:43-48.

Desvergne B, Wahli W. Peroxisome proliferator-activated receptors: nuclear control of metabolism. *Endocr Rev* 1999;20:649-688.

Dey S, Spring PM, Arnold S, Valentino J, Chendil D, Regine WF, Mohiuddin M, Ahmed MM. Low-dose fractionated radiation potentiates the effects of Paclitaxel in wild-type and mutant p53 head and neck tumor cell lines. *Clin Cancer Res* 2003;9:1557–1565.

Diker-Cohen T, Koren R, Liberman UA, Ravid A. Vitamin D Protects Keratinocytes from Apoptosis Induced by Osmotic Shock, Oxidative Stress, and Tumor Necrosis Factor. *Ann N Y Acad Sci* 2003;1010:350–353.

Di Loreto S, Sebastiani P, Benedetti E, Zimmiti V, Caracciolo V, Amicarelli F, Cimini A, Adorno D. Transient maintenance in bioreactor improves health of neuronal cells. *In Vitro Cell Dev Biol Anim* 2006;42:134-142.

Di-Poi N, Ng CY, Tan NS, Yang Z, Hemmings BA, Desvergne B, Michalik L, Wahli W. Epithelium-mesenchyme interactions control the activity of peroxisome proliferator-activated receptor beta/delta during hair follicle development. *Mol Cell Biol* 2005;25:1696-1712.

Di-Poi N, Tan NS, Michalik L, Wahli W, Desvergne B. Antiapoptotic role of PPARbeta in keratinocytes via transcriptional control of the Akt1 signaling pathway. *Mol Cell* 2002;10:721-733.

- Dubois A, Walker RI. Prospects for management of gastrointestinal injury associated with the acute radiation syndrome. *Gastroenterology* 1988;95:500-507.
- Duval C, Müller M, Kersten S. PPARalpha and dyslipidemia. *Biochim Biophys Acta* 2007;1771:961-971.
- Ehlen HW, Buelens LA, Vortkamp A. Hedgehog signaling in skeletal development. *Birth Defects Res C Embryo Today* 2006;78:267– 279.
- El Marjou F, Janssen KP, Chang BH, Li M, Hindie V, Chan L, Louvard D, Chambon P, Metzger D, Robine S. Tissue-specific and inducible Cre-mediated recombination in the gut epithelium. *Genesis* 2004; 39:186–193.
- Escher P, Braissant O, Basu-Modak S, Michalik L, Wahli W, Desvergne B. Rat PPARs: quantitative analysis in adult rat tissues and regulation in fasting and refeeding. *Endocrinology* 2001;142:4195-4202.
- Fevr T, Robine S, Louvard D, Huelsken J. Wnt/ β -Catenin Is Essential for Intestinal Homeostasis and Maintenance of Intestinal Stem Cells. *Mol Cell Biol* 2007;27:7551-7559.
- Fire A, Xu S, Montgomery MK, Kostas SA, Driver SE, Mello CC. Potent and specific genetic interference by double-stranded RNA in *Caenorhabditis elegans*. *Nature* 1998;391:806-811.
- Flentjar N, Chu PY, Ng AY, Johnstone CN, Heath JK, Ernst M, Hertzog PJ, Pritchard MA. TGF-betaR2 rescues development of small intestinal epithelial cells in Elf3-deficient mice. *Gastroenterology* 2007;132:1410-1419.
- Followill DS, Kester D, Travis EL. Histological changes in mouse colon after single- and split-dose irradiation. *Radiat Res* 1993;136:280-288.
- Forgue-Lafitte ME, Coudray AM, Bréant B, Mester J. Proliferation of the human colon carcinoma cell line HT29: autocrine growth and deregulated expression of the c-myc oncogene. *Cancer Res* 1989;49:6566-6571.
- Forman BM, Chen J, Evans RM. Hypolipidemic drugs, polyunsaturated fatty acids, and eicosanoids are ligands for peroxisome proliferator-activated receptors alpha and delta. *Proc Natl Acad Sci USA* 1997;94:4312-4317.
- Franken NAP, Rodermond HM, Stap J, Haveman J, van Bree C. Clonogenic assay of cells in vitro. *Nat Protoc* 2006;1:2315–2319.
- Fre S, Huyghe M, Mourikis P, Robine S, Louvard D, Artavanis-Tsakonas S. Notch signals control the fate of immature progenitor cells in the intestine. *Nature* 2005;435: 964-968.
- Frisch SM, Ruoslahti E. Integrins and anoikis. *Curr Opin Cell Biol* 1997;9:701–706.
- Giaccia AJ, Kastan MB. The complexity of p53 modulation: Emerging patterns from divergent signals. *Genes Dev* 1998;12:2973-2983.

- Glass CK. Going nuclear in metabolic and cardiovascular disease. *J Clin Invest* 2006;116:556-560.
- Goodrich LV, Johnson RL, Milenkovic L, McMahon JA, Scott MP. Conservation of the hedgehog/ patched signaling pathway from flies to mice: induction of a mouse patched gene by Hedgehog. *Genes Dev* 1996;10:301-312.
- Grimaldi PA. Regulatory functions of PPARbeta in metabolism: implications for the treatment of metabolic syndrome. *Biochim Biophys Acta* 2007;1771:983-990.
- Guillemot F, Lo LC, Johnson JE, Auerbach A, Anderson DJ, Joyner AL. Mammalian achaete-scute homolog 1 is required for the early development of olfactory and autonomic neurons. *Cell*. 1993; 75: 463-476.
- Gupta RA, Tan J, Krause WF, Geraci MW, Willson TM, Dey SK, DuBois RN. Prostacyclin-mediated activation of peroxisome proliferator-activated receptor delta in colorectal cancer. *Proc Natl Acad Sci USA* 2000;97:13275-13280.
- Gupta RA, Wang D, Katkuri S, Wang H, Dey SK, DuBois RN. Activation of nuclear hormone receptor peroxisome proliferator-activated receptor-delta accelerates intestinal adenoma growth. *Nat Med* 2004;10:245-247.
- Hallahan DE, Virudachalam S, Sherman ML, Huberman E, Kufe DW, Weichselbaum RR. Tumor necrosis factor gene expression is mediated by protein kinase C following activation by ionizing radiation. *Cancer Res* 1991;51:4565-4569.
- Han J, Flemington C, Houghton AB, Gu Z, Zambetti GP, Lutz RJ, Zhu L, Chittenden T. Expression of *bbc3*, a pro-apoptotic BH3-only gene, is regulated by diverse cell death and survival signals. *Proc Natl Acad Sci USA* 2001;98:11318-11323.
- Harman FS, Nicol CJ, Marin HE, Ward JM, Gonzalez FJ, Peters JM. Peroxisome proliferator-activated receptor-delta attenuates colon carcinogenesis. *Nat Med* 2004;10: 481-483.
- Hauer-Jensen M, Richter KK, Wang J, Abe E, Sung CC, Hardin JW. Changes in transforming growth factor beta1 gene expression and immunoreactivity levels during development of chronic radiation enteropathy. *Radiat Res* 1998;150:673-680.
- Hauer-Jensen M. Late radiation injury of the small intestine. Clinical, pathophysiologic and radiobiologic aspects. A review. *Acta Oncol* 1990;29:401-415.
- He TC, Chan TA, Vogelstein B, Kinzler KW. PPARdelta is an APC-regulated target of nonsteroidal anti-inflammatory drugs. *Cell* 1999;99:335-345.
- Hellemans K, Michalik L, Dittie A, Knorr A, Rombouts K, De Jong J, Heirman C, Quartier E, Schuit F, Wahli W, Geerts A. Peroxisome proliferator-activated receptor-beta signaling contributes to enhanced proliferation of hepatic stellate cells. *Gastroenterology* 2003;124:184-201.

- Höcker M, Wiedenmann B. Molecular mechanisms of enteroendocrine differentiation. *Ann N Y Acad Sci* 1998;859:160-174.
- Hollingshead HE, Killins RL, Borland MG, Girroir EE, Billin AN, Willson TM, Sharma AK, Amin S, Gonzalez FJ, Peters JM. Peroxisome proliferator-activated receptor-beta/delta (PPARbeta/delta) ligands do not potentiate growth of human cancer cell lines. *Carcinogenesis* 2007;28:2641-2649.
- Holst D, Luquet S, Kristiansen K, Grimaldi PA. Roles of peroxisome proliferator-activated receptors delta and gamma in myoblast transdifferentiation. *Exp Cell Res* 2003;288:168-176.
- Houchen CW, Stenson WF, Cohn SM. Disruption of cyclooxygenase-1 gene results in an impaired response to radiation injury. *Am J Physiol* 2000;279:G858-G865.
- Huangfu D, Anderson KV. Signaling from Smo to Ci/Gli: conservation and divergence of Hedgehog pathways from Drosophila to vertebrates. *Development* 2006;133:3-14.
- Hui CC, Slusarski D, Platt KA, Holmgren R, Joyner AL. Expression of three mouse homologs of the Drosophila segment polarity gene cubitus interruptus, Gli, Gli-2, Gli-3, in ectoderm- and mesoderm-derived tissues suggests multiple roles during postimplantation development. *Dev Biol* 1994;162:402-413.
- Ibuki Y, Goto R. Enhancement of NO production from residual peritoneal macrophages by *in vitro* irradiation and its relationship to reactive oxygen intermediates. *Free Radic Biol Med* 1997;22:1029-1035.
- Ijiri K, Potten CS. The re-establishment of hypersensitive cells in the crypts of irradiated mouse intestine. *Int J Radiat Biol Relat Stud Phys Chem Med* 1984;46:609-623.
- Incardona JP, Gruenberg J, Roelink H. Sonic hedgehog induces the segregation of patched and smoothed in endosomes. *Curr Biol* 2002;12:983-995.
- Ireland H, Kemp R, Houghton C, Howard L, Clarke AR, Sansom OJ, Winton DJ. Inducible Cre-mediated control of gene expression in the murine gastrointestinal tract: effect of loss of beta-catenin. *Gastroenterology* 2004;126:1236-1246.
- Jenny M, Uhl C, Roche C, Duluc I, Guillermin V, Guillemot F, Jensen J, Kedinger M, Gradwohl G. Neurogenin3 is differentially required for endocrine cell fate specification in the intestinal and gastric epithelium. *EMBO J* 2002;21:6338-6347.
- Jensen J, Pedersen EE, Galante P, Hald J, Heller RS, Ishibashi M, Kageyama R, Guillemot F, Serup P, Madsen OD. Control of endodermal endocrine development by Hes-1. *Nat Genet* 2000;24:36-44.
- Johnson RJ, Carrington BM. Pelvic radiation disease. *Clin Radiol* 1992;45:4-12.
- Jones RM, Sloane VM, Wu H, Luo L, Kumar A, Kumar MV, Gewirtz AT, Neish AS. Flagellin administration protects gut mucosal tissue from irradiation-induced apoptosis via MKP-7 activity. *Gut* 2011;60:648-657.

- Jung J, Zheng M, Goldfarb M, Zaret KS. Initiation of mammalian liver development from endoderm by fibroblast growth factors. *Science* 1999; 284:1998–2003.
- Jung M, Dritschilo A. Signal transduction and cellular responses to ionizing radiation. *Semin Radiat Oncol* 1996;6:268–272.
- Kang JS, Mulieri PJ, Hu Y, Taliana L, Krauss RS. BOC, an Ig superfamily member, associates with CDO to positively regulate myogenic differentiation. *EMBO J* 2002;21:114–124.
- Kang JS, Mulieri PJ, Miller C, Sassoon DA, Krauss RS. CDO, a robo-related cell surface protein that mediates myogenic differentiation. *J Cell Biol* 1998;143:403–413.
- Kao MS. Intestinal complications of radiotherapy in gynecologic malignancy—clinical presentation and management. *Int J Gynaecol Obstet* 1995;49:S69-S75.
- Kastan MB, Onyekwere O, Sidransky D, Vogelstein B, Craig RW. Participation of p53 protein in the cellular response to DNA damage. *Cancer Res* 1991;51:6304–6311.
- Kastan MB, Zhan Q, el-Deiry WS, Carrier F, Jacks T, Walsh WV, Plunkett BS, Vogelstein B, Fornace AJ Jr. A mammalian cell cycle checkpoint pathway utilizing p53 and GADD45 is defective in ataxia-telangiectasia. *Cell* 1992;71:587–597.
- Katz JP, Perreault N, Goldstein BG, Lee CS, Labosky PA, Yang VW, Kaestner KH. The zinc-finger transcription factor Klf4 is required for terminal differentiation of goblet cells in the colon. *Development*. 2002;129:2619-2628.
- Kavanagh BD, Dent P, Schmidt-Ullrich RK, Chen P, Mikkelsen RB. Calcium-dependent stimulation of mitogen-activated protein kinase activity in A431 cells by low doses of ionizing radiation. *Radiat Res* 1998;149:579-87.
- Kawakami T, Kawcak T, Li YJ, Zhang W, Hu Y, Chuang PT. Mouse dispatched mutants fail to distribute hedgehog proteins and are defective in hedgehog signaling. *Development* 2002;129:5753–5765.
- Kharroubi I, Lee CH, Hekerman P, Darville MI, Evans RM, Eizirik DL, Cnop M. BCL-6: a possible missing link for anti-inflammatory PPAR-delta signalling in pancreatic beta cells. *Diabetologia* 2006;49:2350-2358.
- Kim DJ, Murray IA, Burns AM, Gonzalez FJ, Perdew GH, Peters JM. Peroxisome proliferator-activated receptor-beta/delta inhibits epidermal cell proliferation by down-regulation of kinase activity. *J Biol Chem* 2005;280:9519-9527.
- Kim KA, Kakitani M, Zhao J, Oshima T, Tang T, Binnerts M, Liu Y, Boyle B, Park E, Emtage P, Funk WD, Tomizuka K. Mitogenic Influence of Human R-Spondin1 on the Intestinal Epithelium. *Science* 2005;309:1256–1259.
- Knutsen HK, Olstørn HB, Paulsen JE, Husøy T, Goverud IL, Løberg EM, Kristiansen K, Alexander J. Increased levels of PPARbeta/delta and cyclin D1 in flat dysplastic ACF and adenomas in Apc(Min/+) mice. *Anticancer Res* 2005;25:3781-3789.

- Kolomiitseva IK. Activation of cholesterologenesis in response to ionizing irradiation of the animal body. *Radiobiologia* 1986;26:3-10.
- Koren R, Wacksberg S, Weitsman GE, Ravid A. Calcitriol sensitizes colon cancer cells to H₂O₂-induced cytotoxicity while inhibiting caspase activation. *J Steroid Biochem Mol Biol* 2006;101:151–160.
- Korinek V, Barker N, Moerer P, van Donselaar E, Huls G, Peters PJ, Clevers H. Depletion of epithelial stem-cell compartments in the small intestine of mice lacking Tcf-4. *Nat Genet* 1998;19:379–383.
- Korinek V, Barker N, Willert K, Molenaar M, Roose J, Wagenaar G, Markman M, Lamers W, Destree O, Clevers H. Two members of the Tcf family implicated in Wnt/beta-catenin signaling during embryogenesis in the mouse. *Mol Cell Biol* 1998;18:1248-1256.
- Kosinski C, Stange DE, Xu C, Chan AS, Ho C, Yuen ST, Mifflin RC, Powell DW, Clevers H, Leung SY, Chen X. Indian hedgehog regulates intestinal stem cell fate through epithelial-mesenchymal interactions during development *Gastroenterology* 2010;139:893–903.
- Kuerbitz SJ, Plunkett BS, Walsh WV, Kastan MB. Wild-type p53 is a cell cycle checkpoint determinant following irradiation. *Proc Natl Acad Sci USA* 1992;89:7491–7495.
- Kuhnert F, Davis CR, Wang HT, Chu P, Lee M, Yuan J, Nusse R, Kuo CJ. Essential requirement for Wnt signaling in proliferation of adult small intestine and colon revealed by adenoviral expression of Dickkopf-1. *Proc Natl Acad Sci USA* 2004;101:266-271.
- Labi V, Erlacher M, Kiessling S, Villunger A. BH3-only proteins in cell death initiation, malignant disease and anticancer therapy. *Cell Death Differ* 2006;13:1325-1338.
- Lander HM, Ogiste JS, Teng KK, Novogrodsky A. p21ras as a common signaling target of reactive free radicals and cellular redox stress. *J Biol Chem* 1995;270:21195–21198.
- Langberg CW, Hauer-Jensen M. Influence of fraction size on the development of late radiation enteropathy. An experimental study in the rat. *Acta Oncol* 1996;35:89-94.
- Lee JJ, Ekker SC, von Kessler DP, Porter JA, Sun BI, Beachy PA. Autoproteolysis in hedgehog protein biogenesis. *Science* 1994;266:1528 –1537.
- Lee JJ, von Kessler DP, Parks S, Beachy PA. Secretion and localized transcription suggest a role in positional signaling for products of the segmentation gene hedgehog. *Cell* 1992;71:33–50.
- Lee JM, Bernstein A. p53 mutations increase resistance to ionizing radiation. *Proc Natl Acad Sci USA* 1993;90:5742–5746.
- Lee SR, Kwon KS, Kim SR, Rhee SG. Reversible inactivation of protein-tyrosine phosphatase 1B in A431 cells stimulated with epidermal growth factor. *J Biol Chem* 1998;273:15366-15372.

Leibowitz MD, Fiévet C, Hennuyer N, Peinado-Onsurbe J, Duez H, Bergera J, Cullinan CA, Sparrow CP, Baffic J, Berger GD, Santini C, Marquis RW, Tolman RL, Smith RG, Moller DE, Auwerx J. Activation of PPARdelta alters lipid metabolism in db/db mice. *FEBS Lett* 2000;473:333-336.

Leist M, Jäättelä M. Four Deaths and A Funeral: From Caspases to Alternative Mechanisms. *Nat Rev Mol Cell Biol* 2001;2:589–598.

Lemasters JJ, DiGuseppi J, Nieminen A-L, Herman B. Blebbing, free Ca²⁺ and mitochondrial membrane potential preceding cell death in hepatocytes. *Nature* 1987;325:78–81.

Letavernier E, Perez J, Joye E, Bellocq A, Fouqueray B, Haymann JP, Heudes D, Wahli W, Desvergne B, Baud L. Peroxisome proliferator-activated receptor beta/delta exerts a strong protection from ischemic acute renal failure. *J Am Soc Nephrol* 2005;16:2395–2402.

Lewis PM, Dunn MP, McMahon JA, Logan M, Martin JF, St-Jacques B, McMahon AP. Cholesterol modification of sonic hedgehog is required for long-range signaling activity and effective modulation of signaling by Ptc1. *Cell* 2001;105:599-612.

Li Y, Zhang H, Litingtung Y, Chiang C. Cholesterol modification restricts the spread of Shh gradient in the limb bud. *Proc Natl Acad Sci USA* 2006;103:6548 – 6553.

Lim H, Gupta RA, Ma WG, Paria BC, Moller DE, Morrow JD, DuBois RN, Trzaskos JM, Dey SK. Cyclo-oxygenase-2-derived prostacyclin mediates embryo implantation in the mouse via PPARdelta. *Genes Dev* 1999;13:1561-1574.

Liou JY, Ghelani D, Yeh S, Wu KK. Nonsteroidal anti-inflammatory drugs induce colorectal cancer cell apoptosis by suppressing 14-3-3epsilon. *Cancer Res* 2007;67: 3185-3191.

Liou JY, Lee S, Ghelani D, Matijevic-Aleksic N, Wu KK. Protection of endothelial survival by peroxisome proliferator-activated receptor-delta mediated 14-3-3 upregulation. *Arterioscler Thromb Vasc Biol* 2006; 26:1481-1487.

Liou JY, Aleksic N, Chen SF, Han TJ, Shyue SK, Wu KK. Mitochondrial localization of cyclooxygenase-2 and calcium-independent phospholipase A2 in human cancer cells: Implication in apoptosis resistance. *Experimental Cell Research* 2005;306:75–84.

Luquet S, Lopez-Soriano J, Holst D, Fredenrich A, Melki J, Rassoulzadegan M, Grimaldi PA. Peroxisome proliferator-activated receptor delta controls muscle development and oxidative capability. *FASEB J* 2003;17:2299-2301.

Ma TL, Ni PH, Zhong J, Tan JH, Qiao MM, Jiang SH. Low expression of XIAP-associated factor 1 in human colorectal cancers. *Chin J Dig Dis* 2005;6:10–14.

Ma Y, Erkner A, Gong R, Yao S, Taipale J, Basler K, Beachy PA. Hedgehog-mediated patterning of the mammalian embryo requires transporter-like function of Dispatched. *Cell* 2002;111:63–75.

- MacNaughton WK. New insights into the pathogenesis of radiation-induced intestinal dysfunction. *Aliment Pharmacol Ther* 2000;14:523-528.
- Mahida YR, Galvin AM, Gray T, Makh S, McAlindon ME, Sewell HF, Podolsky DK. Migration of human intestinal lamina propria lymphocytes, macrophages and eosinophils following the loss of surface epithelial cells. *Clin Exp Immunol* 1997;109:377-386.
- Maj JG, Paris F, Haimovitz-Friedman A, Venkatraman E, Kolesnick R, Fuks Z. Microvascular function regulates intestinal crypt response to radiation. *Cancer Res* 2003;63:4338-4341.
- Mann RK, Beachy PA. Novel lipid modifications of secreted protein signals. *Annu Rev Biochem* 2004;73:891-923.
- Mao J, Wang J, Liu B, Pan W, Farr GH 3rd, Flynn C, Yuan H, Takada S, Kimelman D, Li L, Wu D. Low-density lipoprotein receptor-related protein-5 binds to Axin and regulates the canonical Wnt signaling pathway. *Mol Cell* 2001;7:801-809.
- Marigo V, Roberts DJ, Lee SM, Tsukurov O, Levi T, Gastier JM, Epstein DJ, Gilbert DJ, Copeland NG, Seidman CE, Jenkins NA, Seidman JG, McMahon AP, Tabin C. Cloning, expression, chromosomal location of SHH and IHH: two human homologues of the *Drosophila* segment polarity gene hedgehog. *Genomics* 1995;28:44-51.
- Matsusue K, Peters JM, Gonzalez FJ. PPARbeta/delta potentiates PPARgamma-stimulated adipocyte differentiation. *FASEB J* 2004;18:1477-1479.
- Meador JA, Ghandhi SA, Amundson SA. p53-Independent Downregulation of Histone Gene Expression in Human Cell Lines by High- and Low-LET Radiation. *Radiat Res* 2011;175:689-699.
- Merritt AJ, Potten CS, Kemp CJ, Hickman JA, Balmain A, Lane DP, Hall PA. The role of p53 in spontaneous and radiation-induced apoptosis in the gastrointestinal tract of normal and p53-deficient mice. *Cancer Res* 1994;54:614-617.
- Merritt AJ, Potten CS, Watson AJ, Loh DY, Nakayama K, Nakayama K, Hickman JA. Differential expression of bcl-2 in intestinal epithelia. Correlation with attenuation of apoptosis in colonic crypts and the incidence of colonic neoplasia. *J Cell Sci* 1995;108:2261-2271.
- Michalik L, Desvergne B, Tan NS, Basu-Modak S, Escher P, Rieusset J, Peters JM, Kaya G, Gonzalez FJ, Zakany J, Metzger D, Chambon P, Duboule D, Wahli W. Impaired skin wound healing in peroxisome proliferator-activated receptor (PPAR) α and PPAR β mutant mice. *J Cell Biol* 2001;154:799-814.
- Milano J, McKay J, Dagenais C, Foster-Brown L, Pognan F, Gadiant R, Jacobs RT, Zacco A, Greenberg B, Ciaccio PJ. Modulation of Notch processing by γ -secretase inhibitors causes intestinal goblet cell metaplasia and induction of genes known to specify gut secretory lineage differentiation. *Toxicol Sci* 2004;82:341-358.

- Mohler J, Vani K. Molecular organization and embryonic expression of the hedgehog gene involved in cell-cell communication in segmental patterning of *Drosophila*. *Development* 1992;115:957–971.
- Moreno S, Farioli-Vecchioli S, Cerù MP. Immunolocalization of peroxisome proliferator-activated receptors and retinoid X receptors in the adult rat CNS. *Neuroscience* 2004;123:131-145.
- Morgan SE, Kastan MB. p53 and ATM: Cell cycle, cell death, and cancer. *Adv Cancer Res* 1997;71:1–25.
- Mori-Akiyama Y, van den Born M, van Es JH, Hamilton SR, Adams HP, Zhang J, Clevers H, de Crombrughe B. SOX9 is required for the differentiation of paneth cells in the intestinal epithelium. *Gastroenterology* 2007;133:539-546.
- Motoyama J, Takabatake T, Takeshima K, Hui C. Ptch2, a second mouse Patched gene is co-expressed with Sonic hedgehog. *Nat Genet* 1998;18:104-106.
- Müller-Brüsselbach S, Kömhoff M, Rieck M, Meissner W, Kaddatz K, Adamkiewicz J, Keil B, Klose KJ, Moll R, Burdick AD, Peters JM, Müller R. Deregulation of tumor angiogenesis and blockade of tumor growth in PPARbeta-deficient mice. *EMBO J* 2007; 26:3686-3698.
- Murmu N, Jung J, Mukhopadhyay D, Houchen CW, Riehl TE, Stenson WF, Morrison AR, Arumugam T, Dieckgraefe BK, Anant S. Dynamic antagonism between RNA-binding protein CUGBP2 and cyclooxygenase-2-mediated prostaglandin E2 in radiation damage. *Proc Natl Acad Sci USA* 2004;101:13873-13878.
- Nadra K, Anghel SI, Joye E, Tan NS, Basu-Modak S, Trono D, Wahli W, Desvergne B. Differentiation of trophoblast giant cells and their metabolic functions are dependent on peroxisome proliferator-activated receptor beta/delta. *Mol Cell Biol* 2006;26:3266-3281.
- Nagy L, Tontonoz P, Alvarez JG, Chen H, Evans RM. Oxidized LDL regulates macrophage gene expression through ligand activation of PPARgamma. *Cell* 1998;93:229-240.
- Nakano K, Vousden KH. PUMA, a novel proapoptotic gene, is induced by p53. *Mol Cell* 2001;7:683-694.
- Ng AY, Waring P, Ristevski S, Wang C, Wilson T, Pritchard M, Hertzog P, Kola I. Inactivation of the transcription factor Elf3 in mice results in dysmorphogenesis and altered differentiation of intestinal epithelium. *Gastroenterology* 2002;122:1455-1466.
- Nho RS, Xia H, Diebold D, Kahm J, Kleidon J, White E, Henke CA. PTEN regulates fibroblast elimination during collagen matrix contraction. *J Biol Chem* 2006;281:33291-33301.
- Nho RS, Xia H, Kahm J, Kleidon J, Diebold D, Henke CA. Role of integrin-linked kinase in regulating phosphorylation of Akt and fibroblast survival in type I collagen matrices through a beta1 integrin viability signaling pathway. *J Biol Chem* 2005;280:26630-26639.

- Nüsslein-Volhard C, Wieschaus E. Mutations affecting segment number and polarity in *Drosophila*. *Nature* 1980;287:795-801.
- Oliver WR Jr, Shenk JL, Snaith MR, Russell CS, Plunket KD, Bodkin NL, Lewis MC, Winegar DA, Sznaidman ML, Lambert MH, Xu HE, Sternbach DD, Kliewer SA, Hansen BC, Willson TM. A selective peroxisome proliferator-activated receptor delta agonist promotes reverse cholesterol transport. *Proc Natl Acad Sci USA* 2001;98:5306-5311.
- Ormestad M, Astorga J, Landgren H, Wang T, Johansson BR, Miura N, Carlsson P. Foxf1 and Foxf2 control murine gut development by limiting mesenchymal Wnt signaling and promoting extracellular matrix production. *Development* 2006;133:833-843.
- Osterlund T, Kogerman P. Hedgehog signalling: how to get from Smo to Ci and Gli. *Trends Cell Biol* 2006;16:176–180.
- Panakova D, Sprong H, Marois E, Thiele C, Eaton S. Lipoprotein particles are required for Hedgehog and Wingless signaling. *Nature* 2005;435:58–65.
- Paris F, Fuks Z, Kang A, Capodici P, Juan G, Ehleiter D, Haimovitz-Friedman A, Cordon-Cardo C, Kolesnick R. Endothelial apoptosis as the primary lesion initiating intestinal radiation damage in mice. *Science* 2001;293:293–297.
- Park BH, Vogelstein B, Kinzler KW. Genetic disruption of PPARdelta decreases the tumorigenicity of human colon cancer cells. *Proc Natl Acad Sci USA*. 2001;98:2598-25603.
- Pawlik TM, Keyomarsi K. Role of cell cycle in mediating sensitivity to radiotherapy *Int J Radiat Oncol Biol Phys* 2004;59:928–942.
- Peters JM, Lee SS, Li W, Ward JM, Gavrilova O, Everett C, Reitman ML, Hudson LD, Gonzalez FJ. Growth, adipose, brain, and skin alterations resulting from targeted disruption of the mouse peroxisome proliferator-activated receptor beta (delta). *Mol Cell Biol* 2000;20:5119-5128.
- Peters LJ, Withers HR, Thames HD, Jr, Fletcher GH. Tumor radioresistance in clinical radiotherapy. *Int J Radiat Oncol Biol Phys* 1982;8:101–108.
- Pinto D, Gregorieff A, Begthel H, Clevers H. Canonical Wnt signals are essential for homeostasis of the intestinal epithelium. *Genes Dev* 2003;17:1709-1713.
- Piqueras L, Reynolds AR, Hodivala-Dilke KM, Alfranca A, Redondo JM, Hatae T, Tanabe T, Warner TD, Bishop-Bailey D. Activation of PPARbeta/delta induces endothelial cell proliferation and angiogenesis. *Arterioscler Thromb Vasc Biol* 2007;27: 63-69.
- Pomp J, Wike JL, Ouwerkerk IJ, Hoogstraten C, Davelaar J, Schrier PI, Leer JW, Thames HD, Brock WA. Cell density dependent plating efficiency affects outcome and interpretation of colony forming assays. *Radiother Oncol* 1996;40:121–125.

Porter EM, Bevins CL, Ghosh D, Ganz T. The multifaceted Paneth cell. *Cell Mol Life Sci* 2002;59:156-170.

Porter JA, Ekker SC, Park WJ, von Kessler DP, Young KE, Chen CH, Ma Y, Woods AS, Cotter RJ, Koonin EV, Beachy PA. Hedgehog patterning activity: role of a lipophilic modification mediated by the carboxy-terminal autoprocessing domain. *Cell* 1996;86:21-34.

Porter JA, von Kessler DP, Ekker SC, Young KE, Lee JJ, Moses K, Beachy PA. The product of hedgehog autoproteolytic cleavage active in local and long-range signalling. *Nature* 1995;374:363-366.

Potten CS, Booth C, Tudor GL, Booth D, Brady G, Hurley P, Ashton G, Clarke R, Sakakibara S, Okano H. Identification of a putative intestinal stem cell and early lineage marker; musashi-1. *Differentiation* 2003;71:28-41.

Potten CS, Bullock JC. Cell kinetic studies in the epidermis of the mouse. I. Changes in labeling index with time after tritiated thymidine administration. *Experientia* 1983;39:1125-1129.

Potten CS, Grant HK. The relationship between ionizing radiation-induced apoptosis and stem cells in the small and large intestine. *Br J Cancer* 1998;78:993-1003.

Potten CS, Merritt A, Hickman J, Hall P, Faranda A. Characterization of radiation-induced apoptosis in the small intestine and its biological implications. *Int J Radiat Biol* 1994;65:71-78.

Potten CS. Radiation, the ideal cytotoxic agent for studying the cell biology of tissues such as the small intestine. *Radiat Res* 2004;161:123-136.

Potten CS. The significance of spontaneous and induced apoptosis in the gastrointestinal tract of mice. *Cancer Metastasis Rev* 1992;11:179-195.

Qiu W, Carson-Walter EB, Liu H, Epperly M, Greenberger JS, Zambetti GP, Zhang L, Yu J. PUMA regulates intestinal progenitor cell radiosensitivity and gastrointestinal syndrome. *Cell Stem Cell* 2008;2:576-583.

Qiu W, Leibowitz B, Zhang L, Yu J. Growth factors protect intestinal stem cells from radiation-induced apoptosis by suppressing PUMA through the PI3K/AKT/p53 axis. *Oncogene* 2010;29:1622-1632.

Quastler H. The nature of intestinal radiation death. *Radiat Res* 1956;4:303-320.

Ramalho-Santos M, Melton DA, McMahon AP. Hedgehog signals regulate multiple aspects of gastrointestinal development. *Development* 2000;127:2763-2772.

Reed KR, Sansom OJ, Hayes AJ, Gescher AJ, Winton DJ, Peters JM, Clarke AR. PPARdelta status and Apc-mediated tumorigenesis in the mouse intestine. *Oncogene* 2004;23:8992-8996.

- Riccio O, Van Gijn ME, Bezdek AC, Pellegrinet L, Van Es JH, Zimmer-Strobl U, Strobl LJ, Honjo T, Clevers H, Radtke F. Loss of intestinal crypt progenitor cells owing to inactivation of both Notch1 and Notch2 is accompanied by derepression of CDK inhibitors p27Kip1 and p57Kip2. *EMBO Rep* 2008;9:377-383.
- Ritov VB, Banni S, Yalowich JC, Day BW, Claycamp HG, Corongiu FP, Kagan VE. Non-random peroxidation of different classes of membrane phospholipids in live cells detected by metabolically integrated cis-parinaric acid. *Biochim Biophys Acta* 1996;1283:127-140.
- Roberts DM, Slep KC, Peifer M. It takes more than two to tango: Dishevelled polymerization and Wnt signaling. *Nat Struct Mol Biol* 2007;14:463-465.
- Rødningen OK, Overgaard J, Alsner J, Hastie T, Børresen-Dale A-L. Microarray analysis of the transcriptional response to single or multiple doses of ionizing radiation in human subcutaneous fibroblasts. *Radiother Oncol* 2005;77:231-240.
- Roots R, Okada S. Protection of DNA molecules of cultured mammalian cells from radiation induced single-strand scissions by various alcohols and SH compounds. *Int J Radiat Biol* 1972;21:329-342.
- Roy L, Gruel G, Vaurijoux A. Cell response to ionising radiation analysed by gene expression patterns. *Ann Ist Super Sanità* 2009;45:272-277.
- Rubio CA, Jalnas M. Dose-time-dependent histological changes following irradiation of the small intestine of rats. *Dig Dis Sci* 1996;41:392-401.
- Russell AP, Hesselink MK, Lo SK, Schrauwen P. Regulation of metabolic transcriptional co-activators and transcription factors with acute exercise. *FASEB J* 2005;19:986-988.
- Saluja I, Granneman JG, Skoff RP. PPAR delta agonists stimulate oligodendrocyte differentiation in tissue culture. *Glia* 2001;33:191-204.
- Sancho E, Batlle E, Clevers H. Signaling pathways in intestinal development and cancer. *Annu Rev Cell Dev Biol* 2004;20:695-723.
- Sangiorgi E, Capecchi MR. *Bmi1* is expressed in vivo in intestinal stem cells. *Nat Genet* 2008;40:915-920.
- Schmidt-Ullrich RK, Dent P, Grant S, Mikkelsen RB, Valerie K. Signal Transduction and Cellular Radiation Responses. *Radiat Res* 2000;153:245-257.
- Schmuth M, Haqq CM, Cairns WJ, Holder JC, Dorsam S, Chang S, Lau P, Fowler AJ, Chuang G, Moser AH, Brown BE, Mao-Qiang M, Uchida Y, Schoonjans K, Auwerx J, Chambon P, Willson TM, Elias PM, Feingold KR. Peroxisome proliferator-activated receptor (PPAR)-beta/delta stimulates differentiation and lipid accumulation in keratinocytes. *J Invest Dermatol* 2004;122:971-983.
- Schug TT, Berry DC, Shaw NS, Travis SN, Noy N. Opposing effects of retinoic acid on cell growth result from alternate activation of two different nuclear receptors. *Cell* 2007;129:723-733.

- Schuler M, Ali F, Chambon C, Duteil D, Bornert JM, Tardivel A, Desvergne B, Wahli W, Chambon P, Metzger D. PGC1alpha expression is controlled in skeletal muscles by PPARbeta, whose ablation results in fiber-type switching, obesity, and type 2 diabetes. *Cell Metab* 2006;4:407-414.
- Shao J, Sheng H, DuBois RN. Peroxisome proliferator-activated receptors modulate K-Ras-mediated transformation of intestinal epithelial cells. *Cancer Res* 2002;62:3282-3288.
- Shearer BG, Steger DJ, Way JM, Stanley TB, Lobe D C, Grillot DA, Iannone MA, Lazar MA, Willson TM, Billin AN. Identification and characterization of a selective peroxisome proliferator-activated receptor beta/delta (NR1C2) antagonist *Mol Endocrinol* 2008;22:523-529.
- Sheng H, Shao J, DuBois RN. Akt/PKB activity is required for Ha-Ras-mediated transformation of intestinal epithelial cells. *J Biol Chem* 2001;276:14498-144504.
- Shiojima I, Walsh K. Role of Akt signaling in vascular homeostasis and angiogenesis. *Circ Res* 2002;90:1243-1250.
- Shroyer NF, Wallis D, Venken KJ, Bellen HJ, Zoghbi HY. Gfi1 functions downstream of Math1 to control intestinal secretory cell subtype allocation and differentiation. *Genes Dev* 2005;19:2412-2417.
- Shureiqi I, Jiang W, Zuo X, Wu Y, Stimmel JB, Leesnitzer LM, Morris JS, Fan HZ, Fischer SM, Lippman SM. The 15-lipoxygenase-1 product 13-S-hydroxyoctadecadienoic acid down-regulates PPAR-delta to induce apoptosis in colorectal cancer cells. *Proc Natl Acad Sci USA* 2003;100:9968-9973.
- Snyder AR, Morgan WF. Gene expression profiling after irradiation: clues to understanding acute and persistent responses *Cancer Metastasis Rev* 2004;23:259-268.
- Sokolov M, Smirnova N, Cameriniotero R, Neumann R, Panyutin I. Microarray analysis of differentially expressed genes after exposure of normal human fibroblasts to ionizing radiation from an external source and from DNA-incorporated iodine-125 radionuclide. *Gene* 2006;382:47-56.
- Somogyi Z, Horvath G, Telbisz A, Rez G, Palfia Z. Morphological aspects of ionizing radiation response of small intestine. *Micron* 2002;33:167-178.
- Stanger BZ, Datar R, Murtaugh LC, Melton DA. Direct regulation of intestinal fate by Notch. *Proc Natl Acad Sci USA* 2005;102:12443-12448.
- Starke PE FJ. Ferric iron and superoxide ions are required for the killing of cultured hepatocytes by hydrogen peroxide. Evidence for the participation of hydroxyl radicals formed by an iron-catalyzed Haber-Weiss reaction. *J Biol Chem* 1985;260:10099-10104.

- Surapureddi S, Yu S, Bu H, Hashimoto T, Yeldandi AV, Kashireddy P, Cherkaoui-Malki M, Qi C, Zhu YJ, Rao MS, Reddy JK. Identification of a transcriptionally active peroxisome proliferator-activated receptor alpha -interacting cofactor complex in rat liver and characterization of PRIC285 as a coactivator. *Proc Natl Acad Sci USA* 2002;99:11836-11841.
- Suzuki H, Minegishi Y, Nomoto Y, Ota T, Masaoka T, van den Brink GR, Hibi T. Down-regulation of a morphogen (sonic hedgehog) gradient in the gastric epithelium of *Helicobacter pylori*-infected Mongolian gerbils. *J Pathol* 2005;206:186-197.
- Széles L, Töröcsik D, Nagy L. PPARgamma in immunity and inflammation: cell types and diseases. *Biochim Biophys Acta* 2007;1771:1014-1030.
- Tabata T, Eaton S, Kornberg TB. The *Drosophila* hedgehog gene is expressed specifically in posterior compartment cells and is a target of engrailed regulation. *Genes Dev* 1992;6:2635-2645.
- Tachiiri S, Katagiri T, Tsunoda T, Oya N, Hiraoka M, Nakamura Y. Analysis of gene-expression profiles after gamma irradiation of normal human fibroblasts. *Int J Radiat Oncol Biol Phys* 2006;64:272-279.
- Taipale J, Cooper MK, Maiti T, Beachy PA. Patched acts catalytically to suppress the activity of Smoothened. *Nature* 2002;418: 892-897.
- Takayama O, Yamamoto H, Damdinsuren B, Sugita Y, Ngan CY, Xu X, Tsujino T, Takemasa I, Ikeda M, Sekimoto M, Matsuura N, Monden M. Expression of PPARdelta in multistage carcinogenesis of the colorectum: implications of malignant cancer morphology. *Br J Cancer* 2006;95:889-895.
- Tamai K, Zeng X, Liu C, Zhang X, Harada Y, Chang Z, He X. A mechanism for Wnt coreceptor activation. *Mol Cell* 2004;16;13:149-156.
- Tammali R, Ramana KV, Srivastava SK. Aldose reductase regulates TNF-alpha-induced PGE2 production in human colon cancer cells. *Cancer Lett* 2007;252:299-306.
- Tan NS, Michalik L, Di-Poi N, Ng CY, Mermoud N, Roberts AB, Desvergne B, Wahli W. Essential role of Smad3 in the inhibition of inflammation-induced PPARbeta/delta expression. *EMBO J* 2004;23:4211-4221.
- Tan NS, Michalik L, Noy N, Yasmin R, Pacot C, Heim M, Flühmann B, Desvergne B, Wahli W. Critical roles of PPAR beta/delta in keratinocyte response to inflammation. *Genes Dev* 200;15:3263-3277.
- Tessner TG, Muhale F, Riehl TE, Anant S, Stenson WF. Prostaglandin E2 reduces radiation-induced epithelial apoptosis through a mechanism involving AKT activation and bax translocation. *J Clin Invest* 2004;114:1676-1685.
- Todd DG, Mikkelsen RB. Ionizing radiation induces a transient increase in cytosolic free [Ca²⁺] in human epithelial tumor cells. *Cancer Res* 1994;54:5224-5230.

- Tolwinski NS, Wehrli M, Rives A, Erdeniz N, DiNardo S, Wieschaus E. Wg/Wnt signal can be transmitted through arrow/LRP5,6 and Axin independently of Zw3/Gsk3beta activity. *Dev Cell* 2003;4:407-418.
- Trifilieff A, Bench A, Hanley M, Bayley D, Campbell E, Whittaker P. PPAR-alpha and -gamma but not -delta agonists inhibit airway inflammation in a murine model of asthma: in vitro evidence for an NF-kappaB-independent effect. *Br J Pharmacol* 2003;139:163-171.
- Van den Brink GR, Hardwick JC, Nielsen C, Xu C, ten Kate FJ, Glickman J, van Deventer SJ, Roberts DJ, Peppelenbosch MP. Sonic hedgehog expression correlates with fundic gland differentiation in the adult gastrointestinal tract. *Gut* 2002;51:628-633.
- Van den Brink GR. Hedgehog signaling in development and homeostasis of the gastrointestinal tract *Physiol Rev* 2007;87:1343-1375.
- Van der Flier LG, Clevers H. Stem cells, self-renewal, and differentiation in the intestinal epithelium. *Annu Rev Physiol* 2009;71:241-260.
- Van der Hoeven F, Zákány J, Duboule D. Gene transpositions in the HoxD complex reveal a hierarchy of regulatory controls. *Cell*. 1996; 85: 1025-1035.
- Van der Veen JN, Kruit JK, Havinga R, Baller JF, Chimini G, Lestavel S, Staels B, Groot PH, Groen AK, Kuipers F. Reduced cholesterol absorption upon PPARdelta activation coincides with decreased intestinal expression of NPC1L1. *J Lipid Res* 2005;46:526-534.
- Van Dongen JM, Kooyman J, Visser WJ. The influence of 400 r x-irradiation on the number and the localization of mature and immature goblet cells and Paneth cells in intestinal crypt and villus. *Cell Tissue Kinet* 1976;9:65-75.
- Van Dongen JM, Visser WJ, Daems WT, Galjaard H. The relation between cell proliferation, differentiation and ultrastructural development in rat intestinal epithelium. *Cell Tissue Res* 1976;174:183-199.
- Van Dop WA, Heijmans J, Büller NV, Snoek SA, Rosekrans SL, Wassenberg EA, van den Bergh Weerman MA, Lanske B, Clarke AR, Winton DJ, Wijgerde M, Offerhaus GJ, Hommes DW, Hardwick JC, de Jonge WJ, Biemond I, van den Brink GR. Loss of Indian Hedgehog activates multiple aspects of a wound healing response in the mouse intestine *Gastroenterology* 2010;139:1665-16676.
- Van Es JH, Jay P, Gregorieff A, van Gijn ME, Jonkheer S, Hatzis P, Thiele A, van den Born M, Begthel H, Brabletz T, Taketo MM, Clevers H. Wnt signalling induces maturation of Paneth cells in intestinal crypts. *Nat Cell Biol* 2005;7:381-386.
- Van Es JH, Van Gijn ME, Riccio O, Van den Born M, Vooijs M, Begthel H, Cozijnsen M, Robine S, Winton DJ, Radtke F, Clevers H. Notch/gamma-secretase inhibition turns proliferative cells in intestinal crypts and adenomas into goblet cells. *Nature* 2005;435: 959-963.

- Varnat F, Heggeler BB, Grisel P, Boucard N, Corthesy-Theulaz I, Wahli W, Desvergne B. PPARbeta/delta regulates paneth cell differentiation via controlling the hedgehog signaling pathway. *Gastroenterology* 2006;131:538-553.
- Wallingford JB, Habas R. The developmental biology of Dishevelled: an enigmatic protein governing cell fate and cell polarity. *Development* 2005;132:4421-4436.
- Walsh D. Deep Tissue Traumatism from Roentgen Ray Exposure. *Br Med J* 1897;2:272-273.
- Wang C, Yan R, Luo D, Watabe K, Liao D-F, Cao D. Aldo-keto reductase family 1 member B10 promotes cell survival by regulating lipid synthesis and eliminating carbonyls. *J Biol Chem* 2009;284:26742-26748.
- Wang D, Wang H, Guo Y, Ning W, Katkuri S, Wahli W, Desvergne B, Dey SK, DuBois RN. Crosstalk between peroxisome proliferator-activated receptor delta and VEGF stimulates cancer progression. *Proc Natl Acad Sci USA* 2006; 103: 19069-19074.
- Wang D, Wang H, Shi Q, Katkuri S, Wahli W, Desvergne B, Das SK, Dey SK, DuBois RN. Prostaglandin E(2) promotes colorectal adenoma growth via transactivation of the nuclear peroxisome proliferator-activated receptor delta. *Cancer Cell* 2004;6:285-295.
- Wang YX, Zhang CL, Yu RT, Cho HK, Nelson MC, Bayuga-Ocampo CR, Ham J, Kang H, Evans RM. Regulation of muscle fiber type and running endurance by PPARdelta. *PLoS Biol* 2004;2:1532-1539.
- Watson AJ, Pritchard DM. Lessons from genetically engineered animal models. VII. Apoptosis in intestinal epithelium: lessons from transgenic and knockout mice. *Am J Physiol Gastrointest Liver Physiol* 2000;278:G1-G5.
- Watson AJ, Askew JN, Sandle GI. Characterisation of oxidative injury to an intestinal cell line (HT-29) by hydrogen peroxide. *Gut* 1994;35:1575-1581.
- Weitsman GE, Koren R, Zuck E, Rotem C, Liberman UA, Ravid A. Vitamin D sensitizes breast cancer cells to the action of H₂O₂: mitochondria as a convergence point in the death pathway. *Free Radic Biol Med* 2005;39:266-278.
- Wilkins HR, Ohneda K, Keku TO, D'Ercole AJ, Fuller CR, Williams KL, Lund PK. Reduction of spontaneous and irradiation-induced apoptosis in small intestine of IGF-I transgenic mice. *Am J Physiol Gastrointest Liver Physiol* 2002;283:G457-G464.
- Williams JR, Zhang Y, Zhou H, Russell J, Gridley DS, Koch CJ, Little JB. Genotype-dependent radiosensitivity: Clonogenic survival, apoptosis and cell-cycle redistribution. *Int J Radiat Biol* 2008;84:151-164.
- Williams JR, Zhang Y, Zhou H, Gridley DS, Koch CJ, Russell J, Slater JS, Little JB. A quantitative overview of radiosensitivity of human tumor cells across histological type and TP53 status. *Int J Radiat Biol* 2008;84:253-264.

- Williams JR, Zhang Y, Zhou H, Gridley DS, Koch CJ, Slater JM, Little JB. Overview of radiosensitivity of human tumor cells to low-dose-rate irradiation. *Int J Radiat Oncol Biol Phys* 2008;72:909–917.
- Withers HR, Elkind MM. Microcolony survival assay for cells of mouse intestinal mucosa exposed to radiation. *Int J Radiat Biol Relat Stud Phys Chem Med* 1970;17:261-267.
- Withers HR, Elkind MM. Radiosensitivity and fractionation response of crypt cells of mouse jejunum. *Radiat Res* 1969;38:598-613.
- Wong GT, Manfra D, Poulet FM, Zhang Q, Josien H, Bara T, Engstrom L, Pinzon-Ortiz M, Fine JS, Lee HJ, Zhang L, Higgins GA, Parker EM. Chronic treatment with the γ -secretase inhibitor LY-411,575 inhibits β -amyloid peptide production and alters lymphopoiesis and intestinal cell differentiation. *J Biol Chem* 2004; 279:12876–12882.
- Wong HC, Bourdelas A, Krauss A, Lee HJ, Shao Y, Wu D, Mlodzik M, Shi DL, Zheng J. Direct binding of the PDZ domain of Dishevelled to a conserved internal sequence in the C-terminal region of Frizzled. *Mol Cell* 2003;12:1251-1260.
- Woods JW, Tanen M, Figueroa DJ, Biswas C, Zycband E, Moller DE, Austin CP, Berger JP. Localization of PPAR δ in murine central nervous system: expression in oligodendrocytes and neurons. *Brain Res* 2003;975:10-21.
- Wu LJ, Randers-Pehrson G, Xu A, Waldren CA, Geard CR, Yu Z, Hei TK. Targeted cytoplasmic irradiation with alpha particles induces mutations in mammalian cells. *Proc Natl Acad Sci USA* 1999;96:4959–4964.
- Xia H, Nho RS, Kahm J, Kleidon J, Henke CA. Focal adhesion kinase is upstream of phosphatidylinositol 3-kinase/Akt in regulating fibroblast survival in response to contraction of type I collagen matrices via a beta 1 integrin viability signaling pathway. *J Biol Chem* 2004;279:33024-33034.
- Xu HE, Lambert MH, Montana VG, Plunket KD, Moore LB, Collins JL, Oplinger JA, Kliewer SA, Gampe RT Jr, McKee DD, Moore JT, Willson TM. Structural determinants of ligand binding selectivity between the peroxisome proliferator-activated receptors. *Proc Natl Acad Sci USA* 2001;98:13919-13924.
- Yang Q, Bermingham NA, Finegold MJ, Zoghbi HY. Requirement of Math1 for secretory cell lineage commitment in the mouse intestine. *Science* 2001;294:2155–2158.
- Young RW. Acute radiation syndrome. In: Conklin JJ, Walker RI. Eds.). *Military Radiobiology*. Academic Press Inc, 1987; pp.165-190.
- Yu J, Zhang L, Hwang PM, Kinzler KW, Vogelstein B. PUMA induces the rapid apoptosis of colorectal cancer cells. *Mol Cell* 2001;7:673-682.
- Yu J, Zhang L. Apoptosis in human cancer cells. *Curr Opin Oncol* 2004;16:19-24.

Yu K, Bayona W, Kallen CB, Harding HP, Ravera CP, McMahon G, Brown M, Lazar MA. Differential activation of peroxisome proliferator-activated receptors by eicosanoids. *J Biol Chem* 1995;270:23975-23983.

Zandbergen F, Plutzky J. PPARalpha in atherosclerosis and inflammation. *Biochim Biophys Acta* 2007;1771:972-82.

Zeng X, Goetz JA, Suber LM, Scott WJ Jr, Schreiner CM, Robbins DJ. A freely diffusible form of Sonic hedgehog mediates long-range signaling. *Nature* 2001;411:716–720.

Zhang J, Fu M, Zhu X, Xiao Y, Mou Y, Zheng H, Akinbami MA, Wang Q, Chen YE. Peroxisome proliferator-activated receptor delta is up-regulated during vascular lesion formation and promotes post-confluent cell proliferation in vascular smooth muscle cells. *J Biol Chem* 2002;277:11505-11512.

Zhu L, Gibson P, Curre DS, Tong Y, Richardson RJ, Bayazitov IT, Poppleton H, Zakharenko S, Ellison DW, Gilbertson RJ. Prominin 1 marks intestinal stem cells that are susceptible to neoplastic transformation. *Nature* 2009;457:603-607.

Ziouzenkova O, Plutzky J. Lipolytic PPAR activation: new insights into the intersection of triglycerides and inflammation? *Curr Opin Clin Nutr Metab Care* 2004;7:369-375.

Zoete V, Grosdidier A, Michielin O. Peroxisome proliferator-activated receptor structures: ligand specificity, molecular switch and interactions with regulators. *Biochim Biophys Acta* 2007;1771:915-925.

ANNEXES

Peroxisome proliferator-activated receptor gamma activation is required for maintenance of innate antimicrobial immunity in the colon

Laurent Peyrin-Biroulet^{a,b,c,1}, Julia Beisner^{d,e,1}, Guoxing Wang^{d,e,1}, Sabine Nuding^{d,e,f}, Sajit Thottathil Oommen^g, Denise Kelly^h, Erika Parmentier-Decrucq^{a,i}, Rodrigue Dessein^{i,j,k,l}, Emilie Merour^a, Philippe Chavatte^m, Teddy Grandjean^{i,j,k,l}, Aude Bressenotⁿ, Pierre Desreumaux^{a,i}, Jean-Frédéric Colombel^{a,i}, Béatrice Desvergne^g, Eduard F. Stange^f, Jan Wehkamp^{d,e,f,2,3}, and Mathias Chamailard^{i,j,k,l,2,3}

^aInstitut National de la Santé et de la Recherche Médicale, U795, F-59037 Lille, France; ^bInstitut National de la Santé et de la Recherche Médicale U954, F-54505 Vandoeuvre-lès-Nancy, France; ^cFaculté de Médecine, Nancy-Université, F-54505 Vandoeuvre-lès-Nancy, France; ^dDr. Margarete Fischer-Bosch-Institute of Clinical Pharmacology, 70376 Stuttgart, Germany; ^eUniversity of Tuebingen, 70376 Stuttgart, Germany; ^fDepartment of Internal Medicine I, Robert Bosch Hospital, Stuttgart, Germany; ^gCenter for Integrative Genomics, Genopode Building, University of Lausanne, CH-1015 Lausanne, Switzerland; ^hGut Immunology Group, Rowett Institute of Nutrition & Health, University of Aberdeen, Aberdeen AB21 9SB, Scotland, United Kingdom; ⁱUniv Lille Nord de France, F-59000 Lille, France; ^jInstitut Pasteur de Lille, Center for Infection and Immunity of Lille, F-59019 Lille, France; ^kCentre National de la Recherche Scientifique, Unité Mixte de Recherche 8204, F-59021 Lille, France; ^lInstitut National de la Santé et de la Recherche Médicale, U1019, Team 7, Equipe FRM, F-59019 Lille, France; ^mUniv Lille Nord de France, EA1043, F-59000 Lille, France; and ⁿService de Pathologie, Hôpital Central, CHU Nancy, F-54035 Nancy, France

Edited* by Richard A. Flavell, Yale University School of Medicine, Howard Hughes Medical Institute, New Haven, CT, and approved March 25, 2010 (received for review May 23, 2009)

Crohn's disease (CD), a major form of human inflammatory bowel disease, is characterized by primary immunodeficiencies. The nuclear receptor peroxisome proliferator-activated receptor gamma (PPAR γ) is essential for intestinal homeostasis in response to both dietary- and microbiota-derived signals. Its role in host defense remains unknown, however. We show that PPAR γ functions as an antimicrobial factor by maintaining constitutive epithelial expression of a subset of β -defensin in the colon, which includes mDefB10 in mice and DEFB1 in humans. Colonic mucosa of *Ppar γ* mutant animals shows defective killing of several major components of the intestinal microbiota, including *Candida albicans*, *Bacteroides fragilis*, *Enterococcus faecalis*, and *Escherichia coli*. Neutralization of the colicidal activity using an anti-mDefB10 blocking antibody was effective in a PPAR γ -dependent manner. A functional promoter variant that is required for DEFB1 expression confers strong protection against Crohn's colitis and ileocolitis (odds ratio, 0.559; $P = 0.018$). Consistently, colonic involvement in CD is specifically linked to reduced expression of DEFB1 independent of inflammation. These findings support the development of PPAR γ -targeting therapeutic and/or nutritional approaches to prevent colonic inflammation by restoring antimicrobial immunity in CD.

β -defensin 1 | Crohn's disease | microbiota | nutrition | PPAR γ

Crohn's disease (CD) and ulcerative colitis (UC) are chronic inflammatory disorders of the gastrointestinal tract that are influenced by both genetic and environmental factors. As many as 1.4 million persons in the United States may suffer from these forms of inflammatory bowel disease (IBD) (1). No curative treatment is available for these lifelong and disabling disorders. Although UC lesions are limited to the colon and the rectum, CD lesions can affect any portion of the gastrointestinal tract. Antimicrobial peptides, including α - and β -defensins, are key effectors of the gastrointestinal innate immune response. Ileal CD is specifically characterized by reduced expression of Paneth cell-derived α -defensins, which is independently linked to the CD-associated *NOD2* and *TCF7L2* mutations (2, 3). Reduced antimicrobial activity against certain bacterial groups of the intestinal microbiota has been reported in the colonic mucosa of patients with CD compared with patients with UC and controls (4). The mechanisms underlying this phenomenon of reduced colonic antimicrobial immunity in CD remain poorly understood, however.

The nuclear receptor peroxisome proliferator-activated receptor-gamma (PPAR γ) is expressed primarily in colonocytes. On recognition of either natural or synthetic ligands, a heterodimer of reti-

noid X receptor alpha (RXR α) and PPAR γ is formed that allows the regulation of a specific set of genes involved in intestinal homeostasis through its binding to PPAR γ -response elements (PPREs) (5). Genetic ablation of *PPAR γ* was found to result in increased susceptibility to experimental colitis in rodents (5). Conversely, engagement of PPAR γ -mediated signaling by its cognate agonists, such as rosiglitazone, attenuated the severity of inflammatory lesions in both experimental and spontaneous models of colitis (5) and might be effective in UC (6). Consequently, we evaluated the role of PPAR γ in host defense through regulation of antimicrobial peptides in the intestinal mucosa of patients with IBD.

Results

PPAR γ Directly Regulates DEFB1 Expression in Human Colonocytes.

We first searched for potential binding sites of PPAR γ within the promoter of human β -defensin expressed primarily in the colon, namely the β -defensin 1–4 (DEFB1–4) (3, 7). *In silico* approaches were performed within the 5' vicinity to the starting codon of the DEFB1–4-encoding genes. We failed to detect putative PPRE within the 0.3-kb downstream untranslated region of *DEFB2-4*. In contrast, the promoter region of *DEFB1* had four sites with a potential binding affinity to PPAR γ (Fig. 1A). Next, by combining two *in silico* approaches, we identified five additional putative PPREs within the promoter region of *DEFB1* (Fig. 1A). Among the total of nine potential PPREs, three were of DR1 motif and six were of DR2 motif (Table S1). We then systematically and formally assessed the binding activity of RXR α /PPAR γ heterodimer to each of these potential PPREs through an electrophoretic mobility shift assay. Four potential sites bound avidly to recombinant RXR α and PPAR γ protein (Fig. 1B). Up to a 2-fold increase in luciferase

Author contributions: L.P.-B., J.W., and M.C. designed research; L.P.-B., J.B., G.W., S.N., D.K., E.P.-D., R.D., E.M., T.G., A.B., and M.C. performed research; S.T.O., P.C., P.D., J.-F.C., and B.D. contributed new reagents/analytic tools; L.P.-B., J.B., G.W., S.N., S.T.O., D.K., E.P.-D., R.D., E.M., P.C., T.G., A.B., P.D., J.-F.C., B.D., E.F.S., J.W., and M.C. analyzed data; and L.P.-B., E.F.S., J.W., and M.C. wrote the paper.

The authors declare no conflict of interest.

*This Direct Submission article had a prearranged editor.

Freely available online through the PNAS open access option.

¹L.P.-B., J.B., and G.W. contributed equally to this work.

²J.W. and M.C. contributed equally to this work.

³To whom correspondence may be addressed. E-mail: mathias.chamailard@inserm.fr or jan.wehkamp@ikp-stuttgart.de.

This article contains supporting information online at www.pnas.org/lookup/suppl/doi:10.1073/pnas.0905745107/-DCSupplemental.

been implicated in the pathogenesis of CD. PPAR γ is thought to be involved in the innate immune response to microbial infection, but the mechanisms remain poorly understood (9, 10). Thus, we investigated the antimicrobial activity of PPAR γ against microbes linked to IBD pathogenesis (8). Interestingly, cationic peptides extracted from colonic mucosa of *Ppar γ ^{+/-}* mice exhibited defective killing of cultured *Bacteroides fragilis*, *Enterococcus faecalis*, and *Candida albicans* compared with WT animals (Fig. 3A). The viability of a clinical isolate of *Escherichia coli* also was significantly decreased after a 90-min exposure to colonic biopsy extracts of controls compared with *Ppar γ* mutant animals (Fig. 3A). We then evaluated the regulatory role of PPAR γ on the mDefB10-mediated mucosal antibacterial activity. Most of the colidical activity of colonic cationic extracts isolated from WT mice was blocked using an anti-mDefB10 antibody (Fig. 3B). Conversely, the blocking activity of anti-mDefB10 on colonic biopsy extracts isolated from *Ppar γ ^{+/-}* mice was decreased significantly (Fig. 3B), providing a link between the mDefB10 expression deficiency and impaired antimicrobial immunity in the colon of *Ppar γ* mutant mice.

PPAR γ Is Dispensable for Innate Antimicrobial Immunity in the Mouse Ileum. Given our previous results and the fact that PPAR β regulates Paneth cell differentiation (10), we next explored the hypothesis that reduced expression of PPAR γ might be linked to Crohn's ileitis by failing to regulate antimicrobial immunity in the ileum. In contrast to the expression of DefB10 in the colon, the expression of Paneth cell–derived antimicrobial peptides remained

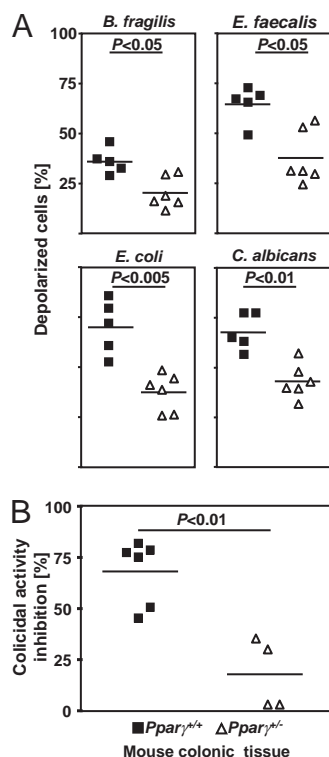


Fig. 3. PPAR γ activation is required for microbicidal activity in the colon. (A) Cationic proteins were extracted from colonic mucosal biopsy specimens from *Ppar γ ^{+/-}* mice ($n = 6$) and controls ($n = 5$). Values represent the mean and normalized antimicrobial activity of each sample against *B. fragilis* (ATCC 25285), *E. faecalis* (clinical isolate 404), *E. coli* (clinical isolate 304446), and *C. albicans* (clinical isolate 526). (B) Anti-mDefB10 antibody was used to inhibit the antimicrobial activity of the colon of *Ppar γ ^{+/-}* mice ($n = 4$) and their WT littermates ($n = 6$) against *E. coli* (clinical isolate 304446). All experiments were performed in duplicate, and P values were determined by the Mann-Whitney test. NS, not significant.

unaffected in *Ppar γ ^{+/-}* mice (Fig. S1). Moreover, no significant difference in small intestine antimicrobial activity was seen between the WT and *Ppar γ* mutant mice (Fig. S2). Similarly, the diversity of the fecal-associated microbiota was similar in *Ppar γ ^{+/-}* and control littermates (Fig. S3), as determined by real-time quantitative PCR (qPCR) on bacterial 16S rDNA of the major bacterial phyla of the fecal flora (9). Collectively, these results demonstrate that PPAR γ is essential for maintaining optimal expression of a subset of β -defensins in the mouse colon, providing a possible mechanism for the impaired microbial killing of the colon in *Ppar γ* -deficient mice and mucosal adherence of certain microorganisms in CD (11).

DEFB1 Expression Is Reduced in CD with Colonic Involvement. We next measured the mucosal level of DEFB1 in patients with CD, patients with UC, and controls. *DEFB1* expression was specifically reduced at the mRNA level in the macroscopically and histologically noninflamed colonic mucosa of patients with colonic involvement (L2 and L3) ($P < 0.001$ by one-way ANOVA) (Fig. 4A), resulting in decreased protein expression of DEFB1 (Fig. 4C). The colonic expression of DEFB1 in colonic biopsy specimens from patients with pure ileal CD (L1) or UC did not differ significantly from that in controls (Fig. 4A). No correlation between *DEFB1* and *IL-8* transcript levels was observed in colonic biopsy specimens from control and CD subjects (Fig. 4B), suggesting that impaired *DEFB1* expression in colonic CD is not linked to inflammation-associated tissue damage. In contrast, and as reported previously (3), constitutive *DEFB1* expression was unchanged in noninflamed colonic mucosa of UC patients expressing low transcript levels of PPAR γ (5). These results indicate PPAR γ -independent regulatory mechanisms of colonic *DEFB1* expression in UC that remain to be identified.

Colonic Involvement in CD Is Associated with a Functional Variant of DEFB1 Promoter. To test the hypothesis that the reduced *DEFB1* expression in L2 and L3 patients may be related to the CD-

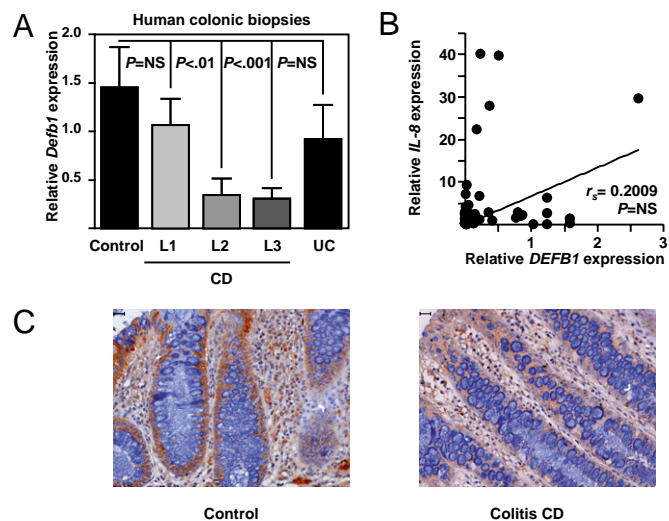


Fig. 4. Reduced expression of DEFB1 is specifically linked to colonic involvement in CD. (A) Relative gene expression in macroscopically noninflamed colonic biopsy specimens from ileal ($n = 16$), colonic ($n = 8$), and ileocolonic ($n = 21$) CD patients compared with UC patients ($n = 8$) and controls ($n = 17$) who underwent colonoscopy. Values represent the mean of normalized data \pm SEM, as measured by real-time qPCR. NS, not significant. P values were determined by the nonparametric Kruskal-Wallis and Mann-Whitney tests. (B) Correlation between *DEFB1* and *IL-8* transcript levels in CD. P values were determined by the nonparametric Spearman test. (C) Immunohistochemical localization of *DEFB1* in control (Left) and Crohn's colitis patients (Right). (Scale bar: 10 μ m.)

associated variants within the promoter of *DEFB1* (12), we next performed a genotype-phenotype analysis in CD. No significant differences were observed between the allele frequencies in the Hungarian cohort (13) and our French cohort of CD patients (Table 1). Consistently, we confirmed that the genetic promoter variation in *DEFB1*, namely rs1800972, was solely associated with colonic involvement in CD (13) (Table 1). Notably, the rs1800972 G allele had a significantly lower frequency in patients with pure colonic disease (L2) compared with L1 patients [odds ratio (OR), 0.524; 95% confidence interval (CI), 0.286–0.961; $P = 0.035$], as well as in patients with colonic involvement (L2 + L3) (OR, 0.559; 95% CI, 0.344–0.909; $P = 0.018$). Unlike rs1800972, the SNP rs11362 G allele was found with a lower frequency in patients with colonic involvement, but this effect was not statistically significant (OR, 0.710; 95% CI, 0.473–1.064; $P = 0.096$).

Discussion

Taken together, our findings suggest a key role of PPAR γ in the maintenance of *DEFB1* expression, thus contributing to the bactericidal and candidacidal activity of the colonic mucosa (4). In CD with colonic involvement, constitutive deficiency of *DEFB1* expression might contribute to diminished microbial killing by the colonic mucosa that subsequently results in increased mucosal adherence of certain microorganisms (11), excessive inflammation, and enhanced antibody response to microbial antigens in CD (14) (Fig. 5). Finally, in line with previous *in vitro* findings (15–17), *DEFB1* expression was inversely correlated with the carriage of *C. albicans* (18) and the humoral response to mannan, a major epitope for anti-*Saccharomyces cerevisiae* antibody (ASCA) production (17). *C. albicans* colonization was significantly increased in CD patients and was identified as an immunogen for ASCA (19), a serologic marker associated mainly with colonic involvement in CD (23). In line with the findings of a recent study (20), we provide a mechanism whereby the rs1800972 G allele might be linked to transactivation of *DEFB1* expression through PPAR γ . It also might account for the inefficacy of PPAR γ -based therapy, such as 5-aminosalicylates, in the colon of CD patients with colonic involvement compared with UC patients. Whether a maintained *DEFB1* expression level might be necessary to account for the protective effect of PPAR γ on the development of colorectal cancer will require additional investigation (21, 22). In summary, we believe that restoring PPAR γ -dependent antimicrobial barrier function might prevent and/or cure inflammatory lesions in the colon of patients with CD.

Materials and Methods

Patients. Through colonoscopy, human colonic biopsy specimens were obtained from macroscopically noninflamed colonic mucosa of healthy individuals (controls, $n = 17$), CD patients with pure ileal disease (L1 according to the Montreal classification; $n = 21$) (Table S4), CD patients with solely colonic

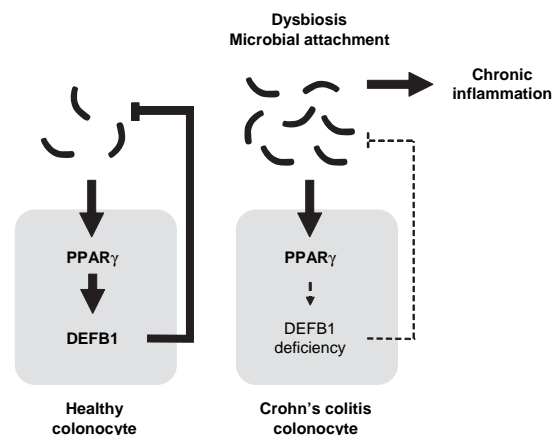


Fig. 5. Model of PPAR γ -mediated antimicrobial immunity in the colon.

disease (L2; $n = 16$) (Table S5), CD patients with ileocolitis (L3; $n = 21$) (Table S6), and UC patients ($n = 8$). The diagnoses of CD and UC were based on standard criteria using clinical, radiologic, endoscopic, and histopathologic findings. All clinical investigations were conducted according to the principles expressed in the Declaration of Helsinki.

Animals. Animal experiments were performed in accredited establishments (B59-108 and B67-218-5) according to European guidelines 86/609/CEE. Age- and sex-matched animals were housed five per cages and had free access to a standard laboratory chow diet in a temperature-controlled specific pathogen-free environment and a half-day light cycle exposure. To avoid estrus variation, 8-week-old PPAR γ mutant males and their WT littermates were bred in a specific pathogen-free environment as reported previously (23). The Ppar γ -null mouse strain was provided by Prof. Béatrice Desvergne. The proximal colon and terminal ileum were dissected out, flushed with cold PBS, and kept frozen in liquid nitrogen until further gene expression analysis. Rosiglitazone was administered orally or rectally to 8-week-old C57BL/6J mice at a dose of 10 mg/kg for 14 days once or twice daily. All animal studies were approved by the local institutional review board.

Plasmids. The *DEFB1* promoter-containing luciferase reporter constructs *DEFB1*-1140 (started from translation codon ATG) were kindly provided by Dr. John A. Petros (Emory University). The human PPAR γ -expressing plasmids pSG5-h-PPAR γ -1 and pSG5-h-PPAR γ -2 contain the cDNA of the human PPAR γ -1 and PPAR γ -2 genes, respectively (23). The pCDNA3.1-RXR α was kindly provided by Dr. Oliver Burk (Dr. Margarete Fischer-Bosch-Institute of Clinical Pharmacology and University of Tübingen).

Promoter Analysis. To screen for potential PPRE within the human *DEFB1*-4 promoter region, we analyzed the nucleotide sequence using two different software types designed to predict transcription factor binding *in silico*. The 1,140 bp upstream of the *DEFB1* promoter region was screened using Mat-

Table 1. Genotype and allele frequencies of *DEFB1* rs1800972 and rs11362 in CD

SNP	Crohn's disease, n (%)	Ileal (L1), n (%)	Colonic (L2), n (%)	Ileocolonic (L3), n (%)		
rs1800972					L1 vs. L2	L1 vs. L2 + L3
CC	170 (68.27)	40 (58.82)	53 (72.60)	77 (71.30)		
CG	70 (28.11)	23 (33.82)	19 (26.03)	28 (25.93)		
GG	9 (3.61)	5 (7.35)	1 (1.37)	3 (2.78)		
C	410 (82.33)	103 (75.74)	125 (85.62)	182 (84.26)	C vs. G	C vs. G
G	88 (17.67)	33 (24.26)	21 (14.38)	34 (15.74)	$P = 0.035$; OR = 0.524	$P = 0.018$; OR = 0.559
rs11362						
GG	82 (33.06)	27 (40.30)	24 (32.88)	31 (28.70)		
GA	113 (45.56)	29 (43.28)	34 (46.58)	50 (46.30)		
AA	53 (21.37)	11 (16.42)	15 (20.55)	27 (25.00)		
G	277 (55.85)	83 (61.94)	82 (56.16)	112 (51.85)	G vs. A	G vs. A
A	219 (44.15)	51 (38.06)	64 (43.84)	104 (48.15)	$P = 0.326$; OR = 1.270	$P = 0.096$; OR = 1.409

Inspector (<http://www.genomatix.de/products/MatInspector/index.html>) and NUBIScan (<http://www.nubiscan.unibas.ch/>).

Electrophoretic Mobility Shift Assay. Gel mobility shift assays were performed as described previously (24). In brief, human PPAR γ and RXR α protein were synthesized using pSG5-h-PPAR γ -1, pSG5-h-PPAR γ -2, and pCDNA3.1-RXR α according to the protocol of the TNT T7 Quick-Coupled Transcription/Translation System (Promega). Nuclear response elements were prepared by annealing 10 μ L each of two complementary oligonucleotide stocks (100 μ M) in 180 μ L of 25 mM NaCl, 25 mM Tris-HCl (pH 7.5), and 5 mM MgCl $_2$. For radioactive labeling, 2 μ L of the annealed oligonucleotides; 5 μ L of 10 \times buffer [500 mM NaCl, 500 mM Tris-Cl (pH 7.5), and 100 mM MgCl $_2$]; 25 μ Ci of (α - 32 P)dCTP; 5 μ L of 2 mM dATP, dGTP, and dTTP; 2 U of Klenow fragment; and water to a final volume of 50 μ L were incubated at 37 $^{\circ}$ C for 1 h and purified through Sephadex columns (MicroSpin G-25; GE Healthcare). The binding reaction contained 10 mM Hepes (pH 7.8), 60 mM KCl, 0.2% Nonidet P-40, 6% glycerol, 2 mM DTT, 0.25 μ g of poly(dI-dC), 2 μ L of 10 μ M non-specific oligonucleotides (5'-AGC TTG CGA AAA TTG TCA CTT CCT GTG TAC ACC CA-3'), 50,000 cpm labeled probe, and 2 μ L of full-length synthesized PPAR γ and/or RXR α in a final volume of 20 μ L. Samples were incubated on ice for 20 min after addition of the labeled probe. Protein-DNA complexes were resolved on a pre-electrophoresed 5% polyacrylamide gel in 44.5 mM boric acid and 1 mM EDTA (pH 8.3) at 200 V at 4 $^{\circ}$ C. Gels were dried and autoradiographed overnight at room temperature and analyzed with a Fuji BAS-1800 II phosphor-storage scanner and AIDA software (Raytest).

Cell Culture and Transient Transfection Assay. Human intestinal epithelium cell line Caco-2 (German Collection of Microorganisms and Cell Cultures, ACC 169), were grown in Dulbecco's modified Eagle's medium containing 25 mM Hepes and 2 mM glutamine supplemented with 10% FCS, 50 μ g of gentamicin/mL, and 5% of nonessential amino acids. Caco-2 cells were stimulated for 24 h with a synthetic activator of the RXR α /PPAR γ heterodimer, rosiglitazone, at 100 nM.

Transient transfections were performed using FuGENE 6 (Roche Diagnostics) according to the manufacturer's protocol. In brief, 1 day before transfection, Caco-2 cells were seeded into the 24-well plates (1.0×10^5 cells/well). Twenty-four hours later, Caco-2 cells (80% confluence) cells were cotransfected with 0.2 μ g of the indicated reporter plasmids plus 0.2 μ g of pSG5-h-PPAR γ -1 or pSG5-h-PPAR γ -2 and 50 ng of Renilla luciferase expression plasmid as an internal control. Total amounts of plasmids were kept constant by adding the empty DNA vector when necessary. The cells were incubated for 48 h and then washed, lysed, and harvested using 100 μ L of passive lysis buffer (Promega) per well. Firefly luciferase and Renilla luciferase activity were analyzed with the Promega Dual-Luciferase reporter assay system using a Berthold luminometer. All experiments were performed in triplicate and repeated independently at least three times by two independent investigators.

Gene Expression Analysis. For gene expression analyses, colonic biopsy specimens were immediately frozen in liquid nitrogen and stored at -80° C. Total RNA from cells and colonic specimens was extracted using the Nucleospin II tissue extraction kit (Macherey Nagel) and reverse-transcribed with the High-Capacity cDNA archive kit (Applied Biosystems), according to the manufacturer's instructions. The resulting cDNA (equivalent to 25 ng of total RNA) was amplified using the SYBR Green real-time PCR kit and detected using the Prism 7300 system (Applied Biosystems). Real-time qPCR was performed with forward and reverse primers (Table S3) designed using Primer Express version 1.0 (Applied Biosystems). On completion of the PCR amplification, a DNA melting curve analysis was carried out to confirm the presence of a single amplicon. β -actin was used as an internal reference gene to normalize the transcript levels. Relative mRNA levels ($2^{-\Delta\Delta Ct}$) were determined by comparing (i) the PCR cycle thresholds (Ct) for the gene of interest and *Actb* (ΔCt) and (ii) ΔCt values for the treated and control groups ($\Delta\Delta Ct$).

Immunohistochemistry. DEF1 immunostaining was performed using a rabbit polyclonal antibody as described previously (15). The specific anti-DEF1 antibody was kindly provided by Dr. T. Ganz (UCLA, Los Angeles, CA). Colonic biopsy specimens were fixed in 4% paraformaldehyde/phosphate-buffered formalin and embedded in paraffin. In brief, sections were first deparaffinized and rehydrated. Human colonic sections were preincubated in 3% H $_2$ O $_2$ methanol for 20 min to quench the endogenous peroxidase activity and with a blocking solution containing avidin D and biotin (Blocking Kit SP2001; Vector Laboratories). Then sections were blocked for 15 min with 5% milk and 1% BSA in PBS and exposed for 30 min to the primary rabbit polyclonal antibody directed against DEF1 (1:300 dilution) at room temperature. Sections

were incubated for 30 min at room temperature with goat anti-rabbit IgG (Dako), and then under the same conditions with an avidin-biotinylated peroxidase complex that was prepared at least 30 min before use.

For mDefB10 immunostaining, we generated an immune affinity-purified rabbit polyclonal F(ab') $_2$ fragment against the mDefB10-derived synthetic peptide Ser-Arg-Phe-Met-Ser-Asn-Cys-His-Pro-Glu-Asn-Leu-Arg. Sections were processed for peroxidase immunostaining using the Dako system following the manufacturer's recommendations. Immunohistochemistry was performed on formalin-fixed, paraffin-embedded tissue sections using the streptavidin-biotin-peroxidase method in a DakoCytomation AutoStainer. Sections were first deparaffinized and rehydrated. Antigen retrieval was performed by incubating the slides in Tris-citrate buffer (pH 6.0) for 20 min at 97 $^{\circ}$ C (PT Link; DakoCytomation). Endogenous peroxidase activity was blocked by incubation in 3% hydrogen peroxide for 10 min. The newly generated polyclonal rabbit anti-mDefB10 (2 mg/L) was incubated on slides for 12 h at 4 $^{\circ}$ C. The biotinylated secondary antibody was a polyclonal swine anti-rabbit (DakoCytomation).

Sections were incubated with 3,3'-diaminobenzidine substrate (Dako) for 1 min, after which the reaction was stopped in distilled water and the sections were counterstained with hematoxylin. Withdrawal of the primary antibody and replacement with a nonspecific antibody were used as negative controls.

Flow Cytometric Antimicrobial Assay. Extraction of cationic proteins from colonic and ileal tissue of Ppar $\gamma^{+/-}$ ($n = 6$) and Ppar $\gamma^{+/+}$ ($n = 5$) mice was performed as described previously (24). *C. albicans* (clinical isolate 526; Institute of Laboratory Medicine, Klinik am Eichert), *E. faecalis* (clinical isolate 404), and *E. coli* (clinical isolate 304446) were grown aerobically at 37 $^{\circ}$ C, whereas *B. fragilis* (ATCC 25285) was cultured anaerobically (Anaero Gen; Oxoid). All clinical isolates were kindly provided by the Institute of Laboratory Medicine, Klinik am Eichert. Then cell suspensions in Schaedler broth bouillon (1:6 dilution) were incubated at a concentration of 1.5×10^6 cells/mL with cationic proteins isolated from 10 μ g total extract at 37 $^{\circ}$ C. After 90 min, 1 μ g/mL of the membrane potential-sensitive dye bis-(1,3-dibutylbarbituric acid) trimethine oxonol [DiBAC $_4$ (3)] (Invitrogen) was added. After 10 min, the suspensions were centrifuged for 10 min at 4,500 $\times g$, and then the bacterial or fungal pellets were resuspended in 300 μ L of PBS (pH 7.4). For blocking experiments with anti-mDefB10 antibody, cationic extracts of colonic tissue from WT and PPAR $\gamma^{+/-}$ mice (35 μ g/mL) were incubated for 1 h at 37 $^{\circ}$ C with or without anti-mDefB10 antibody resuspended in 0.1 M K phosphate buffer at a concentration of 10 mg/L. Subsequently, *E. coli* (clinical isolate 304446) was added in a concentration of 1.5×10^6 cells/mL in Schaedler broth bouillon (1:6) with aqua dest. A total of 10,000 events were analyzed with a FACSCalibur flow cytometer and Cell Quest software (BD) for light scattering and green fluorescence. Antimicrobial activity was determined as percentage of depolarized fluorescent cells with respect to the bacterial control incubated with solvent.

Genotyping. Genotyping for the DEF1 promoter polymorphisms rs11362 and rs1800972 was performed using TaqMan SNP Genotyping Assays (assay c_11636793_20[rs11362] and assay c_11636794_10[rs1800972]) on a Prism 7900 System (Applied Biosystems), according to the supplier's instructions. Initial and postassay analyses were performed using the Sequence Detection System version 2.3 (Applied Biosystems). One-third of the samples were analyzed in duplicates as an internal control, and DNase-free water was used as a non-template control.

Statistics. Data were analyzed using Prism 4.0 (GraphPad Software). The unpaired Student *t* test was used to test for significant differences between activities of different promoter constructs. Statistical analysis was performed using (i) the Spearman test for nonparametric correlation analysis and (ii) the Mann-Whitney test for normalized gene expression in mice and antimicrobial assays, and (iii) Kruskal-Wallis test for normalized gene expression in humans. Differences were considered significant at $P < 0.05$. Values represent the mean of normalized data \pm SEM.

ACKNOWLEDGMENTS. We thank C. Winkler and A. Coutts for their excellent technical assistance; T. Ganz and P. Chavatte for kindly providing the anti-DEF1 antibody and rosiglitazone, respectively; and Professor M-A. Bigard and L. Dubuquoy for helpful discussion. This work was supported by the Association des chefs de service du CHU de Nancy and by grants from the Fondation pour la Recherche Médicale, UCB Pharma, and Sanofi-Aventis. The study also was supported by the Robert Bosch Foundation, the Deutsche Forschungsgemeinschaft Emmy Noether program (WE 436/1-1), and Sonderforschungsbereich 685 (immunotherapy; Project A9).

Evolutionarily Conserved, Growth Plate Zone-Specific Regulation of the Matrilin-1 Promoter: L-Sox5/Sox6 and Nfi Factors Bound near TATA Finely Tune Activation by Sox9[∇]

Andrea Nagy,^{1†} Erzsébet Kénesi,^{1†} Otgonchimeg Rentsendorj,^{1‡} Annamária Molnár,¹ Tibor Szénási,¹ Ildikó Sinkó,¹ Ágnes Zvara,² Sajit Thottathil Oommen,^{1§} Endre Barta,³ László G. Puskás,² Veronique Lefebvre,⁴ and Ibolya Kiss^{1*}

Institute of Biochemistry¹ and Institute of Genetics,² Biological Research Center of the Hungarian Academy of Sciences, Szeged 6701, Hungary; Apoptosis and Genomics Research Group of the Hungarian Academy of Sciences, Research Center for Molecular Medicine, Medical and Health Science Center, University of Debrecen, Debrecen 4010, Hungary³; and Department of Cell Biology, Rheumatologic and Orthopaedic Research Center, Lerner Research Institute, Cleveland Clinic, Cleveland, Ohio 44195⁴

Received 8 January 2010/Returned for modification 1 March 2010/Accepted 15 November 2010

To help uncover the mechanisms underlying the staggered expression of cartilage-specific genes in the growth plate, we dissected the transcriptional mechanisms driving expression of the matrilin-1 gene (*Matn1*). We show that a unique assembly of evolutionarily conserved *cis*-acting elements in the *Matn1* proximal promoter restricts expression to the proliferative and prehypertrophic zones of the growth plate. These elements functionally interact with distal elements and likewise are capable of restricting the domain of activity of a pancartilaginous *Col2a1* enhancer. The proximal elements include a Pe1 element binding the chondrogenic L-Sox5, Sox6, and Sox9 proteins, a SI element binding Nfi proteins, and an initiator Ine element binding the Sox trio and other factors. Sox9 binding to Pe1 is indispensable for functional interaction with the distal promoter. Binding of L-Sox5/Sox6 to Ine and Nfib to SI modulates Sox9 transactivation in a protein dose-dependent manner, possibly to enhance Sox9 activity in early stages of chondrogenesis and repress it at later stages. Hence, our data suggest a novel model whereby Sox and Nfi proteins bind to conserved *Matn1* proximal elements and functionally interact with each other to finely tune gene expression in specific zones of the cartilage growth plate.

Sox proteins play critical roles in lineage specification during development (18, 21, 25). They have an Sry-related high-mobility-group (HMG) box domain, which binds the minor groove of DNA with low affinity. They may act as architectural proteins to organize transcriptional complexes (25). Three Sox proteins direct chondrocyte specification and differentiation, but it is still unclear how they orchestrate the sequential induction of cartilage-specific genes in developing endochondral bones.

Endochondral bones form through tightly intertwined morphogenetic and differentiation events (11, 20, 24, 37). First, mesenchymal cells condense, commit to the chondrocyte lineage, and undergo chondrocyte early differentiation to form cartilage primordia of future bones. They then sequentially differentiate into proliferating, prehypertrophic, hypertrophic, and terminal cells and ultimately die to allow replacement of cartilage by bone. Importantly, the multiple layers of cells that

comprise cartilage primordia proceed through the multiple steps of differentiation in a staggered manner. They thereby establish growth plates (GP), i.e., a series of adjacent tissue zones comprising cells at progressively more advanced stages of maturation. The process is tightly regulated both spatially and temporally to allow GP to continue to grow in one end and to be progressively replaced by bone in the other end throughout fetal and postnatal growth (24). Bone growth is determined by the number of cells proliferating in the columnar zone and progressing toward hypertrophy. It involves complex functional interactions between fibroblast growth factor (FGF), Ihh, parathyroid hormone-related protein (PTHrP), and other factors and signaling pathways that allow chondrocytes to constantly modify their gene expression profile (11, 20, 37). Mutations in these factors and pathways cause severe forms of dwarfism and skeletal malformation diseases (20, 33). Elucidating the transcriptional mechanisms involved in specifying gene expression in specific GP zones has thus special importance to allow development of suitable therapies for such diseases.

The composition of the cartilage extracellular matrix (ECM) progressively changes from one GP zone to the next. This is largely due to staggered expression of the genes encoding the specific components of this matrix (8, 24, 39). *Col2a1* (collagen-2 gene) is activated as soon as prechondrocytes differentiate, whereas *Agc1* (aggrecan gene) and most other cartilage ECM genes are turned on in early chondroblasts (24). In contrast, *Matn1* (matrilin-1 gene) exhibits a narrower spatiotemporal activity (30, 31, 39, 42). It has the unique feature of being

* Corresponding author. Mailing address: Institute of Biochemistry, Biological Research Center of the Hungarian Academy of Sciences, Temesvári krt. 62, Szeged H-6726, Hungary. Phone: 36-(62)-599 633. Fax: 36-(62)-433 506. E-mail: kiss@brc.hu.

† These authors contributed equally to the work and should be considered equal first authors.

‡ Present address: Department of Medicine, Hopkins Bayview Medical Center, Baltimore, MD 21224.

§ Present address: Centre for Integrative Genomics, University of Lausanne, CH-1015 Lausanne, Switzerland.

[∇] Published ahead of print on 20 December 2010.

expressed exclusively in the overtly differentiated chondroblasts of the columnar and prehypertrophic GP zones (4, 5, 19). Chondrocytes turn all these genes off as they undergo hypertrophy and then activate *Col10a1* (collagen-10 gene).

Sox9, L-Sox5, and Sox6 form a trio of transcription factors that are both required and sufficient to induce chondrogenesis (2, 7, 14, 38). Their main functions are to bind and thereby directly induce activation of *Col2a1*, *Agc1*, and several other cartilage ECM genes (1, 13, 23–26). Sox9 features a family-specific HMG box DNA-binding domain and a homodimerization domain, which mediate its binding to pairs of inverted Sox motifs (13, 26). It also features a potent transactivation domain. L-Sox5 and Sox6 are highly related to each other but only distantly related to Sox9 through their HMG box domain. They feature a dimerization domain, distinct from that of Sox9, and lack a transactivation domain. They bind more-variable Sox motifs on cartilage-specific enhancers and cooperate with Sox9 in transactivation by increasing the efficiency of Sox9 binding to its own sites on DNA (13). It remains unknown, however, whether and how the activity of this Sox trio is controlled to confer markedly different expression patterns on the various cartilage ECM genes. We used here the *Matn1* promoter as a model to reach deeper insight into gene regulation orchestrated by the Sox trio.

Matrilin-1 (also called cartilage matrix protein [CMP]) belongs to a family of multidomain adaptor proteins (10, 22, 44). It facilitates assembly of the cartilage ECM by forming collagen-dependent and -independent filaments and interacting with aggrecan. It also forms complexes with biglycan, and decorin, linking collagen-6 microfibrils to aggrecan and collagen-2 (45). We previously showed that the *Matn1* promoter features several blocks of sequences highly conserved in amniotes (34). A 334-bp short promoter is insufficient to direct reporter gene activity in cartilage in transgenic mice (34) but can be activated at a low level in the *Matn1*-specific GP zones upon addition of an intronic enhancer (19). Stronger activity is obtained by using a 2-kb promoter with or without the intronic enhancer (19). These data suggest that the proximal promoter may contain the *cis*-acting elements driving *Matn1* expression in the growth plate but requires distal and intronic enhancers to be activated. This short promoter features highly conserved promoter element 1 (Pe1), recognized by the Sox trio, and two silencer elements (SI and SII) binding Nfi proteins (34, 41).

Here we demonstrate that the short promoter has a central role in conferring on *Matn1* its restricted spatiotemporal expression pattern. We show the respective roles of the Sox-binding sites in the Pe1 and the Ine elements and Nfi-binding sites in the SI element. We show that L-Sox5/Sox6 and Nfi differentially modulate promoter activation by Sox9, according to the relative levels of the proteins. Our data thereby provide new insights into the transcriptional mechanisms that underlie staggered gene expression in the cartilage GP.

MATERIALS AND METHODS

Cell culture. Chicken embryo chondroblasts (CEC) and fibroblasts (CEF) and mesenchymes were prepared and cultured as described previously (41). Low-density mesenchyme (LDM) and high-density mesenchyme (HDM) cultures were made similarly, by plating 1×10^6 cells and 5×10^6 cells, respectively, in 35-mm plates containing F-12 medium–Dulbecco's modified Eagle medium (DMEM) (1:1; HyClone Laboratories) supplemented with 10% fetal bovine

serum (FBS; Sigma and Gibco Laboratories). COS-7 cells were cultured under standard conditions. HDM cultures consisting of early proliferative (stage Ia) chondroblasts and CEC cultures rich in late proliferative (stage Ib) chondroblasts express *Matn1* at low and high levels, respectively (31, 41, 42). LDM, CEF, and COS-7 cultures served as *Matn1*-nonexpressing controls.

Oligonucleotides and plasmid constructions. Nucleotide sequences for wild-type and mutant versions of Pe1 and SI and consensus HMG and SOX9 competitors were described previously (34, 41). Sequences of oligonucleotides for wild-type Ine, Ine derivatives, and mutant versions of Ine are depicted in Fig. 3B.

All positions are given in bp from the first T of the chicken *Matn1* TATA motif. The TR70 (–2011/+67) and NAD1 (–334/+67) *Matn1*-*LacZ* constructs were reported previously (19, 34). PS-NAD1 was produced by inserting the –2011/–948 *Matn1* sequence upstream of NAD1. Eight tandem copies of a 48-bp *Col2a1* enhancer element (E_{Col2a1}) were inserted upstream of NAD1 to obtain $8 \times E_{Col2a1}$ -NAD1. Δ IneM1-TR70 was made by replacing the NAD1 promoter with the –2011/+67 fragment of Δ IneM1-*AC8Luc* (see below).

Luciferase reporters *FO15Luc* and *AC8Luc*, driven by the short and long *Matn1* promoters, respectively, as well as Δ Pe1M1-*FO15Luc* and Δ Pe1M4-*FO15Luc*, carrying point mutations in the Sox motif and spacer of Pe1, respectively, were described (34). To produce $8 \times E_{Col2a1}$ -*FO15Luc*, eight copies of E_{Col2a1} were inserted upstream of *FO15Luc*. Mutations were introduced into Pe1, Ine, and SI elements of reporters by PCR-based QuikChange site-directed mutagenesis (Stratagene) using oligonucleotides carrying the desired mutations. All constructs were verified by restriction enzyme analysis and DNA sequencing.

Generation and histological analysis of transgenic mice. All animal experiments were conducted according to the ethical standards of the Animal Health Care and Control Institute, Csongrád County, Hungary. C57BL/6, CBA, CD-1, and FVB mice were obtained from Charles River Laboratories, Hungary. Transgenic mice were generated essentially as described previously (19). On embryonic day 15.5 (E15.5), foster mothers were sacrificed by cervical dislocation and the transgenes were detected by PCR in founder (G_0) embryos. These embryos were stained with X-Gal (5-bromo-4-chloro-3-indolyl- β -D-galactopyranoside) and photographed as whole mounts with a Leica MZFLIII stereomicroscope equipped with a DC300F camera. Cryosections were counterstained with 0.5% eosin and analyzed using a Nikon Eclipse E600 microscope equipped with Spot RT Slider camera as described previously (19). Figures were made with Adobe Photoshop 8.0 and CorelDraw X4 software.

EMSA and supershift experiments. Full-length cDNAs for L-Sox5 and Sox6 were inserted in frame into the pGEX expression vector. Glutathione S-transferase (GST)-tagged L-Sox5, Sox6, and SOX9 were expressed and purified, and crude cell extracts were made as described previously (34). Twenty to 30 fmol end-labeled DNA probes was incubated with 1 to 2.5 μ g GST-SOX9 or GST-L-Sox5 or 3 μ g crude CEC or CEF cell extracts in the presence of 100 to 500 ng poly(dG-dC) · (dG-dC) and separated on prerun 5% or 6.6% PAGE gel. In competition electrophoretic mobility shift assays (EMSA), 50- and 500-fold molar excesses of cold competitors were added. Supershift experiments were performed as described previously (34) using Sox9, L-Sox5, and Sox6 antisera (26).

In vivo footprinting. CEC and CEF cells and HDM cultures were treated with dimethylsulfate (DMS) or irradiated with UV light and subjected to genomic footprinting as described previously (34). Briefly, 30 μ g of *in vivo*- and *in vitro*-treated DNA samples cleaved with piperidine were amplified by ligation-mediated PCR (LM-PCR) (32) between –227 and +140 using linker primers LP11 and LP25 and gene-specific nested primers PU1 and PU2 (upper strand), PL1 and PL2 (lower strand), and PU3 or PL3 (hybridization probe) (34) (see Fig. 4A).

Transient expression assay. CEC, CEF, and COS-7 cells were transfected with the Ca-phosphate coprecipitation method 4 to 6 h after plating (34, 41). HDM and LDM cultures were transfected similarly, but 24 h after plating. Briefly, 2 μ g (CEF and CEF) or 5 μ g (HDM, LDM, and COS-7) reporters was added with 0.5 μ g pRL-TK vector (Promega) as an internal control to correct for transfection efficiency. Control plates were transfected with *FO15Luc*. Firefly and *Renilla* luciferase activities were measured using Luminoscan Ascent (ThermoLabsystem 2.6) and luciferase assay systems (Promega) 72 h (HDM and LDM) or 48 h (other cells) posttransfection.

Unless indicated otherwise, cotransfections were performed with 2 μ g or 5 μ g *AC8Luc* and increasing amounts (50 to 250 ng) of effector plasmids pcDNA5'UT-FLAG-L-Sox5 (pFSox5) and pcDNA5'UT-FLAG-Sox6 (pFSox6) (26) without or with 250 ng pCDMA-SOX9 (pSOX9) (26). In a typical experiment, 250 ng pSOX9 and 125 ng each of pFSox5 and pFSox6 effector plasmids were used. Other experiments were performed with 0 to 300 ng effector plasmids expressing human CTF-1 (pCTF-1) (36) or mouse Nfia, Nfib, Nfic, and Nfix (pNfia, pNfib, pNfic, and pNfix), homologous to chicken Nfia1.1, Nfib2, Nfic2, and human NFIX2, respectively (9). Transfection mixtures were adjusted with

empty vectors to the same amount of total DNA. Luciferase activities were expressed as fold values relative to that for *FOI5Luc*, taken as 1, unless noted otherwise. Transfections were performed in duplicate or triplicate and repeated 3 to 10 times with at least two different DNA preparations. Results are presented as means \pm standard errors of the means (SEM).

Combined forced expression and Western analysis. To estimate the relative expression levels of Sox and Nfi proteins, we used pcDNA5'UT-FLAG-SOX9 (pFSOX9) (26) and we made pFNfib by inserting fragments of Nfi expression plasmids (9) into pcDNA5'UT-FLAG. COS-7 cells were cotransfected as described above with *AC8Luc*, 1 μ g pFSOX9, and increasing amounts of effector plasmids pFSox5 and pFSox6 or pFNfib. Transfected cells were lysed in 100 μ l buffer containing 14 mM HEPES (pH 7.9), 1.5 mM MgCl₂, 6 mM KCl, 0.44 mM NaCl, 0.08 mM EDTA, 2.3 mM dithiothreitol, 0.5 mM phenylmethylsulfonyl fluoride, 10% glycerol, and a protease inhibitor cocktail (Sigma-Aldrich; P2714). Supernatants were used to measure luciferase activities and in Western blots with rabbit anti-FLAG (Sigma) antisera.

Statistical analysis was carried out using one-way analysis of variance (ANOVA) with KyPlot version 2.0 beta 15.

QRT-PCR. Total RNA was isolated from cultured cells using an RNA isolation kit (Macherey-Nagel). Quantitative real-time PCR (QRT-PCR) was performed on a RotorGene 3000 instrument (Corbett Research) with gene-specific primers and the SYBR green protocol (16). Briefly, 2 μ g of DNase-treated RNA was reverse transcribed using the High-Capacity cDNA Archive kit (Applied Biosystems). Reactions were done with FastStart SYBR green Master mix (Roche Applied Science) at a primer concentration of 250 nM as follows: 15 s at 95°C and 45 cycles of 95°C for 15 s, 60°C for 25 s, and 72°C for 25 s. The quality of the reaction was checked by melting temperature analysis. Individual threshold cycle (C_T) values were normalized to the average C_T values of three internal control genes (glyceraldehyde 3-phosphate dehydrogenase [GAPDH], 18S rRNA, and 28S rRNA genes). The final relative gene expression ratios were calculated as $\Delta\Delta C_T$ values (comparison of the normalized ratios). Gene-specific primer sequences are shown in Table S1 at http://www.brc.hu/pub/Supplemental_Material_Nagy_et_al_MCB2010.pdf.

Genome sequence analysis. The MAF format 44-way vertebrate multiple alignment file of human chromosome 1 was downloaded from the University of California, Santa Cruz (UCSC), website (<http://hgdownload.cse.ucsc.edu/downloads.html>). The corresponding *Matn1* promoter region was extracted from this file using the MAF2FASTA program of the MULTIZ package (http://www.bx.psu.edu/miller_lab/) using the corresponding human positions. The Ine and Pe1 region was extracted and further refined manually. The 75% majority rule consensus and the sequence logo were generated with the Geneious Pro program.

RESULTS

Proximal elements restrict spatiotemporal activation of the *Matn1* promoter by homologous and heterologous enhancers.

We previously reported that a *LacZ* transgene driven by a *Matn1* short promoter (−334/+67; NAD1) exhibited low activity in mouse embryos (34). The addition of the *Matn1* −2011/−948 sequence (PS) markedly increased transgene activity (Fig. 1A and B), but this activity remained lower than that of a transgene harboring the full-length (−2011/+67; TR70) promoter (19) (Fig. 1C). Histological analysis revealed that the transgene activity also increased proximodistally in the limbs and craniocaudally in the vertebral bodies, as with TR70 (Fig. 1D to L). This activity was restricted to columnar and prehypertrophic chondrocytes. The −2011/−1134 region increased the short promoter activity less markedly than the −2011/−948 region but showed similar zonal and proximodistal specificity (see Fig. S1 at http://www.brc.hu/pub/Supplemental_Material_Nagy_et_al_MCB2010.pdf). We therefore concluded that elements in the −2011 to −334 region enhance the activity but not the tissue specificity of the *Matn1* promoter.

Next we tested activation of the *Matn1* short promoter by 8 tandem copies of the pancartilaginous *Col2a1* minimal en-

hancer (8 \times E_{Col2a1}-NAD1). Interestingly, 8 \times E_{Col2a1}-NAD1 dramatically differed in its expression pattern from p3000i3020Col2a1, which contains the *Col2a1* promoter and enhancer (47) (Fig. 2B and C). It was expressed exclusively in distal structures, like digits, caudal vertebral bodies, and nasal cartilage and only in columnar and prehypertrophic GP zones (Fig. 2D to N). Its sporadic or weak activity in epiphyseal and source chondroblasts and lack of activity in condensed mesenchymal cells, perichondrium cells, and prechondrocytes differed markedly from the high activity of the *Col2a1* transgene in these cells (47, 48). Thus, the *Matn1* short promoter inhibited the *Col2a1* enhancer in proximal structures and at early chondrocyte differentiation stages. Even 16 copies of E_{Col2a1} neither increased the transgene activity nor altered its restricted spatiotemporal expression (data not shown).

To sum up, the *Matn1* short promoter plays a critical role in restricting cartilage-specific expression, and its activity is enhanced by distal elements. It is even capable of restricting the activity of a powerful Sox-driven panchondrocytic *Col2a1* heterologous enhancer to distal structures and specific GP zones.

The Sox trio binds to the initiator element *in vitro*. To uncover the powerful mechanism employed by the *Matn1* short promoter, we dissected its elements. We reasoned that Pe1, which is the most conserved element in amniotes, could be involved in Sox-mediated functions, because it bears a palindrome resembling the preferred Sox9-binding site (29) (see Fig. S2B at http://www.brc.hu/pub/Supplemental_Material_Nagy_et_al_MCB2010.pdf) and because it is recognized by the Sox trio *in vitro* and protected in genomic footprinting (34). In addition, we found two conserved pairs of inverted Sox motifs in the Ine element of mammals (Fig. 3A; see Fig. S2A at the URL listed above). The sequence is poorly conserved in the chicken, but the chicken promoter also features two pairs of Sox motifs and a conserved GTGCC motif in the Ine element and an Nfi site upstream of TATA (Fig. 3A). These motifs could thus also play conserved regulatory roles.

We delineated the Sox-binding sites of Ine by EMSA using purified Sox proteins (Fig. 3B to F). GST-fused SOX9, L-Sox5, and Sox6 efficiently bound Ine *in vitro* (Fig. 3C and D and data not shown). Mutations M2 and M5, which disrupted both inverted Sox motifs, abolished complex formation, whereas M1 and M3, which disrupted only one Sox motif, had partial effect. Probes carrying the 5' (Ine5'h1) or 3' (Ine3'h2) Sox motif showed weaker binding than Ine (Fig. 3E and F). Mutation M1 less severely reduced complex formation with L-Sox5 than with SOX9. This was possibly due to the presence of an upstream Sox-like motif, as mutations in this motif (M6), in the 5' half site (M7), or in both sites (M6-7) had a more drastic consequence than M1 (Fig. 3E and F). Mutation M2-3 abolished Sox binding to the 3' site. We concluded that both Sox sites might be functional and might act cooperatively.

CEC nuclear proteins formed three major complexes with Ine. Complexes I and II were supershifted with Sox9, L-Sox5, and Sox6 antibodies (Fig. 3G) and competed with HMG, Sox9, or E_{Col2a1} probes (Fig. 3H). They thus likely contain the Sox trio. In contrast, complex III was not specific to chondrocytes and did not contain Sox factors (Fig. 3G to I).

Ine3'h1, in which the 5' Sox site was mutated, formed two major CEC nucleoprotein complexes (Fig. 3J). These complexes migrated like complexes II and III, and formation of the

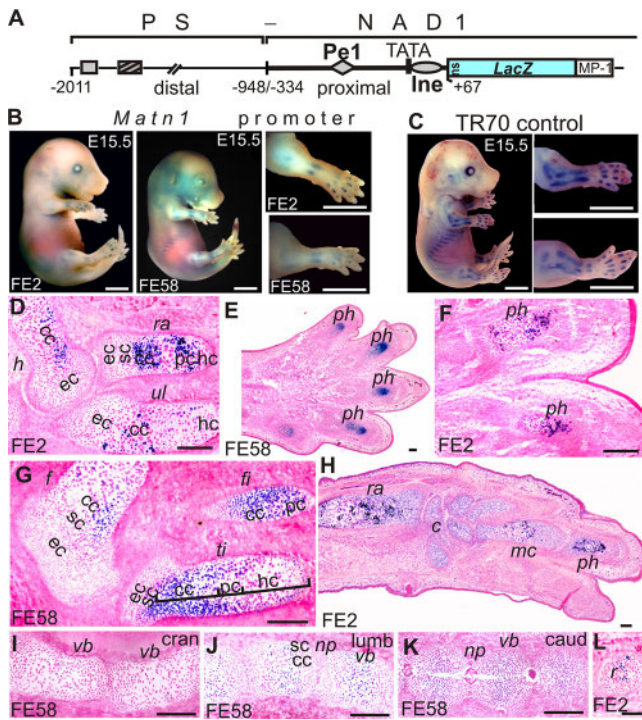


FIG. 1. Upstream elements increase the activity of the *Matn1* proximal promoter *in vivo*. (A) Schematic of PS-NAD1 depicting conserved DNA blocks (rectangles, diamond, and oval) in the distal and proximal *Matn1* promoter regions. (B and C) Expression of PS-NAD1 (B) and TR70 (C; 2-kb *Matn1* promoter) transgenes in founder embryos (FE) stained with X-Gal at E15.5. (D to L) Histological analysis of PS-NAD1 embryo cryosections. In the developing limbs, X-Gal staining increases proximodistally from humerus (h), ulna (ul), and femur (f) to radius (ra), tibia (ti), and fibula (fi) and further from carpals (c) and metacarpals (mc) to phalanges (ph) (D to H). Staining is absent in cranial (cran) vertebral bodies (vb) but increases from lumbar (lumb) to caudal (caud) regions (I to K). *LacZ* activity is restricted to the GP zones of columnar chondroblasts (cc) and prehypertrophic chondrocytes (pc), while it is low or absent in the zones of epiphyseal (ec) and source chondroblasts (sc) and hypertrophic chondrocytes (hc) (D, G, and J to L). np, nucleus pulposus; r, rib. Bars, 2 mm (B and C) and 200 μ m (D to L).

former one was competed by the HMG probe. As complex I was neither efficiently disrupted nor formed with Ine3'h1, we concluded that it likely formed on the 5' Sox site. IneM1, which was mutated in the 5' Sox site, decreased the formation of complex I (Fig. 3K), as judged by reduced supershift formation, especially with Sox9 antibody (compare Fig. 3G and L). Interestingly, a new complex, not supershifted with Sox antibodies, migrated close to or slightly below complex I with probes IneM1, IneM2, and IneM3 (Fig. 3K to N, arrowheads). As IneM1 and IneM3 carried an intact Sox site, they efficiently displaced both the Sox-specific and unrelated complexes of Ine (Fig. 3J). IneM3, which carried mutations in the 3' Sox site, did not produce the Sox-specific complex II, but supershifts with L-Sox5 and Sox6 antibodies indicated that it formed complex I (Fig. 3K and N). IneM2, however, which carried mutations in both Sox sites and in the conserved GTGCC motif, neither formed complexes I to III (Fig. 3K and M) nor competed for those (Fig. 3J). Complex III may contain the unidentified factor binding to the GTGCC motif. Supporting this hypothesis,

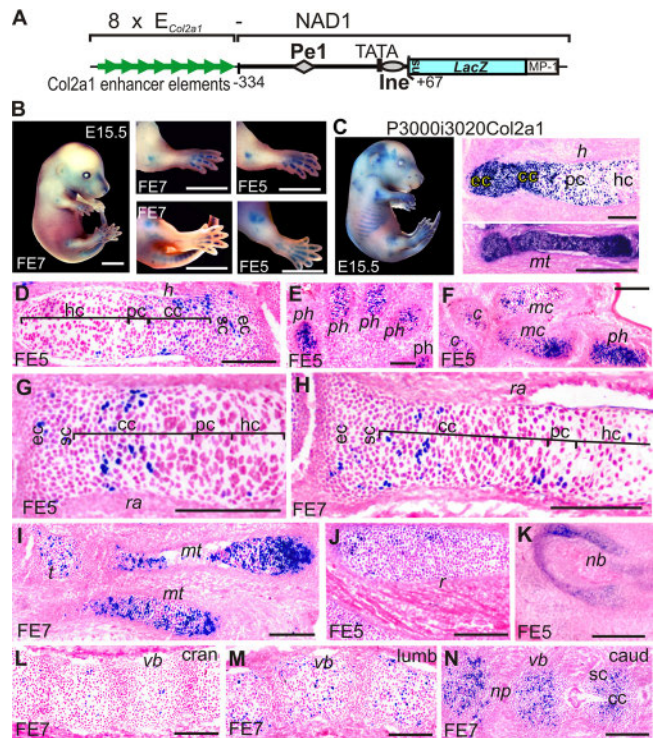


FIG. 2. The short promoter restricts the *Col2a1* enhancer activity *in vivo*. Schematic (A) and expression (B) of the $8 \times E_{Col2a1}$ -NAD1 transgene in comparison with the pattern of P3000i3020*Col2a1* (C) driven by the *Col2a1* promoter and enhancer (47). (D to N) Histological analysis of $8 \times E_{Col2a1}$ -NAD1 cryosections. In the developing limbs (D to I), X-Gal staining is relatively weak in the humerus and radius but sharply increases toward the distal phalanges. *LacZ* activity is completely repressed or limited to a few cells in the cranial and lumbar vertebral bodies but is high in the caudal ones and in the distal part of nasal bone (nb) (K to N). Expression is highest, limited to groups of cells, in the columnar and prehypertrophic zones, but it is strongly reduced in the source and epiphyseal chondroblasts, except for sporadic staining in the distal epiphysis of the humerus (D to N). t, tarsal; mt, metatarsal. Other abbreviations are as defined for Fig. 1. Bars, 2 mm (B) and 200 μ m (D to N).

only complex III efficiently formed with IneM5, which carried mutations in both Sox sites but had part of the GTGCC motif intact (Fig. 3K and O).

We concluded that Sox factors cooperatively bind the Ine 5' and 3' Sox sites. SOX9 binds efficiently only when both sites are intact. Apart from two CEC-specific Sox complexes, an unrelated complex forms on the conserved GTGCC motif in mesenchymal cells. This motif is not listed in the TRANSFAC database and likely interacts with a non-chondrocytic factor.

Cartilage-specific *in vivo* occupancy of Ine and SI. To determine occupancy of the *Matn1* promoter in intact cells, we performed *in vivo* footprinting. We treated CEC and CEF genomic DNA with DMS or UV light to modify G residues at the N-7 position or produce 6-4 photoproducts at TC and CC dinucleotides, respectively (Fig. 4). Bound proteins blocking these modifications appeared as footprints on LM-PCR genomic sequencing ladders compared to LM-PCR of naked CEC and CEF DNA treated with the same reagents *in vitro*. Differences in the modification patterns between the *in vivo*-

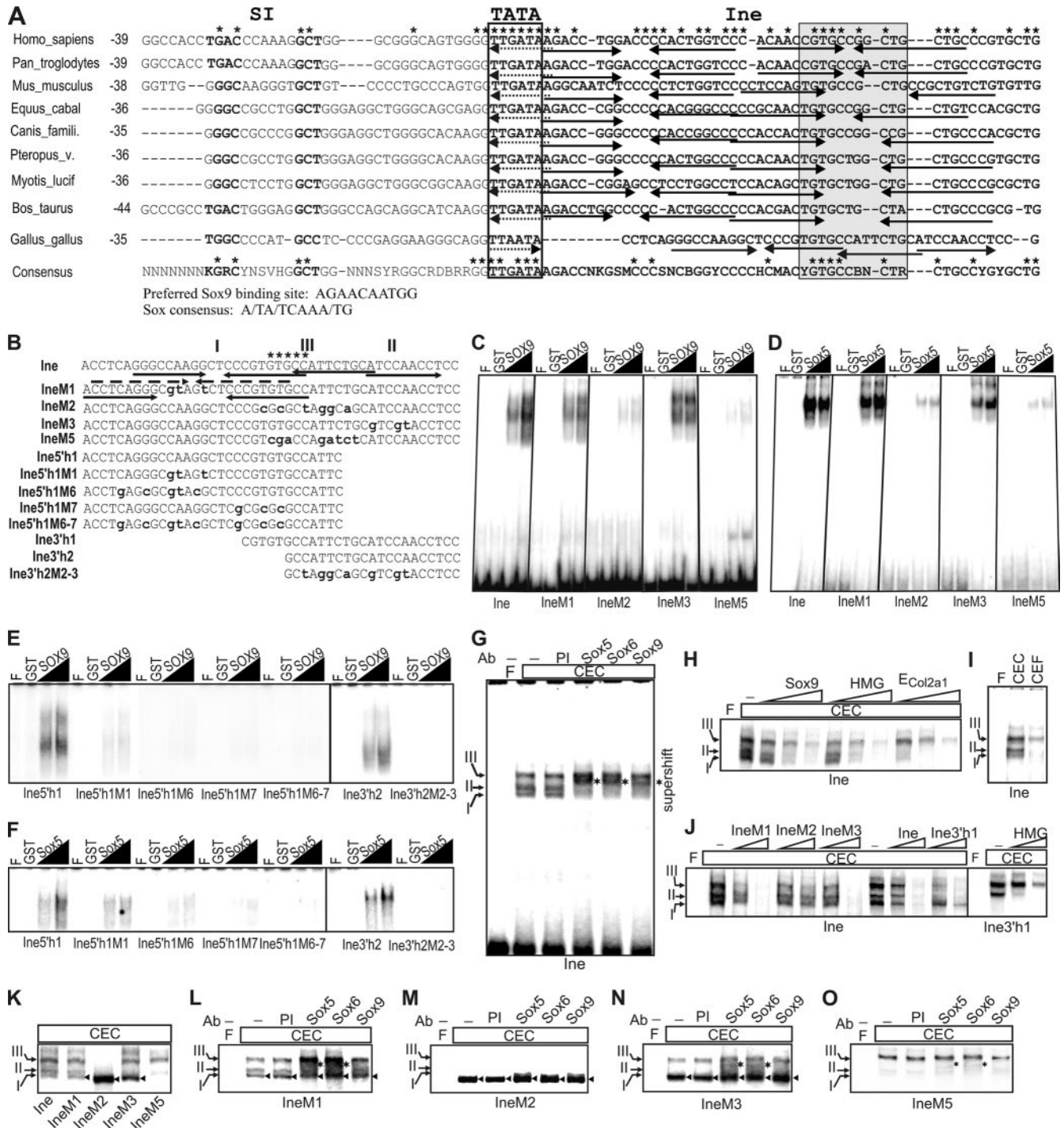


FIG. 3. Binding of Sox proteins to Ine *in vitro*. (A) Ine sequences of selected amniotes and the 75% majority rule consensus for amniotes (see the whole alignment in Fig. S2A at http://www.brc.hu/pub/Supplemental_Material_Nagy_et_al_MCB2010.pdf). TATA and the most conserved motif are boxed; NFI motifs are in boldface. Positions are given from TATA. Nucleotides fully conserved in mammals or in amniotes are marked by asterisks at the top and above the consensus sequence, respectively. Arrows and dotted arrows depict motifs similar to the preferred Sox9-binding site (29) and Sox consensus (21), respectively. Equus_cabal, *Equus caballus*; Canis_famili., *Canis familiaris*; Pteropus_v., *Pteropus vampyrus*; Myotis_lucif, *Myotis lucifugus*. (B) Sequences of Ine and its shorter or mutant derivatives. The conserved GTGCC motif, mutant nucleotides, the 5' (I) and 3' (II) paired Sox sites and unrelated factor-binding site (III) are denoted. (C to F) EMSA of nucleoprotein complexes formed with purified GST-fused Sox proteins on Ine and its derivatives. (G to O) Binding of CEC nuclear proteins to Ine and Ine mutants. (G) Supershift analysis with Sox antibodies (Ab). (H) Competition EMSA with 50-, 100-, and 500-fold molar excesses of the indicated cold competitors. (I) Comparison of CEC and CEF nucleoprotein complexes. (J) Competition EMSA on Ine and Ine3'h1 with the cold probes indicated. (K to O) EMSA (K) and supershifts (L to O) of the wild-type and mutant Ine. The supershifts (asterisks) and new complexes of Ine mutants (arrowheads) are marked. F, free probe; PI, preimmune serum.

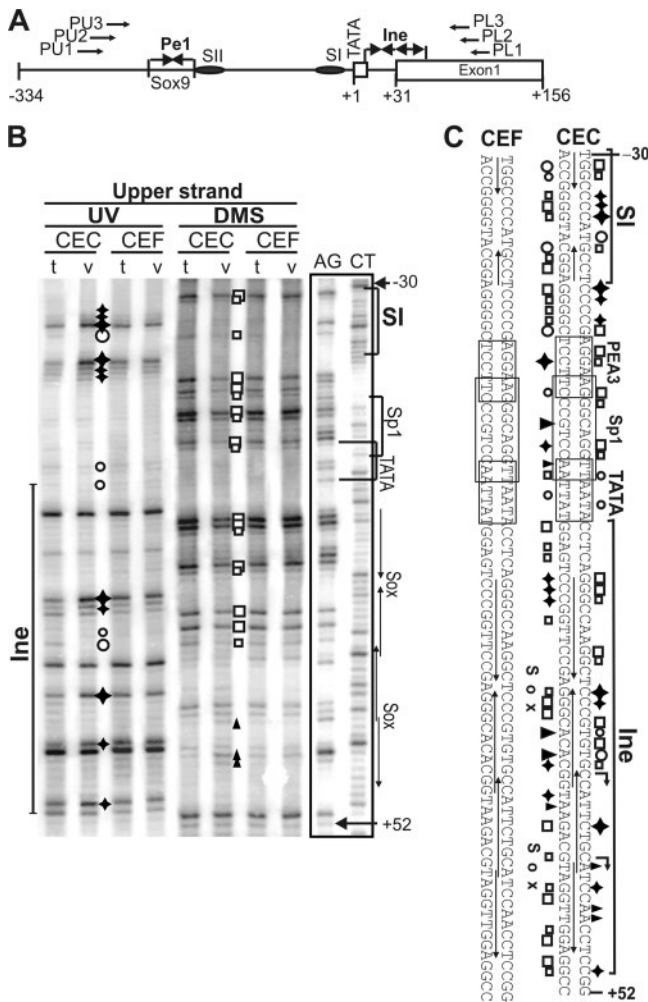


FIG. 4. Tissue-specific occupancy of Ine1 and SI in genomic footprinting. (A) Schematic depicting the primers used in footprinting and the short promoter elements. (B) Footprints on the upper DNA strand. AG and CT are Maxam-Gilbert ladders. DNA from CEC and CEF cultures treated *in vivo* (v) with DMS (open boxes or solid triangles) or UV light (open circles or solid diamonds) is compared with the *in vitro* (t) DNA samples treated with these reagents after isolation from CEC and CEF. Differences in the modification patterns between *in vivo* and *in vitro* treatments appear as hyperactivities (solid diamonds or triangles) or protections (open circles or boxes), revealing specific *in vivo* DNA-protein contacts. (C) Summary of *in vivo* footprinting on both strands.

and *in vitro*-treated samples indicated *in vivo* DNA-protein contacts at specific nucleotides in the promoter area in CEC cultures (Fig. 4B and C). Protection, combined with hyperre-activity on the opposite strand, revealed protein binding to the Sox motifs of Ine and to the conserved TGTGCC motif at the start site. Both treatments revealed *in vivo* occupancy at TATA, at the Nfi contact points of the reported SI element (41), at putative PEA3, Sp1, and GC-rich motifs downstream of SI, and in the Nfi spacer region. In contrast, no footprints were detected in CEF.

In HDM cultures undergoing early chondrogenesis, none or weak occupancy was seen at TATA, Ine, and SI elements on days 0 and 2 (Fig. 5A and B). By day 4, however, the 5' Sox site

of Ine started to be occupied and stronger protection was also observed for the Sox motifs of Pe1 and Nfi contact points of SII (Fig. 5C and D).

We concluded that the CEC-specific *in vivo* footprints at the Ine Sox sites are likely due to stage-specific binding of Sox proteins. The TGTGCC motif, the Nfi site, and other potential ubiquitous factor-binding sites near TATA were also occupied. Gradual protection at the Pe1 and Ine Sox sites and at SII and SI Nfi sites in HDM culture suggests that these elements participate in *Matn1* activation during chondrogenesis.

The Pe1 Sox site and SI Nfi site are indispensable for promoter activation in transiently transfected chondrocytes. To study the contribution of short promoter elements to promoter activity, we introduced point mutations into Ine, Pe1, and SI and measured their effect on the activity of short (*FO15Luc*) and long (*AC8Luc*) promoter constructs. IneM2, which carried mutations in the Sox- and ubiquitous factor-binding sites of Ine, and a double Pe1M1/IneM2 mutation most effectively reduced the activity of the short promoter in CEC (Fig. 6A and B). The -2011/-334 sequence enhanced the short promoter activity ~19-fold in *AC8Luc* in CEC but hardly did so in low- or nonexpressing cultures (Fig. 6C). IneM1, IneM2, and IneM3 cut the long promoter activity by one half or more in CEC. The effect of Pe1M4, which carried a mutation in a factor-binding site in Pe1 (34), was similar, but Pe1M1, in which the Sox site of Pe1 was disrupted, dropped the long promoter activity 13-fold, abolishing CEC-specific enhancement from upstream elements. Pe1M1/IneM2 decreased the activity ($P < 0.05$) to a level even closer to that of *FO15Luc*. Thus, the Sox sites in Pe1 and Ine are needed to mediate promoter activation from upstream elements.

Considering that the SI element was protected in genomic footprinting in CEC culture (Fig. 4) and bound Nfi proteins *in vitro* (41), we also mutated its Nfi contact points. Mutation SI2dm, either alone or in combination with Pe1M1 or Pe1M4, markedly reduced the short promoter activity in mesenchymal cells (Fig. 6A and B). This mutation also dropped the long promoter activity by 10-fold in CEC and similarly in other cultures, indicating non-tissue-specific inhibition (Fig. 6C). Double mutation Pe1M1/SI2dm further diminished the activity ($P < 0.001$) to the basal promoter level in mesenchymal cells, suggesting an additive or synergistic effect. Thus, disruption of the Nfi site of the SI silencer element abolished both the tissue- and stage-specific promoter activity.

We concluded that, although Ine recognition by Sox factors may be involved, Sox factor binding to Pe1 seems to be more crucial for promoter activation in CEC culture rich in late proliferative chondroblasts. In addition, binding of the ubiquitous Nfi to SI near the TATA box may be similarly crucial. The position-specific conservation of motifs similar to the NFI consensus (35) near TATA in amniotes (see Fig. S2A at http://www.brc.hu/pub/Supplemental_Material_Nagy_et_al_MCB2010.pdf) further supports the importance of SI in the regulation of the gene. The significant, but less dramatic, effect of other mutations suggests that the binding of factors to the Pe1 spacer and to the conserved motif of Ine may also be needed for full promoter activity.

Sox and Nfi sites of the short promoter are important for enhancement by *E_{Col2a1}*. Next we tested the activation of the

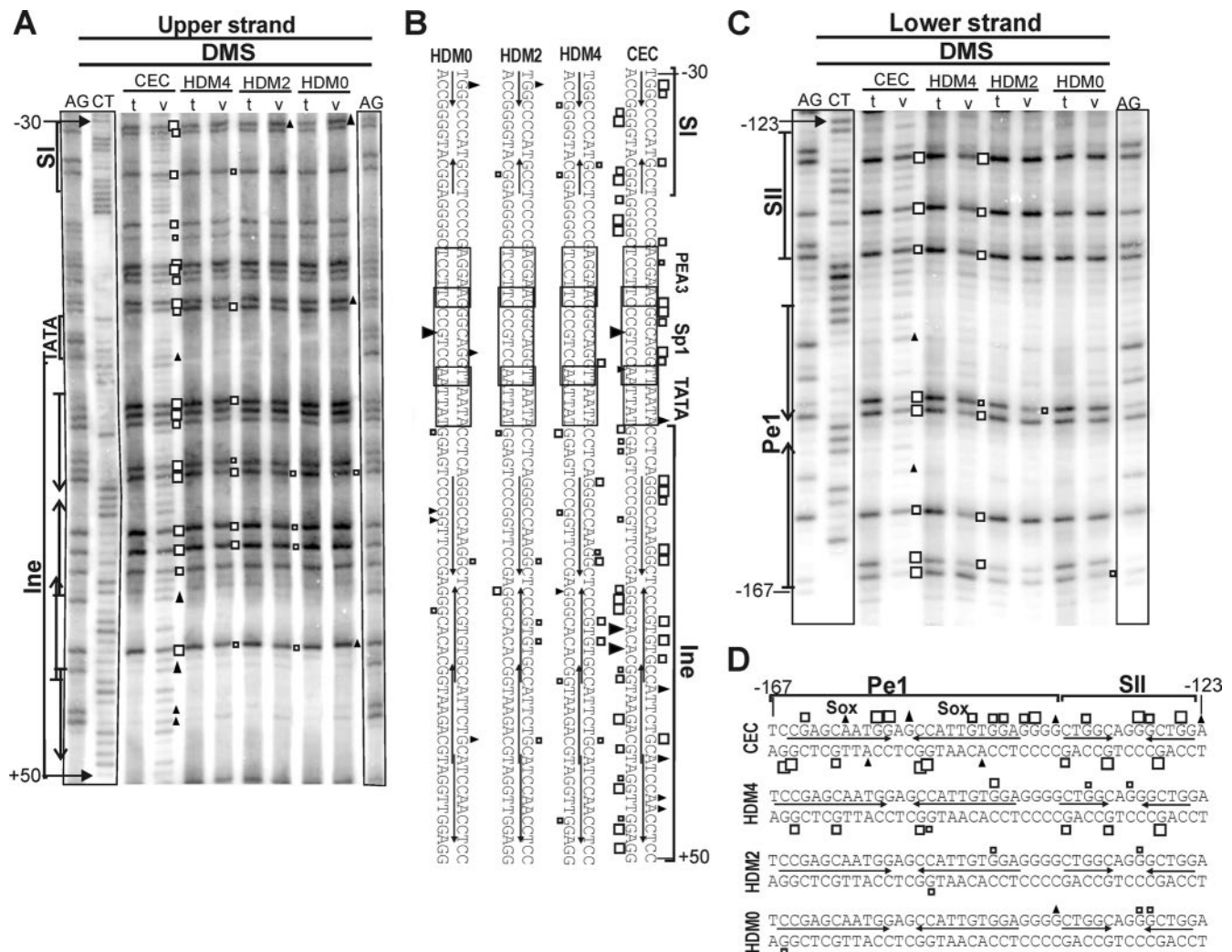


FIG. 5. Slow gradual occupancy of the short promoter elements during chondrogenesis. Shown is a comparison of *in vivo* footprints formed with DMS in the vicinity of the Ine (A) and Pe1 elements (C) in CEC and in day 0, 2, and 4 HDM cultures. (B and D) Summary of *in vivo* footprinting on both strands. Other symbols are as in Fig. 4.

short promoter by a heterologous cartilage enhancer. Eight copies of E_{Col2a1} robustly increased the short promoter activity in CEC but had no effect in CEF or in HDM cultures consisting of early proliferative chondroblasts (Fig. 6D). Lining up with transgenic mouse data, these results indicate that the *Matn1* short promoter also restricted the broad cartilage-specific enhancement by E_{Col2a1} to late proliferative chondroblasts in tissue culture.

Mutations Pe1M1, IneM2, SI2dm, and Pe1M1/IneM2 decreased the relative activity of $8 \times E_{Col2a1}$ -*FO15Luc* by 43.6%, 46.6%, 64.9%, and 78%, respectively, in CEC culture (Fig. 6D). Thus, our data show that, whereas Sox factor binding to Pe1 is crucial for the interaction between the homologous distal and proximal promoter elements, Sox9 binding to Pe1 and Ine is less essential for mediating enhancement from E_{Col2a1} . Disrupting all three Sox sites of Pe1 and Ine or the Nfi site of SI, however, highly diminished the enhancement, supporting the hypothesis that the short promoter elements may

also interact with the heterologous enhancer via the bound Sox and Nfi factors.

Dramatic decrease of transgene activity by mutation of the 5' Sox site in Ine. A transgene carrying the IneM1 mutation displayed very low activity in founder embryos, but this activity remained restricted to the columnar and prehypertrophic GP zones, as with TR70 (Fig. 7). Thus, consistent with the reduced Sox-specific complex formation (Fig. 3L), the IneM1 mutation hampered promoter activation *in vivo* but did not alter the zone- and distal structure-dependent expression pattern of the promoter. The 5' Sox site of Ine is thus needed for optimal promoter activation *in vivo*.

Accumulation of Nfi and Sox mRNAs during *in vitro* chondrogenesis. We compared the kinetics of expression of *Matn1* and other genes in chondrogenic cultures by QRT-PCR. In CEFs, the steady-state mRNA levels of *Matn1* and the Sox trio were very low, while those for Nfi, but not *Nfic*, were elevated relative to those in the committed mesenchyme (HDM, day 0)

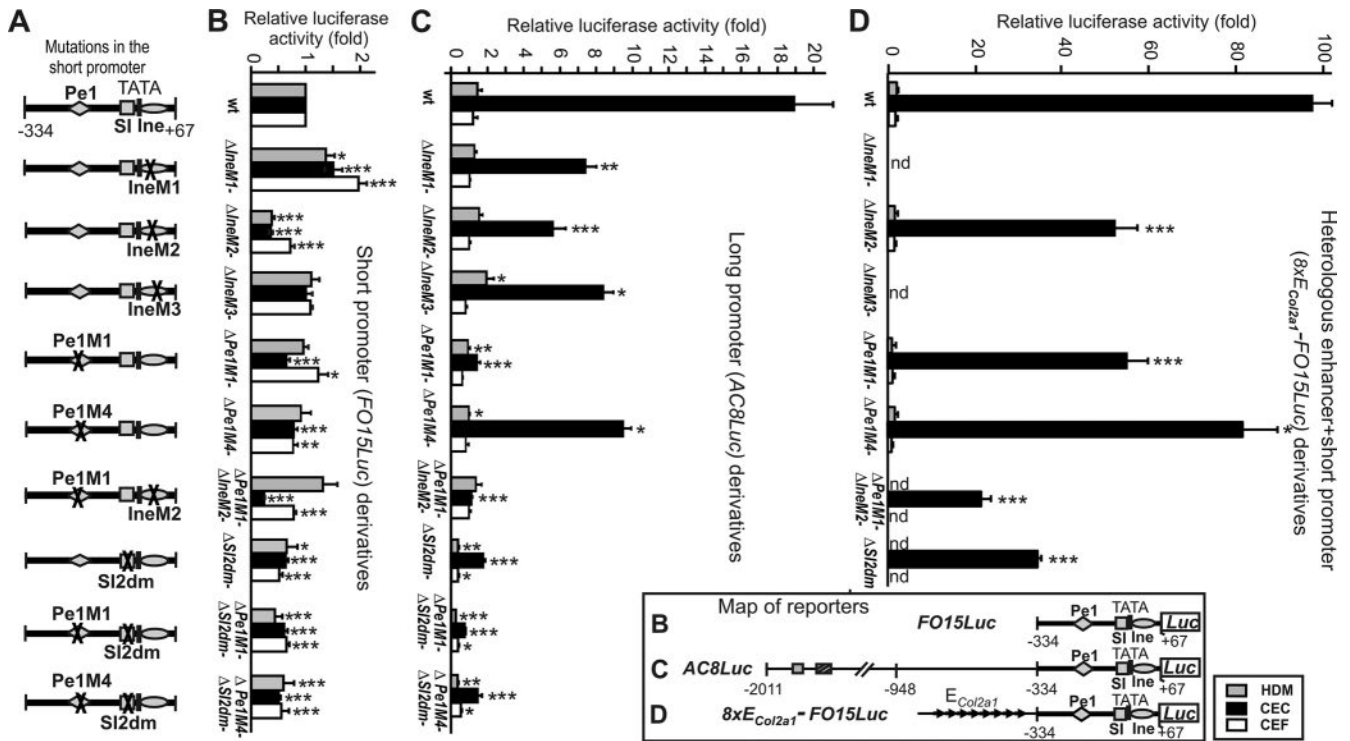


FIG. 6. Effect of Ine, Pe1, and SI mutations on reporter activities in transfected cells. (A) Schematic of single or double mutations introduced into the short promoters of reporters *FO15Luc*, *AC8Luc*, and $8 \times E_{Col2a1}$ -*FO15Luc* driven by the short or long *Matn1* promoter or multiple copies of E_{Col2a1} fused to the short promoter, respectively, as seen on their full maps (bottom). (B to D) Luciferase activities of wild-type (wt) and mutant reporters in the low-, high-, and nonexpressing HDM, CEC, and CEF cultures, respectively, are presented as fold values relative to that for *FO15Luc*. *, $P < 0.05$; **, $P < 0.01$; ***, $P < 0.001$ (compared with wild-type reporter). nd, not determined.

(Fig. 8A to C). In HDM culture, the *Col2a1* mRNA level slowly but continuously accumulated during differentiation, whereas the *Matn1* mRNA level dramatically increased between days 2 and 4 (Fig. 8A). Upon differentiation of CEC, the *Col2a1* and *Matn1* relative mRNA levels rose to values of 181-fold and 2,057-fold, respectively. *Sox9* and *Col2a1* mRNAs accumulated with similar kinetics, but the low levels of L-*Sox5* and *Sox6* mRNAs increased sharply only in CEC culture, except for a small, transient boost of *Sox6* mRNA at days 3 and 4 in HDM culture, just preceding the first peak in the *Matn1* mRNA level (Fig. 8B). The relative Nfi mRNA levels also increased transiently by 2.6- to 22-fold, with two peaks at day 4 and days 6 and 7 in HDM culture, followed by a sharp decline in CEC culture to close to 1 (*Nfia* and *Nfic*) or below 1 (*Nfib* and *Nfic*) (Fig. 8C).

Thus, CEC culture, rich in late proliferative chondroblasts, is characterized by high *Matn1* and Sox trio levels but low Nfi mRNA levels. However, day 4 HDM culture, consisting of early proliferative chondroblasts, exhibits high Nfi mRNA levels but lower *Matn1*, *Sox9*, and *Sox6* mRNA levels and very low L-*Sox5* mRNA expression. *Sox6* and Nfi mRNA levels peaked in HDM culture at the time of *Matn1* activation, suggesting a function in *Matn1* regulation.

Dose-dependent synergy of L-*Sox5*/*Sox6* with SOX9. Next, we assessed activation of the *Matn1* long promoter by cotransfected Sox proteins. While SOX9 doubled it, L-*Sox5*/*Sox6* decreased the promoter activity by about one-half in mesenchymal cells (Fig. 9A). Coexpression of L-*Sox5*/*Sox6* with SOX9

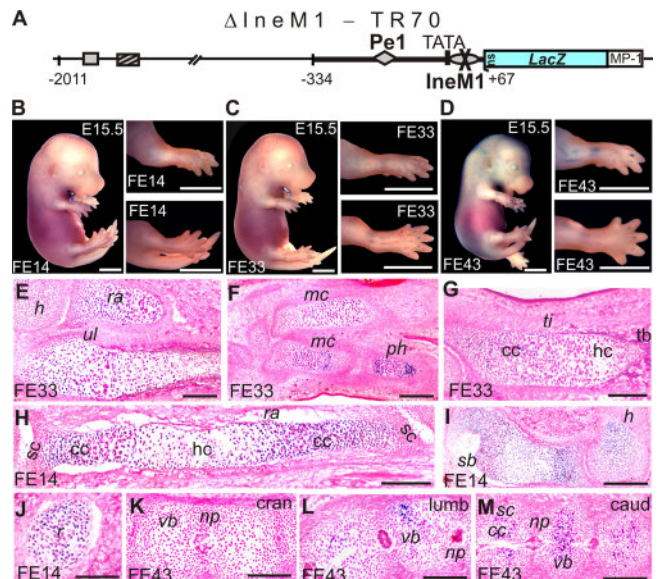


FIG. 7. Low zonal activity of the $\Delta IneM1$ -TR70 transgene. (A to D) Schematic (A) and low activity of the transgene (B to D). (E to M) Histological analysis of cryosections. Weak X-Gal staining in the developing shoulder blade (sb) and limbs slightly increases toward phalanges (E to I). The increase is more pronounced from cranial to caudal vertebral bodies (K to M). Staining is seen in the columnar and prehypertrophic zones (G, H, and M). For other abbreviations, see the Fig. 1 legend. Bars, 2 mm (B to D) and 200 μm (E to M).

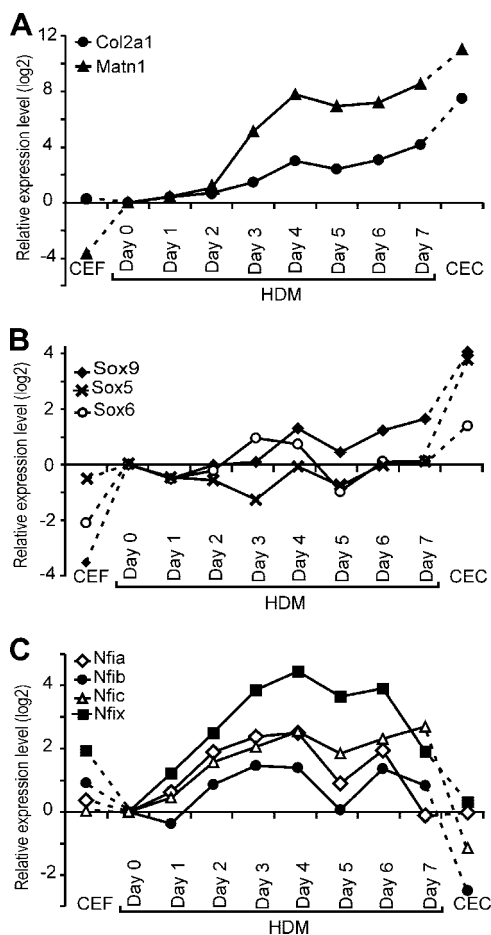


FIG. 8. QRT-PCR analysis of marker gene expression in chondrogenic cultures. (A to C) Marker mRNA levels were determined during chondrogenesis in HDM culture at time points indicated relative to the day 0 values and compared to mRNA levels of high-expressing CEC and nonexpressing CEF cultures. C_T values were normalized and relative gene expression ratios were calculated according to Materials and Methods. Relative expression levels ($\Delta\Delta C_T$) are plotted as \log_2 ratios.

greatly or moderately increased the ability of SOX9 to activate the promoter in CEF and HDM cultures, respectively, but decreased it in CEC culture. This suggests synergy between Sox proteins at early differentiation stages. When we introduced a constant amount of pSOX9 and increasing amounts of pSox5 and pSox6 expression plasmids into CEF, LDM, and HDM cultures, synergistic activation peaked at a low ratio of pL-Sox5 and pSox6 versus pSOX9 and declined at an elevated ratio (Fig. 9B). Highest activation was seen in CEF (3.5-fold), followed by that in LDM and HDM cultures in inverse correlation with the endogenous *Sox5* and *Sox6* expression levels of these cultures (Fig. 8B), raising the possibility that L-Sox5/Sox6 may modulate the activation by SOX9 in a dose-dependent manner.

This hypothesis was confirmed by forced expression of the FLAG-tagged Sox trio in nonchondrocytic COS-7 cells and monitoring of protein expression in Western blots (Fig. 9C). Despite the small effect of SOX9 alone, L-Sox5/Sox6 synergized with SOX9 to activate the long promoter up to ~18- to 20-fold at low molar excess. The activation was high from a 1:1

to 4:1 molar ratio of L-Sox5/Sox6 to SOX9 in repeated experiments, but the synergy dropped above a 5:1 molar ratio (Fig. 9C). When tested individually, L-Sox5 and Sox6 had similar effects (see Fig. S3 at http://www.brc.hu/pub/Supplemental_Material_Nagy_et_al_MCB2010.pdf).

We concluded that L-Sox5/Sox6 may finely tune the activity of the *Matn1* promoter by increasing transactivation by SOX9 at a low molar ratio relative to SOX9 (early stages of chondrogenesis) and by decreasing transactivation by SOX9 at a high ratio (late stage).

Pe1 mutation hampers transactivation by SOX9, and Ine mutation decreases the synergy with L-Sox5/Sox6. Next we studied the effect of Pe1, Ine, and SI mutations on the activity of the Sox trio. In COS-7 cells forced to express L-Sox5/Sox6 in optimal ratio relative to SOX9, the Pe1M1/IneM2 mutation decreased the synergistic activation of the long promoter by 96.1%, followed by the SI2dm and Pe1M1 mutations (85.5 to 89%) (Fig. 9D). The former mutations also repressed SOX9-mediated activation by ~70%. Similar effects were obtained when L-Sox5/Sox6 was expressed in high excess relative to SOX9 in LDM and CEC cultures (Fig. 9D). Thus, disruption of the short promoter Sox sites abolished transactivation by the Sox trio even when upstream sites were intact. The effect of the Pe1M1 mutation was milder, suggesting that SOX9 binding to Pe1 is critical for transactivation by SOX9 in early and late stages of chondrogenesis.

Ine mutations diminished the synergistic activation of SOX9 with an optimal ratio of L-Sox5/Sox6 in COS-7 cells (Fig. 9D). In LDM culture, IneM1 and IneM3 abolished *AC8Luc* activation by SOX9, while IneM2 and IneM3 affected the synergistic activation by the Sox trio more drastically than IneM1. In keeping with the effect of Ine mutations in EMSA, this result indicates that the 3' Sox site in Ine equally interacts with SOX9 and L-Sox5/Sox6, whereas the 5' site preferably binds SOX9 in early chondroblasts. IneM1 also hampers activation by SOX9 in CEC culture (Fig. 9D). Notably, mutation of the SI Nfi site highly decreased SOX9- and Sox trio-mediated promoter activation in the cultures tested. The variable effect of Pe1M4 and the small effect of SOX9 in COS-7 cells suggest that ubiquitous and/or Sox partner factors may also bind the promoter elements.

We concluded that SOX9 binding to Pe1 likely plays a key role in mediating enhancement from distal elements. Based on the data, we suggest a model (see Fig. 10D). L-Sox5/Sox6 expressed at a low level and bound to Ine may synergistically increase activation by Pe1-bound SOX9 in early chondrogenesis. Later on, when produced in excess to SOX9, L-Sox5/Sox6 may decrease activation by SOX9, possibly by competing for binding to the same sites. In addition, Nfi binding to SI and binding of other factors to Pe1 and Ine may also be needed for efficient activation.

Nfi proteins modulate promoter activity. Next we studied the effect of Nfi on *AC8Luc* activity in cotransfection assays. In CEC culture, all Nfi proteins, except Nfia at low concentration, robustly inhibited long promoter activity (Fig. 10A). When NFI and SOX9 were expressed at an optimal ratio, Nfib and Nfic decreased significantly transactivation by SOX9, but all Nfi proteins exerted 74% to 90% repression at higher ratio (see Fig. S4A at http://www.brc.hu/pub/Supplemental_Material_Nagy_et_al_MCB2010.pdf). Notably, CTF-1, an

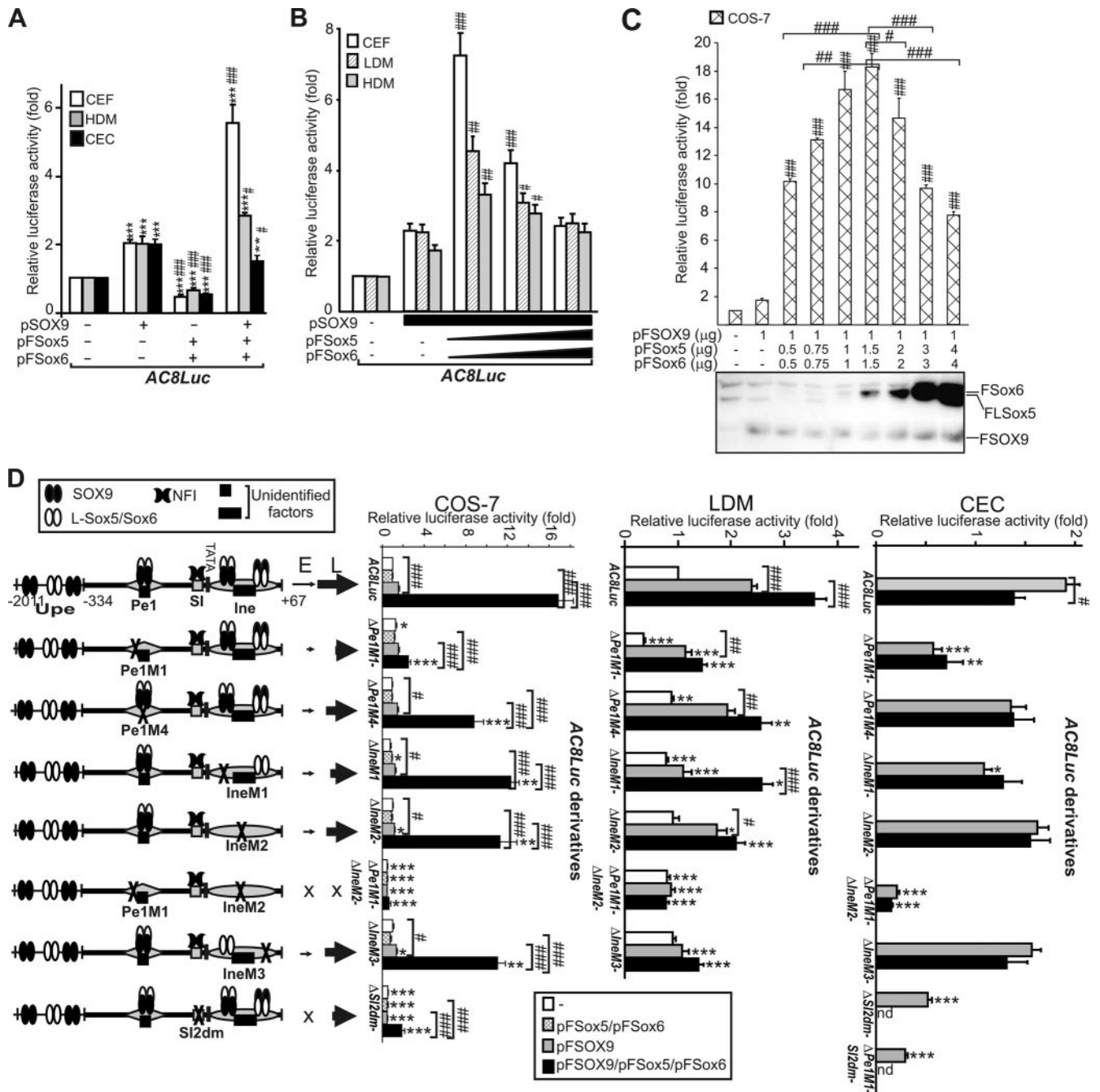


FIG. 9. Functional importance of Sox-binding sites in cotransfection assays. (A to C) *AC8Luc* was cotransfected with Sox expression plasmids in various cultures as indicated. Western analysis with anti-FLAG antibody (C) shows the relative expressions of L-Sox5/Sox6 and SOX9 in the transfected COS-7 samples. (D) Effect of point mutations on the synergistic activation of the long promoter by L-Sox5/Sox6 and SOX9 coexpressed at optimal (2.7:1) molar ratio in COS-7 cells and at a higher ratio in LDM and CEC cultures. The schematic indicates factor binding to the short promoter elements and to the upstream elements (Upe) (not drawn to scale). Thin and thick arrows depict the transcription efficiencies at early (E) and at late (L) stages of chondrogenesis. Luciferase activities are given as fold values relative to that for *AC8Luc*. *, $P < 0.05$; **, $P < 0.01$; ***, $P < 0.001$ (compared with the reporter cotransfected with vectors [A to C] or between the cotransfected mutants and the similarly cotransfected wild-type *AC8Luc* [D]); #, $P < 0.05$; ##, $P < 0.01$; ###, $P < 0.001$ (compared with the SOX9-cotransfected reporters).

isoform of NFIC, only slightly inhibited activation by SOX9 (see Fig. S4B at the URL listed above), suggesting that the various Nfi splice variants may have different effects. In COS-7 cells, Nfia and Nfib in optimal amounts indeed cooperated with SOX9 and potentiated its transactivation of the long promoter

(Fig. 10B). The activation, however, declined at higher levels of Nfia and Nfib. Forced expression of FLAG-tagged proteins in COS-7 cells revealed that the activation increased up to an ~2:1 molar ratio of Nfib to SOX9 but significantly decreased above an ~4:1 molar ratio (Fig. 10C).

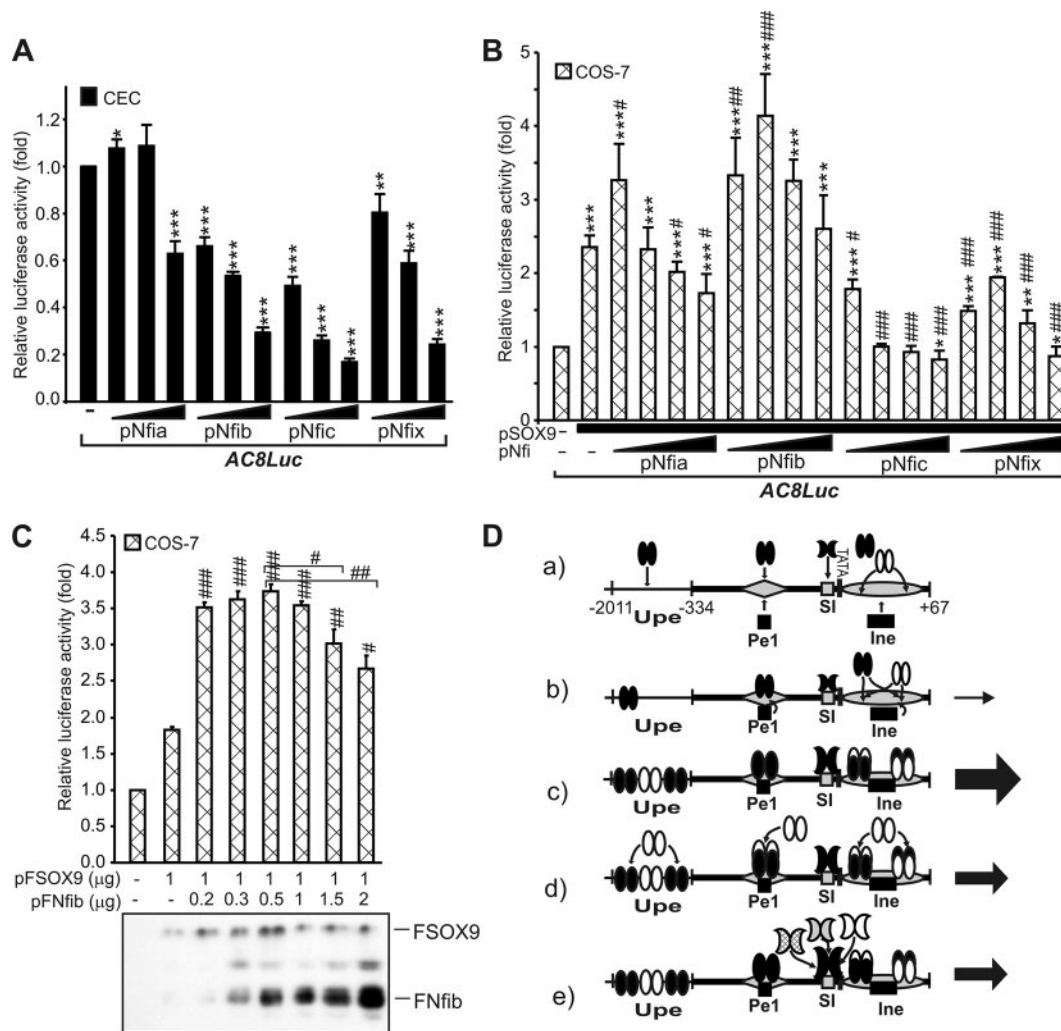


FIG. 10. Modulation of the *Matn1* promoter activity by cotransfected Nfi proteins. (A to C) *AC8Luc* was cotransfected with increasing amounts of Nfi expression plasmids without or with a constant amount of SOX9 expression plasmids in the cultures indicated. (C) Western analysis was made with anti-FLAG antibody to determine the relative ratio of Nfib and SOX9 expressed by force at optimal promoter activation. (D) Model for fine-tuning of the promoter activity by the Sox trio and Nfi. Shown are schematics of factor binding to DNA elements during *Matn1* activation at the onset of chondrogenesis (a), in early (b) and late proliferative chondroblasts (c) at low and optimal occupancy of sites, respectively, and in the late stage at high occupancy of the Sox (d) or Nfi sites (e). See the text for a detailed description. Symbols are as defined for Fig. 9.

These data suggest that Nfi proteins may increase or decrease SOX9-mediated transactivation of *Matn1* depending on their abundance relative to SOX9 (Fig. 10D). The conservation of Nfi sites near TATA and Pe1 (see Fig. S2 at the URL mentioned in the previous paragraph) underlines the importance of Nfi proteins in the restricted cartilage-specific expression of *Matn1* in amniotes.

DISCUSSION

By dissecting the control mechanism that directs *Matn1* expression to specific GP zones, this study sheds new light on a distinctive regulatory network orchestrated by the chondrogenic Sox trio. Focusing on the role of short promoter elements, the present work, in line with former reports (19, 34, 41), reveals the following unique features of *Matn1* regulation. (i) Remarkable sequence and positional conservation of prox-

imal (short) and distal promoter elements strongly suggests an evolutionarily conserved transcriptional mechanism in amniotes. (ii) Fundamentally, the proximal promoter is responsible for conferring spatiotemporal expression. It exerts such a dominant effect that it is even capable of restricting spatially and temporally the activity of the otherwise pancartilaginous *Col2a1* enhancer. (iii) This effect is likely due to a unique set of conserved proximal elements. The Sox site in Pe1, located 95 to 195 bp upstream of TATA, preferably binds SOX9 and is most crucial for promoter activity, while Sox sites in Ine located at the transcription start sites preferably bind L-Sox5/Sox6 and are also important. An Nfi site in SI near TATA is also needed for promoter enhancement, and conservation of Nfi motifs in SII near Pe1 suggests an important function. (iv) The most highly conserved Pe1 element plays a key role in SOX9-mediated transactivation from distal DNA elements, and L-Sox5/Sox6 bound to Ine and Nfi proteins bound to SI

may modulate transactivation by SOX9 in a dose-dependent manner and may thereby fine-tune stage-specific promoter activity.

Cartilage-specific control elements with functional Sox sites in other genes in various locations, e.g., intronic, far-upstream, 5' untranslated, or proximal promoter regions, were described previously (13, 15, 26–28, 46), but none shows similarity to the *Matn1* control region. While the *Matn1* short promoter is sufficient to specify the expression pattern of the gene, the *Col2a1* promoter has no activity on its own and relies on an intronic enhancer capable of directing its activity, as well as that of a heterologous β -globin promoter, to all chondrocytic cells and each GP zone in transgenic mice (47, 48).

Comparison of orthologous promoter regions (known as phylogenetic footprinting) can reveal conserved motifs with important regulatory functions (6). As shown, e.g., for the *Sox2* locus, conservation of extragenic sequences in amniotes can more reliably reflect their functional importance in development than the higher degree of conservation between mammals (17). A conserved cartilage-specific element has been identified, however, only in the far-upstream enhancer of the mammalian orthologs of *Agc1*, but it is not conserved in amniotes (13). Such a high degree of sequence and positional conservation among chicken and mammalian orthologs (34) (see Fig. S2 at http://www.brc.hu/pub/Supplemental_Material_Nagy_et_al_MCB2010.pdf) has not been found for other cartilage ECM genes, strongly suggesting a distance-dependent important function for Pe1 and Ine in amniotes. Pe1 and Ine include one or two pairs of oppositely oriented motifs sharing 6/10 to 8/10 or 5/10 to 7/10 nucleotide identity, respectively, with the preferred Sox9-binding site (29), while Sox9 sites of cartilage enhancers share only 4 or 5 nucleotides with the Sox consensus T/AT/ACAAT/AG (13). In line with our former report (34), the present mutational and functional data confirm the key role of the highly conserved Pe1 in SOX9 binding and SOX9-mediated enhancement from distal elements. Ine is less conserved, but it is also needed for high transgene activity. The 3' paired Sox site of Ine had been shifted to a head-to-head position in the chicken ortholog, and it seems to interact rather with L-Sox5/Sox6 in EMSA and forced-expression studies. Notably, the TATA box also showed similarity to the Sox consensus in most of the *Matn1* orthologs, indicating that, besides the conserved strong Sox9-binding site of Pe1, weaker Sox sites, which seem to be more diverged, are clustered near TATA, while the regulatory module might have been under evolutionary pressure and thus remained more conserved. To our knowledge, this is the first report on Sox sites clustered around the transcription start sites, strongly suggesting their importance in the assembly of the preinitiation complex (PIC).

Matn1 is regulated differently by the Sox trio than other cartilage genes (13, 24, 26). Whereas Sox9 is sufficient for the activation of *Col2a1*, *Agc1*, and *Crt11*, *Sox5* and *Sox6* are required to turn on *Matn1*, as *Matn1* mRNA was not detected in *Sox5*^{-/-}; *Sox6*^{-/-} mice (38). Activation of *Sox6* precedes that of *Matn1* in culture, underlining the importance of Sox6 in turning on *Matn1*. As in cartilage enhancers or the COMP promoter (13, 26, 27), L-Sox5 and Sox6 also synergize with SOX9 in the activation of the *Matn1* promoter, but only in the early stage or at low molar excess. Their role, however, turns to repression in the late stage or at elevated molar ratio. Thus, in

large excess, L-Sox5 and Sox6 may compete with SOX9 for the same binding sites, as for oligodendrocyte-specific genes (40).

In agreement with the transient activation of Nfi genes during *in vitro* chondrogenesis, dominant negative mutation of Nfib interfered with chondrogenesis (43). Overexpression of Nfib increased *Sox9* and *Col2a1* expression, but Nfi sites mediating this regulation have not been identified. By extending this and our former studies (41), here we provide the first evidence that, in addition to the Sox trio, Nfi proteins binding near TATA may also play a critical role in determining the chondrocyte stage-specific activity of the *Matn1* promoter.

According to our model (Fig. 10D), the special geometric arrangement of proximal elements may explain the unique regulation of *Matn1*, as it allows fine-tuning of the promoter activity by L-Sox5/Sox6 and Nfi, depending on their abundances relative to that of SOX9. At the onset of chondrogenesis, binding of Sox and Nfi proteins might be needed to open the chromatin structure around TATA (Fig. 10D, a and b). This hypothesis is based on our observations (34) that *in vivo* footprints were absent from the short promoter in the nonexpressing CEF and that they gradually appeared in differentiating HDM culture, strongly suggesting that activation of *Matn1* involves regulation at the chromatin level. In fact, the Nfi sites of SI and SII were not occupied in CEF, although the Nfi genes are expressed in CEF and Nfi proteins can bind SI and SII from CEF extracts in EMSA and *in vitro* footprinting (41). Based on their interaction with histones (3, 12), Nfi proteins may help disrupt the nucleosome structure during *Matn1* activation.

At the early stage of chondrogenesis, when occupancy of the sites is low and SOX9 is expressed at high molar excess relative to L-Sox5/Sox6, SOX9 preferably binds Pe1 and the Ine-bound L-Sox5/Sox6 synergizes with SOX9 by likely increasing its efficiency for binding Pe1 (Fig. 10D, b). L-Sox5/Sox6 similarly secures Sox9 binding to the *Agc1* and *Col2a1* enhancers (13). Binding of Sox factors in the vicinity of TATA may bend the DNA and facilitate the binding of TATA-binding protein (TBP) and polymerase II during the assembly of PIC (see also Fig. S5 at http://www.brc.hu/pub/Supplemental_Material_Nagy_et_al_MCB2010.pdf). Clustering of Sox motifs in Ine may increase the probability of L-Sox5/Sox6 binding and help recruit SOX9 to Pe1 and TBP to TATA. Bending the DNA may also promote the binding of unidentified factors to Pe1 and Ine. Based on preliminary analysis of mutations, these factors may affect proximodistal transgene activity (data not shown). Further, as NFI proteins can activate transcription through direct interaction with basal transcription factors (e.g., CTF-1 with TFIIB and TBP via its proline-rich transactivation domain) and various coactivators and corepressors (12), Nfi binding to SI (and also possibly to SII near Pe1) may also help the assembly of PIC and the enhanceosome, thus highly contributing to activated transcription (see Fig. S5 at the URL listed above). Pe1 likely plays central role in enhanceosome formation and in SOX9-mediated promoter activation from distal elements, but, due to the low abundance of transcription factors, the transcription activity is low in early proliferative chondroblasts (Fig. 10D, b). The promoter activity is highest in late proliferative chondroblasts, when *in vivo* occupancy is optimal, high at Pe1, and Ine, and moderate at SI (Fig. 10D, c). Nfib exerted activation at an early stage in this study and another

study (43), but we cannot exclude the possibility that another Nfi isoform is active in CEC culture, considering the drop in the relative expression level of Nfib and other Nfi mRNAs. At this late stage, when the Sox trio mRNA level is elevated, forced expression of L-Sox5/Sox6 in large molar excess to SOX9 can decrease transactivation by SOX9, possibly by competing with SOX9 for binding Pe1 and other elements (Fig. 10D, d). High occupancy of the Sox sites of Ine may even physically interfere with the recruitment of PIC to TATA. Overproduction of Nfi may also decrease promoter activity due to competition between activator (e.g., Nfib) and repressor Nfi isoforms, which may even sterically block TBP binding to TATA (Fig. 10D, e).

The unique molecular mechanism described here can facilitate the construction of GP zone-specific vectors and the development of biotechnological therapies for skeletal diseases.

ACKNOWLEDGMENTS

We are grateful to B. de Crombrughe for providing plasmid p3000i3020Col2a1 and SOX9, L-Sox5, and Sox6 antisera, to P. Berta for the GST-SOX9 plasmid, to R. Gronostajski for Nfia, Nfib, Nfic, and Nfix expression plasmids, and to N. Mermod for the CTF1 expression plasmid. We thank P. Szabó for introducing O.R. to genomic footprinting, A. Simon, E. Horváth, I. Kravjár, and K. Kávai for excellent technical assistance, and M. Tóth for the artwork.

This work was supported by grant OTKA PD50006 to E.K., by grants OTKA T049608 from the Hungarian National Scientific Research Foundation, ETT 008/2006 from the Medical Research Council of Hungary, and GVOP-3.1.1.-2004-05-0290/3.0 from the Economic Competitiveness Operative Program of the National Development Plan to I.K., and by NIH/NIAMS grant AR60016 to V.L. Á. Zvara and E. Barta were supported by János Bolyai fellowships from the Hungarian Academy of Sciences (BO/00381/07 and BO/00383/08). This work was also partly supported by grant AVINOMID from the Ányos Jedlik Programme of the National Office for Research and Technology (NKTH) to L.G.P.

REFERENCES

- Akiyama, H. 2008. Control of chondrogenesis by the transcription factor Sox9. *Mod. Rheumatol.* **18**:213–219.
- Akiyama, H., M.-C. Chaboissier, J. F. Martin, A. Schedl, and B. de Crombrughe. 2002. The transcription factor Sox9 has essential roles in successive steps of the chondrocyte differentiation pathway and is required for expression of *Sox5* and *Sox6*. *Genes Dev.* **16**:2813–2828.
- Alevizopoulos, A., et al. 1995. A proline-rich TGF- β -responsive transcriptional activator interacts with histone H3. *Genes Dev.* **9**:3051–3066.
- Aszódi, A., et al. 1996. Cloning, sequencing and expression analysis of mouse cartilage matrix protein cDNA. *Eur. J. Biochem.* **236**:970–977.
- Aszódi, A., et al. 1994. The zonal expression of chicken cartilage matrix protein gene in the developing skeleton of transgenic mice. *Matrix Biol.* **14**:181–190.
- Barta, E., et al. 2005. DoOP: databases of orthologous promoters, collections of clusters of orthologous upstream sequences from chordates and plants. *Nucleic Acids Res.* **33**:D86–D90.
- Bi, W., J. M. Deng, Z. Zhang, R. R. Behringer, and B. de Crombrughe. 1999. Sox9 is required for cartilage formation. *Nat. Genet.* **22**:85–89.
- Cancedda, R., F. D. Cancedda, and P. Castagnola. 1995. Chondrocyte differentiation. *Int. Rev. Cytol.* **159**:265–359.
- Chaudhry, A. Z., A. D. Vitullo, and R. M. Gronostajski. 1998. Nuclear factor I (NFI) isoforms differentially activate simple versus complex NFI-responsive promoters. *J. Biol. Chem.* **273**:18538–18546.
- Deák, F., R. Wagener, I. Kiss, and M. Paulsson. 1999. The matrilins: a novel family of oligomeric extracellular matrix proteins. *Matrix Biol.* **18**:55–64.
- Goldring, M. B., K. Tsuchimochi, and K. Jiri. 2006. The control of chondrogenesis. *J. Cell. Biochem.* **97**:33–44.
- Gronostajski, R. M. 2000. Roles of the NFI/CTF gene family in transcription and development. *Gene* **249**:31–45.
- Han, Y., and V. Lefebvre. 2008. L-Sox5 and Sox6 drive expression of the aggrecan gene in cartilage by securing binding of Sox9 to a far-upstream enhancer. *Mol. Cell. Biol.* **28**:4999–5013.
- Ikeda, T., et al. 2004. The combination of SOX5, SOX6, and SOX9 (the SOX trio) provides signals sufficient for induction of permanent cartilage. *Arthritis Rheum.* **50**:3561–3573.
- Imamura, T., C. Imamura, Y. Iwamoto, and L. J. Sandell. 2005. Transcriptional co-activators CREB-binding protein/p300 increase chondrocyte *Ca-rap* gene expression by multiple mechanisms including sequestration of the repressor CCAAT/enhancer-binding protein. *J. Biol. Chem.* **280**:16625–16634.
- Kálmán, J., et al. 2005. Gene expression profile analysis of lymphocytes from Alzheimer's patients. *Psychiatr. Genet.* **15**:1–6.
- Kamachi, Y., et al. 2009. Evolution of non-coding regulatory sequences involved in the developmental process: reflection of differential employment of paralogous genes as highlighted by Sox2 and group B1 Sox genes. *Proc. Jpn. Acad.* **85**:55–68.
- Kamachi, Y., M. Uchikawa, and H. Kondoh. 2000. Pairing Sox off with partners in the regulation of embryonic development. *Trends Genet.* **16**:182–187.
- Karcagi, I., et al. 2004. Functional analysis of the regulatory regions of the matrilin-1 gene in transgenic mice reveals modular arrangement of tissue-specific control elements. *Matrix Biol.* **22**:605–618.
- Karsenty, G., H. M. Kronenberg, and C. Settembre. 2009. Genetic control of bone formation. *Annu. Rev. Cell Dev. Biol.* **25**:629–648.
- Kiefer, J. C. 2007. Back to basics: Sox genes. *Dev. Dyn.* **236**:2356–2366.
- Kiss, I., et al. 1989. Structure of the gene for cartilage matrix protein, a modular protein of the extracellular matrix. *J. Biol. Chem.* **264**:8126–8134.
- Kou, I., and S. Ikegawa. 2004. SOX9-dependent and -independent transcriptional regulation of human cartilage link protein. *J. Biol. Chem.* **279**:50942–50948.
- Lefebvre, V., and P. Smits. 2005. Transcriptional control of chondrocyte fate and differentiation. *Birth Defects Res. C Embryo Today* **75**:200–212.
- Lefebvre, V., B. Dumitriu, A. Penzo-Méndez, Y. Han, and B. Pallavi. 2007. Control of cell fate and differentiation by Sry-related high-mobility-group box (Sox) transcription factors. *Int. J. Biochem. Cell Biol.* **39**:2195–2214.
- Lefebvre, V., P. Li, and B. de Crombrughe. 1998. A long new form of Sox5 (L-Sox5), Sox6 and Sox9 are coexpressed in chondrogenesis and cooperatively activate the type II collagen gene. *EMBO J.* **17**:5718–5733.
- Liu, C., et al. 2007. Transcriptional activation of cartilage oligomeric matrix protein by Sox9, Sox5, and Sox6 transcription factors and CBP/p300 coactivators. *Front. Biosci.* **12**:3899–3910.
- Liu, Y., H. Li, K. Tanaka, N. Tsumaki, and Y. Yamada. 2000. Identification of an enhancer sequence within the first intron required for cartilage-specific transcription of the $\alpha 2(XI)$ collagen gene. *J. Biol. Chem.* **275**:12712–12718.
- Mertin, S., S. G. McDowell, and V. R. Harley. 1999. The DNA-binding specificity of SOX9 and other SOX proteins. *Nucleic Acids Res.* **27**:1359–1364.
- Mundlos, S., and B. Zabel. 1994. Developmental expression of human cartilage matrix protein. *Dev. Dyn.* **199**:241–252.
- Muratoglu, S., et al. 1995. Expression of the cartilage matrix protein gene at different chondrocyte developmental stages. *Eur. J. Cell Biol.* **68**:411–418.
- Pfeifer, G. P., H. H. Chen, J. Komura, and A. D. Riggs. 1999. Chromatin structure analysis by ligation-mediated and terminal transferase-mediated polymerase chain reaction. *Methods Enzymol.* **304**:548–571.
- Provot, S., and E. Schipani. 2005. Molecular mechanisms of endochondral bone development. *Biochem. Biophys. Res. Commun.* **328**:658–665.
- Rentsendorj, O., et al. 2005. Highly conserved proximal promoter element harbouring paired Sox9-binding sites contributes to the tissue- and developmental stage-specific activity of the matrilin-1 gene. *Biochem. J.* **389**:705–716.
- Roulet, E., et al. 2000. Experimental analysis and computer prediction of CTF/NFI transcription factor DNA binding sites. *J. Mol. Biol.* **297**:833–848.
- Santoro, C., N. Mermod, P. C. Andrews, and R. Tjian. 1988. A family of human CCAAT-box-binding proteins active in transcription and DNA replication: cloning and expression of multiple cDNAs. *Nature* **334**:218–224.
- Shimizu, H., S. Yokoyama, and H. Asahara. 2007. Growth and differentiation of developing limb bud from perspective of chondrogenesis. *Dev. Growth Differ.* **49**:449–454.
- Smits, P., et al. 2001. The transcription factors L-Sox5 and Sox6 are essential for cartilage formation. *Dev. Cell* **1**:277–290.
- Stirpe, N. S., and P. F. Goetinck. 1989. Gene regulation during cartilage differentiation: temporal and spatial expression of link protein and cartilage matrix protein in developing limb. *Development* **107**:23–33.
- Stolt, C. C., et al. 2006. SoxD proteins influence multiple stages of oligodendrocyte development and modulate SoxE protein function. *Dev. Cell* **11**:697–709.
- Szabó, P., et al. 1995. Identification of a nuclear factor-I family protein-binding site in the silencer region of the cartilage matrix protein gene. *J. Biol. Chem.* **270**:10212–10221.
- Szűts, V., et al. 1998. Terminal differentiation of chondrocytes is arrested at distinct stages identified by their expression repertoire of marker genes. *Matrix Biol.* **17**:435–448.
- Uchihashi, T., et al. 2007. Involvement of nuclear factor I transcription/replication factor in the early stage of chondrogenic differentiation. *Bone* **41**:1025–1035.

44. **Wagener, R., et al.** 2005. The matrilins—adaptor proteins in the extracellular matrix. *FEBS Lett.* **579**:3323–3329.
45. **Wiberg, C., et al.** 2003. Complexes of matrilin-1 and biglycan or decorin connect collagen VI microfibrils to both collagen II and aggrecan. *J. Biol. Chem.* **278**:37698–37704.
46. **Zhang, P., S. A. Jimenez, and D. G. Stokes.** 2003. Regulation of human COL9A1 gene expression. *J. Biol. Chem.* **278**:117–123.
47. **Zhou, G., et al.** 1995. A 182 bp fragment of the mouse pro α 1(II) collagen gene is sufficient to direct chondrocyte expression in transgenic mice. *J. Cell Sci.* **108**:3677–3684.
48. **Zhou, G., V. Lefebvre, Z. Zhang, H. Eberspaecher, and B. de Crombrughe.** 1998. Three high mobility group-like sequences within a 48-base pair enhancer of the *Col2a1* gene are required for cartilage-specific expression *in vivo*. *J. Biol. Chem.* **273**:14989–14997.